Theoretical Astroparticle Physics

Contents

1. Topics **1339**

2. Participants **1341**
2.1. ICRANet participants 1341
2.2. Past collaborators 1341
2.3. Ongoing collaborations 1342
2.4. Students 1342

3. Brief description **1343**
3.1. Electron-positron plasma 1343
3.1.1. Thermalization of mildly relativistic plasma with proton loading 1343
3.1.2. Pair plasma relaxation timescales 1344
3.1.3. Hydrodynamic phase of GRB sources 1345
3.2. Neutrinos in cosmology 1345
3.2.1. Massive neutrino and structure formation 1347
3.2.2. Cellular structure of the Universe 1347
3.2.3. Lepton asymmetry of the Universe 1348
3.2.4. Mass Varying Neutrinos 1348
3.3. Indirect Detection of Dark Matter 1349
3.4. Alternative Cosmological Models 1350

4. Publications **1353**
4.1. Publications before 2005 1353
4.2. Publications (2005 - 2008) 1356
4.3. Publications (2009) 1362
4.4. Invited talks at international conferences 1365

5. APPENDICES **1369**

A. Pair plasma relaxation timescales **1371**

B. Hydrodynamic phase of GRB sources **1379**
B.1. Introduction 1379
B.2. Kinetic and hydrodynamical phases 1381
B.3. Physical evolution 1383

B.4. Results 1385
B.4.1. Constant baryonic distribution profile 1385
B.4.2. c) Hybrid profile 1387
B.5. Conclusions 1389
B.6. Numerical approach 1390
B.6.1. Finite difference form of equations 1392
B.6.2. Numerical issues 1393
B.7. test 1395
B.7.1. a) Piran's profile 1395

C. Cosmological structure formation 1397
C.0.2. The Cosmological Principle 1397
C.1. Two-point Correlation Function 1399
C.1.1. Observed Galaxy Distribution 1400
C.1.2. Power Law Clustering and Fractals 1401

D. Massive degenerate neutrinos in Cosmology 1403
D.1. Neutrino decoupling 1403
D.2. The redshifted statistics 1404
D.3. Energy density of neutrinos 1405
D.3.1. Neutrino mass 1406
D.3.2. Chemical potential 1407
D.3.3. Neutrino oscillations 1408
D.4. The Jeans mass of neutrinos 1408
D.5. Joint constraints on the lepton asymmetry of the Universe and neutrino mass from the Wilkinson Microwave Anisotropy Probe 1411
D.5.1. Introduction 1411
D.5.2. Motivation for this work 1414
D.5.3. Basic formulae 1415
D.5.4. Effect of a non-null chemical potential 1419
D.5.5. Method 1421
D.5.6. Results and discussion 1424
D.5.7. Conclusions and perspectives 1428
D.6. Model independent constraints on mass-varying neutrino scenarios 1431
D.6.1. Introduction 1431
D.6.2. Mass-varying neutrinos 1433
D.6.3. Model independent approach 1435
D.6.4. Results and Discussion 1442
D.6.5. Concluding remarks 1448

E. Indirect Detection of Dark Matter **1455**
E.1. Boosting the WIMP annihilation through the Sommerfeld enhancement 1455
E.1.1. The Sommerfeld enhancement 1456
E.1.2. The leptonic branching ratio 1461
E.1.3. CDM substructure: enhancing the Sommerfeld boost . 1463
E.1.4. Discussion 1465
E.2. Constraining the dark matter annihilation cross-section with Cherenkov telescope observations of dwarf galaxies 1468
E.2.1. Introduction 1468
E.2.2. γ-ray flux from Dark Matter annihilation in Draco and Sagittarius 1470
E.2.3. Comparison with the experimental data 1480
E.2.4. Conclusions 1485

F. Alternative Cosmological Models **1489**

Bibliography **1493**

1. Topics

- Electron-positron plasma
  - Thermalization of mildly relativistic plasma with proton loading
  - Relaxation timescales in the pair plasma
  - Hydrodynamic phase of GRB sources
- Neutrinos in cosmology
  - Massive neutrino and structure formation
  - Cellular structure of the Universe
  - Lepton asymmetry of the Universe
  - Mass Varying Neutrinos
- Indirect Detection of Dark Matter
- Alternative Cosmological Models

2. Participants

2.1. ICRANet participants

- Carlo Luciano Bianco
- Massimiliano Lattanzi
- Remo Ruffini
- Gregory Vereshchagin
- She-Sheng Xue

2.2. Past collaborators

- Marco Valerio Arbolino (DUNE s.r.l., Italy)
- Andrea Bianconi (INFN Pavia, Italy)
- Neta A. Bahcall (Princeton University, USA)
- Daniella Calzetti (University of Massachusets, USA)
- Jaan Einasto (Tartu Observatory, Estonia)
- Roberto Fabbri (University of Firenze, Italy)
- Long-Long Feng (University of Science and Technology of China, China)
- Jiang Gong Gao (Xinjiang Institute of Technology, China)
- Mauro Giavalisco (University of Massachusets, USA)
- Gabriele Ingrosso (INFN, University of Lecce, Italy)
- Yi-peng Jing (Shanghai Astronomical Observatory, China)
- Hyung-Won Lee (Inje University, South Korea)
- Marco Merafina (University of Rome "Sapienza", Italy)
- Houjun Mo (University of Massachusetts, USA)

- Enn Saar (Tartu Observatory, Estonia)
- Jay D. Salmonson (Livermore Lab, USA)
- Luis Alberto Sanchez (National University Medellin, Colombia)
- Costantino Sigismondi (ICRA and University of Rome "La Sapienza", Italy)
- Doo Jong Song (Korea Astronomy Observatory, South Korea)
- Luigi Stella (Astronomical Observatory of Rome, Italy)
- William Stoeger (Vatican Observatory, University of Arizona USA)
- Sergio Taraglio (ENEA, Italy)
- Gerda Wiedenmann (MPE Garching, Germany)
- Jim Wilson (Livermore Lab, USA)
- Roustam Zalaletdinov (Tashkent University, Uzbekistan)

2.3. Ongoing collaborations

- Alexey Aksenov (ITEP, Russia)
- Valeri Chechetkin (Keldysh Institute, Russia)
- Urbano França (Instituto de Física Corpuscular, Valencia, Spain)
- Julien Lesgourgues (CERN, Theory Division, Geneva, Switzerland)
- Alessandro Melchiorri (Univ. "Sapienza" di Roma, Italy)
- Lidia Pieri (Institute d'Astrophysique, Paris, France)
- Sergio Pastor (Instituto de Física Corpuscolar, Valencia, Spain)
- Joseph Silk (Oxford University, UK)

2.4. Students

- Gustavo de Barros (IRAP PhD, Brazil)
- Luis Juracy Rangel Lemos (IRAP PhD, Brazil)
- Stefania Pandolfi (IRAP PhD, Italy)
- Ivan Siutsou (IRAP PhD, Belarus)

3. Brief description

Astroparticle physics is a new field of research emerging at the intersection of particle physics, astrophysics and cosmology. Theoretical development in these fields is mainly triggered by the growing amount of experimental data of unprecedented accuracy, coming both from the ground based laboratories and from the dedicated space missions.

3.1. Electron-positron plasma

Electron-positron plasma is of interest in many fields of astrophysics, e.g. in the early universe, gamma-ray bursts, active galactic nuclei, the center of our Galaxy, hypothetical quark stars. It is also relevant for the physics of ultraintense lasers and thermonuclear reactions. We study some properties of dense and hot electron-positron plasmas. In particular, we are interested in the issues of its creation and relaxation, its kinetic properties and hydrodynamic description, baryon loading, transition to transparency and radiation from such plasmas.

Two completely different states exist for electron-positron plasma: optically thin and optically thick. Optically thin pair plasma may exist in active galactic nuclei and in X-ray binaries. The theory of relativistic optically thin nonmagnetic plasma and especially its equilibrium configurations was established in the 80s by Svensson, Lightman, Gould and others. It was shown that relaxation of the plasma to some equilibrium state is determined by a dominant reaction, e.g. Compton scattering or bremsstrahlung.

Developments in the theory of gamma ray bursts from one side, and observational data from the other side, unambiguously point out on existence of optically thick pair dominated non-steady phase in the beginning of formation of GRBs. The spectrum of radiation from optically thick plasma is assumed to be thermal. However, in such a transient phenomena as gamma-ray bursts there could be not enough time for the plasma to relax into equilibrium.

3.1.1. Thermalization of mildly relativistic plasma with proton loading

One of crucial assumptions adopted in the literature on gamma-ray bursts (Ruffini et al. (1999),Ruffini et al. (2000)) is that initial state of the pair plasma,

formed in the source of the gamma-ray burst is supposed to be thermal, with equal temperature of pairs and photons. This assumption was analyzed by Aksenov et al. (2007),Aksenov et al. (2008). The electron-positron-photon plasma was assumed to be homogeneous and isotropic, in the absence of magnetic fields, with average energy per particle bracketing electron rest mass, in the range $0.1\text{MeV} \lesssim \epsilon \lesssim 10\text{MeV}$. Relativistic Boltzmann equations were solved numerically for pairs and photons, starting from arbitrary initial configurations described by the corresponding distribution functions. All binary and triple collisions were accounted for, by the corresponding collisional integrals.

Proton loading of electron-positron plasma was considered by Aksenov et al. (2009c) (2009). This paper systematically presents details of the computational scheme used by Aksenov et al. (2007), as well as generalizes the treatment, considering proton loading of the pair plasma. When proton loading is large, protons thermalize first by proton-proton scattering, and then with the electron-positron-photon plasma by proton-electron scattering. In the opposite case of small proton loading proton-electron scattering dominates over proton-proton one. Thus in all cases the plasma, even with proton admixture, reaches thermal equilibrium configuration on a timescale $t < 10^{-11}$ sec. We show that it is crucial to account for not only binary but also triple direct and inverse interactions between electrons, positrons, photons and protons. Several explicit examples are given and the corresponding timescales for reaching kinetic and thermal equilibria are determined.

3.1.2. Pair plasma relaxation timescales

In previous works (Aksenov et al. (2007),Aksenov et al. (2009c)) relaxation timescales were computed explicitly only in few cases. Systematic exploration of the space of parameters is performed in a separate publication by Aksenov et al. (2009b), see Appendix A. These parameters are: total energy density ρ and the baryonic loading parameter $B = \rho_b/\rho_{e,\gamma}$, the ratio between the energy densities of baryons and of electron-positron pairs and photons. We focused on the time scales of electromagnetic interactions only.

Thermalization timescales are computed for a wide range of values of both the total energy density ($10^{23}\text{erg/cm}^3 \leq \rho \leq 10^{33}\text{erg/cm}^3$) and of the baryonic loading parameter ($10^{-3} \leq B \leq 10^3$). This also allows to study such interesting limiting cases as the almost purely electron-positron plasma or electron-proton plasma as well as intermediate cases.

Both dependencies (thermalization time scales of electron-positron-photon component and final thermalization time scale of pair plasma with baryonic loading) cannot be fitted by simple power laws, though decrease monotonically with increasing total energy density, see Figs. A.1,A.2. Thermalization time scales are not monotonic functions of the baryonic loading parameter.

The relaxation to thermal equilibrium always occurs on a time scale less than 10^{-9} sec. It is interesting that the electron-positron-photon component and/or proton component can thermalize earlier than the time at which complete thermal equilibrium is reached. The relevant time scales are given and compared with the order-of-magnitude estimates.

These results appear to be important both for laboratory experiments aimed at generating optically thick pair plasmas as well as for astrophysical models in which electron-positron pair plasmas play a relevant role.

3.1.3. Hydrodynamic phase of GRB sources

Having established the thermalization timescales of electron-positron plasma with baryonic loading we turn to hydrodynamic evolution of this plasma on much longer timescales. Given that the optical depth of the pair plasma in GRB sources is huge, of the order of 10^{15}, the dynamical equations are the total energy-momentum conservation as well as the continuity equation for baryonic component.

The fireshell model, unlike the fireball model, properly takes into account nonequilibrium processes in the pair plasma by the rate equation of electron-positron component. However, it only operates with volume-averaged macroscopic quantities such as average number densities, average energy densities, average bulk Lorentz factors etc.

We developed an Eulerian relativistic code, which solves hydrodynamic equations in spherically symmetric case (de Barros et al. (2009)). We were mainly interested in the question how different initial spatial distribution for energy and mass densities influence the early evolution of the pair plasma with baryonic loading, for details see Appendix C. We found that deviations from a simple "frozen radial profile" advocated by Piran et al. (1993), see also Piran (1999) in spatial distributions of energy and matter densities are possible. In fact when the expansion occurs not in vacuum but in a cold medium, two peaks in the radial distribution of energy and matter form, the leading one being matter dominated from the very beginning, see e.g. Fig. B.8. Such structures in the energy and matter spatial distributions of the expanding plasma, if survived when transparency is reached, will be reflected in the light curves of GRBs. This gives a fascinating possibility to probe the structure of energy and matter distributions withing the sources of GRBs where the energy is released.

3.2. Neutrinos in cosmology

Many observational facts make it clear that luminous matter alone cannot account for the whole matter content of the Universe. Among them there is the cosmic background radiation anisotropy spectrum, that is well fitted

by a cosmological model in which just a small fraction of the total density is supported by baryons.

In particular, the best fit to the observed spectrum is given by a flat ΛCDM model, namely a model in which the main contribution to the energy density of the Universe comes from vacuum energy and cold dark matter. This result is confirmed by other observational data, like the power spectrum of large scale structures.

Another strong evidence for the presence of dark matter is given by the rotation curves of galaxies. In fact, if we assume a spherical or ellipsoidal mass distribution inside the galaxy, the orbital velocity at a radius r is given by Newton's equation of motion. The peculiar velocity of stars beyond the visible edge of the galaxy should then decrease as $1/r$. What is instead observed is that the velocity stays nearly constant with r. This requires a halo of invisible, dark, matter to be present outside the edge. Galactic size should then be extended beyond the visible edge. From observations is follows that the halo radius is at least 10 times larger than the radius of visible part of the galaxy. Then it follows that a halo is at least 10 times more massive than all stars in a galaxy.

Neutrinos were considered as the best candidate for dark matter about twenty years ago. Indeed, it was shown that if these particles have a small mass $m_\nu \sim 30\,\mathrm{eV}$, they provide a large energy density contribution up to critical density. Tremaine and Gunn (1979) have claimed, however, that massive neutrinos cannot be considered as dark matter. Their paper was very influential and turned most of cosmologists away from neutrinos as cosmologically important particles.

Tremaine and Gunn paper was based on estimation of lower and upper bounds for neutrino mass; when contradiction with these bounds was found, the conclusion was made that neutrinos cannot supply dark matter. The upper bound was given by cosmological considerations, but compared with the energy density of clustered matter. It is possible, however, that a fraction of neutrinos lays outside galaxies.

Moreover, their lower bound was found on the basis of considerations of galactic halos and derived on the ground of the classical Maxwell-Boltzmann statistics. Gao and Ruffini (1980) established a lower limit on the neutrino mass by the assumption that galactic halos are composed by degenerate neutrinos. Subsequent development of their approach Arbolino and Ruffini (1988) has shown that contradiction with two limits can be avoided.

At the same time, in 1977 the paper by Lee and Weinberg (1977) appeared, in which authors turned their attention to massive neutrinos with $m_\nu > 2\,\mathrm{GeV}$. Such particles could also provide a large contribution into the energy density of the Universe, in spite of much smaller value of number density.

Recent experimental results from laboratory (see Dolgov (2002) for a review) rule out massive neutrinos with $m_\nu > 2\,\mathrm{GeV}$. However, the paper by Lee and Weinberg was among the first where very massive particles were

considered as candidates for dark matter. This can be considered as the first of cold dark matter models.

Today the interest toward neutrinos as a candidate for dark matter came down, since from one side, the laboratory limit on its mass do not allow for significant contribution to the density of the Universe, and from other side, conventional neutrino dominated models have problems with formation of structure on small scales. However, in these scenarios the role of the chemical potential of neutrinos was overlooked, while it could help solving both problems.

3.2.1. Massive neutrino and structure formation

Lattanzi et al. (2003) have studied the possible role of massive neutrinos in the large scale structure formation. Although now it is clear, that massive light neutrinos cannot be the dominant part of the dark matter, their influence on the large scale structure formation should not be underestimated. In particular, large lepton asymmetry, still allowed by observations, can affect cosmological constraints on neutrino mass.

3.2.2. Cellular structure of the Universe

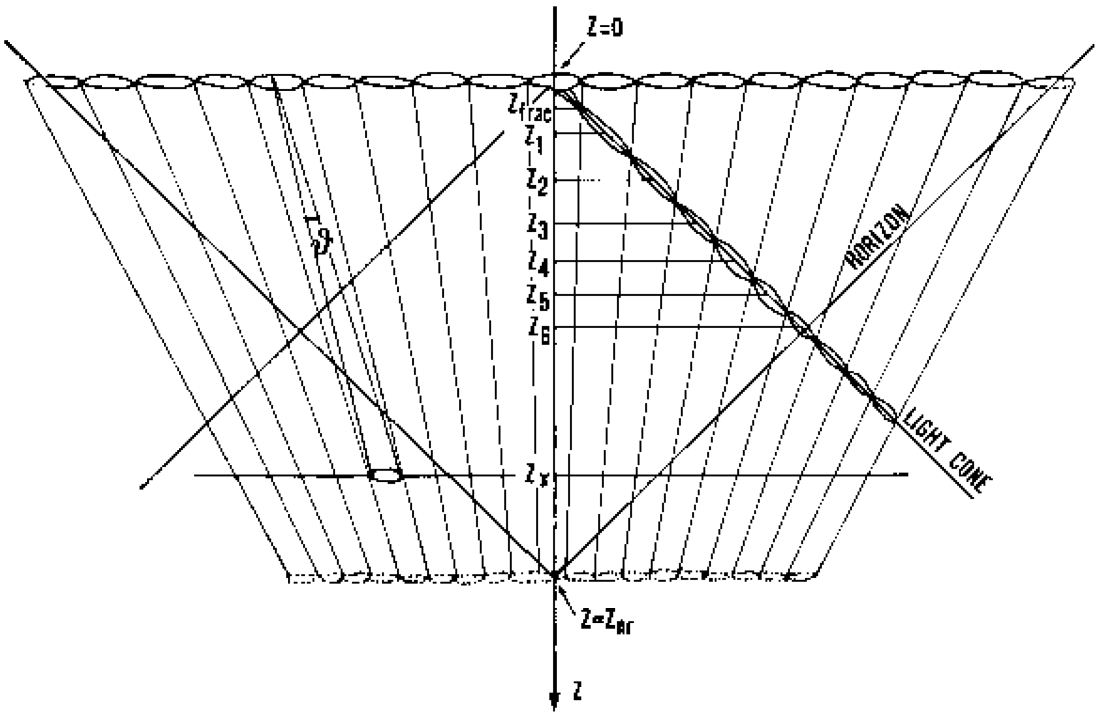

Figure 3.1.: Cellular structure of the Universe.

One of the interesting possibilities, from a conceptual point of view, is the change from the description of the physical properties by a continuous function, to a new picture by introducing a self-similar fractal structure. This approach has been relevant, since the concept of homogeneity and isotropy formerly apply to any geometrical point in space and leads to the concept of a Universe observer-homogeneous Ruffini (1989). Calzetti et al. (1987),Giavalisco (1992),Calzetti et al. (1988) have defined the correlation length of a fractal

$$r_0 = \left(1 - \frac{\gamma}{3}\right)^{1/\gamma} R_S, \tag{3.2.1}$$

where R_S is the sample size, $\gamma = 3 - D$, and D is the Hausdorff dimension of the fractal. Most challenging was the merging of the concepts of fractal, Jeans mass of dark matter and the cellular structure in the Universe, advanced by Ruffini et al. (1988). The cellular structure emerging from this study is represented in Figure 3.1. There the upper cutoff in the fractal structure $R_{\rm cutoff} \approx$ 100 Mpc, was associated to the Jeans mass of the "ino" $M_{\rm cell} = \left(\frac{m_{pl}}{m_{ino}}\right)^2 m_{pl}$. Details see in Appendix C.

3.2.3. Lepton asymmetry of the Universe

Lattanzi et al. (2005),Lattanzi et al. (2006) studied how the cosmological constraints on neutrino mass are affected by the presence of a lepton asymmetry. The main conclusion is that while constraints on neutrino mass do not change by the inclusion into the cosmological model the dimensional chemical potential of neutrino, as an additional parameter, the value of lepton asymmetry allowed by the present cosmological data is surprisingly large, being

$$L = \sum_{\nu} \frac{n_\nu - n_{\bar{\nu}}}{n_\gamma} \lesssim 0.9, \tag{3.2.2}$$

Therefore, large lepton asymmetry is not ruled out by the current cosmological data. Details see in Appendix D.

3.2.4. Mass Varying Neutrinos

A possible interesting link between neutrinos and cosmology is given by those models of dark energy in which neutrinos interact with the scalar field supposed to be responsible for the acceleration of the universe. In these models, the interaction between neutrinos and the scalar field usually implies a variation of the neutrino masses on cosmological time scales. For this reason they are known as mass-varying neutrinos (MaVaNs in short) models.

Several candidates for the accelerating component of the universe, generically dubbed dark energy (DE), have been proposed, but understanding them

theoretically and observationally has proven to be challenging. On the theoretical side, explaining the small value of the observed dark energy density component, $\rho_\phi \sim (10^{-3}\ \mathrm{eV})^4$, as well as the fact that both dark energy and matter densities contribute significantly to the energy budget of the present universe requires in general a strong fine tuning on the overall scale of the dark energy models. On the observational side, choosing among the dark energy models is a complicated task. Most of them can mimic a cosmological constant at late times and all data until now are perfectly consistent with this limit. In this sense, looking for different imprints that could favor the existence of a particular model of dark energy is a path worth taking.

Recently, Franca et al. (2009) found that the MaVaNs scenario could be constrained not only via the dark energy effects, but also by indirect signs of the neutrino mass variation during cosmological evolution, since neutrinos play a key role in several epochs. In particular, they proposed a parameterization for the neutrino mass variation that captures the essentials of those scenarios and allows to constrain them in a model independent way, that is, without resorting to any particular scalar field model. Using WMAP 5yr data combined with the matter power spectrum of SDSS and 2dFGRS, the limit on the present value of the neutrino mass is $m_0 \equiv m_\nu(z=0) < 0.43\ (0.28)$ eV at 95% C.L. for the case in which the neutrino mass was lighter (heavier) in the past, a result competitive with the ones imposed for standard (*i.e.*, constant mass) neutrinos. Moreover, for the ratio of the mass variation of the neutrino mass Δm_ν over the current mass m_0 it is found that $\log[|\Delta m_\nu|/m_0] < -1.3\ (-2.7)$ at 95% C.L. for $\Delta m_\nu < 0\ (\Delta m_\nu > 0)$, totally consistent with no mass variation.

3.3. Indirect Detection of Dark Matter

The motivation for studying dark matter annihilation signatures (see e.g. Bertone et al. (2005)) has received considerable recent attention following reports of a 100 GeV excess in the PAMELA data on the ratio of the fluxes of cosmic ray positrons to electrons Adriani et al. (2009). In the absence of any compelling astrophysical explanation, the signature is reminiscent of the original prediction of a unique dark matter annihilation signal Silk and Srednicki (1984), although there are several problems that demand attention before any definitive statements can be made. By far the most serious of these is the required annihilation boost factor. The remaining difficulties with a dark matter interpretation, including most notably the gamma ray signals from the Galactic Centre and the inferred leptonic branching ratio, are plausibly circumvented or at least alleviated. Recent data from the ATIC balloon experiment provides evidence for a cut-off in the positron flux near 500 GeV that supports a KK-like candidate for the annihilating particle Chang et al. (2008) or a neutralino with incorporation of suitable radiative corrections (Bergstrom et al., 2008).

In a pioneering paper, it was noted (Profumo, 2005) that the annihilation signal can be boosted by a combination of coannihilations and Sommerfeld corrrection. We remark first that the inclusion of coannihilations to boost the annihilation cross-section modifies the relic density, and opens the 1-10 TeV neutralino mass window to the observed (WMAP5-normalised) dark matter density. As found by Lavalle et al. (2008), the outstanding problem now becomes that of normalisation. A boost factor of around 100 is required to explain the HEAT data in the context of a 100 GeV neutralino. The flux is suppressed by between one and two powers of neutralino mass, and the problem becomes far more severe with the 1-10 TeV neutralino required by the PAMELA/ATIC data (Cirelli et al., 2009), a boost of 10^4 or more being required. These latter authors included a Sommerfeld correction appropriate to our $\beta \equiv v/c = 0.001$ dark halo and incorporated channel-dependent boost factors to fit the data, but the required boosts still fell short of plausible values by at least an order of magnitude.

Recently Lattanzi and Silk (2009) proposed a solution to the boost problem via Sommerfeld correction in the presence of a model of substructure that incorporates a plausible phase space structure for CDM, also reassessing the difficulty with the leptonic branching ratio and showing that it is not insurmountable for SUSY candidates. They also evaluated the possibility of independent confirmation via photon channels.

Then, Pieri et al. (2009b) studied the expected γ-ray flux from two local dwarf galaxies for which Cherenkov Telescope measurements are available, namely Draco and Sagittarius, incorporating the Sommerfeld enhancement of the annihilation cross-section. They used recent stellar kinematical measurements to model the dark matter halos of the dwarfs, and the results of numerical simulations to model the presence of an associated population of subhalos. They compared their predictions with the observations of Draco and Sagittarius performed by MAGIC and HESS, respectively, and derived exclusion limits on the effective annihilation cross-section. They also studied the sensitivities of Fermi and of the future Cherenkov Telescope Array to cross-section enhancements. It is found that the boost factor due to the Sommerfeld enhancement is already constrained by the MAGIC and HESS data, with enhancements greater than $\sim 10^4$ being excluded.

3.4. Alternative Cosmological Models

Precision measurement of the cosmological observables have lead to believe that we leave in a flat Friedmann Universe, seeded by nearly scale-invariant adiabatic primordial fluctuations Komatsu et al. (2009). The majority ($\sim 70\%$) of the energy density of the Universe is in the form of a fluid with a cosmological constant-like equation of state ($w \sim -1$), dubbed dark energy, that is responsible for the observed acceleration of the Universe Frieman et al.

(2008). Although this "concordance model" gives a very satisfactory fit of all available data, nevertheless it should be noted that a convincing theoretical explanation for what the dark energy is, is still missing. For this reason it is worth looking for alternatives to the concordance model. Several interesting ideas have been put forward in this regard. One is that the observed acceleration is an artefact due to small-scale inhomogeneities. However this interpretation has to deal with the fact that hints for the presence of dark energy come not only from the acceleration, but also from the CMB data. Recently, Blanchard et al. (2003) have noted that in fact, by relaxing the hypothesis that the fluctuation spectrum can be described by a single power law, the CMB data can be well fitted by a Universe with zero cosmological constant. In this alternative model, the Hubble constant has to be very low ($\sim 46\,\mathrm{km\,s^{-}1Mpc^{-1}}$) with respect to the value measured by the Hubble space telescope ($\sim 72\,\mathrm{km\,s^{-}1Mpc^{-1}}$), but this could be explained if we were living in an underdense region, so that our local neighborhood was expanding faster that the average. This would imply that the Hubble constant measured by the HST would be larger than the "actual" Hubble constant measuring the average expansion speed of the Universe. However, in the paper by Blanchard et al. (2003) a thorough treatment of the statistical issues related to the problem was missing. We reassessed the statistical significance of their findings in a paper presently in preparation (Giusarma et al.).

4. Publications

4.1. Publications before 2005

1. R. Ruffini, D. J. Song, and L. Stella, "On the statistical distribution off massive fermions and bosons in a Friedmann universe" Astronomy and Astrophysics, Vol. 125, (1983) pp. 265-270.

   The distribution function of massive Fermi and Bose particles in an expanding universe is considered as well as some associated thermodynamic quantities, pressure and energy density. These considerations are then applied to cosmological neutrinos. A new limit is derived for the degeneracy of a cosmological gas of massive neutrinos.

2. R. Ruffini and D. J. Song, "On the Jeans mass of weakly interacting neutral massive leptons", in Gamow cosmology, eds. F. Melchiorri and R. Ruffini, (1986) pp. 370–385.

   The cosmological limits on the abundances and masses of weakly interacting neutral particles are strongly affected by the nonzero chemical potentials of these leptons. For heavy leptons ($m_x >$ GeV), the value of the chemical potential must be much smaller than unity in order not to give very high values of the cosmological density parameter and the mass of heavy leptons, or they will be unstable. The Jeans' mass of weakly interacting neutral particles could give the scale of cosmological structure and the masses of astrophysical objects. For a mass of the order 10 eV, the Jeans' mass could give the scenario of galaxy formation, the supercluster forming first and then the smaller scales, such as clusters and galaxies, could form inside the large supercluster.

3. D. Calzetti, M. Giavalisco, R. Ruffini, J. Einasto, and E. Saar, "The correlation function of galaxies in the direction of the Coma cluster", Astrophysics and Space Science, Vol. 137 (1987) pp. 101-106.

   Data obtained by Einasto et al. (1986) on the amplitude of the correlation function of galaxies in the direction of the Coma cluster are compared with theoretical predictions of a model derived for a self-similar observer-homogeneous structure. The observational samples can be approximated by cones of angular width alpha of about 77 deg. Eliminating sources of large observational error, and by making a specified correction, the observational data are found to agree very well with the theoretical predictions of Calzetti et al. (1987).

4. R. Ruffini, D. J. Song, and S. Taraglio, "The 'ino' mass and the cellular large-scale structure of the universe", Astronomy and Astrophysics, Vol. 190, (1988) pp. 1-9.

   Within the theoretical framework of a Gamow cosmology with massive "inos", the authors show how the observed correlation functions between galaxies and between clusters of galaxies naturally lead to a "cellular" structure for the Universe. From the size of the "elementary cells" they derive constraints on the value of the masses and chemical potentials of the cosmological "inos". They outline a procedure to estimate the "effective" average mass density of the Universe. They also predict the angular size of the inhomogeneities to be expected in the cosmological black body radiation as remnants of this cellular structure. A possible relationship between the model and a fractal structure is indicated.

5. D. Calzetti, M. Giavalisco, and R. Ruffini, "The normalization of the correlation functions for extragalactic structures", Astronomy and Astrophysics, Vol. 198 (1988), pp. 1-15.

   It is shown that the spatial two-point correlation functions for galaxies, clusters and superclusters depend explicitly on the spatial volume of the statistical sample considered. Rules for the normalization of the correlation functions are given and the traditional classification of galaxies into field galaxies, clusters and superclusters is replaced by the introduction of a single fractal structure, with a lower cut-off at galactic scales. The roles played by random and stochastic fractal components in the galaxy distribution are discussed in detail.

6. M. V. Arbolino and R. Ruffini, "The ratio between the mass of the halo and visible matter in spiral galaxies and limits on the neutrino mass", Astronomy and Astrophysics, Vol. 192, (1988) pp. 107-116.

   Observed rotation curves for galaxies with values of the visible mass ranging over three orders of magnitude together with considerations involving equilibrium configurations of massive neutrinos, impose constraints on the ratio between the masses of visible and dark halo comporents in spiral galaxies. Upper and lower limits are derived for the mass of the particles making up the dark matter.

7. A. Bianconi, H. W. Lee, and R. Ruffini, "Limits from cosmological nucleosynthesis on the leptonic numbers of the universe", Astronomy and Astrophysics, Vol. 241 (1991) pp. 343-357.

   Constraints on chemical potentials and masses of 'inos' are calculated using cosmological standard nucleosynthesis processes. It is shown that the electron neutrino chemical potential (ENCP) should not be greater than a value of the order of 1, and that the possible effective chemical potential of the other neutrino species should be about 10 times the ENCP in order not to conflict

with observational data. The allowed region (consistent with the He-4 abundance observations) is insensitive to the baryon to proton ratio η, while those imposed by other light elements strongly depend on η.

8. R. Ruffini, J. D. Salmonson, J. R. Wilson, and S.-S. Xue, "On the pair electromagnetic pulse of a black hole with electromagnetic structure", Astronomy and Astrophysics, Vol. 350 (1999) pp. 334-343.

   We study the relativistically expanding electron-positron pair plasma formed by the process of vacuum polarization around an electromagnetic black hole (EMBH). Such processes can occur for EMBH's with mass all the way up to $6 \cdot 10^5 M_\odot$. Beginning with a idealized model of a Reissner-Nordstrom EMBH with charge to mass ratio $\xi = 0.1$, numerical hydrodynamic calculations are made to model the expansion of the pair-electromagnetic pulse (PEM pulse) to the point that the system is transparent to photons. Three idealized special relativistic models have been compared and contrasted with the results of the numerically integrated general relativistic hydrodynamic equations. One of the three models has been validated: a PEM pulse of constant thickness in the laboratory frame is shown to be in excellent agreement with results of the general relativistic hydrodynamic code. It is remarkable that this precise model, starting from the fundamental parameters of the EMBH, leads uniquely to the explicit evaluation of the parameters of the PEM pulse, including the energy spectrum and the astrophysically unprecedented large Lorentz factors (up to $6 \cdot 10^3$ for a $10^3 M_\odot$ EMBH). The observed photon energy at the peak of the photon spectrum at the moment of photon decoupling is shown to range from 0.1 MeV to 4 MeV as a function of the EMBH mass. Correspondingly the total energy in photons is in the range of 10^{52} to 10^{54} ergs, consistent with observed gamma-ray bursts. In these computations we neglect the presence of baryonic matter which will be the subject of forthcoming publications.

9. R. Ruffini, J. D. Salmonson, J. R. Wilson, and S.-S. Xue, "On the pair-electromagnetic pulse from an electromagnetic black hole surrounded by a baryonic remnant", Astronomy and Astrophysics, Vol. 359 (2000) pp. 855-864.

   The interaction of an expanding Pair-Electromagnetic pulse (PEM pulse) with a shell of baryonic matter surrounding a Black Hole with electromagnetic structure (EMBH) is analyzed for selected values of the baryonic mass at selected distances well outside the dyadosphere of an EMBH. The dyadosphere, the region in which a super critical field exists for the creation of e^+e^- pairs, is here considered in the special case of a Reissner-Nordstrom geometry. The interaction of the PEM pulse with the baryonic matter is described using a simplified model of a slab of constant thickness in the laboratory frame (constant-thickness approximation) as well as performing the integration of the general relativistic hydrodynamical equations. Te validation of the constant-thickness approximation, already presented in a previous paper Ruffini et al. (1999) for a

PEM pulse in vacuum, is here generalized to the presence of baryonic matter. It is found that for a baryonic shell of mass-energy less than 1% of the total energy of the dyadosphere, the constant-thickness approximation is in excellent agreement with full general relativistic computations. The approximation breaks down for larger values of the baryonic shell mass, however such cases are of less interest for observed Gamma Ray Bursts (GRBs). On the basis of numerical computations of the slab model for PEM pulses, we describe (i) the properties of relativistic evolution of a PEM pulse colliding with a baryonic shell; (ii) the details of the expected emission energy and observed temperature of the associated GRBs for a given value of the EMBH mass; $10^3 M_\odot$, and for baryonic mass-energies in the range 10^{-8} to 10^{-2} the total energy of the dyadosphere.

10. M. Lattanzi, R. Ruffini, and G. Vereshchagin, "On the possible role of massive neutrinos in cosmological structure formation", in Cosmology and Gravitation, eds. M. Novello and S. E. Perez Bergliaffa, Vol. 668 of AIP Conference Series, (2003) pp. 263–287.

    In addition to the problem of galaxy formation, one of the greatest open questions of cosmology is represented by the existence of an asymmetry between matter and antimatter in the baryonic component of the Universe. We believe that a net lepton number for the three neutrino species can be used to understand this asymmetry. This also implies an asymmetry in the matter-antimatter component of the leptons. The existence of a nonnull lepton number for the neutrinos can easily explain a cosmological abundance of neutrinos consistent with the one needed to explain both the rotation curves of galaxies and the flatness of the Universe. Some propedeutic results are presented in order to attack this problem.

4.2. Publications (2005 - 2008)

1. A.G. Aksenov, R. Ruffini and G.V. Vereshchagin, "Thermalization of nonequilibrium electron-positron-photon plasmas", Physical Review Letters, Vol. 99 (2007) No 12, 125003.

    Starting from a nonequilibrium configuration we analyze the role of the direct and the inverse binary and triple interactions in reaching thermal equilibrium in a homogeneous isotropic pair plasma. We focus on energies in the range $0.1 - 10$ MeV. We numerically integrate the relativistic Boltzmann equation with the exact QED collisional integrals taking into account all binary and triple interactions. We show that first, when a detailed balance is reached for all binary interactions on a time scale $t_k < 10^{-14}$ sec, photons and electron-positron pairs establish kinetic equilibrium. Subsequently, when triple interactions satisfy the detailed balance on a time scale $t_{eq} < 10^{-12}$ sec, the plasma

reaches thermal equilibrium. It is shown that neglecting the inverse triple interactions prevents reaching thermal equilibrium. Our results obtained in the theoretical physics domain also find application in astrophysics and cosmology.

2. C.L. Bianco, R. Ruffini, G.V. Vereshchagin and S.-S. Xue, "Equations of Motion and Initial and Boundary Conditions for Gamma-ray Burst", Journal of the Korean Physical Society, Vol. 49 (2006) No. 2, pp. 722-731.

   We compare and contrast the different approaches to the optically thick adiabatic phase of GRB all the way to the transparency. Special attention is given to the role of the rate equation to be self consistently solved with the relativistic hydrodynamic equations. The works of Shemi and Piran (1990), Piran, Shemi and Narayan (1993), Meszaros, Laguna and Rees (1993) and Ruffini, Salmonson, Wilson and Xue (1999,2000) are compared and contrasted. The role of the baryonic loading in these three treatments is pointed out. Constraints on initial conditions for the fireball produced by electro-magnetic black hole are obtained.

3. P. Singh, K. Vandersloot and G.V. Vereshchagin, "Nonsingular bouncing universes in loop quantum cosmology", Physical Review D, Vol. 74 (2006) 043510.

   Nonperturbative quantum geometric effects in loop quantum cosmology (LQC) predict a ρ^2 modification to the Friedmann equation at high energies. The quadratic term is negative definite and can lead to generic bounces when the matter energy density becomes equal to a critical value of the order of the Planck density. The nonsingular bounce is achieved for arbitrary matter without violation of positive energy conditions. By performing a qualitative analysis we explore the nature of the bounce for inflationary and cyclic model potentials. For the former we show that inflationary trajectories are attractors of the dynamics after the bounce implying that inflation can be harmoniously embedded in LQC. For the latter difficulties associated with singularities in cyclic models can be overcome. We show that nonsingular cyclic models can be constructed with a small variation in the original cyclic model potential by making it slightly positive in the regime where scalar field is negative.

4. M. Lattanzi, R. Ruffini and G.V. Vereshchagin, "Joint constraints on the lepton asymmetry of the Universe and neutrino mass from the Wilkinson Microwave Anisotropy Probe", Physical Review D, Vol. 72 (2005) 063003.

   We use the Wilkinson Microwave Anisotropy Probe (WMAP) data on the spectrum of cosmic microwave background anisotropies to put constraints on the present amount of lepton asymmetry L, parametrized by the dimensionless chemical potential (also called degeneracy parameter) xi and on the effective

number of relativistic particle species. We assume a flat cosmological model with three thermally distributed neutrino species having all the same mass and chemical potential, plus an additional amount of effectively massless exotic particle species. The extra energy density associated to these species is parametrized through an effective number of additional species $\Delta N_{others}{}^{eff}$. We find that $0 < |\xi| < 1.1$ and correspondingly $0 < |L| < 0.9$ at 2σ, so that WMAP data alone cannot firmly rule out scenarios with a large lepton number; moreover, a small preference for this kind of scenarios is actually found. We also discuss the effect of the asymmetry on the estimation of other parameters and, in particular, of the neutrino mass. In the case of perfect lepton symmetry, we obtain the standard results. When the amount of asymmetry is left free, we find at 2sigma. Finally we study how the determination of |L| is affected by the assumptions on $\Delta N_{others}{}^{eff}$. We find that lower values of the extra energy density allow for larger values of the lepton asymmetry, effectively ruling out, at 2sigma level, lepton symmetric models with $\Delta N_{others}{}^{eff} \simeq 0$.

5. G.V. Vereshchagin, "Gauge Theories of Gravity with the Scalar Field in Cosmology", in "Frontiers in Field Theory", edited by O. Kovras, Nova Science Publishers, New York, (2005), pp. 213-255 (ISBN: 1-59454-127-2).

   Brief introduction into gauge theories of gravity is presented. The most general gravitational lagrangian including quadratic on curvature, torsion and nonmetricity invariants for metric-affine gravity is given. Cosmological implications of gauge gravity are considered. The problem of cosmological singularity is discussed within the framework of general relativity as well as gauge theories of gravity. We consider the role of scalar field in connection to this problem. Initial conditions for nonsingular homogeneous isotropic Universe filled by single scalar field are discussed within the framework of gauge theories of gravity. Homogeneous isotropic cosmological models including ultrarelativistic matter and scalar field with gravitational coupling are investigated. We consider different symmetry states of effective potential of the scalar field, in particular restored symmetry at high temperatures and broken symmetry. Obtained bouncing solutions can be divided in two groups, namely nonsingular inflationary and
   oscillating solutions. It is shown that inflationary solutions exist for quite general initial conditions like in the case of general relativity. However, the phase space of the dynamical system, corresponding to the cosmological equations is bounded. Violation of the uniqueness of solutions on the boundaries of the phase space takes place. As a result, it is impossible to define either the past or the future for a given solution. However, definitely there are singular solutions and therefore the problem of cosmological singularity cannot be solved in models with the scalar field within gauge theories of gravity.

6. R. Ruffini, M. G. Bernardini, C. L. Bianco, L. Caito, P. Chardonnet, M.

G. Dainotti, F. Fraschetti, R. Guida, M. Rotondo, G. Vereshchagin, L. Vitagliano, S.-S. Xue,
"The Blackholic energy and the canonical Gamma-Ray Burst" in Cosmology and Gravitation: XIIth Brazilian School of Cosmology and Gravitation, edited by M. Novello and S.E. Perez Bergliaffa, AIP Conference Proceedings, Vol. 910, Melville, New York, 2007, pp. 55-217.

Gamma-Ray Bursts (GRBs) represent very likely "the" most extensive computational, theoretical and observational effort ever carried out successfully in physics and astrophysics. The extensive campaign of observation from space based X-ray and γ-ray observatory, such as the Vela, CGRO, BeppoSAX, HETE-II, INTEGRAL, Swift, R-XTE, Chandra, XMM satellites, have been matched by complementary observations in the radio wavelength (e.g. by the VLA) and in the optical band (e.g. by VLT, Keck, ROSAT). The net result is unprecedented accuracy in the received data allowing the determination of the energetics, the time variability and the spectral properties of these GRB sources. The very fortunate situation occurs that these data can be confronted with a mature theoretical development. Theoretical interpretation of the above data allows progress in three different frontiers of knowledge: a) the ultrarelativistic regimes of a macroscopic source moving at Lorentz gamma factors up to ~ 400; b) the occurrence of vacuum polarization process verifying some of the yet untested regimes of ultrarelativistic quantum field theories; and c) the first evidence for extracting, during the process of gravitational collapse leading to the formation of a black hole, amounts of energies up to 10^{55} ergs of blackholic energy — a new form of energy in physics and astrophysics. We outline how this progress leads to the confirmation of three interpretation paradigms for GRBs proposed in July 2001. Thanks mainly to the observations by Swift and the optical observations by VLT, the outcome of this analysis points to the existence of a "canonical" GRB, originating from a variety of different initial astrophysical scenarios. The communality of these GRBs appears to be that they all are emitted in the process of formation of a black hole with a negligible value of its angular momentum. The following sequence of events appears to be canonical: the vacuum polarization process in the dyadosphere with the creation of the optically thick self accelerating electron-positron plasma; the engulfment of baryonic mass during the plasma expansion; adiabatic expansion of the optically thick "fireshell" of electron-positron-baryon plasma up to the transparency; the interaction of the accelerated baryonic matter with the interstellar medium (ISM). This leads to the canonical GRB composed of a proper GRB (P-GRB), emitted at the moment of transparency, followed by an extended afterglow. The sole parameters in this scenario are the total energy of the dyadosphere E_{dya}, the fireshell baryon loading M_B defined by the dimensionless parameter $B = M_B c^2 / E_{dya}$, and the ISM filamentary distribution around the source. In the limit $B \longrightarrow 0$ the total energy is radiated in the P-GRB with a vanishing contribution in the afterglow. In this limit, the canonical

GRBs explain as well the short GRBs. In these lecture notes we systematically outline the main results of our model comparing and contrasting them with the ones in the current literature. In both cases, we have limited ourselves to review already published results in refereed publications. We emphasize as well the role of GRBs in testing yet unexplored grounds in the foundations of general relativity and relativistic field theories.

7. M. Lattanzi, R. Ruffini and G.V. Vereshchagin, "Do WMAP data constraint the lepton asymmetry of the Universe to be zero?" in Albert Einstein Century International Conference, edited by J.-M. Alimi, and A. Füzfa, AIP Conference Proceedings, Vol. 861, Melville, New York, 2006, pp.912-919.

   It is shown that extended flat ΛCDM models with massive neutrinos, a sizeable lepton asymmetry and an additional contribution to the radiation content of the Universe, are not excluded by the Wilkinson Microwave Anisotropy Probe (WMAP) first year data. We assume a flat cosmological model with three thermally distributed neutrino species having all the same mass and chemical potential, plus an additional amount of effectively massless exotic particle species X. After maximizing over seven other cosmological parameters, we derive from WMAP first year data the following constraints for the lepton asymmetry L of the Universe (95% CL): $0 < |L| < 0.9$, so that WMAP data alone cannot firmly rule out scenarios with a large lepton number; moreover, a small preference for this kind of scenarios is actually found. We also find for the neutrino mass $m_\nu < 1.2eV$ and for the effective number of relativistic particle species $-0.45 < \Delta N^{eff} < 2.10$, both at 95% CL. The limit on ΔN^{eff} is more restrictive man others found in the literature, but we argue that this is due to our choice of priors.

8. R. Ruffini, C.L. Bianco, G.V. Vereshchagin, S.-S. Xue "Baryonic loading and e^+e^- rate equation in GRB sources" to appear in the proceedings of "Relativistic Astrophysics and Cosmology - Einstein's Legacy" Meeting, November 7-11, 2005, Munich, Germany.

   The expansion of the electron-positron plasma in the GRB phenomenon is compared and contrasted in the treatments of Meszaros, Laguna and Rees, of Shemi, Piran and Narayan, and of Ruffini et al. The role of the correct numerical integration of the hydrodynamical equations, as well as of the rate equation for the electron-positron plasma loaded with a baryonic mass, are outlined and confronted for crucial differences.

9. G.V. Vereshchagin, M. Lattanzi, H.W. Lee, R. Ruffini, "Cosmological massive neutrinos with nonzero chemical potential: I. Perturbations in cosmological models with neutrino in ideal fluid approximation", in proceedings of the Xth Marcel Grossmann Meeting on Recent Develop-

ments in Theoretical and Experimental General Relativity, World Scientific: Singapore, 2005, vol. 2, pp. 1246-1248.

Recent constraints on neutrino mass and chemical potential are discussed with application to large scale structure formation. Power spectra in cosmological model with hot and cold dark matter, baryons and cosmological term are calculated in newtonian approximation using linear perturbation theory. All components are considered to be ideal fluids. Dissipative processes are taken into account by initial spectrum of perturbations so the problem is reduced to a simple system of equations. Our results are in good agreement with those obtained before using more complicated treatments.

10. M. Lattanzi, H.W. Lee, R. Ruffini, G.V. Vereshchagin, "Cosmological massive neutrinos with nonzero chemical potential: II. Effect on the estimation of cosmological parameters", in proceedings of the Xth Marcel Grossmann Meeting on Recent Developments in Theoretical and Experimental General Relativity, World Scientific: Singapore, 2005, vol. 2, pp. 1255-1257.

    The recent analysis of the cosmic microwave background data carried out by the WMAP team seems to show that the sum of the neutrino mass is <0.7 eV. However, this result is not model-independent, depending on precise assumptions on the cosmological model. We study how this result is modified when the assumption of perfect lepton symmetry is dropped out.

11. R. Ruffini, M. Lattanzi and G. Vereshchagin, "On the possible role of massive neutrinos in cosmological structure formation" in Cosmology and Gravitation: Xth Brazilian School of Cosmology and Gravitation, edited by M. Novello and S.E. Perez Bergliaffa, AIP Conference Proceedings, Vol. 668, Melville, New York, 2003, pp.263-287.

    In addition to the problem of galaxy formation, one of the greatest open questions of cosmology is represented by the existence of an asymmetry between matter and antimatter in the baryonic component of the Universe. We believe that a net lepton number for the three neutrino species can be used to understand this asymmetry. This also implies an asymmetry in the matter-antimatter component of the leptons. The existence of a nonnull lepton number for the neutrinos can easily explain a cosmological abundance of neutrinos consistent with the one needed to explain both the rotation curves of galaxies and the flatness of the Universe. Some propedeutic results are presented in order to attack this problem.

12. A.G. Aksenov, C.L. Bianco, R. Ruffini and G.V. Vereshchagin, "GRBs and the thermalization process of electron-positron plasmas" in the Proceedings of the "Gamma Ray Bursts 2007" meeting, AIP Conf.Proc. 1000 (2008) 309-312.

We discuss temporal evolution of the pair plasma, created in Gamma-Ray Bursts sources. A particular attention is paid to the relaxation of plasma into thermal equilibrium. We also discuss the connection between the dynamics of expansion and spatial geometry of plasma. The role of the baryonic loading parameter is emphasized.

13. A. G. Aksenov, R. Ruffini, and G. V. Vereshchagin, "Thermalization of Electron-Positron-Photon Plasmas with an Application to GRB" in RELATIVISTIC ASTROPHYSICS: 4th Italian-Sino Workshop, AIP Conference Proceedings, Vol. 966, Melville, New York, 2008, pp. 191-196.

    The pair plasma with photon energies in the range $0.1 - 10$MeV is believed to play crucial role in cosmic Gamma-Ray Bursts. Starting from a nonequilibrium configuration we analyze the role of the direct and the inverse binary and triple interactions in reaching thermal equilibrium in a homogeneous isotropic pair plasma.We numerically integrate the relativistic Boltzmann equation with the exact QED collisional integrals taking into account all binary and triple interactions. We show that first, when a detailed balance is reached for all binary interactions on a time scale $t_k = 10^{-14}$sec , photons and electronpositron pairs establish kinetic equilibrium. Subsequently, when triple interactions satisfy the detailed balance on a time scale $t_{eq} = 10^{-12}$sec , the plasma reaches thermal equilibrium. It is shown that neglecting the inverse triple interactions prevents reaching thermal equilibrium. Our results obtained in the theoretical physics domain also find application in astrophysics and cosmology.

14. R. Ruffini, and G. V. Vereshchagin, S.-S. Xue, "Vacuum Polarization and Electron-Positron Plasma Oscillations" in RELATIVISTIC ASTROPHYSICS: 4th Italian-Sino Workshop, AIP Conference Proceedings, Vol. 966, Melville, New York, 2008, pp. 207-212.

    We study plasma oscillations of electrons-positron pairs created by the vacuum polarization in an uniform electric field. Our treatment, encompassing the case of $E > E_c$, shows also in the case $E < E_c$the existence of a maximum Lorentz factor acquired by electrons and positrons and allows determination of the a maximal length of oscillation. We quantitatively estimate how plasma oscillations reduce the rate of pair creation and increase the time scale of the pair production.

4.3. Publications (2009)

1. A.G. Aksenov, R. Ruffini and G.V. Vereshchagin, "Thermalization of the mildly relativistic plasma", Physical Review D, Vol. 79 (2009) 043008.

    In the recent Letter Aksenov et al. (2007) we considered the approach of nonequilibrium pair plasma towards thermal equilibrium state adopting a kinetic treatment and solving numerically the relativistic Boltzmann equations. It was

shown that plasma in the energy range 0.1-10 MeV first reaches kinetic equilibrium, on a timescale $t_{\rm k} \lesssim 10^{-14}$ sec, with detailed balance between binary interactions such as Compton, Bhabha and Møller scattering, and pair production and annihilation. Later the electron-positron-photon plasma approaches thermal equilibrium on a timescale $t_{\rm th} \lesssim 10^{-12}$ sec, with detailed balance for all direct and inverse reactions. In the present paper we systematically present details of the computational scheme used in Aksenov et al. (2007), as well as generalize our treatment, considering proton loading of the pair plasma. When proton loading is large, protons thermalize first by proton-proton scattering, and then with the electron-positron-photon plasma by proton-electron scattering. In the opposite case of small proton loading proton-electron scattering dominates over proton-proton one. Thus in all cases the plasma, even with proton admixture, reaches thermal equilibrium configuration on a timescale $t_{\rm th} \lesssim 10^{-11}$ sec. We show that it is crucial to account for not only binary but also triple direct and inverse interactions between electrons, positrons, photons and protons. Several explicit examples are given and the corresponding timescales for reaching kinetic and thermal equilibria are determined.

2. A. G. Aksenov, R. Ruffini, and G. V. Vereshchagin, "Thermalization of pair plasma with proton loading" in the Proceedings of "PROBING STELLAR POPULATIONS OUT TO THE DISTANT UNIVERSE" meeting, AIP Conference Proceedings 1111 (2009) 344-350.

   We study kinetic evolution of nonequilibrium optically thick electron-positron plasma towards thermal equilibrium solving numerically relativistic Boltzmann equations with energy per particle ranging from 0.1 to 10 MeV. We generalize our results presented in Aksenov et al. (2007), considering proton loading of the pair plasma. Proton loading introduces new characteristic timescales essentially due to proton-proton and proton-electron Coulomb collisions. Taking into account not only binary but also triple direct and inverse interactions between electrons, positrons, photons and protons we show that thermal equilibrium is reached on a timescale $t_{\rm th} \simeq 10^{-11}$ sec.

3. M. Lattanzi, J. Silk "Can the WIMP annihilation boost factor be boosted by the Sommerfeld enhancement? ", in Phys. Rev. D79, 083523 (2009).

   We demonstrate that the Sommerfeld correction to cold dark matter (CDM) annihilations can be appreciable if even a small component of the dark matter is extremely cold. Subhalo substructure provides such a possibility given that the smallest clumps are relatively cold and contain even colder substructure due to incomplete phase space mixing. Leptonic channels can be enhanced for plausible models and the solar neighbourhood boost required to account for PAMELA/ATIC data is plausibly obtained, especially in the case of a few TeV mass neutralino for which the Sommerfeld-corrected boost is found to be $\sim 10^4 - 10^5$. Saturation of the Sommerfeld effect is shown to occur below $\beta \sim 10^{-4}$, thereby making this result largely independent on the presence of

substructures below $\sim 10^5 M_\odot$. We find that the associated diffuse gamma ray signal from annihilations would exceed EGRET constraints unless the channels annihilating to heavy quarks or to gauge bosons are suppressed. The lepton channel gamma rays are potentially detectable by the FERMI satellite, not from the inner galaxy where substructures are tidally disrupted, but rather as a quasi-isotropic background from the outer halo, unless the outer substructures are much less concentrated than the inner substructures and/or the CDM density profile out to the virial radius steepens significantly.

4. L. Pieri, M. Lattanzi, J. Silk "Constraining the Sommerfeld enhancement with Cherenkov telescope observations of dwarf galaxies", in Mon. Not. Roy. Astron. Soc., in press (2009).

   The presence of dark matter in the halo of our galaxy could be revealed through indirect detection of its annihilation products. Dark matter annihilation is one possible interpretation of the recently measured excesses in positron and electron fluxes, provided that boost factors of the order of 10^3 or more are taken into account. Such boost factors are actually achievable through the velocity-dependent Sommerfeld enhancement of the annihilation cross-section. Here we study the expected γ-ray flux from two local dwarf galaxies for which Cherenkov Telescope measurements are available, namely Draco and Sagittarius. We use recent stellar kinematical measurements to model the dark matter halos of the dwarfs, and the results of numerical simulations to model the presence of an associated population of subhalos. We incorporate the Sommerfeld enhancement of the annihilation cross-section. We compare our predictions with the observations of Draco and Sagittarius performed by MAGIC and HESS, respectively, and derive exclusion limits on the effective annihilation cross-section. We also study the sensitivities of Fermi and of the future Cherenkov Telescope Array to cross-section enhancements. We find that the boost factor due to the Sommerfeld enhancement is already constrained by the MAGIC and HESS data, with enhancements greater than $\sim 10^4$ being excluded.

5. M. Lattanzi, "Mass Varying Neutrinos: A model-independent approach", in Nucl. Phys. Proc. Suppl. 188, 40, (2009).

   In Mass Varying Neutrinos (MaVaNs) models, the neutrinos are coupled with the quintessence field supposed to be responsible for the acceleration of the Universe. Here we propose a new parameterization for the neutrino mass variation that is independent on the details of the scalar field potential and still captures the essential of most MaVaNs models. We also find an upper limit on the mass variation in the case of decreasing mass models, independent of the particular parameterization.

6. U. Franca, M. Lattanzi, J. Lesgourgues, S. Pastor "Model independent constraints on mass-varying neutrino scenarios", in Phys. Rev. D80,

083506 (2009).

Models of dark energy in which neutrinos interact with the scalar field supposed to be responsible for the acceleration of the universe usually imply a variation of the neutrino masses on cosmological time scales. In this work we propose a parameterization for the neutrino mass variation that captures the essentials of those scenarios and allows to constrain them in a model independent way, that is, without resorting to any particular scalar field model. Using WMAP 5yr data combined with the matter power spectrum of SDSS and 2dFGRS, the limit on the present value of the neutrino mass is $m_0 \equiv m_\nu(z = 0) < 0.43\ (0.28)$ eV at 95% C.L. for the case in which the neutrino mass was lighter (heavier) in the past, a result competitive with the ones imposed for standard (*i.e.*, constant mass) neutrinos. Moreover, for the ratio of the mass variation of the neutrino mass Δm_ν over the current mass m_0 we found that $\log[|\Delta m_\nu|/m_0] < -1.3\ (-2.7)$ at 95% C.L. for $\Delta m_\nu < 0\ (\Delta m_\nu > 0)$, totally consistent with no mass variation.

4.4. Invited talks at international conferences

1. "From thermalization mechanisms to emission processes in GRBs"

   (G.V. Vereshchagin)

   XII Marcel Grossmann Meeting, Paris, 12-18 July 2009.

2. "Kinetics of the mildly relativistic plasma and GRBs"

   (A.G. Aksenov R. Ruffini, and G.V. Vereshchagin)

   "The Sun, the Stars, the Universe, and General Relativity" - International conference in honor of Ya. B. Zeldovich 95th Anniversary, Minsk, Belarus, April 19-23, 2009.

3. "Pair plasma around compact astrophysical sources: kinetics, electrodynamics and hydrodynamics"

   (G.V. Vereshchagin and R. Ruffini)

   Invited seminar at RMKI, Budapest, February 24, 2009.

4. "Thermalization of the pair plasma with proton loading"

   (G.V. Vereshchagin, R. Ruffini, and A.G. Aksenov)

   Probing Stellar Populations out to the Distant Universe, Cefalu', Italy, September 7-19, 2008.

5. "Thermalization of the pair plasma with proton loading"

   (G.V. Vereshchagin, R. Ruffini, and A.G. Aksenov)

   3rd Stueckelberg Workshop, Pescara, Italy, 8-18 July, 2008.

6. "Thermalization of the pair plasma"

   (G.V. Vereshchagin, R. Ruffini, and A.G. Aksenov)

7. "Non-singular solutions in Loop Quantum Cosmology"

   (G.V. Vereshchagin)

   2nd Stueckelberg Workshop, Pescara, Italy, 3-7 September, 2007.

8. "(From) massive neutrinos and inos and the upper cutoff to the fractal structure of the Universe (to recent progress in theoretical cosmology)"

   (G.V. Vereshchagin, M. Lattanzi and R. Ruffini)

   A Century of Cosmology, San Servolo, Venice, Italy, 27-31 August, 2007.

9. "Pair creation and plasma oscillations"

   (G.V. Vereshchagin, R. Ruffini, and S.-S. Xue)
   4th Italian-Sino Workshop on Relativistic Astrophysics, Pescara, Italy, 20-29 July, 2007.

10. "Thermalization of electron-positron plasma in GRB sources"

    (G.V. Vereshchagin, R. Ruffini, and A.G. Aksenov)
    Xth Italian-Korean Symposium on Relativistic Astrophysics, Pescara, Italy, 25-30 June, 2007.

11. "Kinetics and hydrodynamics of the pair plasma"

    (G.V. Vereshchagin, R. Ruffini, C.L. Bianco, A.G. Aksenov)

12. "Pair creation and plasma oscillations"

    (G.V. Vereshchagin, R. Ruffini and S.-S. Xue)
    Cesare Lattes Meeting on GRBs, Black Holes and Supernovae, Mangaratiba-Portobello, Brazil, 26 February - 3 March 2007.

13. "Cavallo-Rees classification revisited"

    (G.V. Vereshchagin, R.Ruffini and S.-S. Xue)

    On recent developments in theoretical and experimental general relativity, gravitation and relativistic field theories: XIth Marcel Grossmann Meeting, Berlin, Germany, 23-29 July, 2006.

14. "Kinetic and thermal equilibria in the pair plasma"

    (G.V. Vereshchagin)

    The 1st Bego scientific rencontre, Nice, 5-16 February 2006.

15. "From semi-classical LQC to Friedmann Universe"

    (G.V. Vereshchagin)

    Loops '05, Potsdam, Golm, Max-Plank Institut für Gravitationsphysik (Albert-Einstein-Institut), 10-14 October 2005.

16. "Equations of motion, initial and boundary conditions for GRBs"

    (G.V. Vereshchagin, R. Ruffini and S.-S. Xue)

    IXth Italian-Korean Symposium on Relativistic Astrophysics, Seoul, Mt. Kumgang, Korea, 19-24 July 2005.

17. "On the Cavallo-Rees classification and GRBs"

    (G.V. Vereshchagin, R. Ruffini and S.-S. Xue)

    II Italian-Sino Workshop on Relativistic Astrophysics, Pescara, Italy, 10-20 June, 2005.

5. APPENDICES

A. Pair plasma relaxation timescales

Current interest toward electron-positron plasmas is due to an exciting possibility to generate such plasmas in the laboratory conditions with already operating facilities or those under construction, see e.g. Myatt et al. (2009), for a review see Ruffini et al. (2009b). An impressive progress with ultraintense lasers Chen et al. (2009) allows to reach unprecedented density of created positrons of 10^{16} cm^{-3} with ultraintense short laser pulses, with dimensions close to the Debye length. However, such densities have not yet reached the creation of optically thick pair plasma Katz (2000),Mustafa and Kämpfer (2009). In the focus of ultra intense lasers pairs are created via the Bethe-Heitler conversion of hard x-ray bremsstrahlung photons Myatt et al. (2009) in collisionless regime Wilks et al. (1992). The approach to optically thick phase may be well envisaged in the near future.

Electron-positron plasmas are known to be present in compact astrophysical objects, leaving characteristic imprint in the observed radiation spectra Churazov et al. (2005). Optically thick electron-positron plasma does indeed have a crucial role in the Gamma-Ray Bursts phenomenon Ruffini et al. (2009b),Ruffini et al. (2009a).

Most theoretical considerations so far assumed that electron-positron plasma is formed either in thermal equilibrium (common temperature, zero chemical potentials) or in chemical equilibrium (nonzero chemical potentials), see e.g. Thoma (2009) and references therein. However, it is necessary to establish the timescale for actually reaching such configuration. The only way for particles to thermalize, i.e. reach equilibrium distributions (Bose-Einstein or Fermi-Dirac) is via collisions. Collisions become relevant when the mean free path of particles becomes smaller than the spatial dimensions of plasma, and so optical thickness condition is crucial for thermalization.

Thermalization, or chemical equilibration timescales for optically thick plasmas are estimated in the literature by an order of magnitude arguments using essentially the reaction rates of dominant particle interaction processes, see e.g. Gould (1981),Stepney (1983). They were computed using various approximations such as ultrarelativistic electrons and constant Coulomb logarithm. Accurate determination of such timescales is here presented by solving the relativistic Boltzmann equations, including collisional integrals representing all possible particle interactions. In that case Boltzmann equations become highly nonlinear coupled partial integro-differential equations, and can be

solved only numerically.

We developed relativistic kinetic code, treating the plasma as homogeneous and isotropic and determined thermalization timescales of electron-positron plasma for selected initial conditions Aksenov et al. (2007). Our approach has been generalized to include protons in Aksenov et al. (2009c). We focus on electromagnetic interactions only which have a timescales of less than 10^{-9} sec for our system, and therefore on the proton and leptonic component. The presence of neutrons and their possible equilibrium due to weak interactions will occur only on much longer timescales.

In this Letter we report on the systematic results, obtained by exploring the wide parameter space characterizing pair plasma with baryonic loading. The two basic parameters are the total energy density ρ and the baryonic loading parameter

$$B \equiv \frac{\rho_b}{\rho_{e,\gamma}} \simeq \frac{n_p m_p c^2}{\rho_{e,\gamma}}, \tag{A.0.1}$$

where ρ_b and $\rho_{e,\gamma}$ are total energy densities of baryons and electron-positron-photon plasma, respectively, n_p and m_p are proton number density and proton mass, c is the speed of light. We choose the following range of plasma parameters

$$10^{23} \leq \rho \leq 10^{33} \text{ erg/cm}^3, \tag{A.0.2}$$

$$10^{-3} \leq B \leq 10^{3}, \tag{A.0.3}$$

allowing one to treat also the limiting cases of almost pure electron-positron plasma with $B \ll 1$, and almost pure electron-ion plasma with $B \simeq m_p/m_e$, respectively. The temperatures in thermal equilibrium, corresponding to (A.0.2) are $0.1 \lesssim k_{\rm B}T \lesssim 10$ MeV.

Given the smallness of plasma parameter $g = (n_e \lambda_{\rm D})^3 \ll 1$, where $\lambda_{\rm D}$ is the Debye length, n_e is electron number density, it is sufficient to use only one-particle distribution functions. In homogeneous and isotropic plasma distribution functions depend on energy of a particle and time $f(\epsilon, t)$. We treat the plasma as nondegenerate, neglecting neutrino channels as well as creation and annihilation of baryons and weak interactions Aksenov et al. (2009c).

Relativistic Boltzmann equations Belyaev and Budker (1956), Mihalas and Mihalas (1984) for photons, electrons, positrons, and protons in our case are

$$\frac{1}{c}\frac{\partial f_i}{\partial t} = \sum_q (\eta_i^q - \chi_i^q f_i), \tag{A.0.4}$$

the index i denotes the type of the particle and η_i^q, χ_i^q are the emission and the absorption coefficients for the production of i-particle via the reaction labeled by q. We account for all relecant binary and triple interactions between electrons, positrons, photons, and protons as summarized in Table A.1, and

Binary interactions	Radiative and pair producing variants
Møller and Bhabha $e_1^{\pm} e_2^{\pm} \longrightarrow e_1^{\pm\prime} e_2^{\pm\prime}$ $e^{\pm} e^{\mp} \longrightarrow e^{\pm\prime} e^{\mp\prime}$	Bremsstrahlung $e_1^{\pm} e_2^{\pm} \leftrightarrow e_1^{\pm\prime} e_2^{\pm\prime} \gamma$ $e^{\pm} e^{\mp} \leftrightarrow e^{\pm\prime} e^{\mp\prime} \gamma$
Single Compton $e^{\pm}\gamma \longrightarrow e^{\pm}\gamma'$	Double Compton $e^{\pm}\gamma \leftrightarrow e^{\pm\prime}\gamma'\gamma''$
Pair production and annihilation $\gamma\gamma' \leftrightarrow e^{\pm} e^{\mp}$	Radiative pair production and 3-photon annihilation $\gamma\gamma' \leftrightarrow e^{\pm} e^{\mp} \gamma''$ $e^{\pm} e^{\mp} \leftrightarrow \gamma\gamma'\gamma''$
	$e^{\pm}\gamma \leftrightarrow e^{\pm\prime} e^{\mp} e^{\pm\prime\prime}$

Table A.1.: Microphysical processes in the pair plasma.

Binary interactions (Coulomb scattering)	Radiative and pair producing variants
$p_1 p_2 \longrightarrow p_1' p_2'$	$p e^{\pm} \leftrightarrow p' e^{\pm\prime} \gamma$
$p e^{\pm} \longrightarrow p' e^{\pm\prime}$	$p\gamma \leftrightarrow p' e^{\pm} e^{\mp}$

Table A.2.: Microphysical processes in the pair plasma involving protons. For details see also Ruffini et al. (2009b).

Table A.2.

It has been shown Aksenov et al. (2007) that independent on the functional form of initial distribution functions $f_i(\epsilon, 0)$ plasma evolves to thermal equilibrium state through the kinetic equilibrium, when distribution functions of all particles acquire the same form

$$f_i(\varepsilon) = \exp\left(-\frac{\varepsilon - \varphi_i}{\theta_i}\right), \tag{A.0.5}$$

where $\varepsilon_i = \epsilon_i/(m_i c^2)$ is the energy of the particles, $\varphi_i \equiv \mu_i/(m_i c^2)$ and $\theta_i \equiv k_{\rm B} T_i/(m_i c^2)$ are their chemical potentials and temperatures, $k_{\rm B}$ is Boltzmann's constant. The unique signature of the kinetic equilibrium is the equal temperature of all particles and nonzero chemical potential of photons. In fact the same is also true for pair plasma with proton loading Aksenov et al. (2009c). Approach to complete thermal equilibrium is more complicated in this latter case and depends on the baryon loading. For $B \ll \sqrt{m_p/m_e}$ protons are rare and thermalize via proton-electron (positron) elastic scattering, while in the opposite case $B \gg \sqrt{m_p/m_e}$ proton-proton Coulomb scattering dominates over the proton-electron one and brings protons in thermal equilibrium first with themselves. Then protons thermalize with the pair

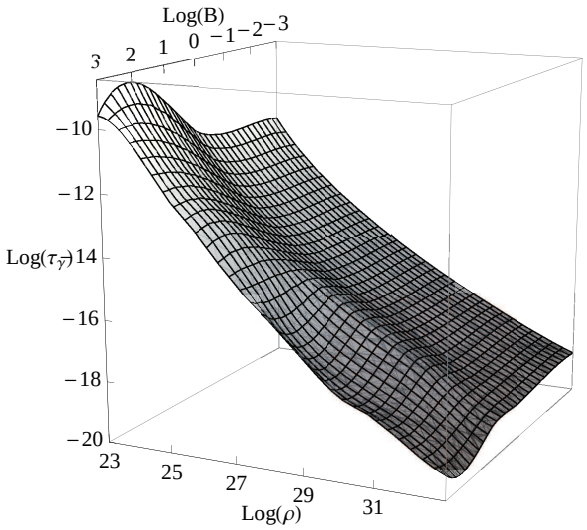

Figure A.1.: The thermalization time scale of electron-positron-photon component of plasma as function of total energy density and baryonic loading parameter. Energy density is measured in erg/cm^3, time is seconds.

plasma by triple interactions. Two-body timescales involving protons should be compared with three-body timescales bringing electron-positron-photon plasma to thermal equilibrium. In fact we found that for $B \ll 1$ electron-positron-photon plasma reaches thermal equilibrium at a given temperature, while protons reach thermal equilibrium with themselves at a different temperature; only later plasma evolves to complete thermal equilibrium with the single temperature on a timescale

$$\tau_{th} \simeq \mathrm{Max}\left[\tau_{3p}, \mathrm{Min}\left(\tau_{ep}, \tau_{pp}\right)\right], \tag{A.0.6}$$

where

$$\tau_{ep} \simeq \frac{m_p c}{\epsilon_e \sigma_{\mathrm{T}} n_e}, \tag{A.0.7}$$

$$\tau_{pp} \simeq \sqrt{\frac{m_p}{m_e}} \left(\sigma_{\mathrm{T}} n_p c\right)^{-1}, \tag{A.0.8}$$

$$\tau_{3p} \simeq \left(\alpha \sigma_{\mathrm{T}} n_e c\right)^{-1} \tag{A.0.9}$$

are the proton-electron (positron) elastic scattering timescale, proton-proton elastic scattering timescale, and three-particle interaction timescale, respectively, σ_{T} is the Thomson cross-section, α is the fine structure constant. In (A.0.7)-(A.0.9) energy dependence of the corresponding timescales is neglected.

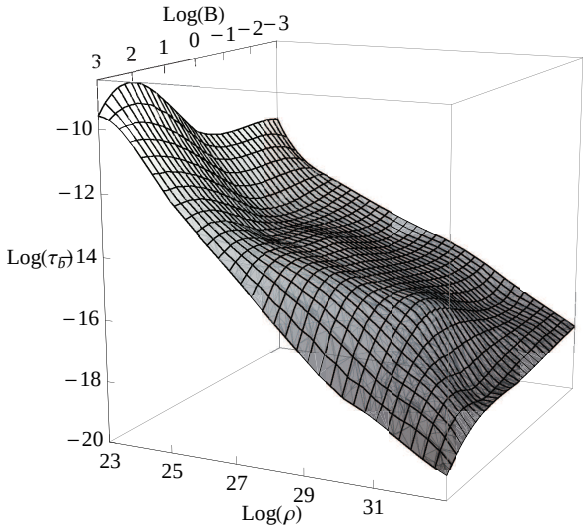

Figure A.2.: The final thermalization timescale of pair plasma with baryonic loading as function of total energy density and baryonic loading parameter. Energy density is measured in erg/cm^3, time is seconds.

The chemical relaxation (thermalization) time scale is usually computed as

$$\tau_i = \lim_{t\to\infty} \left\{ [F_i(t) - F_i(\infty)] \left(\frac{dF_i}{dt} \right)^{-1} \right\}, \tag{A.0.10}$$

where $F_i = \exp(\varphi_i/\theta_i)$ is fugacity of a particle of sort i. We use instead of F_i one of the quantities θ_i, φ_i, n_i, or ρ_i.

We solved the Boltzmann equations with parameters (ρ, B) in the range given by Eqs. (A.0.2) and (A.0.3). Totally 78 models were computed, starting from nonequilibrium configuration until the reaching of steady solution on the computational grid with 20 intervals for particle energy and 16 intervals for angles, details see in Aksenov et al. (2009c). For each model we computed the corresponding timescales for all particles of i kind. For practical purposes instead of (A.0.10) we used the following approximation

$$\tau_{th} = \frac{1}{t_{fin} - t_{in}} \int_{t_{in}}^{t_{fin}} [\theta(t) - \theta(t_{\max})] \left(\frac{d\theta}{dt} \right)^{-1} dt, \tag{A.0.11}$$

with $t_{in} < t_{fin} < t_{\max}$, $t_{\max}$ is the moment of time where steady solution is reached, t_{in} and t_{fin} are the boundaries of time interval over which the averaging is performed, for details see Aksenov et al. (2009a). Thermalization timescales of electron-positron-photon component is shown in Fig. A.1 as function of total energy density of plasma and the baryonic loading parameter. Timescale of electrons, positrons and photons coincide. Final thermalization timescale of pair plasma with baryonic loading is shown in Fig. A.2. Both

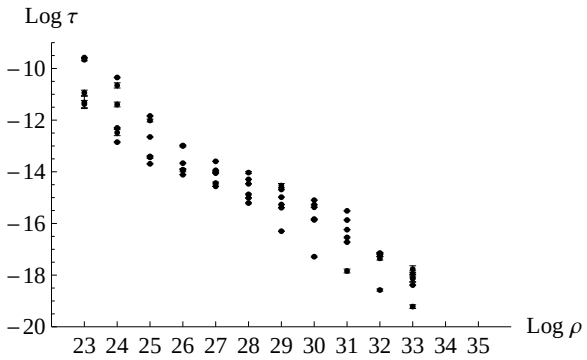

Figure A.3.: The final thermalization timescale of pair plasma with baryonic loading as function of total energy density for selected values of the baryonic loading parameter $B = (10^{-3}, 10^{-1.5}, 1, 10, 10^2, 10^3)$. Energy density is measured in erg/cm^3, time is seconds. Error bars correspond to the standard deviation of the timescale (A.0.11) in the averaging interval $t_{in} \leq t \leq t_{fin}$ from the average value of τ_{th}.

dependencies cannot be fitted by simple power laws, though decrease monotonically with increasing total energy density. Thermalization timescales are not monotonic functions of the baryonic loading parameter.

In Fig. A.3 final thermalization timescale is shown for all models computed, along with the "error bars" which mark the standard deviation of the timescale (A.0.11) in the averaging interval $t_{in} \leq t \leq t_{fin}$ from the average value of τ_{th}. The largest source of errors comes from the small values of time derivative in (A.0.11), though errors are typically below few percent.

In Fig. A.4 we compare for $B = 1$ the actual value of thermalization timescale of electron-positron-photon component with the value estimated from (A.0.9). Both values clearly differ significantly. Actually, the systematic underestimation in more than one order of magnitude, present for $B \leq 1$ disappears for larger baryonic loading.

In Fig. A.5 we present the computed values of final thermalization timescale of the pair plasma with baryonic loading together with the value estimated from (A.0.6), again for $B = 1$. Unlike the previous case, the final thermalization timescale is a more complex function of the total energy density. Interestingly, less significant deviations from the value (A.0.6) occur at the extremes of the interval (A.0.3).

In this Letter we computed for the first time the timescale of thermalization for electron-positron plasma with proton loading in the wide ranges of both total energy density (10 orders of magnitude) and baryonic loading parameter (6 orders of magnitude) allowing to treat limiting cases of almost pure electron-positron plasma, almost pure electron-ion plasma as well as intermediate cases. The final result is presented in Fig. A.1 and A.2. The relaxation to thermal equilibrium for the total energy density (A.0.2) occurs always on

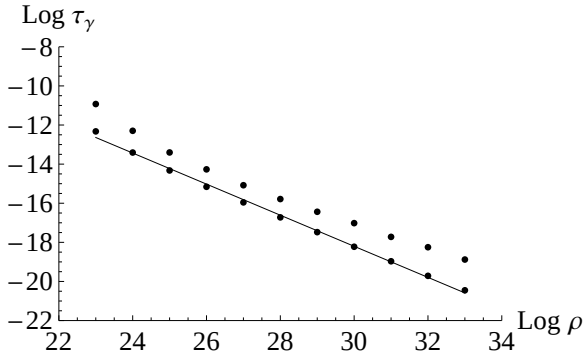

Figure A.4.: The thermalization time scale of electron-positron-photon component of plasma as function of total energy density (points), compared with the τ_{3p} timescale (joined points) computed by (A.0.9) for $B = 1$. Energy density is measured in erg/cm^3, time is seconds.

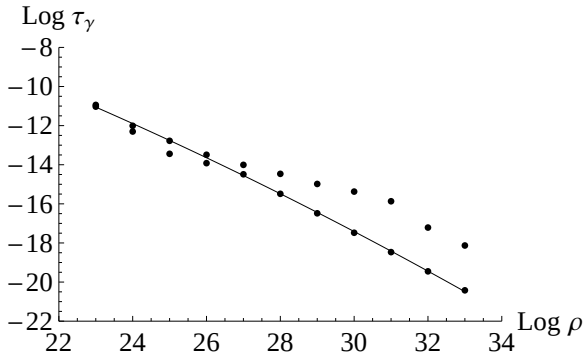

Figure A.5.: The final thermalization timescale of pair plasma with baryonic loading as function of total energy density (points), compared with the τ_{th} timescale (joined points) computed by (A.0.6) for $B = 1$. Energy density is measured in erg/cm^3, time is seconds.

a timescale less than 10^{-9} sec. It is interesting, that electron-positron-photon component and/or proton component can thermalize earlier than the complete thermal equilibrium is reached. The relevant timescales are given, and compared with the order-of-magnitude estimates. Unlike the previous works there is no simplifying assumptions in our method since collisional integrals in the Boltzmann equations are computed directly from the corresponding QED matrix elements. These results are important for the ongoing and future laboratory experiments aimed at creation of electron-positron plasma, as well as for astrophysical models where electron-positron plasmas are present.

B. Hydrodynamic phase of GRB sources

B.1. Introduction

GRBs represent one of the greatest puzzles in astrophysics. They are the brightest and the shortest explosions in the Universe, originating from the most catastrophic events such as gravitational collapse to a Black Hole (BH) taking place at cosmological distances. Such explosions give rise to relativistic outflows with unprecedented Lorentz factors, of the order of hundreds to thousands. Despite the nature of the central engine still remains unclear, one well established fact is the presence of an optically thick relativistic expanding plasma composed of electrons e^-, positrons e^+, photons γ and baryons b. One model for GRBs, the fireball model, involving relativistic outflows was suggested in the early 90's and remain till today the most attractive explanation of large Lorentz factors attained in such outflows (Goodman (1986); Shemi and Piran (1990)). In such a model thermal energy is converted into the bulk kinetic energy due to radiative pressure of relativistic electrons, positrons and photons.

The first study about cosmic fireballs (the plasma originating GRBs) was done by Cavallo and Rees (1978) where the analysis is performed for a plasma composed of pairs and photons for different initial values of optical depth due to Compton scattering, and optical depth due to pair production. This study concludes that average energy of photons should always decrease down to the electron rest mass energy $m_e c^2$ independently on initial conditions. In contrast with this conclusion a recent article by Aksenov et al. (2007) shows that, if the two and three body, direct and inverse processes, are taken into account; thermodynamic equilibrium is always reached, with temperature which, depending on initial conditions, can exceed $m_e c^2$, before beginning of the plasma expansion.

Detailed one-dimensional hydrodynamic simulations were performed (Piran et al. (1993); Mészáros et al. (1993); Ruffini et al. (1999)). In Piran et al. (1993) the equations of energy-momentum conservation are solved numerically. One of the main conclusions derived from these simulations is that in the reference frame of the explosion, short after the beginning of the expansion most of the matter and energy becomes concentrated in a narrow shell which propagates at nearly the speed of light with a simple single peaked "frozen radial

profile". This profile can be reproduced in subsequent time moments by the simple set of scaling laws. In the study by Ruffini et al. (1999)) the same equations were solved, but in addition the departure of e^+e^- from thermal equilibrium with photons was taken into account. This was done adding to the energy-momentum conservation equations, the rate equation for pairs, which reflects the freeze-out of interactions involving electrons and positrons. Initial profiles for the densities were assumed in such a way that e^+e^- plasma is formed in the center, surrounded by the shell of cold baryons. With such configuration a limit was established in order to have a constant width approximation (for details see Ruffini et al. (2000))). In fact it was found for the final baryon loading (after the expanding e^+e^- plasma mixes with baryons)

$$B = Mc^2/E < 10^{-2}, \tag{B.1.1}$$

where Mc^2 is the rest mass energy of baryons, E is the energy of e^+e^- plasma. In Bianco Bianco et al. (2006), the analysis of the similarities and differences between fireshell and other models was performed with the conclusion that it is necessary to take into account the rate equation together with energy and mass conservation conditions, in order to compare theory and observations.

In this paper we revisit the hydrodynamic phase in GRB sources, by studying numerically the evolution of an optically thick plasma. Keeping the assumption of spherical symmetry we focus on the issue how different possible initial spatial distributions of matter and energy in the source of GRBs may influence subsequent evolution of the plasma. We solve the same equations as in Piran et al. (1993) and Ruffini et al. (1999), neglecting for simplicity the rate equation (which is not essential for this scope), instead focusing on various different initial profiles. In addition to considering expansion of γ, e^+, e^-, b in vacuum, we also study the case with expansion into an extended uniform distribution of baryons still satisfying the Ruffini-Wilson condition given by equation (B.1.1). We would like to clarify whether the "frozen radial profile" is the unique radial structure which should be expected in GRB sources, or otherwise a variety of radial profiles in the final evolution of the γ, e^+, e^-, b plasma is also possible.

Our study is expected to shed some light on two different problems. One problem is the emission of plasma at transparency due to Compton scattering, with the light curve clearly depending on the spatial distribution of plasma (what we call the structure of P-GRB) in the optically thick phase. The other problem is purely hydrodynamic possibility to form after transparency multiple shells of collisionless electron-baryon plasma, having different Lorentz factors. This is important in the fireshell model (Ruffini et al. (2009a)) where baryonic shells with different Lorentz factor are expected at tranparecy. The opposite case of a delayed emission by the central engine at different times was considered in internal shock models of GRBs (Piran (1999)).

The structure of the chapter is the following. In section B.2 we briefly remind the concept of fireball and discuss the relevant timescales in the approach of relativistic plasma to thermal equilibrium. In section B.3 we turn to the hydrodynamical evolution of relativistic plasma. We present the results of numerical analysis in section B.4. Conclusions follow in the last section. In section B.6 we review the adopted numerical scheme used to solve relativistic hydrodynamic equations, while in section B.7 we present the results of the test computation.

B.2. Kinetic and hydrodynamical phases

It is generally assumed that the sources of GRBs contain hot relativistic plasma. This plasma is radiation dominated with baryon loading parameter $B \ll 1$. The energy injection resulting in creation of such plasma is assumed to last on a short timescale $t \ll R_0/c$ where R_0 is the initial radius of the plasma. Such plasma is optically thick both to pair production and to Compton scattering with the optical depth

$$\tau \simeq \int (n_{e^+} + n_{e^-})\sigma_T dr \gg 1, \tag{B.2.1}$$

where n stands for the number density and σ_T is the Thompson cross section. Even if initially the energy is injected in the form of γ only, $e^\pm$ pairs will be generated on a timescale $t \simeq 1/(\sigma_T n_\gamma c)$ and vice versa: if only $e^\pm$ pairs are present from the beginning, γ will be generated on a timescale $t^* \simeq 1/(\sigma_T n_{e^+} c)$. Such plasma, which may be non thermal as it forms, will come to thermal equilibrium on a timescale $\alpha^{-1}t^*$, the characteristic timescales for $T = 0.1$ MeV are (Aksenov et al. (2007)):

$$t_{kin} \lesssim 10^{-14}s, \qquad t_{ther} \lesssim 10^{-12}s, \tag{B.2.2}$$

for more details on relaxation timescales see Aksenov et al. (2009b).

Due to radiative pressure of γ and $e^\pm$ pairs the plasma starts to expand adiabatically on a timescale $t_{exp} \simeq R/c$ with $\langle\gamma\rangle \propto r$ where $\langle\gamma\rangle$ is the average Lorentz factor of the bulk radial motion. Such self accelerating phase lasts up to the moment when plasma becomes either matter dominated or transparent to photons (Ruffini et al. (1999)).

Expansion is governed by the relativistic energy-momentum conservation equations and the continuity equation (Goodman (1986); Shemi and Piran (1990); Piran et al. (1993); Mészáros et al. (1993); Ruffini et al. (1999)).

$$T^{\mu\nu}{}_{;\nu} = 0, \tag{B.2.3}$$

$$(n_B U^\nu)_{;\nu} = 0, \tag{B.2.4}$$

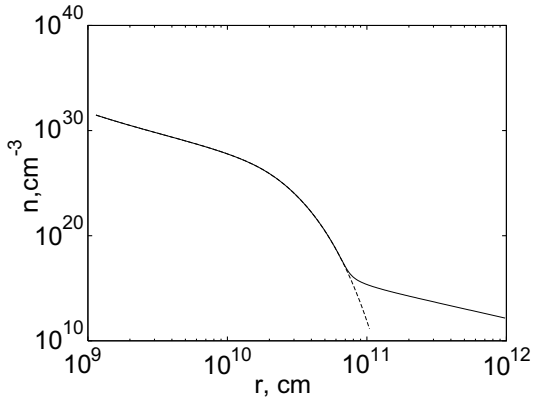

Figure B.1.: The density of pairs as function of radial coordinate. Continuous line is obtained by the rate equation (B.2.5), while dotted line represents thermal distribution. Parameters are: mass of the black-hole $M_{BH} = 10^3 M_\odot$ and charge to mas ratio $Q/\sqrt{G}M = 0.1$. Reproduced from (Ruffini et al. (1999)).

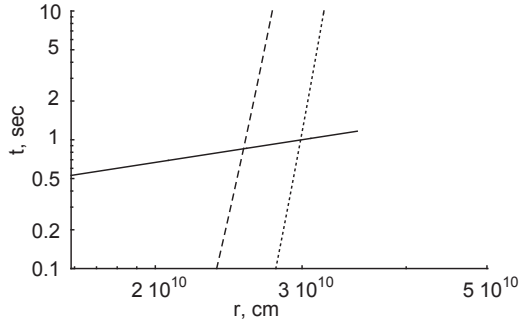

Figure B.2.: Reaction timescales as well as expansion timescale as functions of radius of the fireshell. The radius at which the departure from kinetic and thermal equilibrium occurs is determined respectively by intersections of the dashed and dotted lines with the continuous one. Parameters are: total initial energy $E = 10^{53} erg$ and initial radius $r = 2.4 \times 10^8$ cm.

where $T^{\mu\nu}$ is the energy-momentum tensor of plasma, U^ν and n_B are four-velocity and number density of baryons respectively. However, when the rate of electron-positron pair creation and annihilation, i.e. 2-body processes $t_{2p} \simeq 1/(\sigma_T c n_\pm)$ becomes eventually equal to the expansion rate t_{exp}, pairs freeze out, i.e. go out from thermal equilibrium at t^*_{ther}, see Fig. B.1. In the same way 3-body reactions such as bremsstrahlung freeze out earlier, at the moment t^*_{kin}, when $t_{3p} \simeq 1/(\alpha \sigma_T c n_\pm)$ becomes equal to the expansion rate. We illustrate these processes in Fig. B.2.

Therefore, in order to describe the freeze out of e^+e^- pairs the continuity equation (B.2.4) is phenomenologically modified (Ruffini et al. (1999); Ruffini et al. (2000)).

$$(n_{\pm}U^{\nu})_{;\nu} = \langle \sigma v \rangle \left[n_{\pm}^2(T) - n_{\pm}^2 \right], \tag{B.2.5}$$

where $\langle \sigma v \rangle$ is the average product of the annihilation cross section and particles relative velocity, $n_{\pm}(T)$ is equilibrium density of pairs and $n_{\pm}$ is the density out of equilibrium (see also Grimsrud and Wasserman (1998)). More details about the importance of the equation (B.2.5), within the fireshell model, can be found in Bianco et al. (2006).

Overall, we identify seven important timescales in the evolution of the plasma from the moment of its appearance until it reaches transparency. In chronological order these are:

- energy is injected on the timescale t_{in},
- pair plasma reaches kinetic equilibrium on the timescale t_{kin},
- thermal equilibrium is reached on the timescale t_{ther},
- expansion starts at t_{ex},
- plasma departs from thermal equilibrium at t^*_{ther},
- finally it departs from kinetic equilibrium at t^*_{kin}.
- transparency is reached at t_{tr}.

We can split therefore the entire evolution of plasma in two phases: the *kinetic phase* from its formation at t_{in} until the moment t_{ex} when it begins to expand, and the *hydrodynamic phase* from the beginning of expansion until the moment of transparency t_{tr}. Kinetic evolution of plasma drives it towards thermal equilibrium. Thermodynamics and hydrodynamics can be applied to its description starting from the moment t_{ther}. Finally, when the mean free path of photons exceeds the spatial dimensions of plasma at the moment of reaching transparency it becomes collisionless[1].

During the hydrodynamic phase there are two important moments: when three particle processes such as bremsstrahlung freeze out at t^*_{ther} which marks the end of thermal equilibrium, and the freeze out of two particle processes at t^*_{kin} when even kinetic equilibrium is violated.

B.3. Physical evolution

We study the evolution of a thermal plasma in the hydrodynamic approximation, considering an energy momentum tensor of a perfect fluid (Weinberg

[1]The timescales of Compton scattering and of Coulomb scatterings nearly coincide.

(1972)),

$$T^{\mu\nu} = pg^{\mu\nu} + [\rho(1+\epsilon) + p]U^{\mu}U^{\nu} \tag{B.3.1}$$

where p is pressure, $g_{\mu\nu} = \mathrm{diag}(1, -1, -r^2, -r^2\sin^2\theta)$ is the Minkowski metric tensor, ϵ is specific energy density, ρ is matter density and $U^{\mu} \equiv (\Gamma, \Gamma v, 0, 0)$ is the four velocity, Γ is the Lorentz factor and v is the fluid velocity. Assuming that particles are non relativistic baryons and ultrarelativistic photons, electrons and positrons the fluid variables will be:

$$\begin{aligned}
\epsilon_r &= \epsilon_- + \epsilon_+ + \epsilon_\gamma, \\
\rho_r &= \rho_\gamma + \rho_+ + \rho_-, \\
p_r &= p_\gamma + p_- + p_+,
\end{aligned}$$

where the subscript "r" denotes relativistic component, and

$$\begin{aligned}
\rho_{nr} &= \rho_b, \\
p_{nr} &= p_b \simeq 0,
\end{aligned}$$

where the subscript "nr" denotes non relativistic component. Velocity of both components is the same since they are coupled by collisions, so we have:

$$\epsilon = \epsilon_{nr} + \epsilon_r \simeq \epsilon_r, \tag{B.3.2}$$
$$\rho = \rho_{nr} + \rho_r \simeq \rho_b, \tag{B.3.3}$$
$$p = p_r + p_{nr} \simeq \epsilon_r/3. \tag{B.3.4}$$

It is useful to introduce new variables following Bowers and Wilson (1991):

$$D = \rho\Gamma \quad \text{is the non relativistic component,} \tag{B.3.5}$$
$$E = \epsilon D \quad \text{is the relativistic component,} \tag{B.3.6}$$
$$S = (D + E + \Gamma p)u \quad \text{is the radial momentum.} \tag{B.3.7}$$

In spherically symmetric case we get from the energy-momentum and number of particles conservation (B.2.3)-(B.2.4):

$$\frac{\partial D}{\partial t} = -\frac{\partial (r^2 D v)}{r^2 \partial r}, \tag{B.3.8}$$

$$\frac{\partial E}{\partial t} = -\frac{\partial (r^2 E v)}{r^2 \partial r} - p\frac{\partial (r^2 u)}{r^2 \partial r} - p\frac{\partial \Gamma}{\partial t}, \tag{B.3.9}$$

$$\frac{\partial S}{\partial t} = -\frac{\partial (r^2 S v)}{r^2 \partial r} - \frac{\partial p}{\partial r}, \tag{B.3.10}$$

where u, v and Γ are related as follows:

$$\Gamma = \sqrt{1+u^2}, \qquad v = u/\Gamma. \tag{B.3.11}$$

Equations (B.3.8)-(B.3.10) form a coupled system of partial differential equations, and its solutions cannot be found without further approximations. We implemented a numerical code to solve this system of equations. Explanation of the code and details can be found in section B.6.

B.4. Results

As a test for the code, we performed a simulation with initial conditions taken from Piran et al. (1993), see section B.7. In that paper it is shown that quite independently on initial distribution of matter and energy all solutions for energy-dominated plasma look similar to the one presented in Fig. B.10. Indeed, it was shown that after a brief rearrangement the energy, density and Lorentz factor profiles acquire a certain shape, called there "frozen radial profile", which does not change with time, but just rescales according to simple scaling laws. It is found that this approximation is valid in the energy dominated regime, and in the beginning of the matter dominated regime. Below we show that for different initial distributions of energy and matter the resulting evolution can be also different from the one found in Piran et al. (1993).

B.4.1. Constant baryonic distribution profile

Considering initial profile for E to be

$$E_0 = \frac{\epsilon_0 \rho_0 \Gamma_0}{R_0^8 + r^8}, \tag{B.4.1}$$

(the same as in section B.7), with initial parameters: $\epsilon_0\rho_0 = 0.2, \Gamma_0 = 1$ and $R_0 = 1$, and taking a constant distribution of nonrelativistic matter over space with $D_0 = 2 \times 10^{-9}$, we have the evolution which is presented in Fig. B.3.

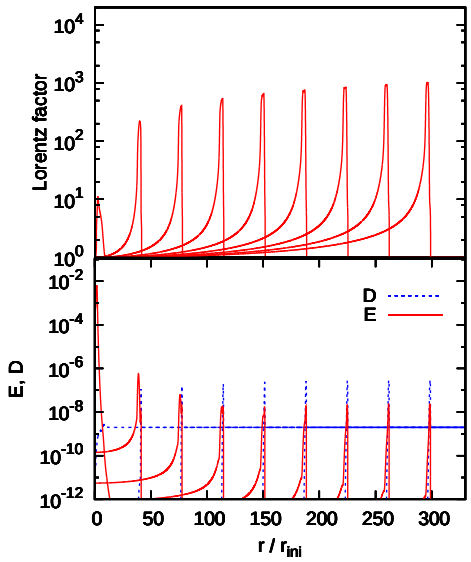

Figure B.3.: Densities and Lorentz factor evolution in the case with a constant baryonic distribution profile.

The plasma in spatial region dominated by the relativistic component E self accelerates like in the previous case. However, it pushes the nonrelativistic baryons which are collected in the front of the shell, creating a leading shell which is matter dominated from the very beginning. Our analysis is different from Ruffini et al. (2000) because we consider uniform baryonic distribution while they consider a shell of baryons located initially at some radius.

Thus unlike the case treated in section B.7, two distinct shells are formed: the outer one being matter dominated and the inner one being energy dominated. The matter dominated shell has from the very beginning a maximum baryon loading of $B \simeq 10^2$. Besides, in this case there is a tail of rarefied energy dominated plasma inside the shell. The baryonic loading at fixed time changes eight orders of magnitude while moving from central region to the matter dominated peak. The Lorentz factor increases very rapidly in the beginning, reaching almost a constant value at the end, see Fig. B.3.

Inspection of Fig. B.3 leads to the following conclusions (see also Figs. B.4, B.5 and B.6):

- the E-shell density is decreasing, its energy is transferred to the baryons which are swept up in the external shell.
- the density of the baryonic shell is increasing, while the shell spreads since it is matter dominated.

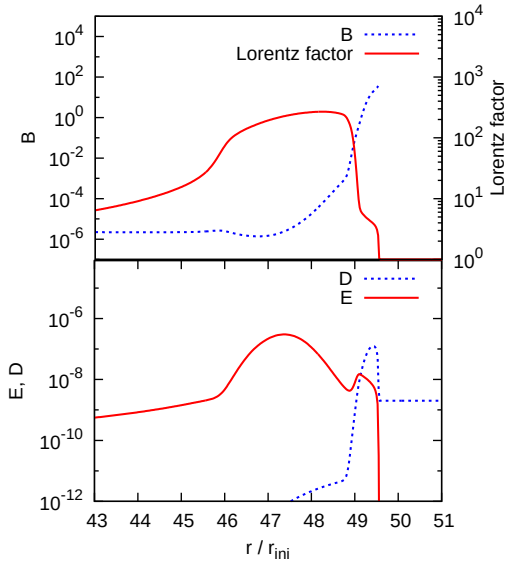

Figure B.4.: Detailed structure of the spatial distribution of Lorentz factor and baryonic loading (upper panel), energy and matter density (lower panel) is shown for the moment $t = 40$. The B parameter changes 8 orders of magnitude in the extension of the shell. B is plotted until the point where Lorentz factor is equal one (also in the following figures).

- the slope of the B parameter is changing, becoming less steep, because of the spreading of the matter dominated shell, and the decreasing of the density in the E-shell.
- the relation $B(r) \propto 1/\Gamma(r)$, whose integral version is true for $10^{-4} \lesssim B \lesssim 1$ is not valid in the differential case.
- B parameter has a constant maximum value in the outer shell.

B.4.2. c) Hybrid profile

Combining the profile used in section B.7 with the previous one, we have now for E, the same profile as in both cases, see Eq. (B.4.1), with the same parameters as in section B.4.1. For the nonrelativistic matter distribution we have instead:

$$D_0 = \frac{\rho_0 \Gamma_0}{a R_0^8 + r^8} + d, \tag{B.4.2}$$

with the following parameters: $\rho_0 = 2 \times 10^{-6}$, $\Gamma_0 = 1$, $a = 10^{-4}$, $d = 2 \times 10^{-11}$ and $R_0 = 1$, which correspond to a dense core inside the radiation

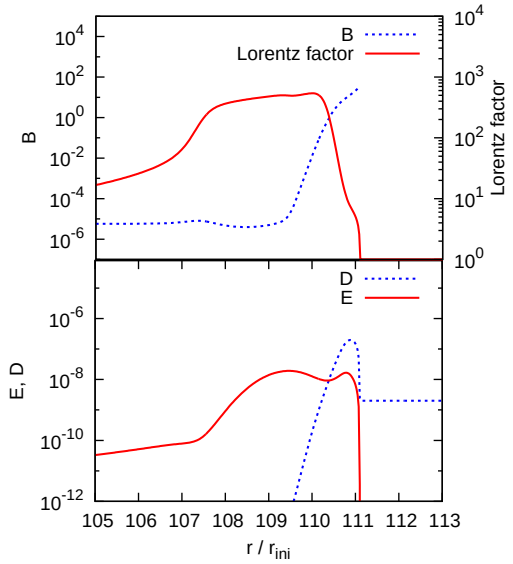

Figure B.5.: The same as in Fig. B.4, for the moment $t = 92$. The density of the outer matter dominated shell increases, and the density of the inner energy dominated one decreases.

dominated region, and a constant density outside.

In this case we have a mixture of two previous cases. In fact, two shells form again: inner one energy dominated, and outer one matter dominated, see Fig. B.7. The "frozen radial profile" is valid for the the inner shell, while the leading shell is matter dominated because of the constant baryon density outside. This kind of initial conditions gives the possibility for the formation of two shells with two maxima in E and D spatial distributions which persists up to large radii, see Fig. B.8. We computed the average values of the Lorentz factors in two regions of space in Fig. 10: for $342 < r < 347$ for the inner shell, and for $347 < r < 349$ for the outer shell. The average Lorentz factors are, respectively, $\Gamma_1 \simeq 400$ and $\Gamma_2 \simeq 10$.

Again, in this case the baryon loading at fixed time changes five orders of magnitude throughout the plasma. The outer matter dominated shell has constant $B \simeq 10^2$, and the energy dominated shell has small B gradually increasing outwards.

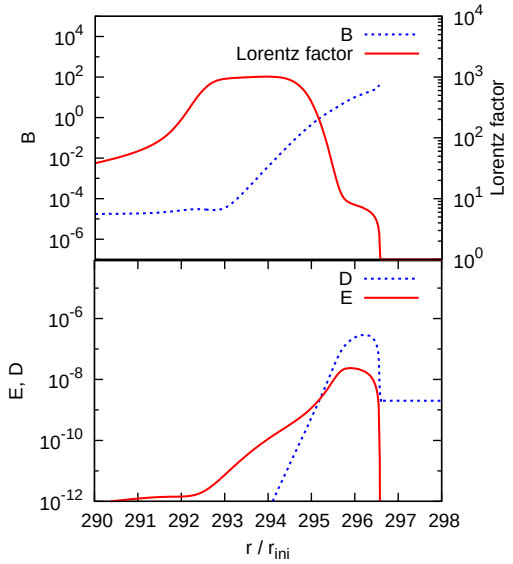

Figure B.6.: The same as in Fig. B.4, for $t = 248$. The maximum B parameter does not change, the ratio between D and E in the outer shell is constant, while in the inner shell it increases.

B.5. Conclusions

We found that the initial spatial distribution for energy density $E(r)$ and matter density $D(r)$, indeed influences the subsequent dynamics of plasma expansion. In particular, the "frozen radial profile" found in Piran et al. (1993) and the constant width approximation established in Ruffini et al. (2000) are not the unique solutions: structures are formed and survive in the expanding shell up to large radii, in the last example 350 times the initial radius when an extended baryon distribution is assumed.

In fact, considering expansion not in vacuum, but in a space uniformly filled by a cold baryonic medium, a leading matter dominated shell is found to form. The local baryonic loading in this shell has a maximum value $B \simeq 10^2$, and it remains constant throughout the evolution although the global baryon loading still respects equation (B.1.1). We found also that the energy density in pairs and photons decreases, being transferred to kinetic energy of baryons. The outer shell spreads with time since it is matter dominated.

We found two peaks in the $D(r)$ profile in the hybrid case: the outer peak is due to swept up baryons, the inner one is due to the dense core located in the center in the beginning of the simulation. Such structure, if survives until the plasma becomes transparent, will give rise to two shells, moving with different Lorentz factors. Since the Lorentz factor of the leading shell

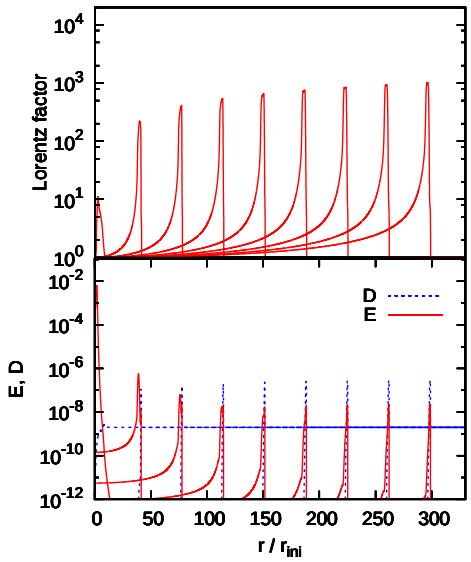

Figure B.7.: The same as in Fig. B.3, but for the hybrid case. The Lorentz factor evolution presents some structure, but its shape is very similar to the case reproduced in section B.7). The densities profiles instead show a very different structure.

is smaller than the one of the inner shell, they will eventually interact in the collisionless regime.

It is conceptually important that the energy budget of photons emitted at transparency versus kinetic energy of remaining baryons will be affected by this more general solution as contrasted to the "frozen radial profile" one.

Finally, the structure seen in energy and matter spatial profiles will be encoded in the light curve of the radiation emitted when transparency is reached. In principle we have now a way to get information from the structure of the P-GRB and the different Lorentz gamma factors in the multiple distribution of accelerated baryons left over at transparency, to infer the information about the matter distribution during the process of the gravitational collapse to a black hole.

B.6. Numerical approach

Finite-difference methods can be applied to solve partial differential equations (B.3.8)-(B.3.10). One approach to the solution of resulting system of coupled nonlinear algebraic equations involves matrix inversion which turns out to be particularly time consuming for our purposes. Instead we fol-

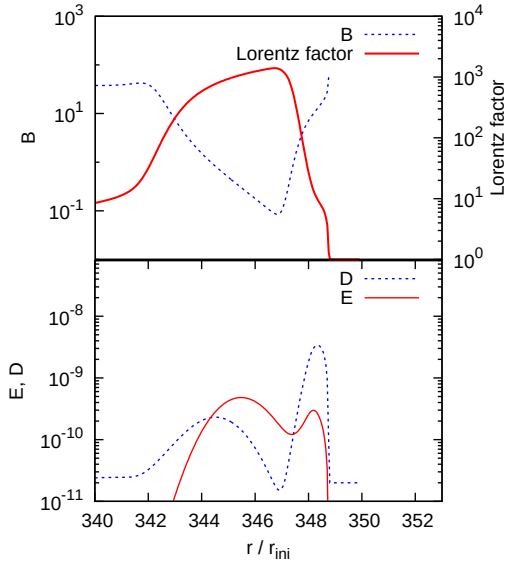

Figure B.8.: The same as in Fig. B.4, for the hybrid case, and $t = 434$. Now we can see two shells for both densities E and D.

low another simpler approach called operator splitting. Below we briefly illustrate the main steps applied for our case (for details of the method see Bowers and Wilson (1991).

The main idea of the operator splitting method is to compute separately the contributions to the "Left Hand Side" (LHS) of equations (B.3.8)-(B.3.10) from different terms on the "Right Hand Side" (RHS). The new values of the physical quantities obtained in this way are then used to compute next different time values to RHS terms.

The order in which terms will be solved is:

INTERACTION

$$\frac{\partial S}{\partial t} = -\frac{\partial p}{\partial r} = -\frac{\partial E/\Gamma}{3\partial r}, \tag{B.6.1}$$

$$u = \frac{S}{D + E + p\Gamma}, \tag{B.6.2}$$

$$\frac{\partial E}{\partial t} = -p\frac{\partial \Gamma}{\partial t}, \tag{B.6.3}$$

$$\frac{\partial E}{\partial t} = -p\frac{\partial (r^2 u)}{r^2 \partial r}, \tag{B.6.4}$$

where we have used (B.3.4), and

ADVECTION

$$\frac{\partial D}{\partial t} = -\frac{\partial (r^2 D v)}{r^2 \partial r}, \tag{B.6.5}$$

$$\frac{\partial E}{\partial t} = -\frac{\partial (r^2 E v)}{r^2 \partial r}, \tag{B.6.6}$$

$$\frac{\partial S}{\partial t} = -\frac{\partial (r^2 S v)}{r^2 \partial r}. \tag{B.6.7}$$

From the physical point of view one may think that first we solve the physical interactions in the plasma, namely

- the acceleration due to radiative pressure,
- the new velocity,
- the new energy densities for the changes in velocity and pressure.

Then we solve the "advection equations" which can be thought just as a rearrangement of the densities in space. As the fluid elements move in space, the "advection equations" will just show where the fluid element located before in r_1 will be after each iteration, to say r_2.

B.6.1. Finite difference form of equations

Using a finite difference method to solve numerically the previous equations, we can have an iteration system in which given initial conditions we can solve step by step in time, the evolution of the variables. Using the following notation:

$$\Delta t = t^n - t^{n-1}, \tag{B.6.8}$$
$$\Delta r = r_k - r_{k-1}, \tag{B.6.9}$$
$$\Delta^t G = G^n - G^{n-1}, \tag{B.6.10}$$
$$\Delta^r G = G_k - G_{k-1}, \tag{B.6.11}$$

where G represents any of the variables, n is a temporal step and k is a spatial step, the system of equations reads

INTERACTION

$$\frac{\Delta^t S}{\Delta t} = -4\pi r^2 \frac{\Delta^r p}{\Delta r}, \tag{B.6.12}$$
$$u = \frac{S}{D + E + p\Gamma}, \tag{B.6.13}$$
$$\frac{\Delta^t E}{\Delta t} = -p\frac{\Delta^t \Gamma}{\Delta t}, \tag{B.6.14}$$
$$\frac{\Delta^t E}{E} = -\frac{\Delta t}{3\Gamma}\frac{\Delta^r (r^2 u)}{r^2 \Delta r}, \tag{B.6.15}$$
$$E^{t+1} = E^t e^{-\frac{\Delta t}{3\Gamma \Delta^r V}\Delta^r (r^2 u)}, \tag{B.6.16}$$

ADVECTION

$$\frac{\Delta^t D}{\Delta t} = -\frac{\Delta^r (r^2 D v)}{\Delta^r V}, \tag{B.6.17}$$
$$\frac{\Delta^t E}{\Delta t} = -\frac{\Delta^r (r^2 E v)}{\Delta^r V}, \tag{B.6.18}$$
$$\frac{\Delta^t S}{\Delta t} = -\frac{\Delta^r (r^2 S v)}{\Delta^r V}. \tag{B.6.19}$$

In order to solve (B.6.12)-(B.6.19), we have to give as initial condition spatial profiles for the physical variables at $t = 0$, then, by iteration method we can calculate the spatial distribution for the variables at any later time. Therefore we have to set initial profiles for: $D(t = 0, r), E(t = 0, r), S(t = 0, r)$.

B.6.2. Numerical issues

Some important points should be kept in mind when making a hydrodynamic code, especially in relativistic case. These points influence both accu-

racy and stability of the scheme. In particular, since our code does not contain treatment of shocks for the moment, distributions of matter, energy and velocity have to be smooth, without any discontinuities.

Centering

The variables have different position on the grid: some are calculated in the center of each volume element ($G_{k+1/2}$) and some are defined in the edge of volume elements (G_k). There is no general rule, but specifically in our case variables related to motion (velocity, momentum) are computed in center of volume element; instead, variables not intrinsically related to motion (densities, temperature) are computed on edges. All this is crucial for numerical stability of the code.

Extrapolating the grid

As in many finite difference methods the differentiation is approximated as:

$$\frac{\partial G_k}{\partial r} = \frac{G_{k+1/2} - G_{k-1/2}}{\Delta r}. \tag{B.6.20}$$

The values on the RHS are the current time step iteration (G^n) while those on the LHS will be used to construct the variables at next time step iteration (G^{n+1}). It means that, at each time step, one spatial value is lost at the ends of the grid. In order to solve this problem we perform an extrapolation after each iteration, restoring the values at the end of the grid ($k_{min-1/2}$ and $k_{max+1/2}$), keeping the same amount of grid points all the time. A linear extrapolation is used to construct these values:

$$G_{k_{max}+1} = 2G_{k_{max}-1} - G_{k_{max}-3} \tag{B.6.21}$$

$$G_{k_{min}-1} = 2G_{k_{min}+1} - G_{k_{min}+3} \tag{B.6.22}$$

We tried also a second order extrapolation, but it does not work well and leads to instability.

Time step and dispersion

The steps in radial coordinate Δr and in time interval Δt are related, the results are quite sensitive to these choices, which should satisfy the Courant condition. Due to relativistic velocities it is better to set the limit for Δt, using the light velocity, $\Delta t < \Delta r/c$, (see Wilson and Mathews (2003)), where $c = 1$ is the light velocity. For a coarse grid we were unable to reproduce known results, in particular the "frozen radial profile" had some dispersion growing with time, while refining Δt leads to better agreement.

B.7. test

B.7.1. a) Piran's profile

As a test for the code, we performed a simulation with initial conditions taken from Piran et al. (1993). Initial profile for E and D with a very steep decay were chosen, namely

$$E_0 = \epsilon_0 D_0 = \frac{\epsilon_0 \rho_0 \Gamma_0}{R_0^8 + r^8} \tag{B.7.1}$$

where parameters are: $\epsilon_0 = 0.001, \rho_0 = 200, \Gamma_0 = 1$ and $R_0 = 1$. The high power in r is needed to represent a dense object with vacuum outside. The material is initially at rest, and it is non relativistic because from the beginning it is matter dominated $D_0 = 10^3 E_0$. Plasma expands like a gas which was initially confined. It just tends to fill all the space with equal density (at infinite time), see Fig. B.9, in good agreement with Fig. 3 of Piran et al. (1993)).

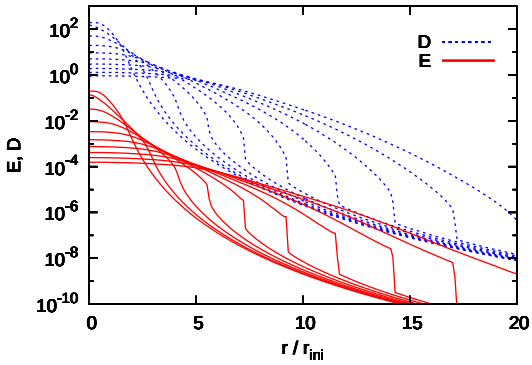

Figure B.9.: Time evolution of the energy density $E(r)$ and matter density $D(r)$ profiles for non relativistic case. All figures are represented in laboratory frame. In this case the baryon loading parameter is $B = 10^3$.

For a relativistic case we use also the equation (B.4.1) for the initial profiles, but with parameters: $\epsilon_0 = 50, \rho_0 = 0.004, \Gamma_0 = 1$ and $R_0 = 1$. It is initially at rest with $\Gamma(0, r) = 1$, but due to the pressure of relativistic particles, the shell self accelerates reaching high Lorentz factors. Because of this peculiarity practically all particles of the shell accelerate almost together and the shell propagates like one-body system accelerating in vacuum. Different from the non relativistic case, just a small part of the density remains in the central region inside the shell, see Fig. B.10.

We also reproduced their relativistic case, shown in their Fig. 1, see our Fig. B.10.

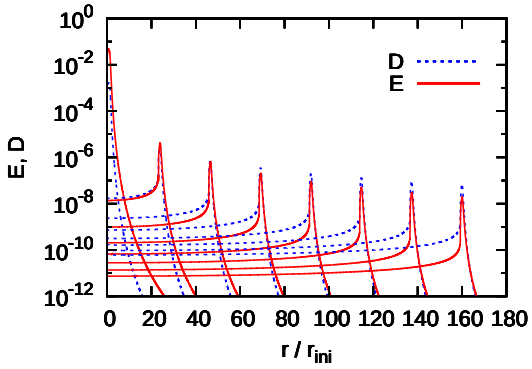

Figure B.10.: The same as in Fig. B.9, but for relativistic case. B parameter is $B = 2 \times 10^{-2}$

C. Cosmological structure formation

C.0.2. The Cosmological Principle

There have been three distinct moments in the developement of the so called *cosmological principle* which is at the very basis of our approach to the analysis of the Universe. The first formulation of the cosmological principle can be simply stated:

All the events in the Universe are equivalent. (C.0.1)

Such cosmological principle was enunciated a few years after the introduction of the field equations of general relativity by Albert Einstein himself (Einstein, 1917) in the quest of visualizing a Universe most democratic with respect to any special point and any possible moment of time: a Universe everlasting in time and totally homogenous in the spatial directions. No solution fulfilling such a cosmological principle could be found, and Einstein was so strongly confident in the validity of this principle that he modified his field equations of general relativity by introducing a cosmological term Λ. George Gamow refers that Einstein later on considered that the biggest mistake in his life. It was through the work of Alexander Friedmann (Friedman, 1922) that a new cosmological principle was advanced:

All the points in the Universe are equivalent. (C.0.2)

As long as we look at our 'neighbour' Universe, this statement is certainly false, because the distribution of matter is far from homogeneous: there are planets, stars, and, going to larger scales, galaxies and clusters of galaxies, separated by almost empty regions. However, Friedmann principle should apply when we average this distribution over a volume containing a large enough amount of galaxies. For such a spatially homogeneous Universe Friedmann (Friedman, 1922) found in 1922 explicit analytic solutions of Einstein equations of general relativity. A remarkable property of this solution is that it describes a non-static Universe. At that time, there were no observational evidences for the temporal evolution of the whole Universe. A first

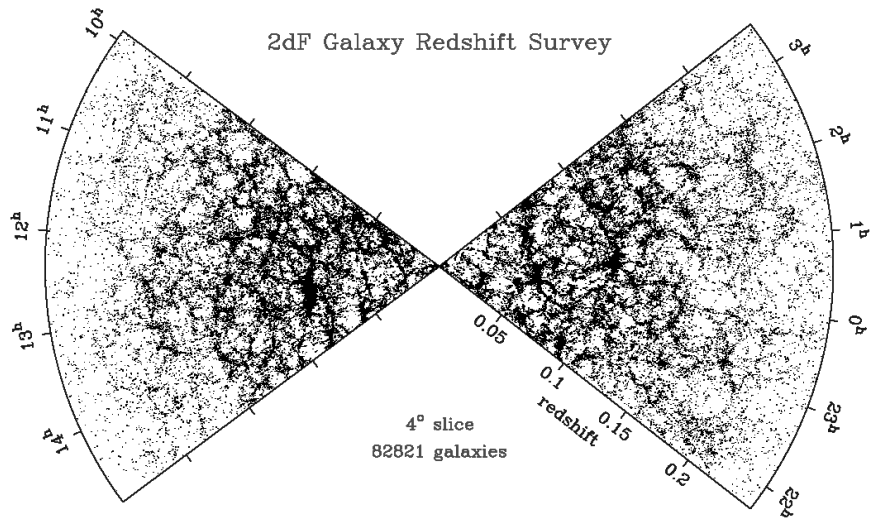

Figure C.1.: The distribution of galaxies in the 2dFGRS (from Peacock (2002)).

evidence came in the 1929 from the observation by Hubble (Hubble, 1929) of the recession of the nebulae. Hubble was the first trying to study the spatial distribution of objects as large as the galaxies, at that time thought to be the largest self-gravitating systems to exist. The Hubble law, interpreted within the framework of Friedmann cosmology, would imply that the galaxy distribution is close to homogenous on the large-scale average (Weyl, 1952; Lemaître, 1927, 1931b,a). It was through the above mentioned work of Hubble first, the remarkable work of George Gamow together with his collaborators (1946-1949) (Gamow, 1946; Alpher et al., 1948; Gamow, 1948; Alpher and Herman, 1948), postulating an initially hot Universe, and the detailed work of Fermi and Turkievich in the same years (Alpher and Herman, 1950) introducing the first computation of cosmological nucleosynthesis, that the Friedmann Universe has grown to become the standard paradigm in cosmology following the discovery of CBR by Penzias & Wilson in 1965 (Penzias and Wilson, 1965).

In effect, one of the strongest predictions of Big Bang model is the presence of a background microwave radiation, relic of the early Universe. This radiation is highly isotropic, reflecting, through the coupling with matter, the high isotropy and homogeneity of the primeval plasma. This tells us that the cosmological principle, and then Friedmann picture, safely applies to the early Universe. Homogeneity on very large scales is confirmed by present day observations of, in particular:

- X-ray background
- radio sources

- gamma ray bursts distribution

- galaxies and clusters of galaxies.

So much so for the very large scales, but what about structures as galaxies and clusters of galaxies? They appear more and more distributed without any apparent homogeneity, but on the contrary showing regularities in an apparent hierarchical distribution of galaxies, clusters of galaxies and superclusters of galaxies separated by large voids (see Fig. C.1). Slowly but more and more clearly the presence of a fractal distribution in the Universe has started to surface and with it a new cosmological principle which can be simply expressed:

All the observers in the Universe are equivalent. (C.0.3)

On the other hand, on smaller scales, distribution of matter is far from homogeneous: galaxies tend to cluster, forming structures separated by large voids. These clusters of galaxies are themselves members of even larger structures, so called superclusters of galaxies. To study such a complicated distribution of matter, it is necessary to use a statistical approach. In the next section we will introduce the mathematical tools usually used to study large scale structure (LSS).

We shall recall in the following a few basic points which have in essential to reach this new principle and make possible the verification of its possible validity.

C.1. Two-point Correlation Function

The statistical description of clustering is based upon the concept of correlation, namely, in a more rigorous way, the probability of finding an object in the vicinity of another one. The standard way to quantify this probability is to define the two-point correlation function $\xi(\vec{x})$ Peebles (1993).

Let's consider a distribution of objects in space, described by the number density function $n(\vec{x})$. The probability that an object is found in an infinitesimal volume δV centered around the point $\vec{x}$ is proportional to the volume itself:

$$\delta P \propto \delta V. \tag{C.1.1}$$

In the absence of structure, the joint probability of finding two objects in two different infinitesimal volumes δV_1 and δV_2, centered respectively around $\vec{x}_1$

and $\vec{x}_2$ is given by the product of the two probabilities:

$$\delta P = \delta P_1 \delta P_2 \propto \delta V_1 \delta V_2 \tag{C.1.2}$$

On the other hand, if objects have a tendence to cluster, we will find an excess probability:

$$\delta P \propto \delta V_1 \delta V_2 \cdot (1 + \xi(\vec{x}_1, \vec{x}_2)) \tag{C.1.3}$$

According to the cosmological principle, we don't expect the correlation function to depend on the position neither on the direction, but only on separation beetween volumes: $\xi(\vec{x}_1, \vec{x}_2) = \xi(r_{12})$, where $r_{12} \equiv |\vec{x}_1 - \vec{x}_2|$.

An equivalent definition of the two-point correlation function is the following:

$$\xi(r_{12}) =< \delta(\vec{x}_1)\delta(\vec{x}_2) >, \tag{C.1.4}$$

where $< ... >$ denotes averaging over all pairs of points in space separated by a distance r_{12}, and $\delta(\vec{x}) \equiv (n(\vec{x}) - \bar{n})/\bar{n}$.

C.1.1. Observed Galaxy Distribution

Observational data coming from galactic surveys are usually expressed in the form of correlation function in redshift space, $\xi(\pi, \sigma)$, where π is a separation along the line of sight and σ is a angular separation on the plane of the sky between two galaxies. It is then possible to obtain the real-space correlation function $\xi(r)$; this step is never a trivial one, but we are not going into details since it is beyond the purpose of this review.

Peebles Peebles (1993) have shown that distribution of galaxies can be described by a two point correlation function with a simple power law form:

$$\xi_g(r) = \left(\frac{r}{r_g}\right)^{-1.77}, \quad r < 10h^{-1}\text{Mpc}, \tag{C.1.5}$$

where h is a Hubble parameter today measured in $100\,\frac{km}{s\,Mpc}$. The correlation length r_g determines the typical distance between objects. For galaxies, it was estimated to be $\simeq 5h^{-1}$Mpc.

For clusters of galaxies the same power law was found first by Bahcall and Soneira Bahcall and Soneira (1983) and Klypin and Kopylov Klypin and Kopylov (1983)

$$\xi_c(r) = \left(\frac{r}{r_c}\right)^{-1.8}, \quad 5h^{-1} < r < 150h^{-1}\text{Mpc}. \tag{C.1.6}$$

with different correlation length, namely $r_c \simeq 25h^{-1}$Mpc. Further, Bahcall and Burgett Bahcall and Burgett (1986) have found correlation function for superclusters of galaxies with the same power law.

Recent observations support these conclusions. Results from the Sloan

Digital Sky Survey (SDSS) on galaxy clustering Zehavi et al. (2005) for about 200,000 galaxies give a real-space correlation function as

$$\xi_g(r) = \left(\frac{r}{r_0}\right)^{-1.8}, \quad 0.1h^{-1} < r < 10h^{-1}\text{Mpc}, \tag{C.1.7}$$

where $r_0 \simeq 5.0h^{-1}$Mpc, although the brightest subsample of galaxies has a significantly steeper $\xi(r)$. The geometry of samples in SDSS is quite close to Las Campanas Redshift Survey Shectman et al. (1996) and the results are very similar, but with much better resolution.

The 2dF Galaxy Redshift Survey Peacock et al. (2001) (see fig.C.1) consists of approximately 250,000 galaxies redshifts. Their result is Hawkins et al. (2003):

$$\xi_g = \left(\frac{r}{r_0}\right)^{-1.67}, \quad 0.1h^{-1} < r < 12h^{-1}\text{Mpc}, \tag{C.1.8}$$

with $r_0 = 5.05h^{-1}$Mpc

Their measurements are in agreement with previous surveys. However, having much smaller statistical errors they were able to find a slight difference of the power law exponent as well as the correlation length on distances or redshifts, colors and types of galaxies. For a summary of measurements of $\xi(r)$ by different surveys other than the ones cited here, see Table 2 of Ref. Hawkins et al. (2003).

C.1.2. Power Law Clustering and Fractals

It is clear that, once a correlation function is given, the density of objects around any randomly chosen member of the system is:

$$n(r) \propto 1 + \xi(r) \tag{C.1.9}$$

If the correlation function has a power law behaviour with exponent γ:

$$\xi(r) \propto r^{-\gamma} \tag{C.1.10}$$

as for galaxies and clusters of galaxies, where $\gamma \simeq 1.8$, then the number of objects in a given volume scales in a similar way:

$$N(r) \propto r^{3-\gamma} \tag{C.1.11}$$

So, for non integer γ, the number of objects scales with a fractional power of the radius of the volume under consideration. This behaviour is typical of fractal sets.

A fractal is a set in which 'mass' and 'radius' are linked by a fractional

power law Mandelbrot (1983):

$$M(r) \propto r^{D_F} \tag{C.1.12}$$

where D_F is the fractional or Hausdorff dimension of the set. So galaxies seem to show, at least up to scales of about 100 Mpc, a fractal distribution with $D_F \simeq 1.2$.

A crucial characteristic of a fractal distribution is the presence of fluctuations at all length scales and, consequently, impossibility of defining an average value for the density. It can be stressed that a fractal structure in a cosmological model, although not spatially homogeneous, is not in conflict with weaker form of the cosmological principle Mandelbrot (1983): in a homogeneous fractal set each observer at a matter point belonging to the set observes the same matter distribution as any other observer belonging to the set.

The question about fractality in galaxy distribution is still under debate Coleman and Pietronero (1992),de Bernardis et al. (2002),Kolb and Turner (1990),Luo and Schram (1992),de Gouveia dal Pino et al. (1995),Durrer and Labini (1998),Gaite et al. (1999),Joyce et al. (2005). There are two main problems that are to be faced with:

1. Most of the matter in the Universe is in the form of dark matter, while observations are about luminous matter. It is still unclear how (and even if) light traces mass: this is in particular related to the problem of matching the clustering of galaxies, that tells us about distribution of luminous (baryonic) matter, with the CMB anisotropies, that tell us about distribution of gravitating matter.

2. On the other hand, still little is known about fluctuations on intermediate scales between those of local galaxy surveys ($\sim 100h^{-1}$ Mpc) and those probed by the observation of CMB anisotropies ($\sim 1000h^{-1}$ Mpc). However, this gap is greatly reduced in recent times de Bernardis et al. (2002),Peacock et al. (2001).

Assuming that the fractal framework is, at least up to some large scale, a good description of the real matter distribution, a consistent model of structure formation has been proposed by Ruffini in the eighties (see Ruffini et al. (1988) and references therein). In this model fractality arises from successive fragmentations of primordial structures, so called 'elementary cells', formed via gravitational instability in the neutrino component of the matter in the Universe. In the following chapter we shall analyse in detail this model.

D. Massive degenerate neutrinos in Cosmology

In Appendix C we have described the evolution of perturbations, and we saw that the nature of dark matter particles is crucial in determining the way structure formation goes. In spite of the fact that a lot of candidates for CDM particles are being considered (see Ref. Bertone et al. (2005) for a review, there are no experimental detections of such particles at present. From the other hand, neutrinos are the only candidates for DM known to exist.

'Light' neutrinos ($m_\nu \ll 1$ MeV) Dolgov (2002), namely neutrinos that decouple while still in their ultrarelativistic regime (see below), may provide a significant contribution to the energy density of the Universe ($\Omega_\nu \sim 1$). Models with light neutrinos were extensively studied in the eighties; a large literature exists on this subject Bisnovatyi-Kogan and Novikov (1980),Zeldovich and Syunyaev (1980),Doroshkevich and Khlopov (1981),Peebles (1982).

The key prediction of the cosmological model with neutrinos is a cellular structure on large scales (see Fig.3.1). The qualitative drawing of cellular structure of the Universe is represented at Fig.C.1.

Ruffini and collaborators have studied such models with particular attention to the problem of clustering on large scales and its relation to the fractal distribution of matter. In the following, we are going to describe their works in detail.

D.1. Neutrino decoupling

The cosmological evolution of a gas of particles can be split in two very different regimes. At early times, the particles are in thermal equilibrium with the cosmological plasma; this corresponds to the situation in which the rate $\Gamma =< \sigma v n >$ of the reactions supposed to mantain the equilibrium (such as $\nu_e + \bar{\nu}_e \leftrightarrow e^+ + e^- \leftrightarrow 2\gamma$ in the case of electronic neutrinos) is much greater than the expansion rate, given by the Hubble parameter. The gas evolves then through a sequence of thermodynamic equilibrium states, described by the usual Fermi-Dirac statistics:

$$f(p) = \frac{1}{\exp\left[(E(p) - \mu)/k_B T\right] + 1}, \tag{D.1.1}$$

where p, μ and T are the momentum, chemical potential and temperature of neutrinos respectively, and k_B is a Boltzmann constant.

However, as the Universe expands and cools, the collision rate Γ becomes lower than the expansion rate; this means that the mean free path is greater than the Hubble radius, thus we can consider the gas as expanding without collisions. It is customary to describe the transition beetween the two regimes by saying that the gas has decoupled from the cosmological plasma.

D.2. The redshifted statistics

Since in a spatially homegeneous and isotropic Universe, described by the Robertson-Walker metric, the product of the three-momentum $p(t)$ of a free particle times the scale factor $a(t)$ is a constant of the motion:

$$p(t) \cdot a(t) = \text{const}, \tag{D.2.1}$$

each particle in the gas changes its momentum according to this relation. This fact, together with Liouville's theorem, implies that the distribuition function after the decoupling time t_d (defined as the time at which $\Gamma = H$) is given by Ruffini et al. (1983):

$$f(p, t > t_d) = f\left(\frac{a(t)}{a_d}p,\, t_d\right) = \frac{1}{\exp\left[(E\left(\frac{a(t)}{a_d}p\right) - \mu_d)/k_B T_d\right] + 1} \tag{D.2.2}$$

where the subscript d denotes quantities evaluated at the decoupling time.

Now let's turn our attention to the special case of neutrinos with $m_\nu \lesssim 10\,\text{eV}$. The ratio Γ/H, as a function of the cosmological temperature, can be evaluated using quantum field theory Kolb and Turner (1990)

$$\frac{\Gamma}{H} \simeq \left(\frac{T}{1\,\text{MeV}}\right)^3 \tag{D.2.3}$$

as long as $T \gg m$.

Therefore, neutrinos decouple from the cosmological plasma, when $T = T_d \simeq 1\,\text{MeV}$. Since $kT_d \gg mc^2$, many of the particles obey $pc \gg mc^2$ and then, when performing integration over the distribution function (D.2.2), we can safely approximate:

$$f(p, t > t_d) = f\left(\frac{a(t)}{a_d}p,\, t_d\right) \simeq \frac{1}{\exp\left[\left(\frac{a(t)}{a_d}pc - \mu_d\right)/k_B T_d\right] + 1}, \tag{D.2.4}$$

since the tail of the distribution function for which $mc^2 \gg pc$ gives little contribution.

In the following, we will need to compute the mean value of physical quantities over this distribution. It will be useful to consider two limiting regimes, namely the nonrelativistic one and the ultrarelativistic one. They correspond to two approximations for the single particle energy Ruffini et al. (1983):

$$\begin{array}{lll} E \simeq mc^2 & kT \ll mc^2 & \text{NR} \\ E \simeq pc & kT \gg mc^2 & \text{UR} \end{array}$$

We stress the fact that this substitution has to be performed only in the function to be integrated, and not on the distribution function. The approximation (D.2.4) depends only on the fact that the particles are ultrarelativistic at the time of decoupling, and then it is valid even when $kT \ll mc^2$.

Then, with a suitable substitution of variables, all the relevant integrals can be recast in a very simple, dimensionless form:

$$I_n(\xi) \equiv \int_0^\infty \frac{y^n dy}{\exp\left[(y-\xi)\right]+1}, \tag{D.2.5}$$

where $\xi \equiv \mu_d / kT_d$ is the dimensionless chemical potential, or degeneracy parameter. These integrals can be expressed using Riemann zeta and related functions.

D.3. Energy density of neutrinos

The present density parameter of neutrinos can be easily evaluated using the method outlined in the previous section. The energy density is given by:

$$\rho_{\nu+\bar{\nu}}(t_0) = \frac{g}{h_P^3} \int_0^\infty E(p) f(p, t_0)\, d^3p \tag{D.3.1}$$

where g is the number of helicity states and h_P is the Planck constant. By normalization with respect to the critical density $\rho_c = 1.054\, h^2 \cdot 10^4 \frac{\text{eV}}{\text{cm}^3}$, we obtain Ruffini and Song (1986),Ruffini et al. (1988):

$$\Omega_{\nu+\bar{\nu}} h^2 \simeq 1.10 \cdot 10^{-1}\, g\, \frac{m}{10\,\text{eV}}\, A(\xi), \tag{D.3.2}$$

where $A(\xi)$ is defined as follows

$$A(\xi) \equiv \frac{I_2(\xi) + I_2(-\xi)}{2 I_2(0)} = \frac{1}{4\eta(3)} \left[\frac{1}{3} |\xi|^3 + 4\eta(2)|\xi| + 4 \sum_{k=1}^{\infty} (-1)^{k+1} \frac{e^{-k|\xi|}}{k^3} \right], \tag{D.3.3}$$

and $\eta(n)$ is the Riemann eta function of index n.

The term $I_2(-\xi)$ appears because we have to take into consideration the

presence of antiparticles, for which the relation $\xi_{\bar{\nu}} = -\xi_{\nu}$ holds. This result follows from the fact that, if we consider a reaction such as

$$\nu + \bar{\nu} \longleftrightarrow ... \longleftrightarrow \gamma + \gamma \tag{D.3.4}$$

we get that, since the chemical potentials of the initial and final states have to be equal, and the chemical potential of the latter is equal to zero, it follows, that $\xi_{\bar{\nu}} = -\xi_{\nu}$.

D.3.1. Neutrino mass

We now know from neutrino oscillation experiments that neutrino do have mass (see Ref. Maltoni et al. (2004) for a review). It is a remarkable fact that neutrino flavour and mass eigenstates do not coincide, but are instead related by a rotation in flavour space:

$$|\nu_\alpha\rangle = \sum_{i=1}^{3} U_{\alpha i} |\nu_i\rangle \tag{D.3.5}$$

where $\alpha = e, \mu, \tau$ labels flavour eigenstates, while $i = 1, 2, 3$ labels mass eigenstates. The "rotation" matrix $U_{\alpha i}$ is called the neutrino mixing matrix. A great deal of effort is presently being put now in measuring the elements of the mixing matrix and the mass differences, which are the parameters actually probed in oscillation experiments. On the other hand, this kind of experiments do not give any information on the absolute scale of the neutrino mass. In this regard, useful information can be obtained by 1. tritium beta decay experiments, 2. neutrinoless beta decay experiments, 3. cosmological observations.

The tritium β decay experiments are sensitive to the "electron neutrino mass" (this is actually a misnomer since the electron neutrino is not a mass eigenstate and thus does not possess a well definite mass) m_e:

$$m_e = \left(\sum_{i=1}^{3} |U_{ei}|^2 \, m_i^2 \right)^{1/2} . \tag{D.3.6}$$

The present 95% CL bounds are:

$$\begin{aligned} m_e &< 2.05\,\text{eV} \qquad \text{Troitsk experiment Lobashev (2003)} \\ m_e &< 2.3\,\text{eV} \qquad \text{Mainz experiment Kraus et al. (2005)} \end{aligned} \tag{D.3.7}$$

The upcoming KATRIN experiment KATRIN collaboration (2001) is expected to improve this bounds by nearly an order of magnitude, reaching a discovery potential for 0.3-0.35 eV masses.

At the same time, no direct measurements or constraints on muonic and

tauonic neutrino masses exist, although we know from oscillation experiments that the difference between masses should in the sub-eV range. Moreover, it is still unknown, whether neutrinos are Majorana or Dirac particles.

Experiments on neutrinoless double β decay (Aalseth et al. (1999),Klapdor-Kleingrothaus et (2001),Arnaboldi et al. (2005)) are instead sensitive to the "Majorana mass" $m_{\beta\beta}$:

$$m_{\beta\beta} = \left| \sum_{i=1}^{3} U_{ei}^2 m_i \right| \tag{D.3.8}$$

A recent paper Strumia and Vissani (2005) gives the following upper bound at 99% CL:

$$|m_{\beta\beta}| \lesssim 0.6\text{eV}. \tag{D.3.9}$$

Cosmology is mainly sensitive, at least to leading order, to the sum of neutrino masses M_ν:

$$M_\nu = \sum_{i=1}^{3} m_i \tag{D.3.10}$$

We should stress that there is no single limit that can be obtained on M_ν by means of cosmological observables, since the exact result depends of several factor, like the datasets considered, and the theoretical assumptions that are made ("priors"). However, we can summarize the present status as follows:

$$M_\nu \lesssim 0.2 - 2.3\text{eV} \tag{D.3.11}$$

where of course the largest value should be taken as the most conservative one, i.e., the one that is obtained by using only the more robust pieces of data (basically the CMB spectrum) and without making any assumption other than the standard FRW cosmological model. It is worth noting that these bounds are competitive with the ones coming from particle physics experiments. They are also expected to improve by an order of magnitude with the next generation of cosmological observations. For a review on the current limits on neutrino mass from cosmology, and how these will be improved in the future, we refer the reader to the work of Lesgourgues and Pastor Lesgourgues and Pastor (2006).

D.3.2. Chemical potential

First constraints on neutrino degeneracy parameter from BBN were obtained in Doroshkevich et al. (1971),Beaudet and Goret (1976). It was shown later Bianconi et al. (1991) that a small value of ξ_e and large values of $|\xi_{\mu,\tau}|$ simultaneously, can lead to BBN abundances which are consistent with observations. It is found in particular that

$$0 \leq \xi_e \lesssim 1.5, \tag{D.3.12}$$

with the additional constraint $F(\xi_\mu) + F(\xi_\tau) \approx F(10\xi_e)$, where $F(\xi) \equiv \xi^2 + \xi^4/2\pi^2$. This, in particular, implies $|\xi_{\mu,\tau}| \lesssim 10\xi_e$.

Recent data both from BBN and CMBR Orito et al. (2001),Kneller et al. (2001),Hansen et al. (2002),Orito et al. (2002),Hansen et al. (2002) strongly constrain neutrino degeneracy parameters. In the paper Orito et al. (2001) these constraints are surprisingly wide, $\xi_e < 1.4$ and $|\xi_{\mu,\tau}| < 40$. Other papers give essentially stronger constraints using additional assumptions,

$$\begin{array}{l} \xi_e < 0.3 \\ |\xi_{\mu,\tau}| < 2.6. \end{array} \tag{D.3.13}$$

Recently, a very robust albeit less stringent limit has been obtained by the analysis of CMB data Lattanzi et al. (2005):

$$|\xi| \leq 1.1 \tag{D.3.14}$$

where the same limit holds for every flavour.

D.3.3. Neutrino oscillations

When one consider different chemical potentials for all neutrino flavors at the epoch prior to BBN, neutrino oscillations equalize chemical potentials Savage et al. (1991), if there is enough time to relaxation process Abazajian et al. (2002). On the basis of large mixing angle solution of the solar neutrino problem,which is favored by recent data Ahmad et al. (2001), the BBN consideration constrains degeneracy parameters of all neutrino flavors Dolgov et al. (2002):

$$|\xi| \leq 0.07. \tag{D.3.15}$$

However the situation when flavor equilibrium is not achieved before BBN is also possible. Thus in the following we consider quite high values of the degeneracy parameter and assume it is positive without loss of generality.

The main result that comes from oscillations consideration is that masses of different neutrino species are nearly equal: $m_{\nu_e} \simeq m_{\nu_\mu} \simeq m_{\nu_\tau}$.

D.4. The Jeans mass of neutrinos

In neutrino dominated Universe the first possible structure occurs when these particles become nonrelativistic, since at earlier times free streaming erases all perturbations. At this epoch the cosmological redshift has the value Ruffini et al. (1988)

$$1 + z_{nr} = 1.698\ 10^4 \left(\frac{m_\nu}{10eV}\right) A(\xi)^{\frac{1}{2}} B(\xi)^{-\frac{1}{2}}, \tag{D.4.1}$$

where

$$B(\xi) \equiv \frac{I_3(\xi) + I_3(-\xi)}{I_3(0)} = \\ = \frac{1}{48\eta_R(5)} \left[\frac{1}{5}\xi^5 + 8\eta_R(2)\xi^3 + 48\eta_R(4)\xi + 48 \sum_{n=1}^{\infty} (-1)^{n+1} \frac{e^{-n\xi}}{n^5} \right]. \quad \text{(D.4.2)}$$

The basic mechanism of fragmentation of the initial inhomogeneities in an expanding Universe is the Jeans instability described in the previous section.

However, in the calculation of Jeans' length of nonrelativistic collisionless neutrinos, we cannot use the velocity of sound obtained by the classical formula $v_s^2 = dp/d\rho$. In fact, since particles are collisionless, their effective pressure is zero and this would lead to a vanishing Jeans length, meaning that even the smallest perturbation would be unstable. This is not the case, since, in the absence of pressure, another mechanism works against gravitational collapse, namely the free streaming of particles. The characteristic velocity associated with this process is simply the dispersion velocity $\sqrt{< v^2 > /3}$, where the factor 3 comes from averaging over spatial directions. Thus, we have to make the substitution $v_s^2 \rightarrow < v^2 > /3$ Ruffini and Song (1986). The correct expression for $< v^2 >$ can be obtained using the method described above:

$$< v^2 > = \begin{cases} c^2 & z > z_{nr} \\ 12 \frac{\eta_R(5)}{\eta_R(3)} \left(\frac{kT_{\nu 0}}{m_\nu} \right)^2 \frac{B(\xi)}{A(\xi)} & z < z_{nr}, \end{cases} \quad \text{(D.4.3)}$$

where $T_{\nu 0} = 1.97\,\mathrm{K}$ is the present temperature of neutrinos.

As a result, the Jeans mass grows in UR regime and decreases in NR regime Bond et al. (1980). The evolution of Jeans mass of neutrinos for $m_\nu = 2.5\,\mathrm{eV}$ and $\xi = 2.5$ with redshift z is represented at fig.D.1.

It is clear, that for such values of neutrino mass the peak of Jeans mass lay above $10^{17}\,M_\odot$ and the corresponding comoving Jeans length is $\lambda_0 > 100\,\mathrm{Mpc}$. From the other hand, Jeans mass today is still larger, than the mass of massive galaxy $10^{12}\,M_\odot$.

Finally, the maximum value of Jeans mass at the moment (D.4.1) is Ruffini and Song (1986)

$$M_J(z_{nr}) = 1.475\ 10^{17} M_\odot g_\nu^{-\frac{1}{2}} N_\nu^{-\frac{1}{2}} \left(\frac{m_\nu}{10eV} \right)^{-2} A(\xi)^{-\frac{5}{4}} B(\xi)^{\frac{3}{4}}. \quad \text{(D.4.4)}$$

The peak of Jeans mass depending on degeneracy parameter for different

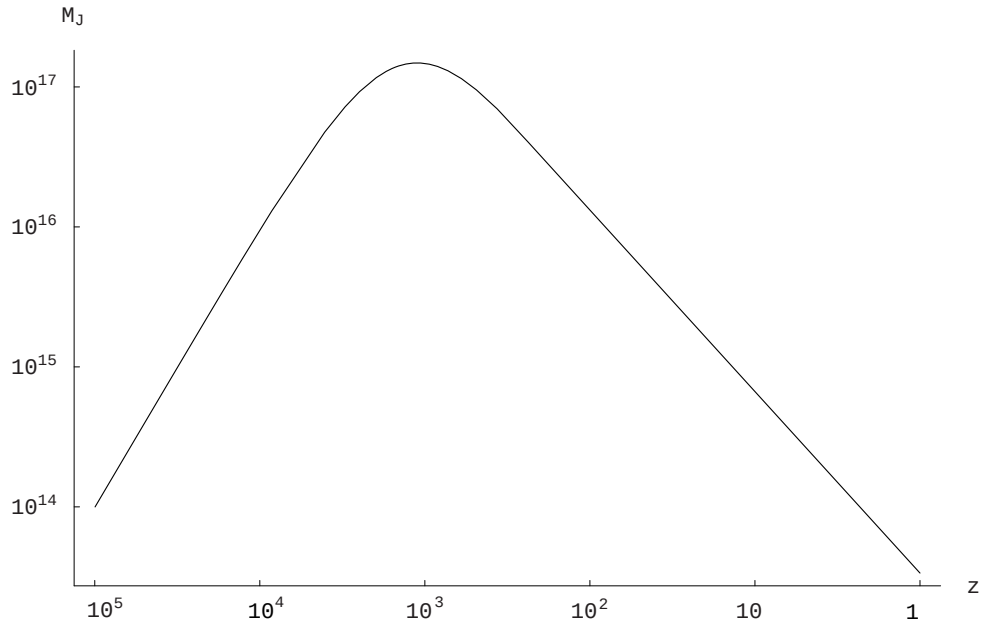

Figure D.1.: The Jeans mass dependence on redshift for neutrinos with mass $m_\nu = 2.5$eV and degeneracy parameter $\xi = 2.5$.

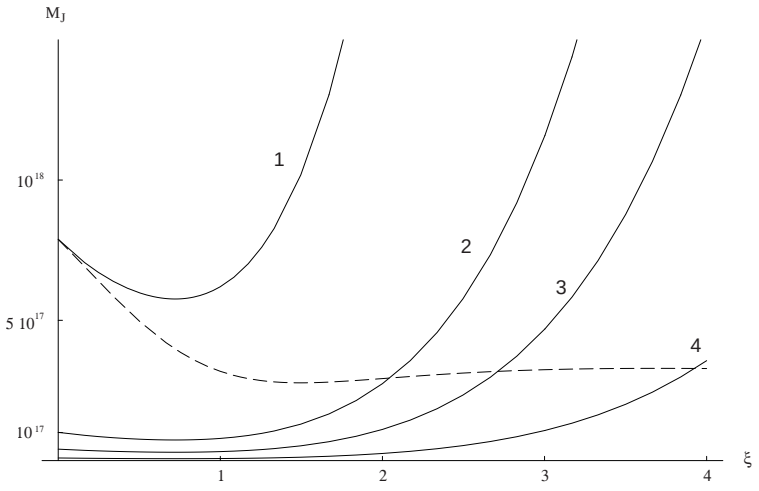

Figure D.2.: The Jeans mass dependence on degeneracy parameter with fixed value of energy density, curves (1-4). Curve (1) corresponds to energy density $\Omega_\nu = 0.11$. Curve (2) corresponds to $\Omega_\nu = 0.3$. Curve (3) represents neutrino energy density $\Omega_\nu = 0.5$ and, finally, curve (4) gives Jeans mass for $\Omega_\nu = 1$. The dashed line represents Jeans mass dependence on degeneracy parameter with fixed neutrino mass $m_\nu = 2.5\,\mathrm{eV}$.

fixed values of energy density as well as with constant mass $m_\nu = 2.5\,\mathrm{eV}$ is shown at Fig.D.2.

By comparing different curves with fixed value of ξ one can find the well known result, that the Jeans mass increases with decreasing of neutrino mass. With growth of degeneracy parameter, however, neutrino mass decreases in the beginning, and its different values correspond to different points at the same curve.

The space above the dashed line at Fig.D.2 represents the region in which the neutrino mass is less than 2.5 eV. It is interesting to note, that this value of m_ν is still sufficient to obtain $\Omega_\nu = 1$ with $\xi \approx 4$.

D.5. Joint constraints on the lepton asymmetry of the Universe and neutrino mass from the Wilkinson Microwave Anisotropy Probe

D.5.1. Introduction

It is a remarkable fact that our observational knowledge of the Universe can be justified in terms of a model, the so-called power-law ΛCDM model, characterized by just six parameters, describing the matter content of our Universe (the physical density of baryons ω_b, the physical density of matter ω_m, the Hubble constant h), the initial conditions from which it evolved (the amplitude A and the spectral index n of the primordial power spectrum) and the optical depth at reionization (τ). In particular, this model provides a good fit to both the cosmic microwave background (CMB) (Spergel et al., 2003) and large scale structure (LSS) data (although in this last case one additional parameter, the bias parameter b, is needed) (Tegmark et al., 2004). Nevertheless, the data leave room for more refined models, described by additional parameters: among them, the spatial curvature, the amplitude of tensor fluctuations, a running spectral index for scalar modes, the equation of state for dark energy, the neutrino fraction in the dark matter component, a non-standard value for the relativistic energy density. All have been considered in previous works. In particular the last two have been studied in order to gain deeper information on the properties of neutrinos (Hannestad, 2002; Spergel et al., 2003; Hannestad, 2003b; Elgaroy and Lahav, 2003; Elgaroy et al., 2002; Allen et al., 2003; Barger et al., 2004; Crotty et al., 2003; Pierpaoli, 2003; Di Bari, 2002, 2003; Barger et al., 2003b; Crotty et al., 2004; Hannestad and Raffelt, 2004; Hannestad, 2003a; Cuoco et al., 2004). Before the measurements of the CMB anisotropy spectrum carried out by the Wilkinson Microwave Anisotropy Probe (WMAP) (Bennett et al., 2003; Hinshaw et al., 2003; Kogut et al., 2003; Page et al., 2003; Peiris et al., 2003; Spergel et al., 2003; Verde et al., 2003), the combined CMB and LSS data yielded the following up-

per bound on the sum of neutrino masses: $\sum m_\nu \leq 3$ eV (Hannestad, 2002). The WMAP precision data allowed to strengthen this limit. Using rather simplifying assumptions, i.e., assuming three thermalized neutrino families all with the same mass and a null chemical potential (thus implying perfect lepton symmetry), the WMAP team found that the neutrino mass should be lower than 0.23 eV (Spergel et al., 2003). This tight limit has been somewhat relaxed to $\sum m_\nu \leq 1$ eV (Hannestad, 2003b) owing to a more careful treatment of the Ly-α data, and its dependence on the priors has been examined (Elgaroy and Lahav, 2003). The LSS data can also be used to put similar constraints, although they are usually weaker. Using the data from the 2 Degree Field Galaxy Redshift Survey (2dFGRS) and assuming "concordance" values for the matter density Ω_m and the Hubble constant h it is found that $\sum m_\nu \leq 1.8$ eV (Elgaroy et al., 2002). A combined analysis of the Sloan Digital Sky Survey (SDSS) and WMAP data gives a similar bound : $\sum m_\nu \leq 1.7$ eV (Tegmark et al., 2004). Quite interestingly, the authors of Ref. (Tegmark et al., 2004) claim that, from a conservative point of view (i.e., making as few assumptions as possible), the WMAP data alone don't give any information about the neutrino mass and are indeed consistent with neutrinos making up the 100% of dark matter. In Allen et al. (2003) it is claimed that the cosmological data favor a non-zero neutrino mass at the 68% confidence limit, while Barger et al. (2004) find the limit $\sum m_\nu < 0.74$.

At the same time, more detailed scenarios with a different structure of the neutrino sector have been studied. The first and more natural extension to the standard scenario is the one in which a certain degree of lepton asymmetry (parameterized by the so-called *degeneracy parameter* ξ, i.e., the dimensionless chemical potential) is introduced (Freese et al., 1983; Ruffini et al., 1983, 1988). Although standard models of baryogenesis (for example those based on $SU(5)$ grand unification models) predict the lepton charge asymmetry to be of the same order of the baryonic asymmetry $B \sim 10^{-10}$, nevertheless there are many particle physics motivated scenario in which a lepton asymmetry much larger than the baryionic one is generated Harvey and Kolb (1981); Dolgov (1992); Foot et al. (1996); Casas et al. (1999); March-Russell et al. (1999); Dolgov et al. (2000); McDonald (2000); Kawasaki et al. (2002); Di Bari and Foot (2002); Yamaguchi (2003); Chiba et al. (2004); Takahashi and Yamaguchi (2004). In some cases, the predicted lepton asymmetry can be of order unity. One of the interesting cosmological implications of a net leptonic asymmetry is the possibility to generate small observed baryonic asymmetry of the Universe (Buchmuller et al., 2004; Falcone and Tramontano, 2001) via the so-called sphaleron process (Kuzmin et al., 1985). The process of Big Bang Nucleosynthesis (BBN) is very sensitive to a lepton asymmetry in the electronic sector, since an excess (deficit) of electron neutrinos with respect to their antiparticles, alters the equilibrium of beta reactions and leads to a lower (higher) cosmological neutron to proton ratio n/p. On the other hand, an asymmetry in the μ or τ sector, even if not influencing directly the beta reactions, can increase the equi-

librium n/p ratio due to a faster cosmological expansion. This can be used to constrain the value of the degeneracy parameter (Bianconi et al., 1991). This leads to the bounds $-0.01 < \xi_e < 0.22$ and $|\xi_{\mu,\tau}| < 2.6$ (Kneller et al., 2001; Hansen et al., 2002).

The effect of a relic neutrino asymmetry on the CMB anisotropy and matter power spectrum was first studied in Ref. (Lesgourgues and Pastor, 1999), and is mainly related to the fact that a lepton asymmetry implies an energy density in relativistic particles larger than in the standard case. The cosmological observables can then be used to constrain this extra energy density, parameterized by the effective number of relativistic neutrino species $N^{\rm eff}$. Although this is somewhat more general than the case of a lepton asymmetry, in the sense that the extra energy density can arise due to other effects as well, nevertheless the case of a non-null chemical potential is not strictly covered by the introduction of $N^{\rm eff}$. This is because the increased relativistic energy density is not the only effect connected to the lepton asymmetry (an additional side effect is for example a change in the Jeans mass of neutrinos (Freese et al., 1983; Ruffini and Song, 1986; Ruffini et al., 1988)). In the hypothesis of a negligible neutrino mass, it has been shown that the WMAP data constrain $N^{\rm eff}$ to be smaller than 9; when other CMB and LSS data are taken into account, the bound shrinks to $1.4 \leq N^{\rm eff} \leq 6.8$ (Crotty et al., 2003; Pierpaoli, 2003). A combined analysis of CMB and BBN data leads to even tighter bounds (Di Bari, 2002, 2003; Hannestad, 2003b; Barger et al., 2003b). A more detailed analysis, in which the effective number of relativistic relics and the neutrino mass are both left arbitrary and varied independently, can be found in Ref. (Crotty et al., 2004). In the same paper, the effect of different mass splittings is also studied. Finally an extension of these arguments to the case in which additional relativistic, low-mass relics (such as a fourth, sterile neutrino or a QCD axion) are present, has been studied in Ref. (Hannestad and Raffelt, 2004).

The goal of this paper is to perform an analysis of the WMAP data using the degeneracy parameter, together with the effective number of relativistic particles, as additional free parameters, in order to put constraints on the lepton number of the Universe. We work in the framework of an extended cosmological model with three thermally distributed neutrino families having all the same mass and chemical potential, plus a certain amount of exotic particles species, considered to be effectively massless. We use the physical neutrino density $\omega_\nu \equiv \Omega_\nu h^2$, the degeneracy parameter ξ and the extra energy density in exotic particles $\Delta N^{\rm eff}_{\rm others}$ as additional parameters that describe the neutrino sector. We perform an analysis in a 8-dimensional parameter space that includes the standard, "core" cosmological parameters.

The paper is organized as follows. After a discussion on the motivations that drive our work in Sec. D.5.2, we shortly review some basic formulae in Sec. D.5.3 and discuss the impact of a non-null degeneracy parameter on the CMB spectrum in Sec. D.5.4. In Sec. D.5.5 we describe the analysis pipeline,

while in Sec. D.5.6 we present our basic results. Finally, we draw our conclusions in Sec. D.5.7.

D.5.2. Motivation for this work

The main motivation for this work comes from the fact that, even though several analyses have been performed which were aimed at putting constraints on the number of effective relativistic degrees of freedom, a statistical analysis of the CMB data aiming to put bounds directly on the degeneracy parameter, instead of on $N^{\rm eff}$, is nevertheless still missing. There are two reasons for this: first of all, in the limit of a vanishing neutrino mass, the increase in $N^{\rm eff}$ is in effect all that is needed to implement the non null chemical potential into the standard model of the evolution of perturbations (Lesgourgues and Pastor, 1999; Ma and Bertschinger, 1995). It is then argued that, since neutrinos with mass smaller than roughly 0.3 eV, being still relativistic at the time of last scattering, would behave as massless, the distinction between ξ and $N^{\rm eff}$ is no more relevant in this case for what concerns their effect on the CMB anisotropy spectrum. Although this is certainly true, it is our opinion that this does not allow to neglect *a priori* the difference between the two parameters. One reason is that the most conservative bound on neutrino mass, coming from the tritium beta decay experiments, reads $m_\nu < 2.2$ eV (at the 2σ level) (Weinheimer et al., 1999; Bonn et al., 2002), that is quite higher than the value of 0.3 eV quoted above. The main evidences for a neutrino mass in the sub-eV range come, in the field of particle physics, from the experiments on neutrinoless double beta decay (Klapdor-Kleingrothaus et al., 2001, 2004), whose interpretation depends on assumptions about the Majorana nature of neutrinos and on the details of the mixing matrix. Other indications of a sub-eV mass come, as stated above, from cosmology and in particular from the power spectrum of anisotropies, but since we want to keep our results as much as possible independent from other analyses, we should not use information on neutrino mass derived from the previous analyses of the CMB data. Moreover, let us note that CMB data analyses are often refined using the results from LSS experiments. Since the structure formation, starting close to the epoch of matter-radiation equality, goes on until very late times, even very light neutrinos (in the range $10^{-3} \div 0.3$ eV) cannot be considered massless for the purpose of evaluating their effect on the matter power spectrum. This means in particular that using $N^{\rm eff}$ would lead to overlook the change in the free streaming length and in the Jeans mass of neutrinos due to the increased velocity dispersion (Lattanzi et al., 2003). It is then our opinion that the use of $N^{\rm eff}$, even if correct with respect to the interpretation of CMB data, precludes the possibility of correctly implementing the LSS data as a subsequent step in the analysis pipeline.

The second point against the cosmological significance of the degeneracy

parameter is related to the constrain from BBN. It was recently shown that, if the Large Mixing Angle (LMA) solution to the solar neutrino problem is correct (as the results of the KamLAND experiment suggest (Eguchi et al., 2003)), then the flavor neutrino oscillations equalize the chemical potentials of e, μ and τ neutrinos prior to the onset of BBN, so that a stringent limit $\xi \lesssim 0.07$ actually applies to all flavours (Dolgov et al., 2002; Abazajian et al., 2002; Wong, 2002). This would constrain the lepton asymmetry of the Universe to such small values that it could be safely ignored in cosmological analyses. However, the presence of another relativistic particle or scalar field would make these limits relax (Barger et al., 2003a), while the effect of the mixing with a light sterile neutrino, whose existence is required in order to account for the results of the Liquid Scintillation Neutrino Detector (LSND) experiment (Aguilar et al., 2001), is still unclear (Abazajian et al., 2002). Moreover, it has been recently shown that a hypothetical neutrino-majoron coupling can suppress neutrino flavor oscillations, thus reopening a window for a large lepton asymmetry (Dolgov and Takahashi, 2004a,b). For all these reasons, we judge it is interesting to study if CMB data alone can constraint or maybe even rule out such exotic scenarios.

D.5.3. Basic formulae

It is customary in cosmology to call ultrarelativistic (or simply relativistic) a species x that decouples from the photon bath at a temperature T_d such that its thermal energy is much larger than its rest mass energy: $k_B T_d \gg m_x c^2$.

Owing to Liouville's theorem, the distribution function in momentum space $f_x(p\,;\,T_x,\xi_x)$ of the species x is given, after decoupling, by (we shall use all throughout the paper units in which $c = \hbar = k_B = 1$):

$$f_x(p\,;\,T_x,\xi_x) = \frac{g_x}{(2\pi)^3}\left[\exp\left(\frac{p}{T_x} - \xi_x\right) \pm 1\right]^{-1}, \tag{D.5.1}$$

where $\xi \equiv \mu_d/T_d$ is the dimensionless chemical potential, often called degeneracy parameter, the sign $+\,(-)$ corresponds to the case in which the x's are fermions (bosons), g is the number of quantum degrees of freedom, and the temperature T evolves in time as the inverse of the cosmological scale factor a, so that $T(t)\cdot a(t) = \text{const}$.

The energy density of the x's at a given temperature is readily calculated:

$$\rho_x(T_x,\xi) = \int E(p)\, f(p\,;\,T_x,\xi_x) d^3\vec{p} = \\ = \frac{g_x}{2\pi^2}\int_0^\infty p^2\sqrt{p^2+m_x^2}\, f(p\,;\,T_x,\xi_x) dp. \tag{D.5.2}$$

Using the dimensionless quantities $y \equiv p/T$ and $\beta \equiv m_x/T$, the expression

for the energy density can be put in the form:

$$\rho_x(T_x, \xi_x) = \frac{g_x}{2\pi^2} T_x^4 \int_0^\infty dy\, y^2 \frac{\sqrt{y^2+\beta^2}}{\exp(y-\xi_x)\pm 1}. \tag{D.5.3}$$

We stress the fact that a temperature dependence is still present in the integral through the term β. However, the temperature dependence disappear from the integral in two notable limits, the ultrarelativistic (UR) and non-relativistic (NR) one, corresponding respectively to the two opposite cases $\beta \ll 1$ and $\beta \gg 1$ (Ruffini et al., 1983). Then, defining

$$J_n^\pm(\xi) \equiv \left(\int_0^\infty \frac{y^n}{e^{y-\xi}\pm 1} dy\right)\left(\int_0^\infty \frac{y^n}{e^y \pm 1} dy\right)^{-1}, \tag{D.5.4}$$

so that $J_n^\pm(0) = 1$, we have

$$\rho_x(T_x, \xi_x) = \begin{cases} \begin{pmatrix} 1 \\ 7/8 \end{pmatrix} g_x \frac{\pi^2}{30} J_3^\pm(\xi_x) T_x^4 & \text{UR} \\ \begin{pmatrix} 1 \\ 3/4 \end{pmatrix} g_x \frac{\zeta(3)}{\pi^2} m_x J_2^\pm(\xi_x) T_x^3 & \text{NR} \end{cases} \tag{D.5.5}$$

where the upper and lower values in parentheses in front of the expression in the right-hand side hold for bosons and fermions respectively, and $\zeta(n)$ is the Riemann Zeta function of order n.

It is useful to express $\rho_x(t)$ in terms of the present day energy density of the cosmic background photons:

$$\rho_x(t) = \begin{pmatrix} 1 \\ 7/8 \end{pmatrix} \left[\frac{g_x}{2}\left(\frac{T_x^0}{T_\gamma^0}\right)^4 J_3^\pm(\xi_x)\right] \rho_\gamma^0 (1+z)^4 \equiv$$

$$\equiv g_x^{\text{eff}} \rho_\gamma^0 (1+z)^4, \tag{D.5.6}$$

having defined an effective number of relativistic degrees of freedom g_x^{eff} as

$$g_x^{\text{eff}} \equiv \frac{g_x}{2} \begin{pmatrix} 1 \\ 7/8 \end{pmatrix} \cdot \left[\left(\frac{T_x^0}{T_\gamma^0}\right)^4 J_3^\pm(\xi_x)\right]. \tag{D.5.7}$$

It is often the case that one has to consider a fermion species x together with its antiparticle $\bar{x}$, the most notable example being the relic neutrinos and antineutrinos. In chemical equilibrium, the relation $\xi_x = -\xi_{\bar{x}}$ holds owing to the conservation of chemical potential, as can be seen considering the reac-

tion:

$$x + \bar{x} \longleftrightarrow \ldots \longleftrightarrow \gamma + \gamma \tag{D.5.8}$$

and noting that the chemical potential in the final state vanishes (Weinberg, 1972). This relation holds for neutrinos and antineutrinos in several cosmological scenarios. There are some exceptions to this, most notably early Universe scenarios in which lepton asymmetry is generated (Foot and Volkas, 1997) or destroyed (Abazajian et al., 2005) by active-sterile neutrino oscillations at low temperatures. However, we shall assume all throughout the paper that the relation $\xi_\nu = -\xi_{\bar{\nu}}$ holds.

It can then be shown that

$$g^{\rm eff}_{x+\bar{x}} = g^{\rm eff}_x + g^{\rm eff}_{\bar{x}} = \\ = \frac{7}{8} g_x \left[1 + \frac{30}{7}\left(\frac{\xi_x}{\pi}\right)^2 + \frac{15}{7}\left(\frac{\xi_x}{\pi}\right)^4\right]\left(\frac{T^0_x}{T^0_\gamma}\right)^4, \tag{D.5.9}$$

where the factor between square parentheses can be recognized as what it is often quoted as the contribution of a non-vanishing chemical potential to the effective number of relativistic species $N^{\rm eff}$.

The definitions introduced above can be easily extended to the case when several ultra-relativistic species x_i are present:

$$g^{\rm eff} \equiv \sum_i g^{\rm eff}_i, \tag{D.5.10}$$

where photons are excluded from the summation. This means that, since $g^{\rm eff}_\gamma = g_\gamma = 1$, the actual number of relativistic degrees of freedom is $(1 + g^{\rm eff})$.

The total density of ultrarelativistic particles at a given time is thus:

$$\rho_{\rm rad} = \rho^0_\gamma \left(1 + g^{\rm eff}\right)(1+z)^4. \tag{D.5.11}$$

Finally we can use this expression to find the dependence on $g^{\rm eff}$ of the redshift of radiation-matter equality z_{eq} (the subscripts b and CDM stands for baryons and cold dark matter respectively):

$$1 + z_{eq} = \frac{\rho^0_b + \rho^0_{\rm CDM}}{\rho^0_\gamma}\left(1 + g^{\rm eff}\right)^{-1}. \tag{D.5.12}$$

So, the larger is the energy density of ultra-relativistic particles in the Universe, parameterized by the effective number of degrees of freedom $g^{\rm eff}$, the smaller z_{eq} will be, i.e., the later the equality between radiation and matter will occur. In other words, supposing that the density in non-relativistic particles (baryons + CDM) is well known and fixed, having more relativistic de-

grees of freedom will shift z_{eq} closer to us and to the CMB decoupling.

In the standard cosmological scenario, the only contribution to the energy density of relativistic particles other than photons is the one due to the three families of standard neutrinos, with zero chemical potential. The ratio of the neutrino temperature to the photon temperature is $T_\nu^0/T_\gamma^0 = (4/11)^{1/3}$, due to the entropy transfer that followed the electron-positron annihilation, shortly after neutrino decoupling. Then

$$g^{\rm eff} = \frac{7}{8}\left(\frac{4}{11}\right)^{4/3} N_\nu \simeq 0.23\, N_\nu, \tag{D.5.13}$$

where $N_\nu = 3$ is the number of neutrino families. The energy density in a single neutrino species is:

$$\rho_\nu^{\rm std} = \frac{7\pi^2}{120}\left(\frac{4}{11}\right)^{4/3} T_\gamma^4. \tag{D.5.14}$$

However, several mechanisms that could increase (or even decrease) the energy density of relativistic particles have been proposed. In the presence of some extra relics (such as sterile neutrinos, majorons, axions, etc.) the energy density of radiation would obviously increase. A non-zero chemical potential for neutrinos or an unaccounted change of ρ_γ, due for example to particle decays that increase the photon temperature, would produce the same result. In all cases the effect is the same: a change in $g^{\rm eff}$, as it can be seen by looking at eq. (D.5.7). It is usual in the literature to parameterize the extra energy density by introducing an effective number of neutrino families $N^{\rm eff}$, defined as:

$$N^{\rm eff} \equiv \frac{\sum_i \rho_i}{\rho_\nu^{\rm std}}, \tag{D.5.15}$$

where again the sum runs over all ultrarelativistic species with the exceptions of photons. It is clear from this definition that $N^{\rm eff}$ is actually the energy density in ultrarelativistic species (apart from photons) normalized to the energy density of a single neutrino species with zero chemical potential and standard thermal history. It is easy to show that a relation formally similar to (D.5.13) holds in the non-standard scenario:

$$g^{\rm eff} = 0.23\, N^{\rm eff}. \tag{D.5.16}$$

In addition, it should be noted that even in the standard scenario $N^{\rm eff} \neq N_\nu = 3$, but instead $N^{\rm eff} \simeq 3.04$. This is due to the fact that neutrino decoupling is not instantaneous, so that neutrino actually share some of the entropy transfer of the e^+e^- annihilation, on one side, and to finite temperature quantum electrodynamics corrections on the other (Dolgov et al., 1997; Mangano et al., 2002).

It is also useful to introduce the effective number of additional relativistic species $\Delta N^{\rm eff}$ defined as:

$$\Delta N^{\rm eff} \equiv N^{\rm eff} - 3.04\,, \tag{D.5.17}$$

so that $\Delta N^{\rm eff} = 0$ in the standard scenario. Please note that $\Delta N^{\rm eff}$ can also be negative, for example in very low reheating scenarios (Giudice et al., 2001).

In this paper we shall consider a scenario in which the radiation content of the Universe at the time of radiation-matter equality is shared among photons, three neutrino families with standard temperature but possibly non-zero chemical potential, and some other relic particle. We shall suppose that the presence of the latter can be completely taken into account through its effect on $N^{\rm eff}$. This is true if the species has been in its ultrarelativistic regime for the most part of the history of the Universe. The presence of this extra relic is required for our analysis, in order to circumvent the equalization of neutrino chemical potentials, as explained at the end of section D.5.2. We also assume that the degeneracy parameters for neutrinos and antineutrinos are equal and opposite, and that e, μ and τ neutrinos all have the same chemical potential.

The extra energy density can thus be split into two distinct contributions, the first due to the non-zero degeneracy parameter of neutrinos and the second due to the extra relic(s):

$$\Delta N^{\rm eff} = \Delta N_\nu^{\rm eff}(\xi) + \Delta N_{\rm others}^{\rm eff}. \tag{D.5.18}$$

Following our assumptions, $\Delta N_\nu^{\rm eff}$ can be expressed as a function of the chemical potential only:

$$\Delta N_\nu^{\rm eff}(\xi) = 3\left[\frac{30}{7}\left(\frac{\xi_x}{\pi}\right)^2 + \frac{15}{7}\left(\frac{\xi_x}{\pi}\right)^4\right]. \tag{D.5.19}$$

D.5.4. Effect of a non-null chemical potential

As anticipated above, the main effect connected to the presence of a non-vanishing degeneracy parameter, is an increase in $g^{\rm eff}$ (or, equivalently, in $N^{\rm eff}$). The presence of this extra number of effective relativistic degrees of freedom can in principle be detected from observations of the CMB radiation. The shift of matter-radiation equality has important consequences for the CMB anisotropy spectrum, these being due to the larger amplitude of the oscillations that enter the horizon during the radiation dominated phase, and to a larger early integrated Sachs-Wolfe (ISW) effect. However these effects, basically due to the speeding up of the cosmological expansion, can be similarly produced by the variation of other cosmological parameters, for example by a smaller CDM density.

Moreover since the change in the redshift of matter-radiation equality depends on the ultra-relativistic species only through the quantity $g^{\rm eff}$, it cannot be used to distinguish between the different species (i.e., it is "flavor blind"), nor to understand if the excess energy density is due to the presence of some unconventional relic, to an extra entropy transfer to photons, or to a non-null chemical potential (i.e., to a lepton asymmetry), or maybe to all of the previous.

However ultrarelativistic particles, other than changing the background evolution, have an effect even on the evolution of perturbations, as it was pointed out in (Bashinsky and Seljak, 2004) with particular regard to the case of neutrinos. First of all, the high velocity dispersion of ultrarelativistic particles damps all perturbations under the horizon scale. Second, the anisotropic part of the neutrino stress-energy tensor couples with the tensor part of the metric perturbations. It was shown in (Weinberg, 2004) that this reduces the amplitude squared of tensor modes by roughly 30% at small scales. Finally, the authors of Ref. (Bashinsky and Seljak, 2004) claimed that the perturbations of relativistic neutrinos produce a distinctive phase shift of the CMB acoustic oscillations. These effects can thus be used to break the degeneracy between $g^{\rm eff}$ and other parameters. It remains to establish whether they can be used to break the degeneracy between the different contributions to $g^{\rm eff}$ or not. Even without performing a detailed analysis, it can be seen by looking at the relevant equations in Ref. (Bashinsky and Seljak, 2004) and (Weinberg, 2004), that both the absorption of tensor modes and the phase shift depend on the quantity $f_\nu \equiv \rho_\nu/(\rho_\gamma + \rho_\nu)$. The effect of free streaming, even if more difficult to express analytically, is also mainly dependent on the value of f_ν (Hu et al., 1998). If we consider the case where the three standard neutrinos are the only contribution to the radiation energy density other than photons, but we allow for the possibility of a non-vanishing chemical potential or for a different T_ν^0/T_γ^0 ratio, we see again that the changes in the shape of the CMB anisotropy spectrum depend only on $g^{\rm eff}$ as whole, as long as eq. (D.5.6) retains its validity, i.e., as long as neutrinos are in their ultra-relativistic regime. Even considering the presence of some additional relic particle x does not seem to change this picture. Supposing that the other ultrarelativistic particles behave as neutrinos for what concerns the effects under consideration, we can argue that in all cases the relevant quantity is $f_x \equiv \rho_x/\rho_{\rm rad}$, so that we are again lead to the conclusions that $g^{\rm eff}$ is the only relevant parameter. This means, for example, that in the case of neutrinos with mass less than ~ 0.3 eV, so that they stay ultrarelativistic until the time of last scattering and for some time after, the effect on CMB perturbations is exactly the same of massless neutrinos, and every change in their temperature or chemical potential, as even the presence of an additional, sterile neutrino, is absorbed in $g^{\rm eff}$ (moreover, we don't have obviously any possibility to extract information about their mass).

However the picture changes when considering neutrinos (or other relic particles) that go out from the ultrarelativistic regime before matter-radiation decoupling. If the neutrino mass is larger than $\sim$ 0.3 eV, the effect of its finite mass is felt by the perturbations that enter the horizon after neutrinos have gone out from the ultrarelativistic regime, because from some point on the evolution the energy density will be given no more by the approximate formula (D.5.6), but instead by eq. (D.5.2) that contains a dependence on mass through the term β. A side effect of this is that it will not be possible to single out the dependence of ρ from T and ξ as an overall factor, so that these two contributions become distinguishable.

Let us make this more clear with an example. Consider a gravitational wave entering the horizon after neutrinos became non-relativistic, but before matter-radiation decoupling. This wave will be absorbed, according to (Weinberg, 2004), proportionally to ρ_ν. On the other hand the free streaming length of neutrinos will vary according to the velocity dispersion $< v^2 >$ (Freese et al., 1983; Ruffini and Song, 1986). The key point is that, for a gas of non-relativistic particles, ρ_ν and $< v^2 >$ will depend on T_ν and ξ_ν in different ways, so that measuring independently the absorption factor and the free streaming length, it would be possible at least in principle to obtain the values of T_ν and ξ_ν without any ambiguity left.

What we have just said is even more true with respect to the LSS data, since even neutrinos with mass greater than 10^{-3} eV are in their non-relativistic regime during the late stages of the process of structure formation. We conclude then by stressing that one should be careful when parameterizing the lepton asymmetry by means of an effective number of degrees of freedom.

D.5.5. Method

We used the `CMBFAST` code (Seljak and Zaldarriaga, 1996), modified as described in (Lesgourgues and Pastor, 1999) in order to account for a non vanishing chemical potential of neutrinos, to compute the temperature (TT) and polarization (TE) CMB spectra for different combinations of the cosmological parameters. As a first step, we added three more parameters, namely the effective number of additional relativistic species $\Delta N^{\rm eff}_{\rm others}$, the neutrino degeneracy parameter ξ (both defined in Sec. D.5.3) and the neutrino physical energy density $\omega_\nu \equiv \Omega_\nu h^2$ to the standard six-parameters ΛCDM model that accounts in a remarkably good way for the WMAP data. As anticipated above, $\Delta N^{\rm eff}_{\rm others}$ accounts only for the extra energy density due to the presence of additional relic relativistic particles other than the three Standard Model neutrinos. We shall refer to the (ω_ν, ξ, $\Delta N^{\rm eff}_{\rm others}$) subspace as the "neutrino sector" of the parameter space (although, as we have just noticed, $\Delta N^{\rm eff}_{\rm others}$ does not refer directly to neutrinos).

With the above mentioned choice of the parameters we can make a con-

sistency check to our results, by verifying that imposing the priors $\xi = 0$, $\omega_\nu = 0$ and $\Delta N^{\rm eff}_{\rm others} = 0$, we obtain results that are in agreement with the ones of the WMAP collaboration. Moreover, by choosing a sufficiently wide range for the variation of the three additional parameters, we can check how much their introduction affects the estimation of the best-fit values of the core parameters. Thus we choose to use the following parameters: the physical baryon density $\omega_b \equiv \Omega_b h^2$, the total density of non relativistic matter $\omega_m \equiv (\Omega_b + \Omega_{\rm CDM})h^2$, the scalar spectral index n, the optical depth to reionization τ, the overall normalization of the CMB spectrum A, the physical neutrino density $\omega_\nu = \Omega_\nu h^2$, the neutrino degeneracy parameter ξ and the extra energy density in non-standard relics $\Delta N^{\rm eff}_{\rm others}$. We will be considering the scenario in which the three standard model neutrinos have all the same mass and chemical potential. We take the chemical potential to be positive (this corresponds to an excess of neutrinos over antineutrinos), but since the effects on the CMB do not depend on the sign of ξ, we quote the limits that we obtain in terms of its absolute value. We do not include as a free parameter the Hubble constant H_0, whose degeneracy with the effective number of relativistic degrees of freedom and with the neutrino mass has been studied in previous works (Elgaroy and Lahav, 2003). Instead we decided, according to the recent measurements of Hubble Space Telescope (HST) Key Project (Freedman et al., 2001), to assume that $h = 0.72$. Moreover, we restrict ourselves to the case of a flat Universe, so that the density parameter of the cosmological constant Ω_Λ is equal to $1 - (\omega_m + \omega_\nu)/h^2$. We are thus dealing with a 8-dimensional parameter space.

Let us discuss in a bit more detail the way we deal with priors in the neutrino sector of parameter space, i.e., with information coming from other observations, and in particular from BBN. As we have stressed in section D.5.2, the standard BBN scenario, together with the equalization of chemical potentials, constraints the neutrino degeneracy parameter to values lower than the ones considered in this paper; on the other hand this conclusion possibly does not hold in non-standard scenarios where additional relativistic relics are present. However, even non-standard scenarios of this kind usually single out some preferred region in parameter space. At the present, several non-standard scenarios that can account for the observed Helium abundance exist (see for example Refs. (Di Bari, 2002) and (Di Bari, 2003)) so that we adopt a conservative approach, and choose not to impose any prior on the neutrino sector, other than the ones that emerge "naturally" as a consequence of our choice of parameters. Anyway, this does not preclude the possibility of successively using the BBN information: in fact once the likelihood function in the neutrino sector has been calculated, it can be convolved with the relevant priors coming from non-standard BBN scenarios.

We span the following region in parameter space: $0.020 \leq \omega_b \leq 0.028$, $0.10 \leq \omega_m \leq 0.18$, $0.9 \leq n \leq 1.10$, $0 \leq \tau \leq 0.3$, $0.70 \leq A \leq 1.10$, $0 \leq \omega_\nu \leq 0.30$, $0 \leq |\xi| \leq 2.0$, $0 \leq \Delta N^{\rm eff}_{\rm others} \leq 2.0$. We shall call this our "(5+3) parameter

space". In order to obtain the likelihood function $\mathcal{L}(\omega_b, \omega_m, n, \tau, A, \omega_\nu, \xi, \Delta N^{\rm eff}_{\rm others})$ in this region, we sample it over a grid consisting of 5 equally spaced points in each dimension. For each point on our grid, corresponding to a combination of the parameters, we compute the likelihood relative to the TT (Hinshaw et al., 2003) and TE (Kogut et al., 2003) angular power spectrum observed by WMAP, using the software developed by the WMAP collaboration (Verde et al., 2003) and kindly made publicly available at their website[1]. To obtain the likelihood function for a single parameter, we should marginalize over the remaining ones. However for simplicity we approximate the multi-dimensional integration required for the marginalization procedure with a maximization of the likelihood, as it is a common usage in this kind of likelihood analysis. This approximation relies on the fact that the likelihood for cosmological parameters is supposed to have a gaussian shape (at least in the vicinity of its maximum) and that integration and maximization are known to be equivalent for a multivariate Gaussian distribution.

According to Bayes' theorem, in order to interpret the likelihood functions as probability densities, they to be inverted through a convolution with the relevant priors, representing our knowledge and assumptions on the parameters we want to constrain. Here we shall assume uniform priors, i.e. we will assume that all values of the parameters are equally probable.

For each of the core parameters, we quote the maximum likelihood value (which we shall refer to also as the "best-fit" value) over the grid and the expectation value over the marginalized distribution function. We quote also the best chi square value χ^2_0 (we recall that $\chi^2 \equiv -2\ln\mathcal{L}$) divided by the number of degrees freedom, that is equal to the number of data (for WMAP, this is 1348) minus the number of parameters. For what concerns the parameters of the neutrino sector, we quote the maximum likelihood and the expectation value as well, and in addition we report a 2σ confidence interval. Using a Bayesian approach, we define the 95% confidence limits as the values at which the marginalized likelihood is equal to $\exp[-(\chi^2_0 - 4)/2]$, i.e., the values at which the likelihood is reduced by a factor $\exp(2)$ with respect to its maximum value [2]. There is one exception to this procedure, namely, when the maximum likelihood value for a parameter that is positively defined (such as ω_ν or the absolute value of ξ), let us call it θ, is equal to zero. In this case, instead than computing the expectation value, we just give an upper bound. In order to do this, we compute the cumulative distribution function $\mathcal{C}(\theta) = \left(\int_0^\theta \mathcal{L}(\bar\theta)d\bar\theta\right) / \left(\int_0^\infty \mathcal{L}(\bar\theta)d\bar\theta\right)$ and quote as the upper limit at the 95% confidence level the value of θ at which $\mathcal{C}(\theta) = 0.95$.

[1] http://lambda.gsfc.nasa.gov/

[2] The 95% confidence level defined in this way is not in general equal to the 2σ region, defined computing the variance of the probability distribution. However, the two are equal for a gaussian probability density. As we shall see, almost all the marginalized distribution have a nearly gaussian shape. When it is not so, we shall point this out.

Once we have obtained constraints on ω_ν, ξ and $\Delta N^{\rm eff}_{\rm others}$, we translate them to limits on the neutrino mass m_ν, the lepton asymmetry L and the extra number of effective relativistic species $\Delta N^{\rm eff}$, using eqs. (D.5.18) and (D.5.19) together with the following relations (Freese et al., 1983; Ruffini and Song, 1986; Lattanzi et al., 2003):

$$\Omega_\nu h^2 = \sum_\nu \frac{m_\nu F(\xi_\nu)}{93.5\,\mathrm{eV}}, \tag{D.5.20}$$

$$L \equiv \sum_\nu \frac{n_\nu - n_{\bar\nu}}{n_\gamma} = \\ = \frac{1}{12\zeta(3)} \left[\sum_\nu \left(\xi^3 + \pi^2 \xi \right) \left(\frac{T^0_\nu}{T^0_\gamma} \right)^3 \right], \tag{D.5.21}$$

where

$$F(\xi) \equiv \frac{2}{3\zeta(3)} \left[\sum_{k=1}^{\infty} (-1)^{k+1} \frac{e^{+k\xi} + e^{-k\xi}}{k^3} \right] = \\ = \frac{1}{3\zeta(3)} \left[\frac{1}{3}\xi^3 + \frac{\pi^2}{3}\xi + 4 \sum_{k=1}^{\infty} (-1)^{k+1} \frac{e^{-k\xi}}{k^3} \right]. \tag{D.5.22}$$

D.5.6. Results and discussion

We start our analysis by looking at the effect of the introduction of the additional parameters to the estimation of the core parameters (ω_b, ω_m, n, τ, A). First of all, we check that imposing the priors $\xi = 0$, $\omega_\nu = 0$ and $\Delta N^{\rm eff}_{\rm others} = 0$ our results are in good agreement with the ones of the WMAP collaboration (we should refer to the values quoted in Table I of Ref. (Spergel et al., 2003)). The mean and maximum likelihood values that we obtain for each parameter are summarized in Table D.1. We see that in all cases our results lie within the 68% confidence interval of WMAP expected values. Then we remove the prior on ω_ν, while still retaining the ones on ξ and $\Delta N^{\rm eff}_{\rm others}$. The maximum likelihood model has still $\omega_\nu = 0$. The best-fit values of the core parameters are left unchanged, and the same happens for the best-fit χ^2, thus suggesting that a non-zero ω_ν is not required in order to improve the goodness of fit. The results for the core parameters are summarized in Table D.2.

Finally, we compute the likelihood over our whole parameter space. The results for the core parameters are summarized in Table D.3. The maximum

Table D.1.: Core Parameters with priors: $\xi = 0$, $\Omega_\nu = 0$, $\Delta N^{\rm eff}_{\rm others} = 0$

Parameter	Mean	Likelihood
Baryon density, ω_b	0.024	0.024
Matter density, ω_m	0.15	0.16
Hubble constant, h (fixed)	0.72	0.72
Spectral index, n	1.00	1.00
Optical depth, τ	0.13	0.075
Amplitude, A	0.8	0.8
χ^2/ν		1437/1343

Table D.2.: Core Parameters with priors: $\xi = 0$, $\Delta N^{\rm eff}_{\rm others} = 0$

Parameter	Mean	Likelihood
Baryon density, ω_b	0.024	0.024
Matter density, ω_m	0.15	0.16
Hubble constant, h (fixed)	0.72	0.72
Spectral index, n	1.00	1.00
Optical depth, τ	0.13	0.075
Amplitude, A	0.8	0.8
χ^2/ν		1437/1342

Table D.3.: Core Parameters with no neutrino priors

Parameter	Mean	Likelihood
Baryon density, ω_b	0.023	0.022
Matter density, ω_m	0.14	0.14
Hubble constant, h (fixed)	0.72	0.72
Spectral index, n	0.98	0.95
Optical depth, τ	0.12	0.075
Amplitude, A	0.8	0.7
χ^2/ν		1431/1340

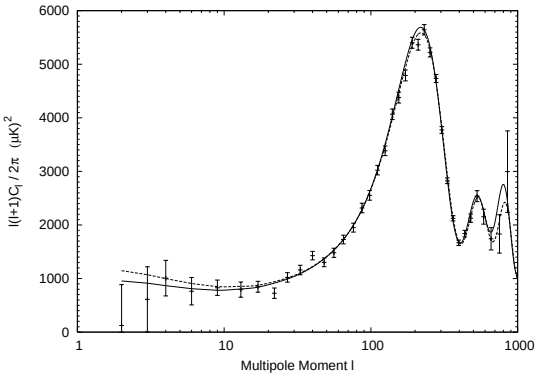

Figure D.3.: Comparison between the best-fit power spectrum obtained assuming the priors $\xi = 0, \Delta N^{\rm eff}_{\rm others} = 0$ (solid line) and without such prior (dashed line). The points are the WMAP data on the temperature angular power spectrum (Hinshaw et al., 2003).

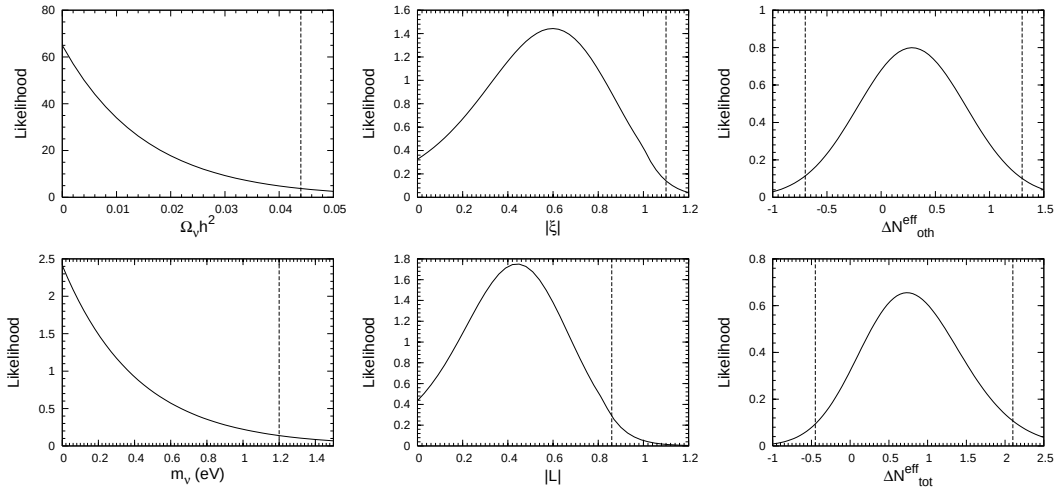

Figure D.4.: Likelihood functions for ω_ν, $|\xi|$, $\Delta N^{\rm eff}_{\rm others}$ and for the derived parameters $|L|$, m_ν and $\Delta N^{\rm eff}$, obtained as a result of the analysis in (5+3) parameter space. The dotted lines bound the 95% confidence interval. The functions are normalized so that their integral is equal to unity.

likelihood model over the grid has $(\omega_b, \omega_m, n, \tau, A, \omega_\nu, \xi, \Delta N^{\rm eff}_{\rm others}) =$, and $(0.022, 0.14, 0.95, 0.075, 0.7, 0, 0.5, 0)$. We see that this time, the best fit values for the five core parameters are slightly changed with respect to the standard case. The changes in ω_m and n could seem strange at a first sight, since intuitively one would expect the opposite behaviour, i.e., a change to larger values for both, because a larger ω_m could keep the time of matter-radiation equality, while a larger n would increase the power on small scales thus leaving more room for neutrino free streaming. This is because the goodness of fit of a particular model with respect of the WMAP data is mainly determined

by its ability to fit the first and second peak. Increasing together ω_m, n, ξ and $\Delta N^{\rm eff}_{\rm others}$ would increase the height of the first peak that can be then lowered back by decreasing the overall amplitude A. We show in fig. D.3 a comparison between the best-fit spectrum in the ($\xi = 0$, $\Delta N^{\rm eff}_{\rm others} = 0$) subspace with the best-fit spectrum on the whole space.

Now let us turn our attention to the neutrino sector of parameter space. The best-fit model over the ($\xi = 0$, $\Delta N^{\rm eff}_{\rm others} = 0$) subspace of the grid has $\omega_\nu = 0$, and the χ^2 changes from 1437 to 1541 when going from $\omega_\nu = 0$ to the next value in our grid, $\omega_\nu = 0.075$. We can compute an upper bound for ω_ν, but since the region in which $\mathcal{L}(\omega_\nu)$ significantly differs from zero is all comprised between the first two values in our grid $\{0, 0.075\}$, the result is rather dependent from the particular interpolation scheme we choose. Using a simple, first order interpolation scheme, we find the bound $\omega_\nu < 0.0045$ (95% CL), corresponding to $m_\nu < 0.14$ eV, while using higher order interpolation schemes the bound weakens up to $\omega_\nu < 0.015$ ($m_\nu < 0.47$ eV). This result should then be taken with caution and we shall simply consider it as an indication that, although we are using a grid-based method with a rather wide grid spacing instead than the more sophisticated Markov Chain Monte Carlo (MCMC) method (Christensen et al., 2001; Lewis and Bridle, 2002), we basically obtain the same results of the WMAP collaboration, namely, $\omega_\nu \leq 0.0072$ (Spergel et al., 2003), when imposing the priors $\xi = 0$, $\Delta N^{\rm eff}_{\rm others} = 0$.

We make a second check by imposing that $\omega_\nu = 0$, $\xi = 0$ and computing the 95% confidence region for $\Delta N^{\rm eff}_{\rm others}$. We find that $0 \leq \Delta N^{\rm eff}_{\rm others} \leq 1.4$. Since the degeneracy parameter is vanishing, the same limit applies to $\Delta N^{\rm eff} = \Delta N^{\rm eff}_{\rm others}$. This is quite in agreement with the results quoted in Ref. (Crotty et al., 2003), although it is more restrictive. This is probably due to the fact that we are imposing a stronger prior on h, keeping it constant and equal to 0.72. This is confirmed by a visual inspection of fig. 2 of Ref. (Crotty et al., 2003).

The best-fit value for neutrino density over the whole parameter space is still $\omega_\nu = 0$, but this time χ^2 changes from 1431 to 1441 as ω_ν goes from 0 to 0.075, so that the probability density spreads out to higher values of ω_ν with respect to the preceding case. The result is that the upper bound raises up to $\omega_\nu < 0.044$, quite independently from the interpolation scheme used. This is probably related to the already observed trend for which, when the energy density of relativistic relics is increased, the possibility for larger neutrino masses reopens (Hannestad, 2003b; Elgaroy and Lahav, 2003; Hannestad and Raffelt, 2004; Lesgourgues and Liddle, 2001).

The maximum likelihood value for the degeneracy parameter is $|\xi| = 0.5$, while the expectation value over the distribution function is $|\xi| = 0.56$ (corresponding to $|L| = 0.43$). At the 2σ level, the degeneracy parameter is constrained in the range $0 \leq |\xi| \leq 1.07$. This corresponds to $0 \leq |L| \leq 0.9$. For what concerns the additional number of relativistic relics, the maximum like-

lihood model has $\Delta N_{\rm others}^{\rm eff} = 0$, and the expectation value over the marginalized probability function is $\Delta N_{\rm others}^{\rm eff} = 0.3$. The 95% confidence region is $-0.7 \leq \Delta N_{\rm others}^{\rm eff} \leq 1.3$. This opening towards smaller, negative values of $\Delta N_{\rm others}^{\rm eff}$ can be ascribed to the fact that such values produce a lowering of the acoustic peak, that can be compensated by a larger degeneracy parameter. The quoted bounds on ω_ν and ξ translate to the following bound on the neutrino mass: $m_\nu < 1.2$ eV (95% CL). In fig. D.4 we show the likelihood functions, while in Table D.4 we summarize our results for the basic and derived parameters describing the neutrino sector.

We remark that, although the maximum likelihood model over the whole grid has $\omega_\nu = 0$, this is not in contradiction with our choice of considering ξ and $\Delta N_{\rm others}^{\rm eff}$ as independent parameters, in spite of the fact that in this limit they should be degenerate. The basic reason is that, as can be seen from the likelihood curves, models with $\omega_\nu > 0$ can be statistically significant. For these models, $\Delta N_\nu^{\rm eff}$ and $\Delta N_{\rm others}^{\rm eff}$ are not exactly degenerate.

In order to better study the partial degeneracy between $|\xi|$ and $\Delta N_{\rm others}^{\rm eff}$, and then to understand how the value of $\Delta N_{\rm others}^{\rm eff}$ affects the estimation of the degeneracy parameter, we compute the likelihood curve for the degeneracy parameter for particular values of $\Delta N_{\rm others}^{\rm eff}$. The results are shown in Table D.5. . From this table, a quite evident trend appears, namely that for large values of $\Delta N_{\rm others}^{\rm eff}$, smaller values of $|\xi|$ are preferred, and viceversa. As already noticed, this is probably related to the fact that when $\Delta N_{\rm others}^{\rm eff}$ is increased, it remains less room for the extra energy density of neutrinos coming from the non-vanishing degeneracy parameter. It is worth noting that, for $\Delta N_{\rm others}^{\rm eff} \simeq 0$, the case $\xi = 0$ lies outside the 95% confidence region. We stress the fact that, according to theoretical predictions, in models of degenerate BBN with "3+1" neutrino mixing, if chemical potentials are large ($\xi > 0.05$), the production of sterile neutrinos is suppressed, effectively resulting in $\Delta N_{\rm others}^{\rm eff} = 0$ (Di Bari, 2002, 2003).

D.5.7. Conclusions and perspectives

In this paper, we have studied the possibility to constraint the lepton asymmetry of the Universe, the sum of neutrino masses, and the energy density of relativistic particles using the WMAP data, in the framework of an extended flat ΛCDM model. Despite the fact that the current amount of cosmological data can be rather coherently explained by the standard picture with three thermally distributed neutrinos, vanishing lepton asymmetry and no additional particle species, nevertheless we think that it is useful to explore how non-standard scenarios are constrained by the cosmological observables. We have concentrated our attention to models with a (eventually large) net lepton asymmetry (corresponding to a non-zero degeneracy parameter for neutrinos). Such models are motivated in the framework of extensions to the

Table D.4.: Neutrino Sector

Parameter	95% Confidence Interval
Physical neutrino density, ω_ν	$\lesssim 0.044$
Degeneracy parameter, $\lvert\xi\rvert$	$0.60^{+0.50}_{-0.60}$
Neutrino mass in eV, m_ν	$\lesssim 1.2$
Lepton asymmetry, $\lvert L\rvert$	$0.46^{+0.43}_{-0.46}$
Effective number of additional relativistic relics, $\Delta N^{\rm eff}_{\rm others}$	0.30 ± 1.0
Effective number of additional relativistic relics, $\Delta N^{\rm eff}$	$0.70^{+1.40}_{-1.15}$

Table D.5.: Correlation between ξ and $\Delta N^{\rm eff}_{\rm others}$

$\Delta N^{\rm eff}_{\rm others}$	ξ (95% Confidence Interval)
0	0.65 ± 0.58
0.5	$0.42^{+0.58}_{-0.42}$
1.0	$0.18^{+0.58}_{-0.18}$
1.5	≤ 0.53
2.0	≤ 0.29

standard model of particle physics, and can possibly explain the observed amount of baryon asymmetry in the Universe. Having in mind this, we have also included the energy density of relativistic species as an independent parameter. In this last aspect, our approach differs from previous ones, where the two parameters where considered degenerate. We have remarked that, although an approximate degeneracy between the two exists, it could be broken by finite mass effect, especially in the case of neutrino masses saturating the tritium beta decay bound.

When considering perfect lepton symmetry , our results are in agreement with previous ones. In the more general case, we have found that, at the 2σ level the bounds on the degeneracy parameter and lepton asymmetry are respectively $0 \leq |\xi| \leq 1.1$ and $0 \leq |L| \leq 0.9$. The effective number of additional relativistic species (excluding the contribution from the non standard thermal distribution of neutrinos) is bounded as follows (95% CL): $-0.7 \leq \Delta N^{\rm eff}_{\rm others} \leq 1.3$. Including also neutrinos, this reads $-0.45 \leq \Delta N^{\rm eff} \leq 2.10$. This limit is much more restrictive than the ones found in similar analysis (Crotty et al., 2003; Pierpaoli, 2003). This is probably due to the fact that we assume a very strong prior on the Hubble parameter, fixing $h = 0.72$. The physical explanation is that the later matter-radiation equality due to $\Delta N^{\rm eff} > 0$ can be compensated by making $\omega_m = \Omega_m h^2$ larger, and viceversa. This gives rise to a partial degeneracy between $\Delta N^{\rm eff}$ and h, thus making the costraints on both parameters looser unless some external prior is imposed to break the degeneracy.

We also find that the data are compatible with ω_ν and m_ν equal to 0, with upper bounds (95% CL) $\omega_\nu \leq 0.044$ and $m_\nu \leq 1.2\,\mathrm{eV}$. This bounds are larger than the ones usually found, and this is probably due on one hand to the presence of a larger energy density of UR particles, and on the other hand to the wide grid spacing we have used.

The usual scenario, with $|L| = 0$ and $\Delta N^{\rm eff} = 0$, is then compatible with WMAP data at the 2σ level; however the likelihood curves show that alternative scenarios with $\xi \simeq 0.6$ and $\Delta N^{\rm eff} \simeq 0.7$ have a larger likelihood with respect to the data. In effect, the standard scenario lies outside the 1σ confidence region. Even if this is not enough to definitely claim evidence, in the CMB anisotropy spectrum, of exotic physics, we think that it is however interesting that non-standard models are not ruled out but actually preferred by the WMAP data.

We have also studied how the results on the lepton asymmetry can change when more precise information on the energy density of relativistic particles is given. We have shown that, the smaller is the extra energy density, the larger is the allowed lepton asymmetry. In particular, for models with vanishing $\Delta N^{\rm eff}_{\rm others}$, perfect lepton symmetry is ruled out at the 2σ level. This is probably due to the approximate degeneracy between $\Delta N^{\rm eff}$ and ξ. The issue of the exact extent of this degeneracy is still open, and we think that it

deserves a deeper attention. It would be desirable to investigate if future precision CMB experiments, and in particular the PLANCK mission, can clearly disentangle the two parameters. Even more promising to this purpose is the power spectrum of LSS, as we have stressed in Sec. D.5.4.

The results presented in this paper have been derived assuming that the three neutrino families have all the same mass and chemical potential, owing to the structure of the `CMBFast` code used to generate the theoretical power spectra. It is yet to investigate the role of a non-uniform distribution of the lepton asymmetry between different families. In a similar way we did not investigate models in which chemical equilibrium between neutrinos and antineutrinos does not hold, implying $\xi_\nu \neq -\xi_{\bar{\nu}}$.

We conclude then that WMAP data still cannot exclude the presence of non-standard physics in the early evolution of the Universe. In particular, they do not exclude the presence of a large neutrino asymmetry, and consequently they do not rule out exotic leptogenesis scenario where a large lepton number is produced.

D.6. Model independent constraints on mass-varying neutrino scenarios

D.6.1. Introduction

Since the accelerated expansion of the universe was first observed with Type Ia supernovae (SN) (Riess et al., 1998; Perlmutter et al., 1999), the case for a cosmological constant-like fluid that dominates the energy density of the universe has become stronger and is well established by now with the new pieces of data gathered (Frieman et al., 2008).

Several candidates for the accelerating component of the universe, generically dubbed dark energy (DE), have been proposed (Frieman et al., 2008; Copeland et al., 2006; Peebles and Ratra, 2003; Caldwell and Kamionkowski, 2009), but understanding them theoretically and observationally has proven to be challenging. On the theoretical side, explaining the small value of the observed dark energy density component, $\rho_\phi \sim (10^{-3}\ \mathrm{eV})^4$, as well as the fact that both dark energy and matter densities contribute significantly to the energy budget of the present universe requires in general a strong fine tuning on the overall scale of the dark energy models. In the case in which the dark energy is assumed to be a scalar field ϕ slowly rolling down its flat potential $V(\phi)$, the so-called quintessence models (Caldwell et al., 1998), the effective mass of the field has to be taken of the order $m_\phi = |d^2V(\phi)/d\phi^2|^{1/2} \sim 10^{-33}$ eV for fields with vacuum expectation values of the order of the Planck mass.

On the observational side, choosing among the dark energy models is a complicated task (Linder, 2008). Most of them can mimic a cosmological con-

stant at late times (that is, an equation of state $w_\phi \equiv p_\phi/\rho_\phi = -1$) (Albrecht et al., 2006), and all data until now are perfectly consistent with this limit. In this sense, looking for different imprints that could favor the existence of a particular model of dark energy is a path worth taking.

Our goal in this paper consists in understanding whether the so-called Mass-Varying Neutrinos (MaVaNs) scenario (Gu et al., 2003; Fardon et al., 2004; Peccei, 2005; Amendola et al., 2008; Wetterich, 2007) could be constrained not only via the dark energy effects, but also by indirect signs of the neutrino mass variation during cosmological evolution, since neutrinos play a key role in several epochs (Hannestad, 2006; Lesgourgues and Pastor, 2006). An indication of the variation of the neutrino mass would certainly tend to favor this models (at least on a theoretical basis) with respect to most DE models. One should keep in mind that MaVaNs scenarios can suffer from stability issues for the neutrino perturbations (Afshordi et al., 2005), although there is a wide class of models and couplings that avoid this problem (Bjaelde et al., 2008; Bean et al., 2008c,b,a; Bernardini and Bertolami, 2008).

Similar analyses have been made in the past, but they have either assumed particular models for the interaction between the neutrinos and the DE field (Brookfield et al., 2006a,b; Ichiki and Keum, 2008), or chosen a parameterization that does not reflect the richness of the possible behavior of the neutrino mass variations (Zhao et al., 2007).

In order to be able to deal with a large number of models, instead of focusing on a particular model for the coupling between the DE field and the neutrino sector, we choose to parameterize the neutrino mass variation to place general and robust constraints on the MaVaNs scenario. In this sense, our work complements previous analyses by assuming a realistic and generic parameterization for the neutrino mass, designed in such a way to probe almost all the different regimes and models within the same framework. In particular, our parameterization allows for fast and slow mass transitions between two values of the neutrino mass, and it takes into account that the neutrino mass variation should start when the coupled neutrinos change their behavior from relativistic to nonrelativistic species. We can mimic different neutrino-dark energy couplings and allow for almost any monotonic behavior in the neutrino mass, placing reliable constraints on this scenario in a model independent way.

Our work is organized as follows: in Section D.6.2 we give a brief review of the MaVaNs scenario and its main equations. In Section D.6.3 we present our parameterization with the results for the background and the perturbation equations obtained within this context. The results of our comparison of the numerical results with the data and the discussion of its main implications are shown in section D.6.4. Finally, in section D.6.5 the main conclusions and possible future directions are discussed.

D.6.2. Mass-varying neutrinos

In what follows, we consider a homogeneous and isotropic universe with a Robertson-Walker flat metric, $ds^2 = a^2\left(d\tau^2 + dr^2 + r^2 d\Omega^2\right)$, where τ is the conformal time, that can be written in terms of the cosmic time t and scale factor a as $d\tau = dt/a$, in natural units ($\hbar = c = k_B = 1$). In this case, the Friedmann equations read

$$\mathcal{H}^2 = \left(\frac{\dot{a}}{a}\right)^2 = \frac{a^2}{3m_p^2}\rho, \tag{D.6.1}$$

$$\dot{\mathcal{H}} = -\frac{a^2}{6m_p^2}\left(\rho + 3p\right), \tag{D.6.2}$$

where the dot denotes a derivative with respect to conformal time, and the reduced Planck mass is $m_p = 1/\sqrt{8\pi G} = 2.436 \times 10^{18}$ GeV. As usual, ρ and p correspond to the total energy density and pressure of the cosmic fluid, respectively. The neutrino mass in the models we are interested in is a function of the scalar field ϕ that plays the role of the dark energy, and can be written as

$$m_\nu(\phi) = M_\nu f(\phi)\,, \tag{D.6.3}$$

where M_ν is a constant and different models are represented by distinct $f(\phi)$.

The fluid equation of the neutrino species can be directly obtained from the Boltzmann equation for its distribution function (Brookfield et al., 2006b),

$$\dot{\rho}_\nu + 3\mathcal{H}\rho_\nu\left(1 + w_\nu\right) = \alpha(\phi)\dot{\phi}\left(\rho_\nu - 3p_\nu\right)\,, \tag{D.6.4}$$

where $\alpha(\phi) = d\ln[m_\nu(\phi)]/d\phi$ takes into account the variation of the neutrino mass, and $w_x = p_x/\rho_x$ is the equation of state of the species x. For completeness and later use, we will define $\Omega_{x0} = \rho_x/\rho_{c0}$, the standard density parameter, where the current critical density is given by $\rho_{c0} = 3H_0^2 m_p^2 = 8.099\, h^2 \times 10^{-11}$ eV^4 and $H_0 = 100\, h$ km s^{-1} Mpc^{-1} is the Hubble constant.

Since the total energy momentum tensor is conserved, the dark energy fluid equation also presents an extra right-hand side term proportional to the neutrino energy momentum tensor trace, $T^\alpha_{(\nu)\alpha} = (\rho_\nu - 3p_\nu)$, and can be written as

$$\dot{\rho}_\phi + 3\mathcal{H}\rho_\phi\left(1 + w_\phi\right) = -\alpha(\phi)\dot{\phi}\left(\rho_\nu - 3p_\nu\right)\,. \tag{D.6.5}$$

For a homogeneous and isotropic scalar field, the energy density and pressure are given by

$$\rho_\phi = \frac{\dot{\phi}^2}{2a^2} + V(\phi)\,, \quad p_\phi = \frac{\dot{\phi}^2}{2a^2} - V(\phi)\,, \tag{D.6.6}$$

and both equations lead to the standard cosmological Klein-Gordon equation

for an interacting scalar field, namely,

$$\ddot{\phi} + 2\mathcal{H}\dot{\phi} + a^2 \frac{dV(\phi)}{d\phi} = -a^2 \alpha(\phi) \left(\rho_\nu - 3p_\nu\right) \ . \tag{D.6.7}$$

From the above equations one sees that, given a potential $V(\phi)$ for the scalar field and a field-dependent mass term $m_\nu(\phi)$ for the neutrino mass, the coupled system given by equations (D.6.1), (D.6.4), and (D.6.7), together with the fluid equations for the baryonic matter, cold dark matter and radiation (photons and other massless species) can be numerically solved (Brookfield et al., 2006b). Notice that a similar approach has been used for a possible variation of the dark matter mass (Anderson and Carroll, 1997) and its possible interaction with the dark energy (Amendola, 2000; Amendola and Tocchini-Valentini, 2001), with several interesting phenomenological ramifications (Farrar and Peebles, 2004; Franca and Rosenfeld, 2004; Huey and Wandelt, 2006; Das et al., 2006; Quartin et al., 2008; La Vacca et al., 2009).

Following (Franca and Rosenfeld, 2004; Das et al., 2006), equations (D.6.4) and (D.6.5) can be rewritten in the standard form,

$$\begin{aligned} \dot{\rho}_\nu &+ 3\mathcal{H}\rho_\nu \left(1 + w_\nu^{(\mathrm{eff})}\right) = 0 \,, \\ \dot{\rho}_\phi &+ 3\mathcal{H}\rho_\phi \left(1 + w_\phi^{(\mathrm{eff})}\right) = 0 \,, \end{aligned} \tag{D.6.8}$$

if one defines the *effective* equation of state of neutrinos and DE as

$$\begin{aligned} w_\nu^{(\mathrm{eff})} &= \frac{p_\nu}{\rho_\nu} - \frac{\alpha(\phi)\dot{\phi}\left(\rho_\nu - 3p_\nu\right)}{3\mathcal{H}\rho_\nu} \,, \\ w_\phi^{(\mathrm{eff})} &= \frac{p_\phi}{\rho_\phi} + \frac{\alpha(\phi)\dot{\phi}\left(\rho_\nu - 3p_\nu\right)}{3\mathcal{H}\rho_\phi} \,. \end{aligned} \tag{D.6.9}$$

The effective equation of state can be understood in terms of the dilution of the energy density of the species. In the standard noncoupled case, the energy density of a fluid with a given constant equation of state w scales as $\rho \propto a^{-3(1+w)}$. However, in the case of interacting fluids, one should also take into account the energy transfer between them, and the energy density in this case will be given by

$$\rho(z) = \rho_0 \exp\left[3\int_0^z \left(1 + w^{(\mathrm{eff})}(z')\right) d\ln(1+z')\right] \ , \tag{D.6.10}$$

where the index 0 denotes the current value of a parameter, and the redshift z is defined by the expansion of the scale factor, $a = a_0(1+z)^{-1}$ (in the rest of this work we will assume $a_0 = 1$). For a constant effective equation of state one obtains the standard result, $\rho \propto a^{-3(1+w^{(\mathrm{eff})})}$, as expected.

Notice that this mismatch between the effective and standard DE equations of state could be responsible for the "phantom behavior" suggested by supernovae data when fitting it using a cosmological model with noninteracting components (Das et al., 2006). This effect could be observable if dark energy was coupled to the dominant dark matter component. For the models discussed here, however, it cannot be significant: the neutrino fraction today ($\Omega_{\nu 0}/\Omega_{\phi 0} \sim 10^{-2}$) is too small to induce an "effective phantom-like" behavior.

As we commented before, the analysis until now dealt mainly with particular models, that is, with particular functional forms of the dark energy potential $V(\phi)$ and field dependence of the neutrino mass $\alpha(\phi)$. A noticeable exception is the analysis of Ref. (Zhao et al., 2007), in which the authors use a parameterization for the neutrino mass *a là* Chevallier-Polarski-Linder (CPL) (Albrecht et al., 2006; Chevallier and Polarski, 2001; Linder, 2003): $m_\nu(a) = m_{\nu 0} + m_{\nu 1}(1-a)$. However, although the CPL parameterization works well for the dark energy equation of state, it cannot reproduce the main features of the mass variation in the case of variable mass particle models. In the case of the models discussed here, for instance, the mass variation is related to the relativistic/nonrelativistic nature of the coupled neutrino species. With a CPL mass parameterization, the transition from m_1 to m_0 always takes place around $z \sim 1$, which is in fact only compatible with masses as small as 10^{-3} eV. Hence, the CPL mass parameterization is not suited for a self-consistent exploration of all interesting possibilites.

One of the goals in this paper is to propose and test a parameterization that allows for a realistic simulation of mass-varying scenarios in a model independent way, with the minimum possible number of parameters, as explained in the next section.

D.6.3. Model independent approach

Background equations

As usual, the neutrino energy density and pressure are given in terms of the zero order Fermi-Dirac distribution function by

$$f^0(q) = \frac{g_\nu}{e^{q/T_{\nu 0}} + 1}\,, \tag{D.6.11}$$

where $q = ap$ denotes the modulus of the comoving momentum $q_i = q n_i$ ($\delta^{ij} n_i n_j = 1$), g_ν corresponds to the number of neutrino degrees of freedom, and $T_{\nu 0}$ is the present neutrino background temperature. Notice that in the neutrino distribution function we have used the fact that the neutrinos decouple very early in the history of the universe while they are relativistic, and therefore their equilibrium distribution depends on the comoving momentum, but not on the mass (Lesgourgues and Pastor, 2006). In what follows we

have neglected the small spectral distortions arising from non-instantaneous neutrino decoupling (Mangano et al., 2005). Thus, the neutrino energy density and pressure are given by

$$\rho_\nu = \frac{1}{a^4}\int \frac{dq}{(2\pi)^3}\, d\Omega\, q^2 \epsilon f^0(q)\ , \tag{D.6.12}$$

$$p_\nu = \frac{1}{3a^4}\int \frac{dq}{(2\pi)^3}\, d\Omega\, q^2 f^0(q)\frac{q^2}{\epsilon}\ , \tag{D.6.13}$$

where $\epsilon^2 = q^2 + m_\nu^2(a)a^2$ (assuming that m_ν depends only on the scale factor). Taking the time-derivative of the energy density, one can then obtain the fluid equation for the neutrinos,

$$\dot{\rho}_\nu + 3\mathcal{H}\left(\rho_\nu + p_\nu\right) = \frac{d\ln m_\nu(u)}{du}\mathcal{H}\left(\rho_\nu - 3p_\nu\right)\ , \tag{D.6.14}$$

where $u \equiv \ln a = -\ln(1+z)$ is the number of e-folds counted back from today. Due to the conservation of the total energy momentum tensor, the dark energy fluid equation is then given by

$$\dot{\rho}_\phi\ + 3\mathcal{H}\rho_\phi\left(1+w_\phi\right) = -\frac{d\ln m_\nu(u)}{du}\mathcal{H}\left(\rho_\nu - 3p_\nu\right)\ . \tag{D.6.15}$$

We can write the effective equations of state, defined in eqs. (D.6.8), as

$$\begin{aligned} w_\nu^{\rm eff} &= \frac{p_\nu}{\rho_\nu} - \frac{d\ln m_\nu(u)}{du}\left(\frac{1}{3} - \frac{p_\nu}{\rho_\nu}\right)\ , \\ w_\phi^{\rm eff} &= \frac{p_\phi}{\rho_\phi} + \left(\frac{\Omega_\nu}{\Omega_\phi}\right)\frac{d\ln m_\nu(u)}{du}\left(\frac{1}{3} - \frac{p_\nu}{\rho_\nu}\right)\ . \end{aligned} \tag{D.6.16}$$

The above results only assume that the neutrino mass depends on the scale factor a, and up to this point, we have not chosen any particular parameterization. Concerning the particle physics models, it is important to notice that starting from a value of w_ϕ and a function $m_\nu(a)$ one could, at least in principle, reconstruct the scalar potential and the scalar interaction with neutrinos following an approach similar to the one in Ref. (Rosenfeld, 2007).

Mass variation parameters

Some of the main features of the MaVaNs scenario are: *(i)* that the dark energy field gets kicked and moves away from its minimum (if $m_\phi > H$) or from its previous slow-rolling trajectory (if $m_\phi < H$) when the neutrinos become non-relativistic, very much like the case when it is coupled to the full matter content of the universe in the so-called *chameleon* scenarios (Brax et al., 2004);

and *(ii)* that as a consequence, the coupling with the scalar field generates a neutrino mass variation at that time. Any parameterization that intends to mimic scalar field models interacting with a mass-varying particle (neutrinos, in our case) for the large redshift range to which the data is sensitive should at least take into account those characteristics. Moreover, the variation of the mass in most models (see (Brookfield et al., 2006b), for instance) can be well approximated by a transition between two periods: an earlier one, in which the mass is given by m_1, and the present epoch, in which the mass is given by m_0 (we will not consider here models in which the neutrino mass behavior is nonmonotonic). The transition for this parameterization, as mentioned before, starts when neutrinos become nonrelativistic, which corresponds approximately to

$$z_{\rm NR} \approx 1.40 \left(\frac{1\ {\rm eV}}{3\ T_{\gamma 0}}\right) \left(\frac{m_1}{1\ {\rm eV}}\right) \approx 2 \times 10^3 \left(\frac{m_1}{1\ {\rm eV}}\right) \tag{D.6.17}$$

where m_1 corresponds to the mass of the neutrino during the period in which it is a relativistic species. Before $z_{\rm NR}$ we can treat the neutrino mass as essentially constant, since the right-hand side (RHS) of the fluid equation is negligible compared to the left-hand side (LHS), and therefore there is no observable signature of a possible mass variation.

When the neutrinos become nonrelativistic, the RHS of the DE and neutrino fluid equations becomes important, and the neutrino mass starts varying. In order to model this variation, we use two parameters, namely the current neutrino mass, m_0, and Δ, a quantity related to the amount of time that it takes to complete the transition from m_1 to m_0. That behavior resembles very much the parameterization of the dark energy equation of state discussed in (Corasaniti and Copeland, 2003), except for the fact that in our case the transition for the mass can be very slow, taking several e-folds to complete, and must be triggered by the time of the nonrelativistic transition, given by equation (D.6.17). Defining $f = [1 + e^{-[u\ (1+\Delta) - u_{\rm NR}]/\Delta}]^{-1}$ and $f_* = [1 + e^{u_{\rm NR}/\Delta}]^{-1}$ we can use the form

$$m_\nu = m_0 + (m_1 - m_0) \times \Gamma(u, u_{\rm NR}, \Delta)\ , \tag{D.6.18}$$

where

$$\begin{aligned} \Gamma(u, u_{\rm NR}, \Delta) &= 1 - \frac{f}{f_*} \\ &= \left[1 - \frac{1 + e^{u_{\rm NR}/\Delta}}{1 + e^{-[u\ (1+\Delta) - u_{\rm NR}]/\Delta}}\right]\ . \end{aligned} \tag{D.6.19}$$

Starting at $u_{\rm NR} = -\ln(1 + z_{\rm NR})$, the function $\Gamma(u, u_{\rm NR}, \Delta)$ decreases from 1 to 0, with a velocity that depends on Δ. The top panel in Figure D.5 gives the

behavior of eq. (D.6.18) with different parameters; the bottom panels shows that in this parametrization, the derivative of the mass with respect to e-fold number resembles a Gaussian function. The peak of the quantity dm/du occurs at the value $\bar{u} = u_{\rm NR}/(1+\Delta)$; hence, for $\Delta \ll 1$, the mass variation takes place immediately after the non-relativistic transition ($\bar{u} \simeq u_{\rm NR}$) and lasts a fraction of e-folds (roughly, 3Δ e-folds); for $1 \leq \Delta \leq |u_{\rm NR}|$ the variation is smooth and centered on some intermediate redshift between z_{NR} and 0; while for $\Delta \gg |u_{NR}|$, the transition is still on-going today, and the present epoch roughly coincides with the maximum variation.

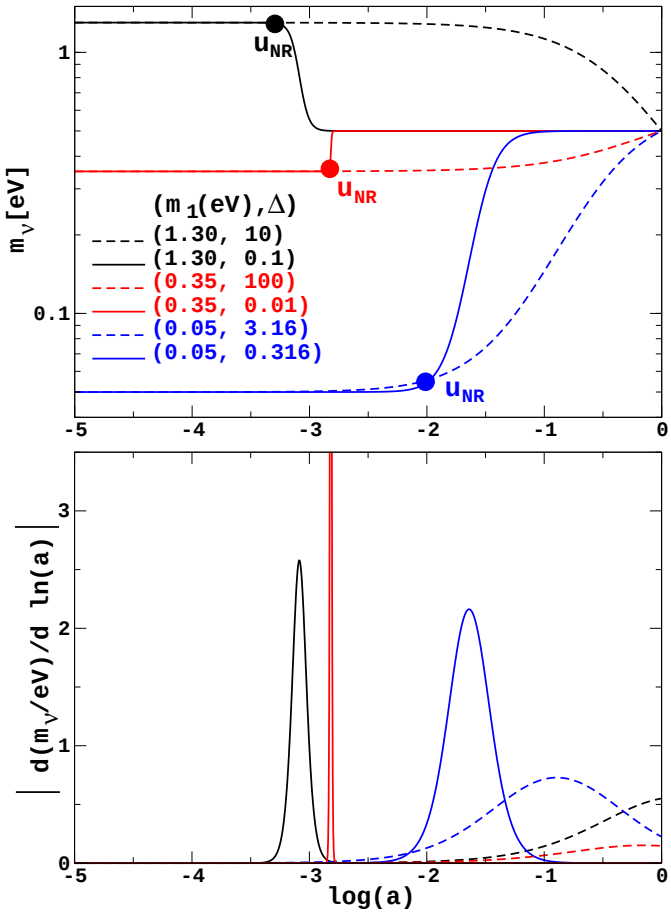

Figure D.5.: (Color online) Neutrino mass behavior for the parameterization given by equation (D.6.18). *Top panel*: Neutrino mass as a function of $\log(a) = u/\ln(10)$ for models with $m_0 = 0.5$ eV and different values of m_1 and Δ. *Bottom panel:* Neutrino mass variation for the same parameters as in the top panel.

Although the functional form of Γ, eq. (D.6.19), seems complicated, one should note that it is one of the simplest forms satisfying our requirements with a minimal number of parameters. An example that could look simpler, but that for practical purposes is not, would be to assume that the two

plateaus are linked together by a straight line. In this case, we would need a parameterization of the form

$$m_\nu = \begin{cases} m_1 & , \quad u < u_{\rm NR} \, , \\ m_0 + (m_1 - m_0)\left[\frac{u-u_{\rm end}}{u_{\rm NR}-u_{\rm end}}\right] & , \quad u_{\rm NR} \leq u \leq u_{\rm end} \, , \\ m_0 & , \quad u > u_{\rm end} \end{cases}$$

where $u_{\rm end}$ corresponds to the chosen redshift in which the transition stops. Notice that in this case not only we still have three parameters to describe the mass variation, but also the function is not smoooth. Moreover, the derivative of the mass with respect to u gives a top-hat-like function which is discontinuous at both $u_{\rm NR}$ and $u_{\rm end}$. In this sense, it seemed to us that equation (D.6.18) would give us the best "price-to-earnings ratio" among the possibilities to use phenomenologically motivated parameterizations for the mass-varying neutrinos, although certainly there could be similar proposals equally viable, such as for instance the possibility of adapting for the mass variation the parameterization used for the dark energy equation of state in (Douspis et al., 2006; Linden and Virey, 2008). There, the transition between two constant values of the equation of state exhibits a $\tanh\left[\Gamma_t(u-u_t)\right]$ dependence, where Γ_t is responsible for the duration of the transition and u_t is related to its halfway point.

In the rest of our analysis, we will use a couple of extra assumptions that need to be taken into account when going through our results. First, we will consider that only one of the three neutrino species is interacting with the dark energy field, that is, only one of the mass eigenstates has a variable mass. The reason for this approximation is twofold: it is a simpler case (compared to the case with 3 varying-mass neutrinos), since instead of 6 extra parameters with respect to the case of constant mass, we have only 2, namely the early mass of the neutrino whose mass is varying, m_1, and the velocity of the transition, related to Δ.

Besides simplicity, the current choice is the only one allowed presently in the case in which neutrinos were heavier in the past. Indeed, we expect our stronger constraints to come from those scenarios, especially if the neutrino species behaves as a nonrelativistic component at the time of radiation-matter equality, given by $1 + z_{\rm eq} \sim 4.05 \times 10^4 (\Omega_{c0}h^2 + \Omega_{b0}h^2)/(1 + 0.23 N_{\rm eff})$ (here the indexes c and b stand for cold dark matter and baryons, respectively, and $N_{\rm eff}$ is the effective number of relativistic neutrinos). Taking the three neutrino species to be nonrelativistic at equality would change significantly the value of $z_{\rm eq}$, contradicting CMB data (according to WMAP5, $1 + z_{\rm eq} = 3141^{+154}_{-157}$ (68% C.L.) (Komatsu et al., 2009)). Instead, a single neutrino species is still marginally allowed to be non-relativistic at that time.

To simplify the analysis, we also assumed that the dark energy field, when not interacting with the neutrinos, reached already the so-called scaling so-

lution [see, *e.g.*, Copeland et al. (2006) and references therein], i.e., the dark energy equation of state w_ϕ in eq. (D.6.15) is constant in the absence of interaction. Notice however that when the neutrinos become non-relativistic the dark energy fluid receives the analogous of the chameleon kicks we mentioned before, and the dark energy effective equation of state, eq. (D.6.16), does vary for this period in a consistent way.

The upper panel of Figure D.6 shows how the density parameters of the different components of the universe evolve in time, in a typical MaVaNs model. The lower panel displays a comparison between mass-varying and constant mass models, in particular during the transition from m_1 to m_0. As one would expect, far from the time of the transition, the densities evolve as they would do in the constant mass case.

Perturbation equations

The next step is to calculate the cosmological perturbation equations and their evolution using this parameterization. We chose to work in the synchronous gauge, and our conventions follow the ones by Ma and Bertschinger (Ma and Bertschinger, 1995). In this case, the perturbed metric is given by

$$ds^2 = -a^2 d\tau^2 + a^2 \left(\delta_{ij} + h_{ij}\right) dx^i dx^j \,. \tag{D.6.20}$$

In this gauge, the equation for the three-momentum of the neutrinos reads (Ichiki and Keum, 2008)

$$\frac{dq}{d\tau} = -\frac{1}{2} q \dot{h}_{ij} n_i n_j - a^2 \frac{m_\nu^2}{q} \beta \frac{\partial \rho_\phi}{\partial x^i} \frac{\partial x^i}{d\tau} \,, \tag{D.6.21}$$

where, as in equation (D.6.4), we define

$$\beta(a) \equiv \frac{d \ln m_\nu}{d\rho_\phi} = \frac{d \ln m_\nu}{d \ln a} \left(\frac{d\rho_\phi}{d \ln a}\right)^{-1} \,. \tag{D.6.22}$$

Since the neutrino phase space distribution (Ma and Bertschinger, 1995) can be written as $f\left(x^i, q, n_j, \tau\right) = f^0(q)\left[1 + \Psi\left(x^i, q, n_j, \tau\right)\right]$, one can show that the first order Boltzmann equation for a massive neutrino species, after Fourier transformation, is given by (Brookfield et al., 2006b; Ichiki and Keum, 2008)

$$\begin{aligned} \frac{\partial \Psi}{\partial \tau} &+ i\frac{q}{\epsilon}(\hat{\mathbf{n}} \cdot \mathbf{k})\Psi + \left(\dot{\eta} - (\hat{\mathbf{k}} \cdot \hat{\mathbf{n}})^2 \frac{\dot{h} + 6\dot{\eta}}{2}\right) \frac{d \ln f^0}{d \ln q} \\ &= -i\beta \frac{qk}{\epsilon}(\hat{\mathbf{n}} \cdot \mathbf{k}) \frac{a^2 m_\nu^2}{q^2} \frac{d \ln f^0}{d \ln q} \delta\rho_\phi \,, \end{aligned} \tag{D.6.23}$$

where η and h are the synchronous potentials in the Fourier space. Notice that the perturbed neutrino energy density and pressure are also going to be modified due to the interaction, and are written as

$$\delta\rho_\nu = \frac{1}{a^4}\int \frac{d^3q}{(2\pi)^3} f^0 \left(\epsilon\Psi + \beta\frac{m_\nu^2 a^2}{\epsilon}\delta\rho_\phi\right) , \tag{D.6.24}$$

$$3\delta p_\nu = \frac{1}{a^4}\int \frac{d^3q}{(2\pi)^3} f^0 \left(\frac{q^2}{\epsilon}\Psi - \beta\frac{q^2 m_\nu^2 a^2}{\epsilon^3}\delta\rho_\phi\right) . \tag{D.6.25}$$

This extra term comes from the fact that the comoving energy ϵ depends on the dark energy density, leading to an extra-term which is proportional to β.

Moreover, if we expand the perturbation $\Psi\left(\mathbf{k}, q, \mathbf{n}, \tau\right)$ in a Legendre series (Ma and Bertschinger, 1995), the neutrino hierarchy equations will read,

$$\begin{aligned}
\dot{\Psi}_0 &= -\frac{qk}{\epsilon}\Psi_1 + \frac{\dot{h}}{6}\frac{d\ln f^0}{d\ln q} , \\
\dot{\Psi}_1 &= \frac{qk}{3\epsilon}\left(\Psi_0 - 2\Psi_2\right) + \kappa , \\
\dot{\Psi}_2 &= \frac{qk}{5\epsilon}(2\Psi_1 - 3\Psi_3) - \left(\frac{1}{15}\dot{h} + \frac{2}{5}\dot{\eta}\right)\frac{d\ln f^0}{d\ln q}, \\
\dot{\Psi}_\ell &= \frac{qk}{(2\ell+1)\epsilon}\left[\ell\Psi_{\ell-1} - (\ell+1)\Psi_{\ell+1}\right] .
\end{aligned} \tag{D.6.26}$$

where

$$\kappa = -\frac{1}{3}\beta\,\frac{qk}{\epsilon}\frac{a^2 m_\nu^2}{q^2}\frac{d\ln f^0}{d\ln q}\delta\rho_\phi . \tag{D.6.27}$$

For the dark energy, we use the "fluid approach" (Hu, 1998) (see also (Bean and Dore, 2004; Hannestad, 2005; Koivisto and Mota, 2006)), so that the density and velocity perturbations are given by,

$$\begin{aligned}
\dot{\delta}_\phi = \left[1 + \beta\rho_\nu(1-3w_\nu)\right]^{-1}\Bigg\{ & 3\mathcal{H}(w_\phi - \hat{c}_\phi^2)\left(\delta_\phi + \frac{3\mathcal{H}(1+w_\phi)}{1+\beta\rho_\nu(1-3w_\nu)}\frac{\theta_\phi}{k^2}\right) + \\
& - (1+w_\phi)\left(\theta_\phi + \frac{\dot{h}}{2}\right) - \left(\frac{\rho_\nu}{\rho_\phi}\right)\left[\beta\dot{\rho}_\phi(1-3c_\nu^2)\delta_\nu + \dot{\beta}\rho_\phi(1-3w_\nu)\delta_\phi\right]\Bigg\} ,
\end{aligned} \tag{D.6.28}$$

$$\dot{\theta}_\phi = -\left[\frac{\mathcal{H}(1-3\hat{c}_\phi^2)+\beta\rho_\nu(1-3w_\nu)\mathcal{H}(1-3w_\phi)}{1+\beta\rho_\nu(1-3w_\nu)}\right]\theta_\phi + \\ + \frac{k^2}{1+w_\phi}\hat{c}_\phi^2\delta_\phi - \beta(1-3w_\nu)\left(\frac{\rho_\nu}{\rho_\phi}\right)\left[\frac{k^2}{1+w_\phi}\rho_\phi\delta_\phi - \dot{\rho}_\phi\theta_\phi\right] , \quad \text{(D.6.29)}$$

where the dark energy anisotropic stress is assumed to be zero (Mota et al., 2007), and the sound speed $\hat{c}_\phi^2$ is defined in the frame comoving with the dark energy fluid (Weller and Lewis, 2003). So, in the synchronous gauge, the quantity $c_\phi^2 \equiv \delta p_\phi/\delta\rho_\phi$ is related to $\hat{c}_\phi^2$ through

$$c_\phi^2\delta_\phi = \hat{c}_\phi^2\left(\delta_\phi - \frac{\dot{\rho}_\phi}{\rho_\phi}\frac{\theta_\phi}{k^2}\right) + w_\phi\frac{\dot{\rho}_\phi}{\rho_\phi}\frac{\theta_\phi}{k^2} . \quad \text{(D.6.30)}$$

In addition, from eqs. (D.6.15) and (D.6.22), we have that

$$\frac{\dot{\rho}_\phi}{\rho_\phi} = \frac{-3\mathcal{H}(1+w_\phi)}{1+\beta\rho_\nu(1-3w_\nu)} . \quad \text{(D.6.31)}$$

D.6.4. Results and Discussion

Numerical approach

Equipped with the background and perturbation equations, we can study this scenario by modifying the numerical packages that evaluate the CMB anisotropies and the matter power spectrum. In particular, we modified the CAMB code[3] (Lewis et al., 2000), based on CMBFast[4] (Seljak and Zaldarriaga, 1996) routines. We use CosmoMC[5] (Lewis and Bridle, 2002) in order to sample the parameter space of our model with a Markov Chain Monte Carlo (MCMC) technique.

We assume a flat universe, with a constant equation of state dark energy fluid, cold dark matter, 2 species of massless neutrinos plus a massive one, and ten free parameters. Six of them are the standard ΛCDM parameters, namely, the physical baryon density $\Omega_{b0}h^2$, the physical cold dark matter density $\Omega_{c0}h^2$, the dimensionless Hubble constant h, the optical depth to reionization $\tau_{\rm reion}$, the amplitude (A_s) and spectral index (n_s) of primordial density fluctuations. In addition, we vary the constant dark energy equation of state parameter w_ϕ and the three parameters accounting for the neutrino mass: the present mass m_0, the logarithm of the parameter Δ related to the duration of the transition, and the logarithm of the ratio of the modulus of

[3] http://camb.info/

[4] http://cfa-www.harvard.edu/~mzaldarr/CMBFAST/cmbfast.html

[5] http://cosmologist.info/cosmomc/

Table D.6.: Assumed ranges for the MaVaNs parameters

Parameter	Range
w_ϕ	$-1 < w_\phi < -0.5$
m_0	$0 < m_0/\mathrm{eV} < 5$
Δ	$-4 < \log\Delta < 2$
μ	$-6 < \log(\mu_+) < 0$
	$-6 < \log(\mu_-) < 0$

the mass difference over the current mass, $\log\mu$, where we define

$$\mu \equiv \frac{|m_1 - m_0|}{m_0} \begin{cases} \mu_+ \equiv \frac{m_1}{m_0} - 1 \ , & m_1 > m_0 \ , \\ \mu_- \equiv 1 - \frac{m_1}{m_0} \ , & m_1 < m_0 \ . \end{cases}$$

All these parameters take implicit flat priors in the regions in which they are allowed to vary (see Table D.6).

Table D.7.: Results for increasing and decreasing neutrino mass, using WMAP 5yr + small scale CMB + LSS + SN + HST data.

	$(+)$Region 95% (68%) C.L.	$(-)$Region 95% (68%) C.L.
w_ϕ	< -0.85 (< -0.91)	< -0.87 (< -0.93)
m_0 (eV)	< 0.28 (< 0.10)	< 0.43 (< 0.21)
$\log\mu_+$	< -2.7 (< -4.5)	—
$\log\mu_-$	—	< -1.3 (< -3.1)
$\log\Delta$	$[-3.84; 0.53]$ $([-2.20; 0.05])$	$[-0.13; 4]$ $([0.56; 4])$

Concerning the last parameter, notice that we choose to divide the parameter space between two regions: one in which the mass is decreasing over time (μ_+) and one in which it is increasing (μ_-). We chose to make this separation because the impact on cosmological observables is different in each regime, as we will discuss later, and by analyzing this regions separately we can gain a better insight of the physics driving the constraints in each one of them. Moreover, we do not allow for models with $w_\phi < -1$, since we are only considering scalar field models with standard kinetic terms.

For given values of all these parameters, our modified version of CAMB first integrates the background equations backward in time, in order to find the initial value of ρ_ϕ leading to the correct dark energy density today. This problem does not always admit a solution leading to well-behaved perturbations: the dark energy perturbation equations (D.6.28), (D.6.29) become singular whenever one of the two quantities, ρ_ϕ or $[1 + \beta\rho_\nu(1 - 3w_\nu)]$, appearing in the denominators vanishes. As we shall see later, in the case in

which the neutrino mass decreases, the background evolution is compatible with cases in which the dark energy density crosses zero, while the second term can never vanish. We exclude singular models by stopping the execution of CAMB whenever $\rho_\phi < 0$, and giving a negligible probability to these models in CosmoMC. The physical interpretation of these pathological models will be explained in the next sections. For other models, CAMB integrates the full perturbation equations, and passes the CMB and matter power spectra to CosmoMC for comparison with the data.

We constrain this scenario using CMB data (from WMAP 5yr (Komatsu et al., 2009; Dunkley et al., 2009), VSA (Scott et al., 2003), CBI (Pearson et al., 2003) and ACBAR (Kuo et al., 2004)); matter power spectrum from large scale structure (LSS) data (2dFGRS (Cole et al., 2005) and SDSS (Tegmark et al., 2006)); supernovae Ia (SN) data from (Kowalski et al., 2008), and the HST Key project measurements of the Hubble constant (Freedman et al., 2001)[6].

Once the posterior probability of all ten parameters has been obtained, we can marginalize over all but one or two of them, to obtain one- or two-dimensional probability distributions. We verified that the confidence limits on the usual six parameters do not differ significantly from what is obtained in the "vanilla model" (Komatsu et al., 2009), and therefore we only provide the results for the extra neutrino and dark energy parameters (Figures D.11, D.10, D.8, D.7, and Table D.7).

Increasing neutrino mass

In this model, the background evolution of the dark energy component obeys to equation (D.6.15), which reads after division by ρ_ϕ:

$$\begin{aligned} \frac{\dot{\rho}_\phi}{\rho_\phi} &= -3\mathcal{H}(1+w_\phi) - \frac{d\ln m_\nu}{du}\frac{\rho_\nu}{\rho_\phi}\mathcal{H}(1-3w_\nu) \\ &\equiv -\Gamma_d - \Gamma_i \end{aligned} \tag{D.6.32}$$

where the two positive quantities Γ_d and Γ_i represent respectively the dilution rate and interaction rate of the dark energy density. For any parameter choice, ρ_ϕ can only decrease with time, so that the integration of the dark energy background equation backward in time always find well-behaved solutions with positive values of ρ_ϕ. Moreover, the quantity $[1+\beta\rho_\nu(1-3w_\nu)]$ appearing in the denominator of the dark energy perturbation equations is equal to the contribution of the dilution rate to the total energy loss rate,

[6] While this work was being finished, the SHOES (Supernova, HO, for the Equation of State) Team (Riess et al., 2009) reduced the uncertainty on the Hubble constant by more than a factor 2 with respect to the value obtained by the HST Key Project, finding $H_0 = 74.2 \pm 3.6$ km s^{-1} Mpc^{-1}. However, since we are taking a flat prior on H_0, and our best fit value for H_0 is contained in their 1σ region, we do not expect our results to be strongly affected by their results.

$\Gamma_d/(\Gamma_d + \Gamma_i)$. This quantity is by construction greater than zero, and the dark energy equations cannot become singular. However, when the the interaction rate becomes very large with respect to the dilution rate, this denominator can become arbitrarily close to zero. Then, the dark energy perturbations can be enhanced considerably, distorting the observable spectra and conflicting the data. Actually, this amplification mechanism is well-known and was studied by various authors (Bean et al., 2008b; Valiviita et al., 2008; Gavela et al., 2009). It was found to affect the largest wavelengths first, and is usually refered as the large scale instability of coupled dark energy models. The condition for avoiding this instability can be thought to be roughly of the form

$$\Gamma_i < A\Gamma_d \,, \tag{D.6.33}$$

where A is some number depending on the cosmological parameters and on the data set (since a given data set tells how constrained is the large scale instability, i.e. how small can be the denominator $[1 + \beta\rho_\nu(1 - 3w_\nu)]$, i.e. how small should the interaction rate remain with respect to the dilution rate). The perturbations are amplified when the denominator is much smaller than one, so A should be a number much greater than one. Intuitively, the condition (D.6.39) will lead to the rejection of models with small values of (w_ϕ, Δ) and large values of μ_-. Indeed, the interaction rate is too large when the mass variation is significant (large μ_-) and rapid (small Δ). The dilution rate is too small when w_ϕ is small (close to the cosmological constant limit). Because of that, it seems that when the dark energy equation of state is allowed to vary one can obtain a larger number of viable models if $w_\phi > -0.8$ early on in the cosmological evolution (Majerotto et al., 2009; Valiviita et al., 2009).

We ran CosmoMC with our full data set in order to see how much this mass-varying scenario can depart from a standard cosmological model with a fixed dark energy equation of state and massive neutrinos. In our parameter basis, this standard model corresponds to the limit $\log\mu_- \to -\infty$, with whatever value of $\log\Delta$. The observational signature of a neutrino mass variation during dark energy or matter domination is encoded in well-known effects, such as: (i) a modification of the small-scale matter power spectrum [due to a different free-streaming history], or (ii) a change in the time of matter/radiation equality [due to a different correspondence between the values of (ω_b, ω_m, ω_ν) today and the actual matter density at the time of equality]. On top of that, the neutrino and dark energy perturbations can approach the regime of large-scale instability discussed above.

Our final results - namely, the marginalized 1D and 2D parameter probabilities - are shown in figures D.7 and D.8. The shape of the contours in $(\log\mu_-, \log\Delta)$ space is easily understandable with analytic approximations. The necessary condition (D.6.33) for avoiding the large-scale instability reads

in terms of our model parameters

$$\mu_- \left[\frac{1+\Delta(1+\Gamma)}{\Delta}\right] < A \left[\frac{1}{(1-\Gamma)\,(1-f)}\right] \frac{3\Omega_\phi(1+w_\phi)}{\Omega_\nu(1-3w_\nu)}\,, \tag{D.6.34}$$

where we expressed the mass variation as

$$\frac{d\ln m_\nu}{du} = \left(\frac{\mu_-}{1-\mu_-\Gamma}\right)\left(\frac{1+\Delta}{\Delta}\right)(1-\Gamma)\,(1-f)\ . \tag{D.6.35}$$

Two limits can be clearly seen from this equations. For $\Delta \ll 1$ (fast transitions), the upper limit on μ_- reads

$$\mu_- \lesssim A\Delta \left[\frac{1}{(1-\Gamma)\,(1-f)}\right] \frac{3\Omega_\phi(1+w_\phi)}{\Omega_\nu(1-3w_\nu)}\,. \tag{D.6.36}$$

This corresponds to the diagonal limit in the lower half of the right upper panel of figure D.8. In fact, the appearance of the large-scale instability is seen in models localized at the edge of the allowed region, as shown in figure D.9.

In the opposite case of a very slow transition, $\Delta \gg 1$, it is clear from eq. (D.6.34) that the limit on μ_- should be independent on Δ,

$$\mu_- \lesssim A \left[\frac{1}{(1-\Gamma)\,(1-f)}\right] \frac{3\Omega_\phi(1+w_\phi)}{\Omega_\nu(1-3w_\nu)}\,. \tag{D.6.37}$$

This limit corresponds to the almost vertical cut in the upper part of the plane $(\log\mu_-, \log\Delta)$ (upper right panel, fig. D.8).

These conditions are easier to satisfy when at the time of the transition, $\Omega_\phi(1+w_\phi)$ is large. So, in order to avoid the instability, large values of w_ϕ are preferred. However, it is well-known that cosmological observables (luminosity distance relation, CMB and LSS power spectra) better fit the data for w close to -1 (cosmological constant limit). In the present model, the role of the large-scale instability is to push the best-fit value from -1 to -0.96, but $w_\phi = -1$ is still allowed at the 68% C.L.

The main result of this section is that the variation of the neutrino mass is bounded to be small, not so much because of the constraining power of large-scale structure observations in the regime where neutrino free-streaming is important (i.e., small scales), but by CMB and LSS data on the largest scales, which provide limits on the possible instability in DE and neutrino perturbations.

Indeed, for the allowed models, the mass variation could be at most of order 10% for masses around 0.05 eV, and less than 1% for masses larger than 0.3 eV: this is undetectable with small scale clustering data, showing that the limit really comes from large scales.

With those results, we conclude that there is no evidence for a neutrino mass variation coming from the present data. In fact, as for most cosmological data analyses, the concordance ΛCDM model remains one of the best fits to the data, lying within the 68% interval of this analysis.

Nonetheless, better constraints will possibly be obtained with forthcoming data, especially the ones that probe patches of the cosmological "desert" between $z \simeq 1100$ and $z \simeq 1$, like CMB weak lensing (Lesgourgues et al., 2006), and/or cross-correlations of different pieces of data, like CMB and galaxy-density maps (Lesgourgues et al., 2008). We can estimate, for instance, what is the favored redshift range for the neutrino mass variation according to our results. Taking $m_0 = 0.1$ eV and the mean likelihood values for $\log \Delta$ and $\log[m_1/m_0]$, one can see that the bulk of the mass variation takes place around $z \sim 20$, a redshift that possibly will be probed by future tomographic probes like weak lensing (Hannestad et al., 2006; Kitching et al., 2008) and especially 21 cm absorption lines (Loeb and Zaldarriaga, 2004; Loeb and Wyithe, 2008; Mao et al., 2008; Pritchard and Pierpaoli, 2008). Those will help not only to disentangle some degeneracies in the parameter space, but will also allow for direct probes of the neutrino mass in different redshift slices.

Decreasing neutrino mass

In this case, the evolution rate of the dark energy density is still given by equation (D.6.32) but with an opposite sign for the interaction rate: in can be summarized as

$$\frac{\dot{\rho}_\phi}{\rho_\phi} = -\Gamma_d + \Gamma_i \,, \tag{D.6.38}$$

with Γ_d and Γ_i both positive. In principle, the interaction rate could overcome the dilution rate, leading to an increase of ρ_ϕ. Hence, the integration of the dark energy evolution equation backward in time can lead to negative values of ρ_ϕ, and the prior $\rho_\phi > 0$ implemented in our CAMB version is relevant. Still, the denominator $[1 + \beta\rho_\nu(1 - 3w_\nu)]$ can never vanish since it is equal to $\Gamma_d/(\Gamma_d - \Gamma_i)$.

Well before before the transition, the interaction rate is negligible and $\dot{\rho}_\phi$ is always negative. We conclude that $\beta = d\ln m_\nu/d\rho_\phi$ starts from small positive values and increases. If the condition

$$\Gamma_i < \Gamma_d \tag{D.6.39}$$

is violated during the transition, $\dot{\rho}_\phi$ will cross zero and become positive. This corresponds to β growing from zero to $+\infty$, and from $-\infty$ to some finite negative value. After Γ_i/Γ_d has reached its maximum, β undergoes the opposite evolution. Reaching $\rho_\phi = 0$ is only possible if ρ_ϕ has a non-monotonic evolution, i.e. if (D.6.39) is violated. However, the perturbations diverge even before reaching this singular point: when β tends to infinity, it is clear from eq.

(D.6.26) that the neutrino perturbation derivatives become arbitrarily large. We conclude that in this model, the condition (D.6.39) is a necessary condition for avoiding instabilities, but not a sufficient condition: the data is expected to put a limit on the largest possible value of β, which will always be reached before $\dot{\rho}_\phi$ changes sign, i.e. before the inequality (D.6.39) is saturated. Hence, the condition for avoiding the instability is intuitively of the form of (D.6.33), but now with A being a number smaller than one.

We then ran CosmoMC with the full data set and obtained the marginalized 1D and 2D parameter probabilities shown in figures D.10 and D.11. The major differences with respect to the increasing mass case are: a stronger bound on m_0, a much stronger bound on μ_-, and the fact that large values of Δ are now excluded. This can be understood as follows. In order to avoid instabilites, it is necessary to satisfy the inequalities (D.6.36), (D.6.37), but with a much smaller value of A than in the increasing mass case; hence, the contours should look qualitatively similar to those obtained previously, but with stronger bounds. This turns out to be the case, although in addition, large Δ values are now excluded. Looking at the mass variation for large Δ in figure D.5, we see that in this limit the energy transfer takes place essentially at low redhsift. Hence, the interaction rate is large close to $z = 0$. In many models, this leads to positive values of $\dot{\rho}_\phi$ at the present time, to a non- behavior of the dark energy density, and to diverging perturbations. This can only be avoided when w is large with respect to -1, i.e. when the dilution rate is enhanced. Hence, in this model, the need to avoid diverging perturbations imposes a strong parameter correlation between w and Δ. However, values of w greater than -0.8 are not compatible with the supernovae, CMB and LSS data set; this slices out all models with large Δ.

The fact that the bound on m_0 is stronger in the decreasing mass case is also easily understandable: for the same value of the mass difference $\mu_\pm = |m_1 - m_0|/m_0$, a given m_0 corresponds to a larger mass m_1 in the decreasing mass case. It is well-known that CMB and LSS data constrain the neutrinos mass through its background effect, i.e. through its impact on the time of matter/radiation equality for a given dark matter abundance today. The impact is greater when m_1 is larger, i.e. in the decreasing mass case; therefore, the bounds on m_0 are stronger.

D.6.5. Concluding remarks

In this work we analysed some mass-varying neutrino scenarios in a nearly model independent way, using a general and well-behaved parameterization for the neutrino mass, including variations in the dark energy density in a self-consistent way, and taking neutrino/dark energy perturbations into account.

Our results for the background, CMB anisotropies, and matter power spec-

tra are in agreement with previous analyses of particular scalar field models, showing that the results obtained with this parameterization are robust and encompass the main features of the MaVaNs scenario.

Moreover, a comparison with cosmological data shows that only small mass variations are allowed, and that MaVaNs scenario are mildly disfavored with respect to the constant mass case, especially when neutrinos become lighter as the universe expands. In both cases, neutrinos can change significantly the evolution of the dark energy density, leading to instabilities in the dark energy and/or neutrino perturbations when the transfer of energy between the two components per unit of time is too large. These instabilities can only be avoided when the mass varies by a very small amount, especially in the case of a decreasing neutrino mass. Even in the case of increasing mass, constraining better the model with forthcoming data will be a difficult task, since it mimics a massless neutrino scenario for most of the cosmological time.

One should keep in mind that our analysis assumes a constant equation of state for dark energy and a monotonic behavior for the mass variation. Even though those features are present in most of the simplest possible models, more complicated models surely can evade the constraints we obtained in our analysis.

Finally, those constraints will improve with forthcoming tomographic data. If any of the future probes indicate a mismatch in the values of the neutrino mass at different redshifts, we could arguably have a case made for the mass-varying models.

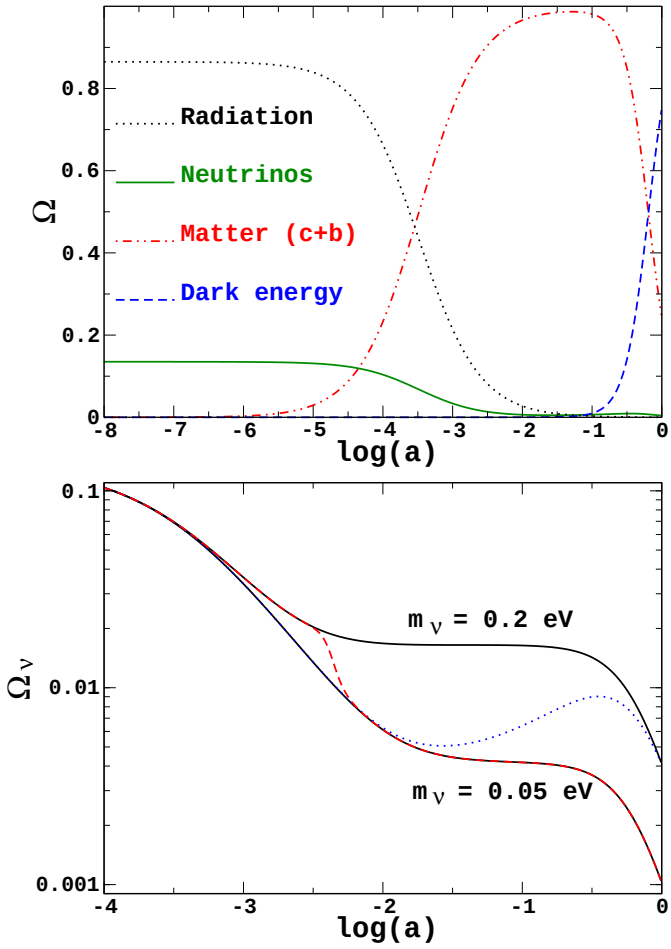

Figure D.6.: (Color online) *Top panel*: Density parameters for the different components of the universe versus $\log(a) = u/\ln(10)$ in a model with $m_1 = 0.05$ eV, $m_0 = 0.2$ eV, $\Delta = 10$, and all the other parameters consistent with present data. The radiation curve include photons and two massless neutrino species, and matter stands for cold dark matter and baryons. The bump in the neutrino density close to $\log(a) = -0.5$ is due to the increasing neutrino mass. *Bottom panel:* Density parameters for two different mass-varying neutrino models. The solid black curves show the density parameter variation for two distinct constant mass models, with masses $m_\nu = 0.05$ eV and $m_\nu = 0.2$ eV. The dashed (red) curve shows a model in which the mass varies from $m_1 = 0.2$ eV to $m_0 = 0.05$ eV, with $\Delta = 0.1$, and the dotted (blue) line corresponds a model with $m_1 = 0.05$ eV to $m_0 = 0.2$ eV, with $\Delta = 10$.

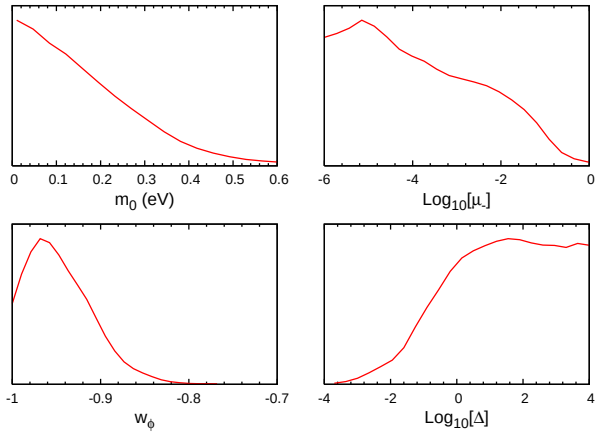

Figure D.7.: Marginalised 1D probability distribution in the increasing mass case $m_1 < m_0$, for the neutrino / dark energy parameters: m_0, $\log_{10}[\mu_-]$ (top panels), w_ϕ, and $\log \Delta$ (bottom panels).

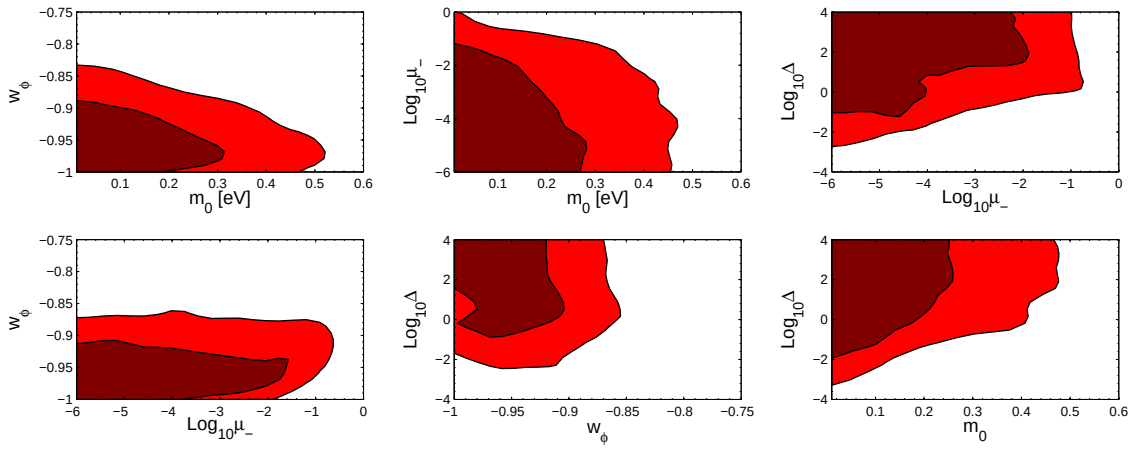

Figure D.8.: Marginalised 2D probability distribution in the increasing mass case $m_1 < m_0$.

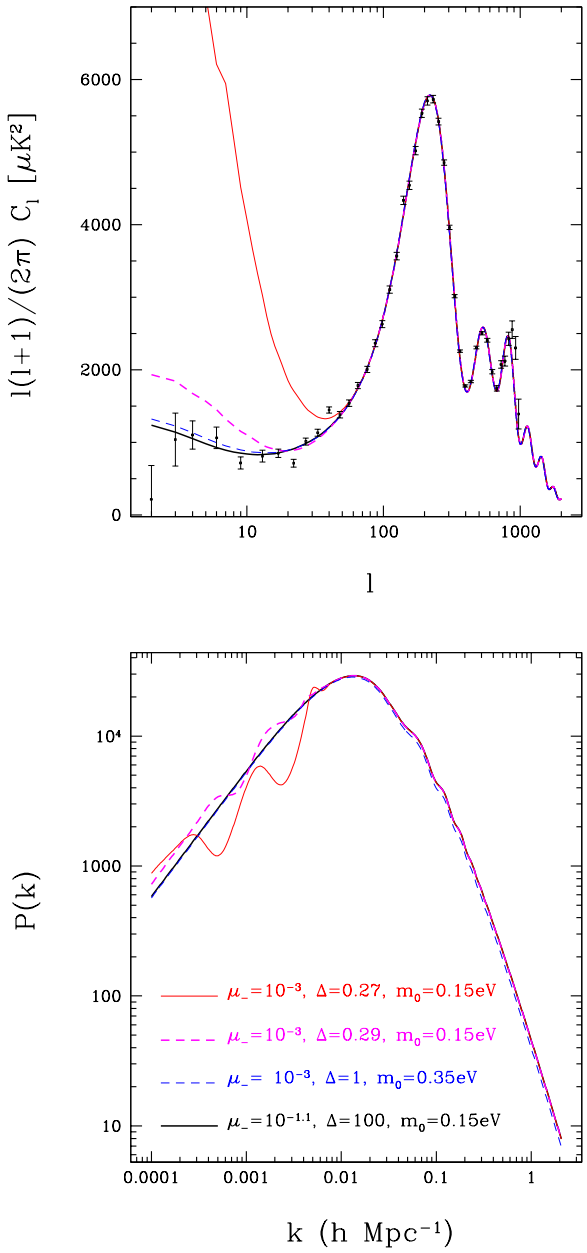

Figure D.9.: (Color on-line) CMB anisotropies and matter power spectra for some mass varying models with increasing mass, showing the development of the large scale instability. The cosmological parameters are set to our best fit values, except for the ones shown in the plot. The data points in the CMB spectrum correspond to the binned WMAP 5yr data.

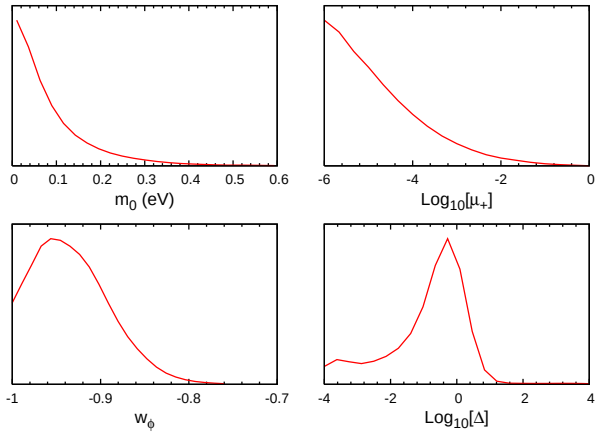

Figure D.10.: (Color online:) Marginalised 1D probability distribution (red/solid lines) for the decreasing mass case $m_1 > m_0$, for neutrino / dark energy parameters: m_0, $\log[\mu_+]$ (top panels), w_ϕ, and $\log \Delta$ (bottom panels).

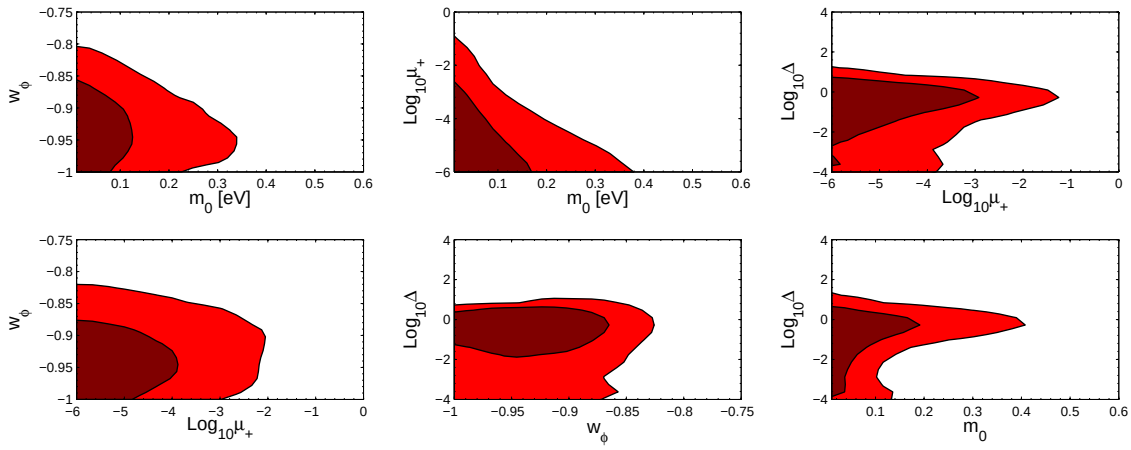

Figure D.11.: (Color online) Marginalised 2D probability distribution for decreasing mass, $m_1 > m_0$.

E. Indirect Detection of Dark Matter

E.1. Boosting the WIMP annihilation through the Sommerfeld enhancement

The motivation for studying dark matter annihilation signatures (see e.g. (Bertone et al., 2005)) has received considerable recent attention following reports of a 100 GeV excess in the PAMELA data on the ratio of the fluxes of cosmic ray positrons to electrons (Adriani et al., 2009). In the absence of any compelling astrophysical explanation, the signature is reminiscent of the original prediction of a unique dark matter annihilation signal (Silk and Srednicki, 1984), although there are several problems that demand attention before any definitive statements can be made. By far the most serious of these is the required annihilation boost factor. The remaining difficulties with a dark matter interpretation, including most notably the gamma ray signals from the Galactic Centre and the inferred leptonic branching ratio, are, as we argue below, plausibly circumvented or at least alleviated. Recent data from the ATIC balloon experiment provides evidence for a cut-off in the positron flux near 500 GeV that supports a Kaluza-Klein-like candidate for the annihilating particle (Chang et al., 2008) or a neutralino with incorporation of suitable radiative corrections (Bergstrom et al., 2008).

In a pioneering paper, it was noted (Profumo, 2005) that the annihilation signal can be boosted by a combination of coannihilations and Sommerfeld corrrection. We remark first that the inclusion of coannihilations to boost the annihilation cross-section modifies the relic density, and opens the 1-10 TeV neutralino mass window to the observed (WMAP5-normalised) dark matter density. As found by Lavalle et al. (2008), the outstanding problem now becomes that of normalisation. A boost factor of around 100 is required to explain the HEAT data in the context of a 100 GeV neutralino. The flux is suppressed by between one and two powers of neutralino mass, and the problem becomes far more severe with the 1-10 TeV neutralino required by the PAMELA/ATIC data (Cirelli et al., 2009), a boost of 10^4 or more being required. These latter authors included a Sommerfeld correction appropriate to our $\beta \equiv v/c = 0.001$ dark halo and incorporated channel-dependent boost factors to fit the data, but the required boosts still fell short of plausible values by at least an order of magnitude.

Here we propose a solution to the boost problem via Sommerfeld correction in the presence of a model of substructure that incorporates a plausible phase space structure for cold dark matter (CDM). We reassess the difficulty with the leptonic branching ratio and show that it is not insurmountable for supersymmetric candidates. Finally, we evaluate the possibility of independent confirmation via photon channels.

Substructure survival means that as much as 10% of the dark matter is at much lower β. This is likely in the solar neighbourhood and beyond, but not in the inner galaxy where clump destruction is prevalent due to tidal interactions. Possible annihilation signatures from the innermost galaxy such as the WMAP haze of synchrotron emission and the EGRET flux of diffuse gamma rays are likely to be much less affected by clumpy substructure than the positron flux in the solar neighbourhood. We show in the following section that incorporation of the Sommerfeld correction means that clumps dominate the annihilation signal, to the extent that the initial clumpiness of the dark halo survives.

E.1.1. The Sommerfeld enhancement

Dark matter annihilation cross sections in the low-velocity regime can be enhanced through the so-called "Sommerfeld effect" (Sommerfeld, 1931; Hisano et al., 2004, 2005; Cirelli et al., 2007; March-Russell et al., 2008; Arkani-Hamed et al., 2009; Pospelov and Ritz, 2009). This non-relativistic quantum effect arises because, when the particles interact through some kind of force, their wave function is distorted by the presence of a potential if their kinetic energy is low enough. In the language of quantum field theory, this correspond to the contribution of "ladder" Feynman diagrams like the one shown in Fig. E.1 in which the force carrier is exchanged many times before the annihilation finally occurs. This gives rise to (non-perturbative) corrections to the cross section for the process under consideration. The actual annihilation cross section times velocity will then be:

$$\sigma v = S\,(\sigma v)_0 \tag{E.1.1}$$

where $(\sigma v)_0$ is the tree level cross section times velocity, and in the following we will refer to the factor S as the "Sommerfeld boost" or "Sommerfeld enhancement" [1].

In this section we will study this process in a semi-quantitative way using a simple case, namely that of a particle interacting through a Yukawa potential. We consider a dark matter particle of mass m. Let $\psi(r)$ be the reduced two-body wave function for the s-wave annihilation; in the non-relativistic limit,

[1] In the case of repulsive forces, the Sommerfeld "enhancement" can actually be $S < 1$, although we will not consider this possibility here.

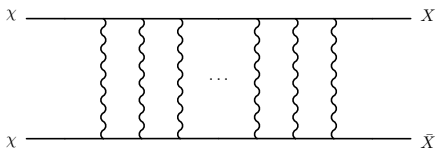

Figure E.1.: Ladder diagram giving rise to the Sommerfeld enhancement for $\chi\chi \to X\bar{X}$ annihilation, via the exchange of gauge bosons.

it will obey the radial Schrödinger equation:

$$\frac{1}{m}\frac{d^2\psi(r)}{dr^2} - V(r)\psi(r) = -m\beta^2\psi(r), \tag{E.1.2}$$

where β is the velocity of the particle and $V(r) = -\frac{\alpha}{r}e^{-m_V r}$ is an attractive Yukawa potential mediated by a boson of mass m_V.

The Sommerfeld enhancement S can be calculated by solving the Schrödinger equation with the boundary condition $d\psi/dr = im\beta\psi$ as $r \to \infty$. Eq. (E.1.2) can be easily solved numerically. It is however useful to consider some particular limits in order to gain some qualitative insight into the dependence of the Sommerfeld enhancement on particle mass and velocity. First of all, we note that for $m_V \to 0$, the potential becomes Coulomb-like. In this case the Schrödinger equation can be solved analytically; the resulting Sommerfeld enhancement is:

$$S = \frac{\pi\alpha}{\beta}(1 - e^{-\pi\alpha/\beta})^{-1}. \tag{E.1.3}$$

For very small velocities ($\beta \to 0$), the boost $S \simeq \pi\alpha/\beta$: this is why the Sommerfeld enhancement is often referred as a $1/v$ enhancement. On the other hand, $S \to 1$ when $\alpha/\beta \to 0$, as one would expect.

It should however be noted that the $1/v$ behaviour breaks down at very small velocities. The reason is that the condition for neglecting the Yukawa part of the potential is that the kinetic energy of the collision should be much larger than the boson mass m_V times the coupling constant α, i.e., $m\beta^2 \gg \alpha m_V$, and this condition will not be fulfilled for very small values of β. This is also evident if we expand the potential in powers of $x = m_V r$; then, neglecting terms of order x^2 or smaller, the Schrödinger equation can be written as (the prime denotes the derivative with respect to x):

$$\psi'' + \frac{\alpha}{\varepsilon}\frac{\psi}{x} = \left(-\frac{\beta^2}{\varepsilon^2} + \frac{\alpha}{\varepsilon}\right)\psi, \tag{E.1.4}$$

having defined $\varepsilon = m_V/m$. The Coulomb case is recovered for $\beta^2 \gg \alpha\varepsilon$, or exactly the condition on the kinetic energy stated above. It is useful to define $\beta^* \equiv \sqrt{\alpha m_V/m}$ such that $\beta \gg \beta^*$ is the velocity regime where the Coulomb approximation for the potential is valid.

Another simple, classical interpretation of this result is the following. The range of the Yukawa interaction is given by $R \simeq m_V^{-1}$. Then the crossing time scale is given by $t_{cross} \simeq R/v \simeq 1/\beta m_V$. On the other hand, the dynamical time scale associated to the potential is $t_{dyn} \simeq \sqrt{R^3 m/\alpha} \simeq \sqrt{m/\alpha m_V^3}$. Then the condition $\beta \gg \beta^*$ is equivalent to $t_{cross} \ll t_{dyn}$, i.e., the crossing time should be much smaller than the dynamical time-scale. Finally, we note that since in the Coulomb case $S \sim 1/\beta$ for $\alpha \gg \beta$, the region where the Sommerfeld enhancement actually has a $1/v$ behaviour is $\beta^* \ll \beta \ll \alpha$. It is interesting to notice that this region does not exist at all when $m \lesssim m_V/\alpha$.

The other interesting regime to examine is $\beta \ll \beta^*$. Following the discussion above, this corresponds to the potential energy dominating over the kinetic term. Referring again to the form (E.1.4) for $x \ll 1$ of the Schrödinger equation, this becomes:

$$\psi'' + \frac{\alpha}{\varepsilon}\frac{\psi}{x} = \frac{\alpha}{\varepsilon}\psi. \tag{E.1.5}$$

The positiveness of the right-hand side of the equation points to the existence of bound states. In fact, this equation has the same form as the one describing the hydrogen atom. Then bound states exist when $\sqrt{\alpha/\varepsilon}$ is an even integer, i.e. when:

$$m = 4m_V n^2/\alpha, \qquad n = 1, 2, \ldots \tag{E.1.6}$$

From this result, we expect that the Sommerfeld enhancement will exhibit a series of resonances for specific values of the particle mass spaced in a $1 : 4 : 9 : ...$ fashion. The behaviour of the cross section close to the resonances can be better understood by approximating the electroweak potential by a well potential, for example: $V(r) = -\alpha m_V \theta(R - r)$, where $R = m_V^{-1}$ is the range of the Yukawa interaction, and the normalization is chosen so that the well potential roughly matches the original Yukawa potential at $r = R$. The external solution satisfying the boundary conditions at infinity is simply an incoming plane wave, $\psi_{out}(r) \propto e^{ik_{out}r}$, with $k_{out} = m\beta$. The internal solution is: $\psi_{in}(r) = Ae^{ik_{in}r} + Be^{-ik_{in}r}$, where $k_{in} = \sqrt{k_{out}^2 + \alpha m m_V} \simeq \sqrt{\alpha m m_V}$ (the last approximate equality holds because $\beta \ll \beta^*$). The coefficients A and B are as usual obtained by matching the wave function and its first derivative at $r = R$; then the enhancement is found to be:

$$S = \left[\cos^2 k_{in}R + \frac{k_{out}^2}{k_{in}^2}\sin^2 k_{in}R\right]^{-1}. \tag{E.1.7}$$

When $\cos k_{in}R = 0$, i.e., when $\sqrt{\alpha m/m_V} = (2n+1)\pi/2$, the enhancement assumes the value $k_{in}^2/k_{out}^2 \simeq \beta^{*2}/\beta^2 \gg 1$. This is however cut off by the finite width of the state.

In summary, the qualitative features that we expect to observe are

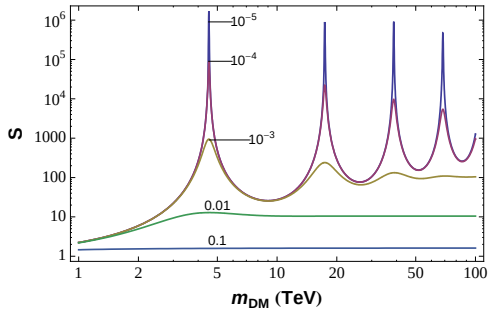

Figure E.2.: Sommerfeld enhancement S as a function of the dark matter particle mass m, for different values of the particle velocity. Going from bottom to top $\beta = 10^{-1}, 10^{-2}, 10^{-3}, 10^{-4}, 10^{-5}$.

i) at large velocities ($\beta \gg \alpha$) there is no enhancement, $S \simeq 1$;
ii) in the intermediate range $\beta^* \ll \beta \ll \alpha$, the enhancement goes like $1/v$: $S \simeq \pi\alpha/\beta$, this value being independent of the particle mass;
iii) at small velocities ($\beta \ll \beta^*$), a series of resonances appear, due to the presence of bound states. Close to the resonances, $S \simeq (\beta^*/\beta)^2$. In this regime, the enhancement strongly depends on the particle mass, because it is this that determines whether we are close to a resonance or not. Similar results have been independently obtained in Ref. (March-Russell and West, 2009).

We show the result of the numerical integration of Eq. (E.1.2) in Figure E.2, where we plot the enhancement S as a function of the particle mass m, for different values of β. We choose specific values of the boson mass $m_V = 90\,\text{GeV}$ and of the gauge coupling $\alpha = \alpha_2 \simeq 1/30$. These values correspond to a particle interacting through the exchange of a Z boson.

We note however that, as can be seen by the form of the equation, the enhancement depends on the boson mass only through the combination $\varepsilon = m_V/m$, so that a different boson mass would be equivalent to rescaling the abscissa in the plot. Moreover, the evolution of the wave function only depends on the two quantities α/ε and β/ε, so that a change $\alpha \to \alpha'$ in the gauge coupling would be equivalent to: $\beta \to \beta' = \frac{\alpha'}{\alpha}\beta$, $\varepsilon \to \varepsilon' = \frac{\alpha'}{\alpha}\varepsilon$. This shows that Fig. E.2 does indeed contain all the relevant information on the behaviour of the enhancement S.

We see that the results of the numerical evaluation agree with our qualitative analysis above. When $\beta = 10^{-1}$ (bottom curve), we are in the $\beta > \alpha \simeq 3 \times 10^{-2}$ regime and there is basically no enhancement. The next curve $\beta = 10^{-2}$ is representative of the $\beta \gtrsim \beta^*$ regime, at least for m larger than a few TeV. The enhancement is constant with the particle mass and its value agrees well with the expected value $\pi\alpha/\beta \simeq 10$. The drop of the enhancement in the mass region below ~ 3 TeV is due to the fact that here $\beta \lesssim \beta^*$,

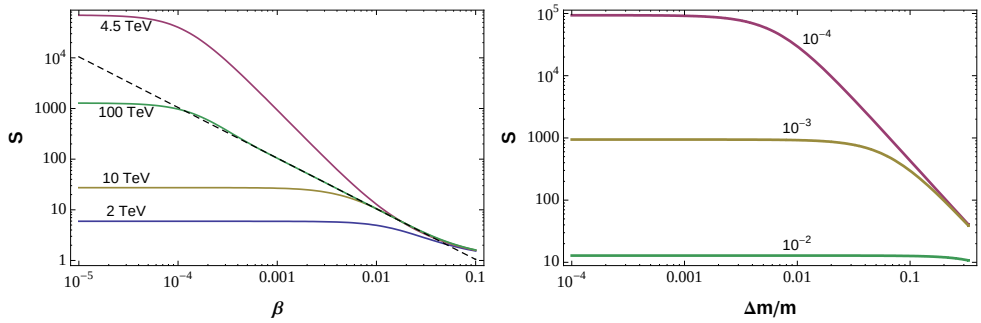

Figure E.3.: Top panel: Sommerfeld enhancement S as a function of the particle velocity β for different values of the dark matter mass. From bottom to top: $m = 2$, 10, 100, 4.5 TeV, the last value corresponding to the first resonance in Fig. E.2. The black dashed line shows the $1/v$ behaviour that is expected in the intermediate velocity range (see text for discussion). Bottom panel: Sommerefeld enhancement S as a function of the relative distance from the first resonance shown in Fig. E.2, occurring at $m \simeq 4.5$ TeV, for different values of β. From top to bottom: $\beta = 10^{-4}$, 10^{-3}, 10^{-2}.

and that there are no resonances for this value of the mass. Decreasing β again (top three curves, corresponding to $\beta = 10^{-3}$, 10^{-4}, 10^{-5} from bottom to top) we observe the appearance of resonance peaks. The first peak occurs for $m = \bar{m} = 4.5$ TeV, so that expression (E.1.6) based on the analogy with the hydrogen atom overestimates the peak position by a factor 2. However, the spacing between the peaks is as expected, going like n^2, as the next peaks occur roughly at $m = 4$, 9, $16\,\bar{m}$. The height of the first peak agrees fairly well with its expected value of $(\beta^*/\beta)^2$. The other peaks are damped; this is particularly evident for $\beta = 10^{-3}$, and in this case it is due to the fact that β^* decreases as m increases, so that for $m \sim 100$ TeV we return to the non-resonant, $1/\beta$ behaviour, and the enhancement takes the constant value $\pi\alpha/\beta \simeq 100$.

Complementary information can be extracted from the analysis of the upper panel of Fig. E.3, where we plot the Sommerfeld enhancement as a function of β, for different values of the particle mass. Far from the resonances, the enhancement factor initially grows as $1/\beta$ and then saturates to some constant value. This constant value can be estimated by solving the Schrödinger equation with $\beta = 0$. We find that a reasonable order of magnitude estimate is given by $S_{max} \sim 6\alpha/\varepsilon$; the corresponding value of $\beta \sim 0.5\varepsilon$. The $1/\beta$ behaviour holds down to smaller velocities for larger particle masses, leading to larger enhancement factors. However, when the particle mass is close to a resonance, S initially grows like $1/\beta$ but at some point the $1/\beta^2$ behaviour "turns on", leading to very large values of the boost factor, until this also saturates to some constant value.

It is clear from the discussion until this point that the best hope for obtaining a large enhancement comes from the possibility of the dark matter mass lying close to a resonance; for the choice of parameter used above this would mean $m \simeq \bar{m} \simeq 4.5\,\mathrm{TeV}$. However, one could be interested in knowing how close the mass should be to the center of the resonance in order to obtain a sizeable boost in the cross-section. In order to understand this, we show in Fig. E.3 the enhancement as a function of $\mu \equiv |m - \bar{m}|/m$, i.e., of the fractional shift from the center of the resonance. Clearly, for $\beta \leq 10^{-3}$, a boost factor of $\gtrsim 100$ can be obtained for $\mu \lesssim 0.2$, i.e., for deviations of up to 20% from $\bar{m}$, corresponding to the range between 3.5 and 5.5 TeV. This is further reduced to the 4 to 5 TeV range if one requires $S \gtrsim 10^3$.

E.1.2. The leptonic branching ratio

The relevance of the Sommerfeld enhancement for the annihilation of supersymmetric particles was first pointed out in Refs (Hisano et al., 2004, 2005), in the context of the minimal supersymmetric standard model where the neutralino is the lightest supersymmetric particle. A wino-like or higgsino-like neutralino would interact with the W and Z gauge bosons due to its $\mathrm{SU}(2)_L$ nonsinglet nature. In particular, the wino $\tilde{W}^0$ is the neutral component of a $\mathrm{SU}(2)_L$ triplet , while the higgsinos $(\tilde{H}_1^0, \tilde{H}_2^0)$ are the neutral components of two $\mathrm{SU}(2)_L$ doublets. The mass (quasi-) degeneracy between the neutralino and the other components of the multiplet leads to transitions between them, mediated by the exchange of weak gauge bosons; this gives rise to a Sommerfeld enhancement at small velocities. On the other hand, the bino-like neutralino being a SU(2) singlet, would not experience any Sommerfeld enhancement, unless a mass degeneracy with some other particle is introduced into the model.

The formalism needed to compute the enhancement when mixing among states is present is slightly more complicated than the one described above, but the general strategy is the same. As shown in the paper by Hisano et al. (Hisano et al., 2005) through direct numerical integration of the Schrödinger equation, the qualitative results of the previous section still hold: for dark matter masses $\gtrsim 1\,\mathrm{TeV}$, a series of resonances appear, and the annihilation cross section can be boosted by several order of magnitude.

An interesting feature of this "multi-state" Sommerfeld effect is the possibility of boosting the cross section for some annihilation channels more than others. This happens when one particular annihilation channel is very suppressed (or even forbidden) for a given two-particle initial state, but not for other initial states. This can be seen as follows. The general form for the total annihilation cross section after the enhancement has been taken into account is

$$\sigma v = N \sum_{ij} \Gamma_{ij} d_i(v) d_j^*(v), \tag{E.1.8}$$

where N is a multiplicity factor, Γ_{ij} is the absorptive part of the action, responsible for the annihilation, the d_i are coefficients describing the Sommerfeld enhancement, and the indices i, j run over the possible initial two-particle states. Let us consider for definiteness the case of the wino-like neutralino: the possible initial states are $\{\chi^0\chi^0, \chi^+\chi^-\}$. The neutralino and the chargino are assumed to be quasi-degenerate, since they are all members of the same triplet. What we will say can anyway be easily generalized to the case of the higgsino-like neutralino. Let us also focus on two particular annihilation channels: the W^+W^- channel and the e^+e^- channel. It can be assumed that, close to a resonance, $d_1 \sim d_2$. This can be inferred for example using the square well approximation as in Ref. (Hisano et al., 2005), where it is found that, in the limit of small velocity, $d_1 \simeq \sqrt{2}(\cos\sqrt{2}p_c)^{-1} - \sqrt{2}(\cosh p_c)^{-1}$ and $d_2 \simeq (\cos\sqrt{2}p_c)^{-1} + 2(\cosh p_c)^{-1}$, where $p_c \equiv \sqrt{2\alpha_2 m/m_W}$. The elements of the Γ matrix for the annihilation into a pair of W bosons are $\sim \alpha_2^2/m_\chi^2$, so that we can write the following order of magnitude estimate:

$$\sigma v(\chi^0\chi^0 \to W^+W^-) \sim |d_1|^2 \frac{\alpha_2^2}{m_\chi^2}. \tag{E.1.9}$$

On the other hand, the non-enhanced neutralino annihilation cross section to an electron-positron pair $\Gamma_{22} \sim \alpha_2^2 m_e^2/m_\chi^4$, so that it is suppressed by a factor $(m_e/m_\chi)^2$ with respect to the gauge boson channel. This is a well-known general feature of neutralino annihilations to fermion pairs and is due to the Majorana nature of the neutralino. The result is that all low velocity neutralino annihilation diagrams to fermion pairs have amplitudes proportional to the final state fermion mass. The chargino annihilation cross section to fermions, however, does not suffer from such an helicity suppression, so that it is again $\Gamma_{11} \sim \alpha_2^2/m_\chi^2 \gg \Gamma_{22}$. Then:

$$\sigma v(\chi^0\chi^0 \to e^+e^-) \sim |d_1|^2 \frac{\alpha_2^2}{m_\chi^2}. \tag{E.1.10}$$

Then we have that, after the Sommerfeld correction, the neutralino annihilates to W bosons and to e^+e^- pairs (and indeed to all fermion pairs) with similar rates, apart from $O(1)$ factors. This means that while the W channel is enhanced by a factor $|d_1|^2$, the electron channel is enhanced by a factor $|d_1|^2 m_\chi^2/m_e^2$. The reason is that the annihilation can proceed through a ladder diagram like the one shown in Fig. E.4, in which basically the electron-positron pair is produced by annihilation of a chargino pair close to an on-shell state. This mechanism can be similarly extended to annihilations to other charged leptons, neutrinos or quarks.

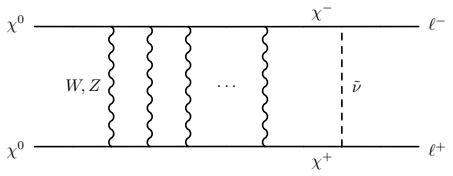

Figure E.4.: Diagram describing the annihilation of two neutralinos into a charged lepton pair, circumventing helicity suppression.

E.1.3. CDM substructure: enhancing the Sommerfeld boost

There is a vast reservoir of clumps in the outer halo where they spend most of their time. Clumps should survive perigalacticon passage over a fraction (say ν) of an orbital time-scale, $t_d = r/v_r$, where v_r is the orbital velocity (given by $v_r^2 = GM/r$). It is reasonable to assume that the survival probability is a function of the ratio between t_d and the age of the halo t_H, and that it vanishes for $t_d \to 0$. Thus, at linear order in the (small) ratio t_d/t_H, a first guess at the clump mass fraction as a function of galactic radius would be $f_{clump} \propto t_d$. We conservatively adopt the clump mass fraction $\mu_{cl} = \nu r v_r^{-1} t_H^{-1}$ with $\nu = 0.1 - 1$. This gives a crude but adequate fit to the highest resolution simulations, which find that the outermost halo has a high clump survival fraction, but that near the sun only 0.1-1 % survive (Springel et al., 2008c). In the innermost galaxy, essentially all clumps are destroyed.

Suppose the clump survival fraction $S(r) \propto f_{clump} \propto r^{3/2}$ to zeroth order. The annihilation flux is proportional to $\rho^2 \times$ Volume $\times\, S(r) \propto S(r)/r$. This suggests we should expect to find an appreciable gamma ray flux from the outer galactic halo. It should be quasi-isotropic with a $\sim$10% offset from the centre of the distribution. The flux from the Galactic Centre would be superimposed on this. High resolution simulations demonstrate that clumps account for as much luminosity as the uniform halo (Diemand et al., 2008), (Springel et al., 2008a). However much of the soft lepton excess from the inner halo will be suppressed due to the clumpiness being much less in the inner galaxy.

We see from the numerical simulations of our halo, performed at a mass resolution of 1000$M_\odot$ that the subhalo contribution to the annihilation luminosity scales as $M_{min}^{-0.226}$ (Springel et al., 2008a). For $M_{min} = 10^5 M_\odot$, this roughly equates the contribution of the smooth halo at $r = 200$ kpc from the center. This should continue down to the minimum subhalo mass. We take the latter to be $10^{-6}M_\odot$ clumps, corresponding the damping scale of a bino-like neutralino (Hofmann et al., 2001; Loeb and Zaldarriaga, 2005). We consider this as representative of the damping scale of neutralino dark matter, although it should be noted that the values of this cutoff for a general weakly interacting massive particle (WIMP) candidate can span several orders of

magnitude, depending on the details of the underlying particle physics model (Profumo et al., 2006; Bringmann, 2009). It should also be taken into account that the substructure is a strong function of galactic radius. Since the dark matter density drops precipitously outside the solar circle (as r^{-2}), the clump contribution to boost is important in the solar neighbourhood. However absent any Sommerfeld boost, it amounts only to a factor of order unity. Incidentally the simulations show that most of the luminosity occurs in the outer parts of the halo (Springel et al., 2008a) and that the boost here due to substructure is large, typically a factor of 230 at r_{200}.

However there is another effect of clumpiness, namely low internal velocity dispersion. In fact, the preceding discussion greatly underestimates the clump contribution to the annihilation signal. This is because the coldest substructure survives clump destruction albeit on microscopic scales. Within the clumps, the velocity dispersion σ initially is low. Thus, the annihilation cross section is further enhanced by the Sommerfeld effect in the coldest surviving substructure. We now estimate that including this effect results in a Sommerfeld-enhanced clumpiness boost factor at the solar neighborhood of 10^4 to 10^5.

To infer σ from the mass M of the clump is straightforward. The scalings can be obtained by combining dynamically self-consistent solutions for the radial dependence of the phase space density in simulated CDM halos (Dehnen and McLaughlin, 2005) as well as directly from the simulations (Vass et al., 2009) $\rho/\sigma^\epsilon \propto r^{-\alpha}$, combined with our ansatz about clump survival that relates minimum clump mass to radius and the argument that marginally surviving clumps have density contrast of order unity. With $\epsilon = 3$ and $\alpha = 1.875$ (Navarro et al., 2008), we infer (for the isotropic case) that $\sigma \propto \rho^{1/\epsilon} r^{\alpha/\epsilon} \propto M^{1/4}$. This is a compromise between the two exact solutions for nonlinear clumps formed from hierarchical clustering of CDM: spherical ($M \propto r^3$) or Zeldovich pancakes ($M \propto r$), and is just the self-similar scaling limiting value. The numerical simulations of Springel et al. (2008c) suggest a scaling $M_{sub} \propto v_{max}^{3.5}$ down to the resolution limit of $\sim 10^3 \mathrm{M}_\odot$, somewhat steeper than self-similar scaling.

So one can combine this result with the previous scaling to compute the total boost, i.e., taking into account both the clumpiness and the Sommerfeld enhancement. We know from the analysis of Springel et al. (Springel et al., 2008a) that for a minimum halo mass of $10^{-6}\, M_\odot$ the luminosity of the subhalo component should more or less equate to that of the smooth halo at the galactocentric radius, i.e. $L^0_{sh} \simeq L^0_{sm}$ at $r = 8\,\mathrm{kpc}$, where the superscript 0 stands for the luminosity in the absence of any Sommerfeld correction. Thus the boost factor with respect to a smooth halo is of order unity, after the presence of subhalos is taken in consideration. Next we take into account the Sommerfeld enhancement. The velocity dispersion in the halo is $\beta \sim 10^{-3}$, while the velocity dispersion in the subhalos is $\beta \sim 10^{-5}$ for a $10^5\, M_\odot$ clump,

and can be scaled down to smaller clumps using the $\sigma \overset{\propto}{\sim} M^{1/4}$ relation. From the discussion in sec. E.1.1 and in particular from Figs. E.2 and E.3 it appears that, if the dark matter mass is $\lesssim 10\,\mathrm{TeV}$ and far from the resonance occurring for $m \simeq 4.5\,\mathrm{TeV}$: (1) the Sommerfeld enhancement is the same for the halo and for the subhalos, since it has already reached the saturation regime; (2) it is of order 30 at most, so that the resulting boost factor still falls short by at least one order of magnitude with respect to the value needed to explain the PAMELA data. On the other hand, if the dark matter mass is close to its resonance value, then a larger value of the boost can be achieved inside the cold clumps, since (1) the enhancement is growing like $1/v^2$ and (2) it is saturating at a small value of β. Referring for definiteness to the top curve in the top panel of Fig. E.3 ($m = 4.5\,\mathrm{TeV}$), one finds $S \simeq 10^4 - 10^5$ for all clumps with mass $M \lesssim 10^9\,M_\odot$ (that is roughly the mass of the largest clumps) while the smooth halo is enhanced by a factor 1000. Then the net result is that the boost factor is of order $10^4 - 10^5$ and is mainly due to the Sommerfeld enhancement in the cold clumps (the enhancement in the diffuse halo only contributing a fraction 1-10%). Of course the details will be model dependent; it should also be stressed that the enhancement strongly depends on the value of the mass when this is close to the resonance.

E.1.4. Discussion

In the previous section we have shown how it is possible to get a boost factor of order $10^4 - 10^5$ for a dark matter particle mass of order 4.5 TeV. This is tantalizing because this is roughly the value one needs to explain the PAMELA data for a dark matter candidate with this given mass, as can be inferred by analysis of Fig. 9 of Ref (Cirelli et al., 2009). Although we have made several approximations concerning the clump distribution and velocity, it should be noted that our results still hold as long as the majority of the clumps are very cold ($\beta \lesssim 10^{-4}$) because this is the regime in which the enhancement becomes constant. The saturation of the Sommerfeld effect also plays a crucial role in showing that the very coldest clumps are unable to contribute significantly to the required boost factor if the dark matter mass is not close to one of the Sommerfeld resonances. Because of saturation below $\beta \sim 10^{-4}$, the Sommerfeld boost is insensitive to extrapolations beyond the currently resolved scales in simulations. Note however that the precise value for the dark matter particle mass is uncertain because of such model-dependent assumptions as the adopted mass-splitting, the multiplet nature of the supersymmetric particles, and the possibility of different couplings, weaker than weak.

The model presented here does not pose any problem from the point of view of the high energy gamma-ray emission from the centre of the galaxy, since very few clumps are presents in the inner core and thus there is no Sommerfeld enhancement. Thus there is no possibility of violating the EGRET

or HESS observations of the galactic center or ridge, contrary to what is argued in Ref. (Bertone et al., 2009). There is a potential problem however with gamma ray production beyond the solar radius out to the outer halo. From (Springel et al., 2008a), the simulations are seen to yield an additional enhancement due to clumpiness alone above $10^5 M_\odot$ of around 80% at r_{200} in the annihilation luminosity. Extrapolating to earth mass clumps, the enhancement is 230 in the annihilation luminosity at the same radius. This is what a distant observer would see. The incorporation of the Sommerfeld factor would greatly amplify this signal by $S \sim 10^4 - 10^5$.

The expected flux that would be observed by looking in a direction far from the galactic center can be readily estimated. Assuming an effective cross section $\sigma v = 3 \times 10^{-22}$ cm^3 s^{-1}, corresponding to a Sommerfeld boost of 10^4 on top of the canonical value of the cross section times velocity, the number of annihilations on the line of sight is roughly $4 \times 10^{-9} (m/\mathrm{TeV})^{-2}$ cm^{-2} s^{-1}. We have assumed a Navarro-Frenk-White (NFW) profile. The effect of the clumpiness is still not included in this estimate. Following the results of the simulation in Ref. (Springel et al., 2008a), this value should be multiplied by a factor $\sim$ 200. Convolving with the single annihilation spectrum of a 5 TeV dark matter particle yields the flux shown in Fig. E.5. There we show the spectrum that would be produced if the dark matter particle would annihilate exclusively either to W bosons, b quarks or τ leptons (blue, red and green curves, respectively). We also consider a candidate that annihilates to τ leptons 90% of the time and to Ws the remaining 10% of the time (model "Hyb1") and a candidate that annihilates only to quarks and leptons, with the same cross section apart from color factors (model "Hyb2").

The gamma ray signal mostly originates from the outer halo and should be detectable as an almost isotropic hard gamma-ray background. Candidates annihilating to heavy quarks or to gauge bosons seem to be excluded by EGRET. On the other hand, a dark matter particle annihilating to τ leptons is compatible with the measurements of EGRET at these energies (Strong et al., 2004), and within the reach of FERMI.

There are however at least two reasons that induce significant uncertainty into any estimates. Firstly, the halo density profile in the outer galaxy may be substantially steeper than is inferred from an NFW profile, as current models are best fit by an Einasto profile (Gao, 2008), $\rho(r) \propto \exp[(-2/\alpha((r/r_s)^\alpha - 1)]$, as opposed to the asymptotic NFW profile $\rho(r) \propto r^{-3}$. Using the Einasto profile yields at least a 10% reduction. Another possibility is to use a Burkert profile (Burkert, 1996), that gives a better phenomenological description of the dark matter distribution inside the halo, as it is inferred by the rotation curves of galaxies (Gentile et al., 2004; Salucci et al., 2007). Using a Burkert profile, the flux is reduced by a factor 3. Secondly, and more importantly, the subhalos are much less concentrated at greater distances from the Galactic Centre (Diemand et al., 2007). These effects should substantially reduce the gamma ray contribution from the outer halo. A future application will be to evalu-

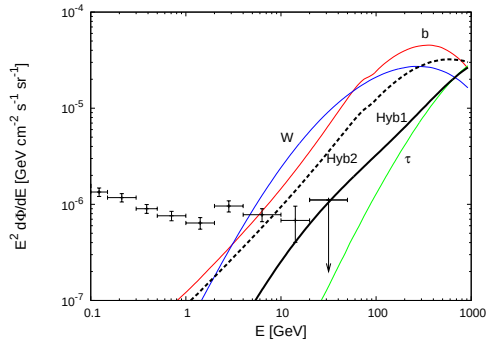

Figure E.5.: Contribution to the diffuse galactic photon background from the annihilation of a 5 TeV dark matter particle, for different channels, when both clumpiness and the Sommerfeld enhancement in cold clumps are taken into account, compared with the measurements of the diffuse gamma background from EGRET (Strong et al., 2004). The label "Hyb1" (solid black line) stands for a hybrid model in which the dark matter annihilates to τ leptons 90% of the time and to W pairs the rest of the time. The label "Hyb2" (dashed black line) stands for a model in which the dark matter annihilates to leptons and quarks only, with the same cross-section apart from color factors. The latter could be realized through the circumvention of helicity suppression.

ate the extragalactic diffuse gamma ray background where the evolution of clumpiness with redshift should play an interesting role in producing a possible spectral feature in the isotropic component. Note that the annihilation rate originating from very high redshift subhalo substructure and clumpiness near the neutralino free-streaming scale (Kamionkowski and Profumo, 2008) is mostly suppressed due to the saturation of the Sommerfeld effect that we described above.

Because of the saturation of the Sommerfeld boost, it should be possible to focus future simulations on improved modelling of the radial profiles and concentrations of substructures in the outer halo. It is these that contribute significantly to the expected diffuse gamma if our interpretation of the PAMELA and the ATIC data, and in particular the required normalisation and hence boost, is correct. Of course, there are other possible explanations of the high energy positron data, most notably the flux from a local pulsar (Aharonian et al., 1995; Yuksel et al., 2009; Hooper et al., 2009a) that has recently been detected as a TeV gamma ray source.

An interesting consequence of the model proposed here is the production of synchrotron radiation emitted by the electrons and positrons produced in the dark matter annihilations, similar to the one that is possibly the cause of the observed "WMAP haze" (Hooper et al., 2007; Cumberbatch et al., 2009). For a TeV candidate, this synchrotron emission would be visible in the $\nu \gtrsim$ 100 GHz frequency region. This region will be probed by the Planck mis-

sion; the synchrotron radiation would then give rise to a galactic foreground "Planck haze" in the microwave/far infrared part of the spectrum. This quasi-isotropic high frequency synchrotron component will be an additional source of B-mode foregrounds that will need to be incorporated into proposed attempts to disentangle any primordial B-mode component in the cosmic microwave background. Another interesting application would be to look at the gamma-ray emission from specific objects, like the Andromeda Galaxy (M31). M31 has been observed in the relevant energy range by the CELESTE and HEGRA atmospheric Cherenkov telescopes, and limits on the partial cross section to photons, in the absence of boost, were obtained by Mack et al. (2008).

Finally, we note that in Sec. E.1.2 we have described a mechanism that can enhance the production of leptons (especially light leptons) in neutralino dark matter annihilations, making the leptonic channel as important as the gauge boson channel. A dark matter candidate annihilating mainly into leptons can simultaneously fit the PAMELA positron and antiproton data, owing to the fact that no antiproton excess is produced. The enhancement of the lepton branching ratio can possibly alleviate the problem of antiproton production following neutralino annihilation into a pair of gauge bosons. It should however be noted that the mechanism in question also enhances the quark channel in a similar way, thus introducing an additional source of antiprotons. It would thus be desirable to suppress in some way the quark annihilation channel. This could be realised in a variation of the above mentioned mechanism, if the lightest neutralino is quasi-degenerate in mass with the lightest slepton $\tilde{l}$; this is what happens for example in the $\tilde{\tau}$ coannihilation region. In this case, the Sommerfeld enhancement would proceed through the creation of an intermediate $\tilde{l}^+\tilde{l}^-$ bound state that would subsequently annihilate to the corresponding standard model lepton pair, without producing any (tree-level) quark. This points to the necessity of further investigating different models in order to assess if the boost in the leptonic branching ratio is indeed compatible with the PAMELA data.

E.2. Constraining the dark matter annihilation cross-section with Cherenkov telescope observations of dwarf galaxies

E.2.1. Introduction

Detection of a rise in the high energy cosmic ray e^+ fraction by the PAMELA satellite experiment (Adriani et al., 2009) and of a possible peak in the $e^+ + e^-$ flux by the ATIC balloon experiment (Chang et al., 2008) has stimulated considerable recent theoretical activity in indirect detection signatures of particle

dark matter via annihilations of the Lightest Supersymmetric Particle (LSP) and other massive particle candidates (Bergstrom et al., 2008; Cirelli and Strumia, 2008; Cholis et al., 2008; Liu et al., 2009; Hooper et al., 2009b; Grajek et al., 2009; Donato et al., 2009; de Boer, 2009; Hooper and Zurek, 2009). Several hurdles must be surmounted if these signals are to be associated with dark matter annihilations. Firstly, a high boost factor $(10^3 - 10^4)$ is needed within a kiloparsec of the solar circle (Cirelli et al., 2008). Secondly, the boost factor must be suppressed in the inner galaxy to avoid excessive γ-ray and synchrotron radio emission (Bertone et al., 2009). Thirdly, the annihilation channels must be largely lepton–dominated to avoid $\bar{p}$ production (Cirelli et al., 2009). Finally, account must be taken of the FERMI/HESS observations of electron/positron fluxes that do not reproduce part of the ATIC data (Abdo et al., 2009; Aharonian, 2009).

The third of these requirements is addressed in various particle physics models for the dark matter candidate (Cirelli et al., 2009). Here we explore the implications of the first two requirements, and comment on the implications of the newest data on particle fluxes. The higher annihilation cross-section needed for the interpretation of the positron excess in terms of dark matter annihilations can be obtained via the Sommerfeld effect (Arkani-Hamed et al., 2009; Lattanzi and Silk, 2009). This effect occurs only at low relative velocities of the annihilating particles, and does not change the thermal cross-section required by cosmological measurements. Robertson and Zentner (2009) examined possible signatures of the Sommerfeld enhancement arising from the non-trivial dependence of the DM velocity distribution upon position within a DM halo. Here we consider the Sommerfeld enhancement in the substructures of our galaxy, where the velocity dispersion is as low as $10\,\mathrm{km\,s^{-1}}$ in the dwarf galaxies and becomes even lower for smaller subhalo masses. The boost, which is inversely proportional to the particle velocity, is especially relevant on the smallest scales that are unresolved by numerical simulations (Springel et al., 2008b). Throughout this paper, we will not consider the full velocity distribution function but will take the central values as a reference for computing the boost.

The second requirement can be understood because the unresolved substructures that dominate the local boost are likely to be tidally disrupted in the inner galaxy (Lattanzi and Silk, 2009). The predictions for signals coming from the Galactic Center (GC) are also reduced by adopting a shallower DM profile. We note that these effects also lower the local $\bar{p}$ contribution.

In this paper, we focus on the γ-ray signal coming from the Draco dwarf galaxy. We choose Draco because its DM density profile is determined in detail (Walker et al., 2009) and because it has been observed by the MAGIC Cherenkov Telescope (Albert et al., 2008). Our aim is to constraint the Sommerfeld enhancement through such a measurement. We will show how the constraints depend sensitively on the astrophysical uncertainties due to both numerical simulations and astronomical measurements. Moreover, we will

show how the result is mainly dominated by the smooth DM halo of the dwarf galaxy, so that it is almost independent of the sub-substructure model used. We also derive exclusion plots for the effective annihilation cross-section obtained with the available measurements, as well as for the sensitivities achievable with future detectors. We apply our results to the case of the Sagittarius dwarf galaxy, which has also been observed with the HESS Cherenkov Telescope (Aharonian, 2008). This galaxy, much closer to us than Draco, would give a higher γ-ray flux and thus sets the greatest constraint. Unfortunately, the tidal stripping of Sagittarius because of its proximity to the GC makes it difficult to model the DM profile. In this paper we will assume that its mass profile can be modeled in the same way as Draco, by adopting the universality of mass profiles in the dwarf galaxies found in Walker et al. (2009). Since neither MAGIC nor HESS have observed any signal along the direction of the targets, we therefore set 95% CL upper limits on the γ-ray coming from these sources.

The paper is organized as follows: in Sec.E.2.2 we model the particle physics scenarios where the Sommerfeld enhancement is largest, as well as the astrophysical uncertainties in the determination of the γ-ray flux; in Sec.E.2.3 we derive the constraints on the effective cross-section set with the available Cherenkov Telescope measurements, and give exclusion plots achievable with the next generation of experiments that make use of Cherenkov Telescope technology, namely the proposed Cherenkov Telescope Array (CTA). We give our conclusions in Sec. E.2.4.

E.2.2. γ-ray flux from Dark Matter annihilation in Draco and Sagittarius

The observed photon flux from DM annihilations inside a halo can be factorized into two terms:

$$\frac{d\Phi_\gamma}{dE_\gamma}(M, E_\gamma, M_h, \mathbf{r}, d, \theta) = \frac{d\Phi_{PP}}{dE_\gamma}(M, E_\gamma) \times LOS(M_h, \mathbf{r}, d, \theta) \tag{E.2.1}$$

where M denotes DM particle mass, E_γ is photon energy, M_h halo mass, $\mathbf{r}$ the position inside the halo, d the distance from the observer and θ the angular resolution of the instrument ($\theta \sim 0.1^\circ$ for the Cherenkov Telescopes). The first term depends on the nature of the DM and describes the yields of photons in a single annihilation:

$$\frac{d\Phi_{PP}}{dE_\gamma}(M, E_\gamma) = \frac{1}{4\pi}\frac{(\sigma v)_0}{2M^2} \cdot \sum_f \frac{dN_\gamma^f}{dE_\gamma} B_f. \tag{E.2.2}$$

Here, dN_γ^f/dE_γ is the differential photon spectrum per annihilation relative to the final state f, which is produced with branching ratio B_f, and $(\sigma v)_0$ denotes the tree level s-wave annihilation cross section, which we assume to be equal to its thermal value necessary for reproducing the observed cosmological abundance today: $(\sigma v)_0 = 3 \times 10^{-26}\,\mathrm{cm}^3\,\mathrm{s}^{-1}$. The second term in Eq. E.2.1 is the line of sight integral of the DM density squared which describes the number of the annihilations which happen along the cone of view defined by the instrument:

$$LOS(M_h, \mathbf{r}, d, \theta) = \int\int_{\Delta\Omega} d\theta d\phi \int_{\mathrm{los}} d\lambda \left[\frac{\rho_{DM}^2(M_h, c, \mathbf{r}(\lambda, \psi, \theta, \phi))}{d^2} J(x, y, z|\lambda, \theta, \phi)\right] \tag{E.2.3}$$

Here, ρ_{DM} is the DM density profile inside the halo, c being the concentration parameter of the halo, defined as the ratio between virial radius and scale radius and computed following the prescriptions of Bullock et al. (2001); $\mathbf{r}$ is the galactocentric distance, which, inside the cone, can be written as a function of the line of sight λ, the angular coordinates θ and ϕ coordinates and the pointing angle with respect to the observed ψ through the relation $r = \sqrt{\lambda^2 + {R_\odot}^2 - 2\lambda R_\odot C}$, where $R_\odot$ is the distance of the Sun from the GC ($R_\odot = 8.5$kpc) and $C = \cos(\theta)\cos(\psi) - \cos(\phi)\sin(\theta)\sin(\psi)$; finally, inside the cone, $d = \lambda$ and $J(x, y, z|\lambda, \theta, \phi)$ is the Jacobian determinant from cartesian to polar coordinates. The presence of the Sommerfeld effect is reflected by setting $\sigma v = S(\beta(M_h, \mathbf{r}), M)(\sigma v)_0$. The Sommerfeld enhancement S now enters the line of sight integral of Eq.E.2.3.

The particle physics sector

The dark matter annihilation cross section can be enhanced, with respect to its primordial value, in the presence of the so-called Sommerfeld effect. This is a (non-relativistic) quantum effect occurring when the slow-moving annihilating particles interact through a potential (Sommerfeld, 1931). The idea that the gamma-ray flux from dark matter annihilations can be enhanced in this way was first proposed in a pioneering paper by Hisano et al. (2004) (see also Hisano et al., 2005). Recently, the possibility of explaining the large boost factor required by PAMELA using this mechanism has stimulated several studies of this effect (see for example Cirelli et al., 2007; March-Russell et al., 2008; Arkani-Hamed et al., 2009; Pospelov and Ritz, 2009; Lattanzi and Silk, 2009; March-Russell and West, 2009).

As already noticed, in the presence of the enhancement, the effective s-

wave annihilation cross section times velocity can be written as:

$$\sigma v = S(\beta, M)\,(\sigma v)_0\,, \tag{E.2.4}$$

where $(\sigma v)_0$ is the tree level s-wave annihilation cross section, and the Sommerfeld enhancement S depends (for a given interaction potential) on the annihilating particle mass M and velocity $\beta = v/c$.

The enhancement is effective in the low-velocity regime, and disappears ($S = 1$) in the limit $\beta \to 1$. In general, one can distinguish two distinct behaviours, resonant and non-resonant, depending on the value of the annihilating particle mass. In the non-resonant case, the cross section grows like $1/\beta$ before saturation occurs at a certain value $S_{\max}$ of the enhancement. In the resonant case, occurring for particular values of M, the cross-section first grows like $1/\beta$ (as in the non-resonant case), then at some point it grows like $1/\beta^2$ before saturating. The Sommerfeld boost can reach very large values. Both in the resonant and non-resonant case, the values of β and S for which the saturation occurs depend, other than on the particle mass, on the parameters of the interaction potential, namely the coupling constant α and the mass of the exchange boson m_V.

In this paper, we will consider two different particle physics scenarios. In the first, we consider a weakly interacting massive particle (WIMP) dark matter candidate. In this case the Sommerfeld effect is caused by the standard model weak interaction, mediated by W and Z bosons, so that $m_V = 90$ GeV and $\alpha = 1/30$. If the dark matter is a Majorana particle, such as for example the supersymmetric neutralino, its annihilation into a fermionic final state f is helicity-suppressed by a factor $(m_f/M)^2$. For a dark matter particle in the 1 to 10 TeV range, this is a factor $10^{-2} \div 10^{-4}$ even for the heaviest possible final state, i.e. the top quark. Thus we are naturally led to consider a candidate that annihilates mainly to weak gauge bosons. However, for completeness we have also considered the heavy quark and lepton annihilation channels. The differential photon spectra per annihilation dN_γ^f/dE_γ for the various final states have been computed using PYTHIA (Sjostrand et al., 2001), including also the contribution from final state radiation.

We consider the following values for the mass of the particle: $M = (4.3,\ 4.45,\ 4.5,\ 4.55\,\mathrm{TeV})$. This values are chosen because, in the case of a weak interaction potential, a resonance in the Sommerfeld-enhanced cross section occurs for $M \simeq 4.5$TeV (Lattanzi and Silk, 2009). Being so close to the resonance, even a relatively small change in the mass of the particle can produce order of magnitude changes in the Sommerfeld boost. In fact, the maximum achievable boost goes from $S \simeq 1.5 \times 10^3$ for $M = 4.3\,\mathrm{TeV}$ to $S \simeq 4 \times 10^5$ for $M = 4.55\,\mathrm{TeV}$.

The second scenario we consider has been introduced by Arkani-Hamed et al. (2009) [AH]. In this model, a new force with a coupling constant $\alpha \sim 10^{-2}$ is introduced in the dark sector, mediated by a boson ϕ having a mass $m_V =$

Mass (TeV)	m_V(GeV)	α	S_{max}	$\bar{\beta}$
4.3	80	$1/30$	1.5×10^3	8.0×10^{-4}
4.45	80	$1/30$	1.2×10^4	2.8×10^{-4}
4.5	80	$1/30$	7.0×10^4	1.1×10^{-4}
4.55	80	$1/30$	4.2×10^5	4.7×10^{-5}
0.7	1	10^{-2}	750	2.4×10^{-5}
0.7	0.1	10^{-2}	750	8.5×10^{-6}

Table E.1.: Values of the maximum possible boost S_{max} and of the saturation velocity $\bar{\beta}$, for different dark matter models. Each model is defined by the value of the dark matter particle mass M, and by the parameters of the Yukawa potential responsible for the enhancement, namely the mass m_V of the exchange boson and the coupling constant α.

$m_\phi \lesssim 1$ GeV. It is this new force that is responsible for the Sommerfeld enhancement. In this case, it is found that the large boosts required to explain the PAMELA and ATIC data can be obtained for a dark matter particle of mass $M \simeq 700$ GeV. In AH models, the dark matter annihilates mainly to ϕ bosons, that in turn decay into electrons or muons (depending on the mass of the ϕ). The gamma rays are produced in the decay of the ϕ as final state radiation (Bergstrom et al., 2009). We consider two particular realisations of this scenario: we take the dark matter mass to be $M = 700\,\mathrm{GeV}$ in both, and m_ϕ equal to either 100 MeV or 1 GeV. We note that the dark matter interaction cross section in the first case is only one order of magnitude away from the upper bound coming from observations of the mass distribution inside clusters of galaxies (Miralda-Escudé, 2002).

The enhancement as a function of velocity in the models considered is depicted in Fig. E.6. The main properties of the enhancement, i.e. the maximum value S_{max} and the saturation velocity $\bar{\beta}$, are summarised in Table E.1 for the different models, together with the parameters of the interaction potential that is responsible for the Sommerfeld boost. We point out that, in the case of dwarf galaxies and their subhalos, the dispersion velocity is of the order of $10\,\mathrm{km\,s^{-1}}$, which means that we are always in the saturation regime, and the enhancement is always maximum, and equal to S_{max}. As we show in the next sections, these large boost factors can be tested through Cherenkov telescope observations of dwarf galaxies.

The astrophysical sector: smooth dark matter halo

We discuss here the modeling of the dark matter inside the Draco dwarf galaxy. Walker et al. (2009) have recently demostrated the existence of a universal mass profile for the dwarf spheroidal galaxies of the Local Group, find-

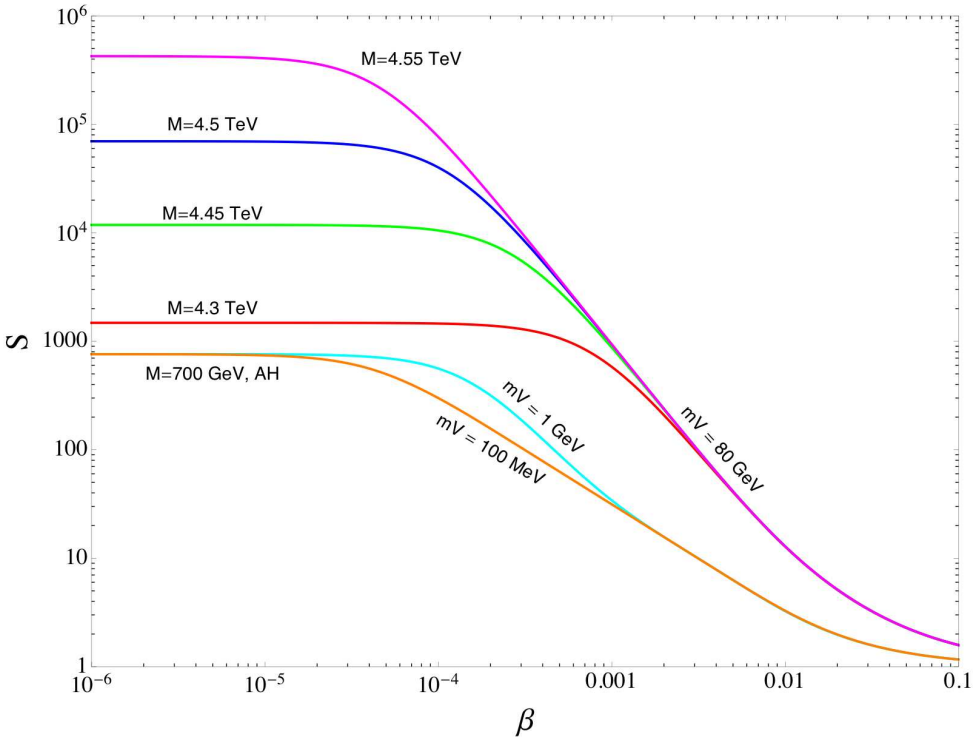

Figure E.6.: Sommerfeld enhancement S as a function of the particle velocity β for different values of the dark matter mass close to the resonance in our model with α= 1/30 and $m_V = 80$ GeV, as well as for a model with $\alpha = 10^{-2}$ and $m_V = 1$ GeV and 100 MeV (labeled AH).

ing that the enclosed mass at the half-light radius is well constrained and robust within a wide range of halo models and velocity anisotropies and that the dwarfs can be characterized by a universal dark matter halo of fixed shape and narrow range in normalization. The Draco galaxy lies about 80 kpc away from us, almost at the zenith with respect to the GC ($\psi_D \sim 85°$). Walker et al. (2009) found that a cuspy NFW halo:

$$\rho_{DM}(r) = \frac{\rho_s}{\left(\frac{r}{rs}\right)\left(1+\frac{r}{rs}\right)^2} \tag{E.2.5}$$

with scale radius $r_s \sim 1$kpc is the best fit to the data on the stellar velocity dispersions, although a cored universal halo:

$$\rho_{DM}(r) = \frac{\rho_s}{\left(1+\frac{r}{rs}\right)^3} \tag{E.2.6}$$

with scale radius $r_s \sim 200\,\mathrm{pc}$ is not yet ruled out. The scale density ρ_s is fixed by requiring that the mass embedded in the inner 300 pc equals the measured value of $M_{300} = 1.9 \times 10^7\,\mathrm{M}_\odot$. In Table E.2 we list the central values as well as the 95 % CL ones for the scale radius as universally found for the dwarfs by Walker et al. (2009). We note the King radius of Draco is $\sim 650\,\mathrm{pc}$ (Armandroff et al., 1995), which roughly corresponds to the scale for the mass universality in the dwarf galaxy (600 pc). The mass measured within 600 pc in the case of Draco is about $7 \times 10^7\,\mathrm{M}_\odot$, and the mass enclosed by the maximum radius with stellar velocity dispersion measurements is $\sim 9 \times 10^7\,\mathrm{M}_\odot$, while the virial mass is estimated to be $4 \times 10^9\,\mathrm{M}_\odot$ with a concentration parameter $c_{NFW} \sim 18$ (Walker et al., 2007).

The satellites, or subhalos, of our Galaxy suffer from external tidal stripping due to the interaction with the Milky Way. To account for gravitational tides, we follow Hayashi et al. (2003) and assume that all the mass beyond the subhalo tidal radius is lost in a single orbit without affecting its central density profile. The tidal radius is defined as the distance from the subhalo center at which the tidal forces of the host potential equal the self-gravity of the subhalo. In the Roche limit, it is expressed as:

$$r_{tid}(r) = \left(\frac{M_{sub}}{2M_{host}(<r)}\right)^{1/3} r \tag{E.2.7}$$

where r is the distance from the halo center, M_{sub} the subhalo mass and $M_{host}(<r)$ the host halo mass enclosed in a sphere of radius r.
In our case, the host halo is the Milky Way (MW), which we model after the recent high resolution N-body simulations *Aquarius* (Springel et al., 2008b,c) and *Via Lactea II* (Diemand et al., 2008): while the latter describes the MW with an NFW profile ($M_h \sim 1.9 \times 10^{12}\,\mathrm{M}_\odot$, $r_s = 21$kpc, $\rho_s = 8.09 \times 10^6\,\mathrm{M}_\odot\mathrm{kpc}^{-3}$),

the former finds a shallower profile in the inner regions. We have checked that the difference between the two profiles are irrelevant for our analysis.
At the distance of Draco, we find $r_{tid} = 11.2$kpc. We note that the condition $r_{tid} > r_s$ holds, which guarantees that the binding energy is negative and the system is not dispersed by tides. The value of r_{tid} found making use of the Roche criterium is indeed an upper limit since it has been computed in the pointlike approximation.
The LOS integral for the Draco galaxy is computed by numerically integrating Eq. E.2.3, assuming that the integral is different from zero only in the interval $[d - r_{tid}, d + r_{tid}]$.

In the case of the dwarf galaxies, their mass and therefore the masses of the sub-subhalos lie in the region at low β where the Sommerfeld enhancement saturates. This is true for every DM mass except for the one which lies closest to the resonance (in our model, $M = 4.55$TeV). In this case, however, the radial dependence of the enhancement produces a variation of a few percent, so that as a good approximation, the Sommerfeld enhancement S can be considered constant and taken out of the LOS integral. The result of the computation of the LOS integral ($S = 1$) according to Eq.E.2.3 in the case of Draco is depicted in Fig.E.7 as a function of the angle of view ψ with respect to the center of Draco. Only the LOS relative to the central value for the NFW fit to the data is shown.

In view of the dark matter profile universality, we model the inner regions of the closer Sagittarius galaxy using the same profile parameters as in the case of Draco (see also Evans et al. (2004) for a comparison between the Draco and Sagittarius inner DM profiles), although there is no direct evidence of the shape of its DM halo. The Sagittarius dwarf galaxy is located at a distance of about 24 kpc from us, at low latitudes $\psi_S = 15^\circ$. Its vicinity to the Galactic Center causes significant tidal stripping due to the interaction with the gravitational potential of the Milky Way. Yet the surviving stellar component suggests that its inner dark matter halo also survives. Moreover, the observations show that Sagittarius is indeed dark matter-dominated with a central stellar velocity dispersion of about 10 km s^{-1} (Ibata et al., 1997), similar to the one observed in Draco. At the distance of Sagittarius, the tidal radius is $r_{tid} = 4$kpc, still larger than the scale radius.

The results of the line of sight integral towards the center of each dwarf galaxy are shown in Table E.2, for the central value and the 95 % CL values of both the best fit NFW and the cored profile obtained by Walker et al. (2009).

In Table E.3 we list the values of the LOS computed for the smooth component of the MW in the direction of the dwarf galaxies, which will provide a foreground for the detection of the dwarfs themselves. We do not describe in this paper the details of these computations, which are studied extensively in Pato et al. (2009) and Pieri, Bertone & Branchini (in preparation). We observe

Draco fit	r_s(kpc)	$LOS^D_{\psi_D=0}$	$LOS^S_{\psi_S=0}$
NFW	0.795	1.05×10^{-3}	4.43×10^{-3}
NFW $+2\sigma$	3.0	7.85×10^{-4}	2.8×10^{-3}
NFW -2σ	0.3	1.91×10^{-3}	9.8×10^{-3}
Core	0.15	7.5×10^{-4}	2.17×10^{-3}
Core $+2\sigma$	0.3	5.2×10^{-4}	9.4×10^{-4}
Core -2σ	0.085	1.54×10^{-3}	6.9×10^{-3}

Table E.2.: Line of sight integral for the smooth halo of the dwarf galaxies. First column: models reflecting the astronomical uncertainties from a fit to the Draco stellar velocity dispersion. Second column: scale radius for each model. Third column: values for the LOS integral toward the center of Draco. Fourth column: values for the LOS integral toward the center of Sagittarius.

MW model	$LOS_{\psi_{MW}=\psi_D}$	$LOS_{\psi_{MW}=\psi_S}$
VL2	1.18×10^{-5}	2.73×10^{-4}
Aquarius	1.13×10^{-5}	4×10^{-4}

Table E.3.: Line of sight integral for the smooth component of the Milky Way integrated along a direction pointing towards the center of the dwarf galaxies. First column: MW model from numerical simulation. Second column: line of sight integral towards the center of Draco. Third column: line of sight integral towards the center of Sagittarius.

that, both for Draco and for Sagittarius, the dwarf center is brighter in γ-ray than the MW foreground.

The astrophysical sector: substructures

The recent *Aquarius* and the *Via Lactea II* simulations have succeeded in determining the properties of the subhalos and sub-subhalos such as spatial and mass distribution, density profiles and spatial dependence of the concentration parameter. We therefore study the effects on the expected γ-ray flux of a population of sub-subhalos inside the dwarfs according to the recent findings of numerical simulations, although we do not expect a significant impact on the expected flux towards the center of the dwarf, where the smooth halo flux is larger (Giocoli et al., 2008, 2009). We populate Draco with sub-subhalos with masses as small as $10^{-6}M_\odot$, corresponding to the damping scale of a typical DM candidate with $M = 100$GeV (Hofmann et al., 2001; Green et al., 2004, 2005; Loeb and Zaldarriaga, 2005). It should howevere be noted that such a minimum mass may vary between 10^{-12} and $10^{-4}M_\odot$ depending on the particle physics model considered (Profumo et al., 2006).

We follow the results of *Via Lactea II* to model the population of sub-substructures:

$$\rho_{sh}(M_h, M_{sub}, r) = \frac{A M_{sub}^{-\alpha}}{\left(1 + \frac{r}{r_s^h}\right)^2} \, \mathrm{M}_\odot{}^{-1}\mathrm{kpc}^{-3} \tag{E.2.8}$$

where r_s^h is the scale radius of the host halo and r is the radial coordinate inside the host halo. We normalize the subhalo distribution function $\rho_{sh}(M_h, M_{sub}, r)$ such that 10 % of the mass of the host halo before the tidal stripping is distributed in substructures with masses between $10^{-5}M_h$ and $10^{-2}M_h$, adopting two choices for the mass slope $\alpha = 2$ and $\alpha = 1.9$. We have checked that modeling the spatial substructure distribution function according to *Aquarius* does not significantly change our results.

As a second step, we remove all of the subhalos which lie beyond r_{tid}. This is indeed an upper value for the number of surviving sub-subhaloes, since we are not considering here the fifty percent of the subhalos that exit the virial radius of the parent halo during their first orbit (Tormen et al., 2004) and are therefore dispersed into the halo of the Milky Way.
The contribution of such a population of sub-substructures to the annihilation signal can be written as (Pieri et al., 2008):

$$LOS(M_h, \mathbf{r}, d, \theta) \propto \int_{M_{sub}} dM_{sub} \int_c dc \int \int_{\Delta\Omega} d\theta d\phi$$

$$\int_{los} d\lambda [\rho_{sh}(M_h, M_{sub}, \mathbf{r}) P(c(M_{sub}, r)) LOS_{sh}(M_{sh}, \mathbf{r}, d, \theta)] \tag{E.2.9}$$

where the contribution from each sub-subhalo (LOS_{sh}) is convolved with its distribution function (ρ_{sh}). $P(c)$ is the lognormal distribution of the concentration parameter with dispersion σ_c = 0.24 (Bullock et al., 2001) and mean value $\bar{c}$:

$$P(\bar{c}, c) = \frac{1}{\sqrt{2\pi}\sigma_c c} \, e^{-\left(\frac{\ln(c) - \ln(\bar{c})}{\sqrt{2}\sigma_c}\right)^2}. \tag{E.2.10}$$

Again, the integral along the line-of-sight will be different from zero only in the interval $[d - r_{tid}, d + r_{tid}]$.

For each sub-substructure, we use an NFW density profile whose concentration parameter $c(M_{sub}, r)$ relative to the radius R_{vir} that encloses an average density of 200 $\times$ the critical one, depends on its mass and on its position inside the host halo, according to the results of *Via Lactea II* and Bullock et al.

Draco fit	mass slope	$LOS^{D,sub}_{\psi_D=0}$	$LOS^{S,sub}_{\psi_S=0}$
NFW	-2	4.13×10^{-5}	5.40×10^{-5}
NFW	-1.9	1.03×10^{-5}	1.34×10^{-5}
NFW $+2\sigma$	-2	3.85×10^{-6}	4.25×10^{-6}
NFW $+2\sigma$	-1.9	9.5×10^{-7}	1.05×10^{-6}
NFW -2σ	-2	1.98×10^{-4}	3.10×10^{-4}
NFW -2σ	-1.9	4.94×10^{-5}	7.71×10^{-5}

Table E.4.: Line of sight integral for the clumpy component of the dwarf galaxies. First column: models reflecting the astronomical uncertainties from a fit to the Draco stellar velocity dispersion. Second column: subhalo mass slope. Third column: values for the LOS integral toward the center of Draco. Fourth column: values for the LOS integral toward the center of Sagittarius.

(2001) extrapolated to $10^{-6}\,\mathrm{M}_\odot$:

$$c(M_{sub}, r) = \left(\frac{r}{R_{vir}}\right)^{-0.286} \times \left(89.04 \left(\frac{M_{sub}}{\mathrm{M}_\odot}\right)^{-0.0135} - 42.43 \left(\frac{M_{sub}}{\mathrm{M}_\odot}\right)^{0.006}\right) \quad \text{(E.2.11)}$$

We numerically integrate Eq. E.2.9 to estimate the LOS contribution from the sub-substructures in a 10^{-5} sr solid angle along the direction ψ_D or ψ_S towards the center of the dwarfs. The result of this computation for the subhalo population of Draco is depicted in Fig.E.7 as a function of ψ_D, for the central value of the NFW fit to the stellar kinematics and for a mass slope of -2. As expected, this contribution becomes relevant only away from the center, where it anyway gives a flux which is one order of magnitude smaller.

We repeat the same analysis for Sagittarius, assuming its sub-subhalo population is modeled in the same way as the Draco's one, yet with a smaller todal radius. The result of the integration of Eq. E.2.9 along a direction pointing towards the center of the dwarfs is listed in Table E.4. Although the values in the case of Sagittarius are slightly larger than for Draco, due to its proximity to us, the relative strength of the smooth to clumpy component is larger in Draco, making the presence of sub-subhalos in Sagittarius almost irrelevant with respect to the smooth component.

In Table E.5 we compute the values of the LOS flux computed for the clumpy component of the MW in the direction of the dwarf galaxies. We observe that, both for Draco and for Sagittarius, the dwarf center is brighter in γ-rays than the MW clumpy foreground. We do not describe in this pa-

subhalo mass slope	$LOS^{sub}_{\psi_{MW}=\psi_D}$	$LOS^{sub}_{\psi_{MW}=\psi_S}$
-2	2×10^{-5}	5.5×10^{-5}
-1.9	2.5×10^{-6}	6.5×10^{-6}

Table E.5.: Line of sight integral for the clumpy component of the Milky Way integrated along a direction pointing towards the center of the dwarf galaxies. First column: Subhalo mass slope. Second column: line of sight integral towards the center of Draco. Third column: line of sight integral towards the center of Sagittarius.

per the details of these computations, which can be found in Pato et al. (2009) and Pieri, Bertone & Branchini (in preparation). The MW foreground contribution to Draco, computed including its smooth and clumpy component, is shown in Fig.E.7. The band of values accounts for the different simulations as well as for the different subhalo mass slope. The MW foreground begins hiding Draco at around 0.3 degrees from the Draco center. We have checked that the same happens in the case of Sagittarius.

The mass modeling of the dwarf galaxies at large distances from their centers is just an educated guess; as a check of consistency of our results, we repeated our calculations in the case when the DM halo extends only up to 600 pc, that is to say to the King radius (we remind that the mass within the King radius is directly measured through stellar kinematics). The differences between the computations extending to R_{vir} and the ones extending to the 600 pc amount to 5% at most.

In the following section we will compare our predictions with the available data and expected sensitivities from the atmospheric Cherenkov telescopes (ACTs). To compare with the data, we will consider the sum of the four contributions to the photon flux: 1) annihilations in the smooth halo of the dwarf galaxy, 2) annihilations in the subhalos of the dwarf galaxy, 3) annihilations in the smooth halo of the Milky Way and 4) in the subhalos of the Milky Way, computed along the direction which corresponds to the position of the dwarf galaxy in the sky. The relative importance of the four terms depends on the angle of view from the centre of the dwarf galaxy, as well as on the particle physics model. The contribution due to the annihilation in the smooth halo of the dwarf galaxy is always predominant when looking at the dwarf center.

E.2.3. Comparison with the experimental data

The MAGIC and HESS ACTs have put 95 % upper limits on the γ-ray fluxes from Draco and Sagittarius, respectively. The upper limit for Draco inte-

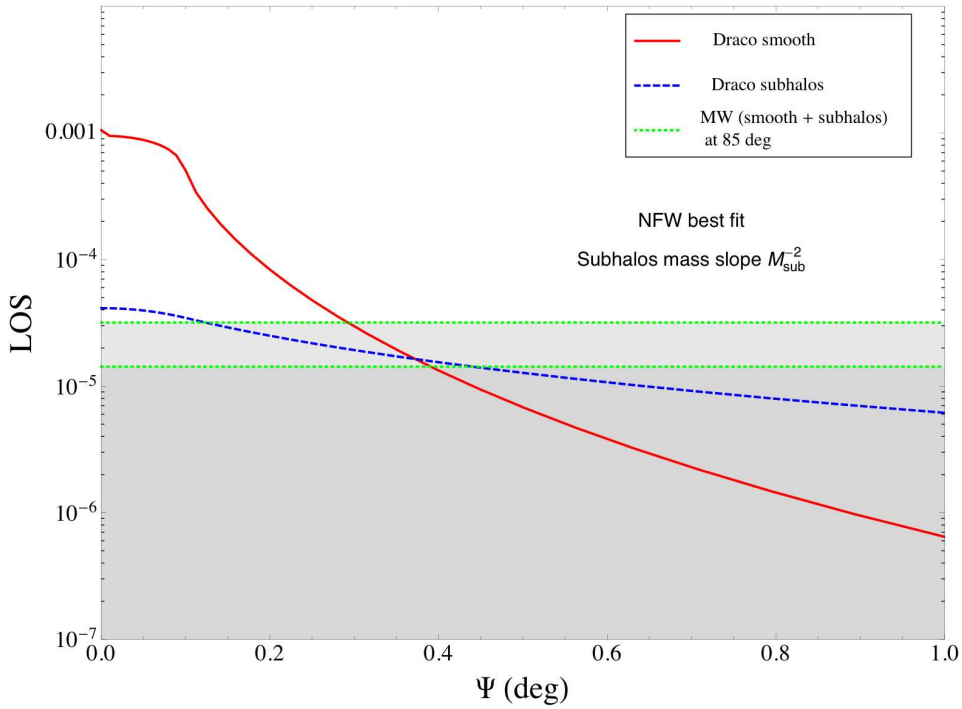

Figure E.7.: Φ_{cosmo} as a function of the angle of view ψ from the centre of halo, computed in the case of Draco and Sagittarius, for the smooth halo and from the subhalo population.

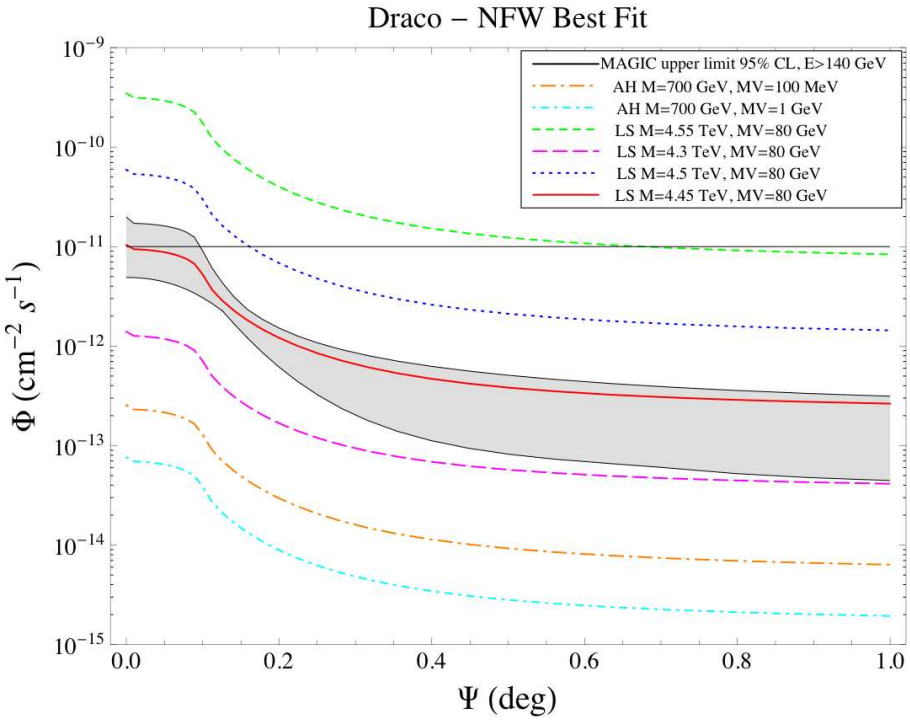

Figure E.8.: Expected γ-ray flux above 140 GeV as a function of the angle of view ψ from the centre of Draco.

grated over energies above 140 GeV is 10^{-11} ph cm^{-2} s^{-1}. In the case of Sagittarius, this limit is 3.6×10^{-12} ph cm^{-2} s^{-1}, integrated above 250 GeV.

In Fig. E.8 and E.9 we compare these values with the prediction of the γ-ray flux from DM annihilations. We compute the flux for the particle DM models described in Sec.E.2.2. We show the result in the case of the central value for the scale radius in the NFW best fit to the kinematic data, as derived in Walker et al. (2009). Indeed, in the case of M=4.45 TeV, we show the astrophysical uncertainty by plotting the curves relative to NFW and cored fits, for central and 95 % CL values of the scale radius.
We note that our dwarfs actually appear as point sources for an angular resolution of 0.1°.
The data from both MAGIC and HESS already exclude the highest Sommerfeld-enhanced cross-sections.

Since the main contribution to the γ-ray flux at the center of the dwarf comes from halos which are in saturation with respect to the velocity-dependent enhancement, we can present the previous results in terms of an exclusion plot on the effective Sommerfeld-enhanced cross-section. In Fig.E.10 we show the exclusion limit on the effective annihilation cross-section imposed by the MAGIC upper limit on Draco, in the case when the DM particle annihilates

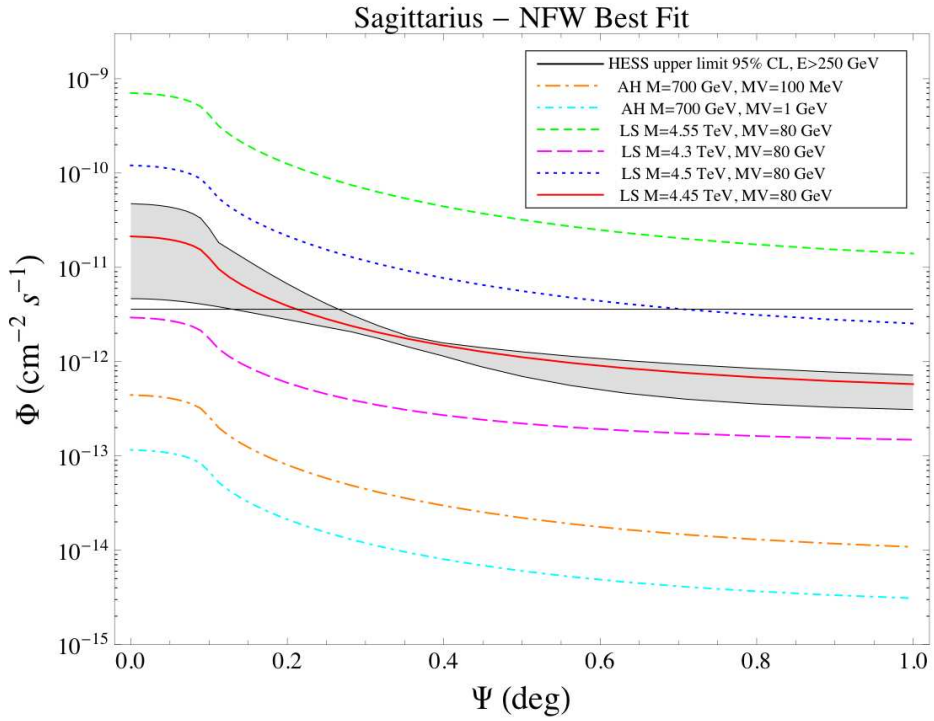

Figure E.9.: Expected γ-ray flux above 250 GeV as a function of the angle of view ψ from the centre of Sagittarius.

in gauge bosons. The band of values reflects the astrophysical uncertainties due to astronomical data and numerical simulations. For comparison, we also show the exclusion plot obtained by the observation of the GC with the HESS telescope. HESS has extensively observed the Galactic Center (GC) source, measuring an integrated flux above 160 GeV of $\Phi(> 160\text{TeV}) = 1.87 \times 10^{-11}\,\text{ph}\,\text{cm}^{-2}\,\text{s}^{-1}$ in 2003 and 2004 (Aharonian et al., 2006).
In order to compute the Sommerfeld enhancement of the MW halo towards the GC, it is necessary to convolve the information on the rotation curve of our Galaxy with the β-dependence of the effect, and including the presence of the black hole at the center of the Galaxy. This computation has been done in Pato et al. (2009) and brings enhancements of the order of 10^3 to 10^4 for the Lattanzi & Silk models, and of the order of 10^2 for the Arkani-Hamed model. In Fig.E.10 we report the exclusion limit with respect to a constant effective Sommerfeld-enhanced annihilation cross-section. The band of values for each experiment reflects the astrophysical uncertainty due to the inner profile. We have used the spiky NFW profiles obtained by *Via Lactea II* and a cored isothermal profile with scale radius $r_s = 5$kpc normalized to the same local value for the DM density as found in *Via Lactea II* (i.e. $\sim 0.4\text{GeV}\,\text{cm}^{-3}$). Since simulations do not include baryons which may play an important role at the GC, the large uncertainty on the inner pro-

file prevents this measurement to put strong limits. As an exercise, we computed the sensitivity to Draco to the space-based telescope Fermi and the future Cherenkov Telescope Array (CTA) [2]. The CTA is a proposed experiment which will make use of Cherenkov Telescope technology on a large scale, in order to lower the threshold energy down to $\sim$ 50GeV. The instrument is being designed. The tens of telescopes in the array could either look at different portions of the sky, thus reaching up to $\sim$ 1 sr of field of view, or focus on the same source, thus dramatically increasing the single telescope sensitivity. We take a sample sensitivity from the CTA home page, according to which the CTA will be able to detect $\Phi(> 50\text{GeV}) = 7 \times 10^{-12}$ ph cm^{-2} s^{-1} and $\Phi(> 1\text{TeV}) = 2.9 \times 10^{-14}$ ph cm^{-2} s^{-1}. Such a sensitivity to a single source could improve if more telescopes could point at the same source. In the case of Fermi, we took the sensitivity to point sources from Baltz et al. (2008), that is to say, $\Phi(> 3\text{GeV}) = 10^{-10}$ ph cm^{-2} s^{-1}. We show the sensitivity bands for Fermi and the CTA in Fig.E.10. The uncertainty always derives from astrophysics. Although a boost to the thermal annihilation cross-section is always required to observe Draco (see also Pieri et al., 2009a), the limits will improve significantly with the future data.
In Fig.E.11 we show the same kind of exclusion limits and expected sensitivities as in Fig.E.10, yet computed for a DM particle annihilating into e^+e^- and producing photons as a final state radiation. The limits and sensitivities at high DM masses are in this case poorly restrictive.

Finally, in Fig.E.12 we show the sensitivity to Sagittarius with Fermi and the CTA, under the assumption that we have used all throughout the paper, namely that the inner DM halo of Sagittarius is modeled as the one of Draco. We superimpose the effective cross-section as a function of the DM particle mass in the case of a Sommerfeld effect mediated by a 80 GeV boson, for different values of β. For TeV DM masses close to the resonance, with a boost of a factor $\sim 10^3$, the CTA would be the only instrument able to detect the signal.

In general, the constraints will depend, among other things, on the final states for annihilation. In the case of the WIMP scenario, the results discussed so far have been obtained considering a dark matter particle of mass $M \simeq 4.5$ TeV annihilating exclusively into gauge bosons. Considering instead annihilation into heavy quarks or leptons as possible final states changes the predicted fluxes by factors of order unity, thus leaving our conclusions basically unchanged. In particular, a particle that annihilates only to heavy quarks would produce a flux 1.6-1.7 times larger than that shown in the figures, for all experiments. The limits on the Sommerfeld boost would then be proportionally tighter. In the case of a particle annihilating to τ leptons, the change in the flux depends on the energy threshold: for MAGIC, HESS and CTA it is respectively 0.5, 0.8, and 3.8 times the flux from the gauge boson channel.

[2] CTA homepage: http://www.cta-observatory.org/

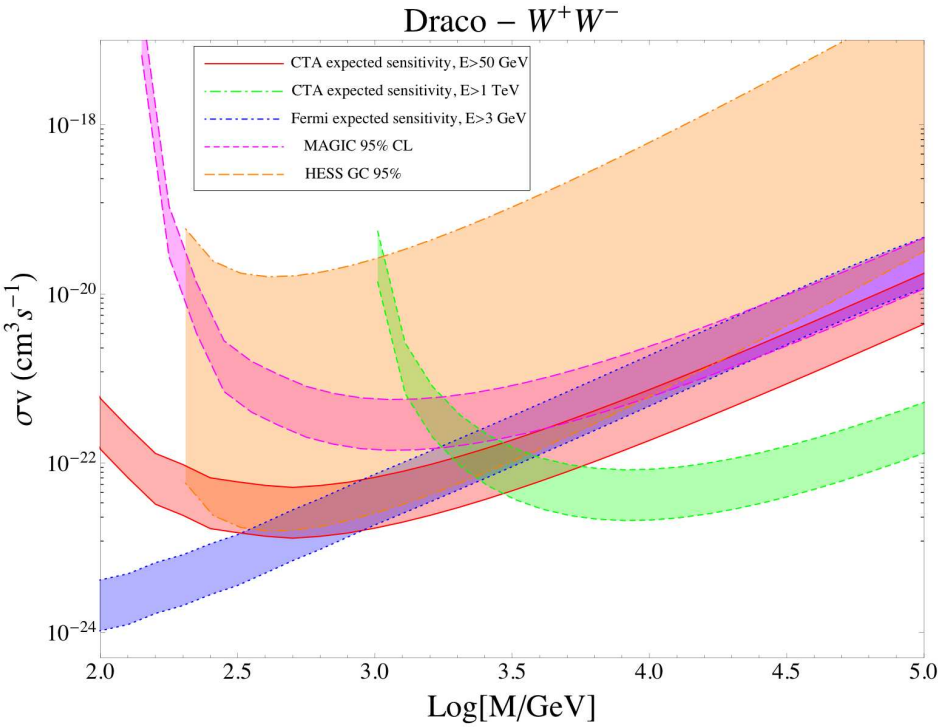

Figure E.10.: Exclusion plot (MAGIC and HESS GC) and expected sensitivity (CTA and Fermi) for the effective annihilation cross section, in the case of γ-ray observations of the Draco galaxy and for dark matter particles annihilating into WW.

Ligther leptonic and quark final states are strongly disfavoured due to the helicity suppression; however they could become important if the helicity suppression is lifted in some way. In the case of the AH scenario, the final spectrum is instead naturally driven to light leptons (electrons and muons) since heavier states are kinematically forbidden.

E.2.4. Conclusions

The excess in cosmic-ray positrons and electrons has motivated a wealth of theoretical efforts in order to be explained in terms of DM. In particular, the annihilation mechanism has been revised in the light of the Sommerfeld enhancement, a velocity-dependent effect. Such an effect is maximal in the dwarf galaxies and in their substructures. The enhancement actually saturates for DM halo masses smaller than the dwarf scale. Several studies (see. e.g. Bertone et al., 2009; Cirelli and Panci, 2009; Galli et al., 2009; Pato et al., 2009) have recently constrained the Sommerfeld enhancement and thus the interpretation of the Pamela excess in terms of dark matter. However, the DM halo of the dwarf galaxies can now be modeled making use of kinematic stel-

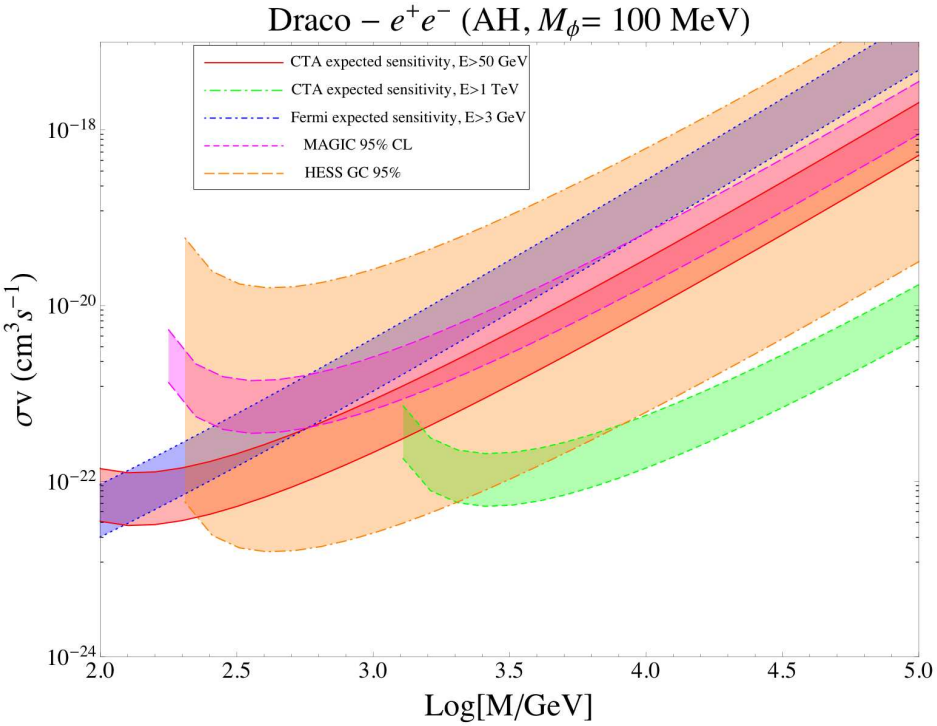

Figure E.11.: Exclusion plot (MAGIC and HESS GC) and expected sensitivity (CTA and Fermi) for the effective annihilation cross section, in the case of γ-ray observations of the Draco galaxy and for dark matter particles annihilating into e^+e^- in the AH case with M_V = 100 MeV.

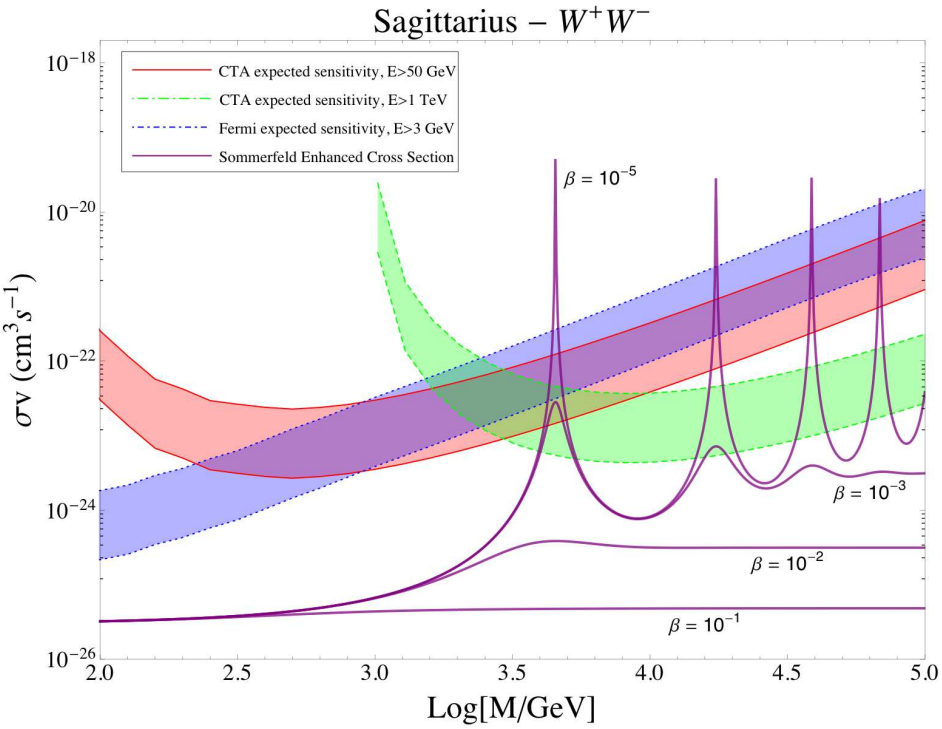

Figure E.12.: Expected sensitivity for the effective annihilation cross section, in the case of γ-ray observations of the Sagittarius galaxy and for dark matter particles annihilating into WW.

lar data with a precision which is far better than the uncertainties on the MW DM profile or on the subhalo population or on the propagation parameters which affect the limits set by antimatter, radio and γ-ray signals. We have computed the expected γ-ray flux from the Draco and the Sagittarius dwarf galaxies, for which upper limits are available from the ACTs. We have computed the flux within the astrophysical uncertainties and we find that the measurements of MAGIC and HESS are able to constrain the enhancement and set an upper limit of $\sim 10^4$. We have shown that the future CTA experiment should be able to test the boost relative to the thermal annihilation cross-sections up to values of a few hundred.

F. Alternative Cosmological Models

Precision measurement of the cosmological observables have lead to believe that we leave in a flat Friedmann Universe, seeded by nearly scale-invariant adiabatic primordial fluctuations Komatsu et al. (2009). The majority ($\sim 70\%$) of the energy density of the Universe is in the form of a fluid with a cosmological constant-like equation of state ($w \sim -1$), dubbed dark energy, that is responsible for the observed acceleration of the Universe Frieman et al. (2008). Although this "concordance model" gives a very satisfactory fit of all available data, nevertheless it should be noted that a convincing theoretical explanation for what the dark energy is, is still missing. For this reason it is worth looking for alternatives to the concordance model. Several interesting ideas have been put forward in this regard. One is that the observed acceleration is an artefact due to small-scale inhomogeneities. However this interpretation has to deal with the fact that hints for the presence of dark energy come not only from the acceleration, but also from the CMB data.

Recently, Blanchard et al. (2003) have noted that in fact, by relaxing the hypothesis that the fluctuation spectrum can be described by a single power law, the CMB data can be well fitted by a Universe with zero cosmological constant. In this alternative model, the Hubble constant has to be very low ($\sim 46\,\mathrm{km\,s^{-}1Mpc^{-1}}$) with respect to the value measured by the Hubble space telescope ($\sim 72\,\mathrm{km\,s^{-}1Mpc^{-1}}$), but this could be explained if we were living in an underdense region, so that our local neighborhood was expanding faster that the average. This would imply that the Hubble constant measured by the HST would be larger than the "actual" Hubble constant measuring the average expansion speed of the Universe.

However, in the paper by Blanchard et al. (2003) a thorough treatment of the statistical issues related to the problem was missing. We reassessed the statistical significance of their findings in a paper presently in preparation (Giusarma et al.). The main point is that the fact that, introducing additional parameters, the WMAP data can be explained by a model with $\Omega_\Lambda = 0$, providing a fit that is as good (or nearly as good) as the fit provided by the concordance model, is not enough. In fact, it could be that the alternative model requires a very fine-tuning of the model parameters. In the language of probabilities, this is the case if there are some combination of the parameters where the probablity *density* is very large, but nevertheless they have a very

small support, i.e. the *volume* in parameter space associated to these models is very small. The overrall result is that the probablity *mass* associated to these models is low as well, even if they fit well the data (i.e they have a high likelihood).

Then, following Blanchard et al. (2003) we have focused on models with a broken power-law spectrum of primordial fluctuations:

$$P(k) = \begin{cases} A_1 k^{n_1} & \text{for } k < k_* \\ A_2 k^{n_2} & \text{for } k \geq k_* \end{cases} \tag{F.0.1}$$

with a continuity condition $A_1 k_*^{n_1} = A_2 k_*^{n_2}$. Thus the primordial power spectrum is defined by five parameters, of which only four are independent instead of two as in the concordance model. We choose the four independent parameters to be A_1, n_1, n_2, k_*. The other parameters defining the model are the standard parameters of the concordance cosmological model. In order to explore the parameter space, we use the Markov Chain Monte Carlo (MCMC) method, through the publicly available code `CosmoMC` (Lewis and Bridle, 2002). In order to be as conservativa as possible, we have used only the WMAP 5-year data. The result for the density parameter of the cosmological constant Ω_Λ is that $0.35 \leq \Omega_\Lambda$ 0.76 at 95% confidence level, with mean value $\Omega_\Lambda = 0.62$. This should be compared with the WMAP 5-year result $\Omega_\Lambda = 0.742 \pm 0.030$. We also show the comparison between the two full posterior probability distributions in Fig. F.1. It can be seen that allowing for a broken power-law primordial spectrum shifts the preferred value for Ω_Λ to lower values and increases the width of the distribution, with the result that the 95% lower limit gows down to $\Omega_\Lambda = 0.35$. Then we find that, contrarily to what claimed by Blanchard et al. (2003), models with $\Omega_\Lambda = 0$ do not provide a satisfactory explanation to the CMB data. We have explicitly checked that the disagreement can be traced down to the fact that there are models with very smallΩ_Λ that have a high likelihood (i.e., a small χ^2) but that have a very small statistical weight associated to them.

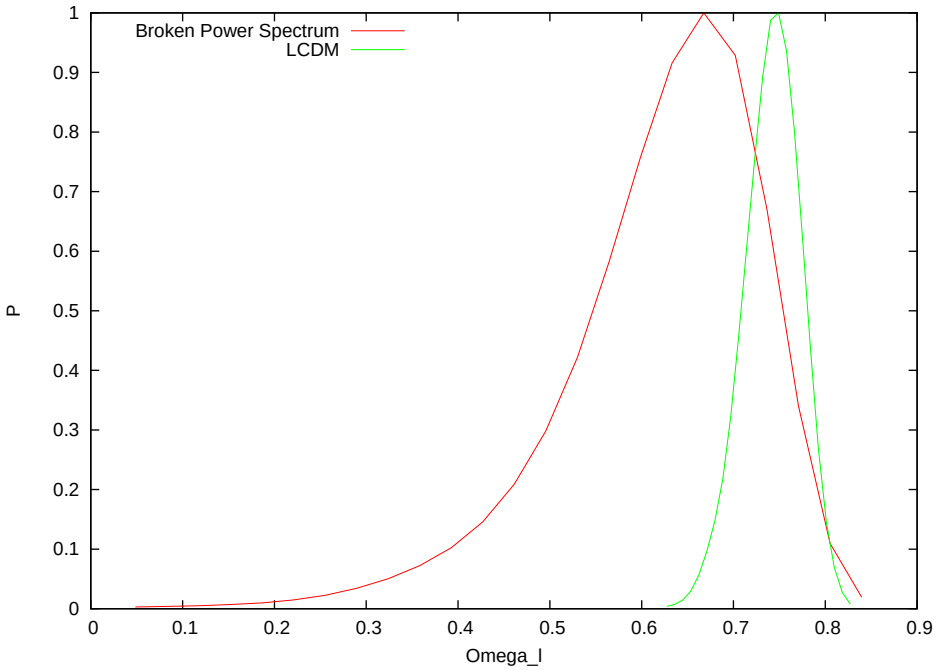

Figure F.1.: Relative probability as a function of Ω_Λ, for the standard concordance model ("LCDM") and for the alternative model described in the text ("Broken power spectrum").

Bibliography

AALSETH, C.E., AVIGNONE, F.T., BRODZINSKI, R.L., COLLAR, J.I., GARCIA, E., GONZÁLEZ, D., HASENBALG, F., HENSLEY, W.K., KIRPICHNIKOV, I.V., KLIMENKO, A.A. ET AL.
«Neutrinoless double-β decay of ^{76}Ge: First results from the International Germanium Experiment (IGEX) with six isotopically enriched detectors».
Phys. Rev. C, **59**, pp. 2108–2113 (1999).

ABAZAJIAN, K.N., BEACOM, J.F. AND BELL, N.F.
«Stringent constraints on cosmological neutrino-antineutrino asymmetries from synchronized flavor transformation».
Phys. Rev. D, **66(1)**, pp. 013008–+ (2002).

ABAZAJIAN, K., BELL, N.F., FULLER, G.M. AND WONG, Y.Y.Y.
«Cosmological lepton asymmetry, primordial nucleosynthesis, and sterile neutrinos».
Phys. Rev., **D72**, p. 063004 (2005).

ABAZAJIAN, K.N., BEACOM, J.F. AND BELL, N.F.
«Stringent constraints on cosmological neutrino antineutrino asymmetries from synchronized flavor transformation».
Phys. Rev., **D66**, p. 013008 (2002).

ABDO, A.A. ET AL.
«Measurement of the Cosmic Ray e+ plus e- spectrum from 20 GeV to 1 TeV with the Fermi Large Area Telescope».
Phys. Rev. Lett., **102**, p. 181101 (2009).

ADRIANI, O. ET AL.
«An anomalous positron abundance in cosmic rays with energies 1.5.100 GeV».
Nature, **458**, pp. 607–609 (2009).

AFSHORDI, N., ZALDARRIAGA, M. AND KOHRI, K.
«On the stability of Dark Energy with Mass-Varying Neutrinos».
Phys. Rev., **D72**, p. 065024 (2005).

AGUILAR, A. ET AL.
«Evidence for neutrino oscillations from the observation of anti-nu/e appearance in a anti-nu/mu beam».
Phys. Rev., **D64**, p. 112007 (2001).

AHARONIAN, .F.
≪Observations of the Sagittarius Dwarf galaxy by the H.E.S.S. experiment and search for a Dark Matter signal≫.
Astropart. Phys., **29**, pp. 55–62 (2008).

AHARONIAN, F. ET AL.
≪HESS observations of the galactic center region and their possible dark matter interpretation≫.
Phys. Rev. Lett., **97**, p. 221102 (2006).

AHARONIAN, F.A., ATOYAN, A.M. AND VOELK, H.J.
≪High energy electrons and positrons in cosmic rays as an indicator of the existence of a nearby cosmic tevatron≫.
A&A , **294**, pp. L41–L44 (1995).

AHARONIAN, H.E.S.S.C.F.
≪Probing the ATIC peak in the cosmic-ray electron spectrum with H.E.S.S≫ (2009).

AHMAD, Q.R., ALLEN, R.C., ANDERSEN, T.C., ANGLIN, J.D., BÜHLER, G., BARTON, J.C., BEIER, E.W., BERCOVITCH, M., BIGU, J., BILLER, S. ET AL.
≪Measurement of the Rate of $\nu_e + d \rightarrow p + p + e^-$ Interactions Produced by ^{8}B Solar Neutrinos at the Sudbury Neutrino Observatory≫.
Phys. Rev. Lett. , **87(7)**, pp. 071301–+ (2001).

AKSENOV, A.G., RUFFINI, R. AND VERESHCHAGIN, G.V.
≪Thermalization of Nonequilibrium Electron-Positron-Photon Plasmas≫.
Phys. Rev. Lett. , **99(12)**, pp. 125003–+ (2007).

AKSENOV, A.G., RUFFINI, R. AND VERESHCHAGIN, G.V.
≪Thermalization of Electron-Positron-Photon Plasmas with an application to GRB≫.
In *American Institute of Physics Conference Series*, volume 966 of *American Institute of Physics Conference Series*, pp. 191–196 (2008).

AKSENOV, A.G., RUFFINI, R. AND VERESHCHAGIN, G.V.
≪Kinetics of the mildly relativistic plasma and GRBs≫.
to appear in the proceeding of the conference "The Sun, the Stars, the Universe, and General Relativity" held in Minsk, Belarus on April 20-23, 2009. (2009a).

AKSENOV, A.G., RUFFINI, R. AND VERESHCHAGIN, G.V.
≪Pair plasma relaxation time scales≫.
Phys. Rev. E, **submitted** (2009b).

AKSENOV, A.G., RUFFINI, R. AND VERESHCHAGIN, G.V.
≪Thermalization of the mildly relativistic plasma≫.
Phys. Rev. D, **79(4)**, pp. 043008–+ (2009c).

ALBERT, J. ET AL.
«Upper limit for gamma-ray emission above 140 GeV from the dwarf spheroidal galaxy Draco».
Astrophys. J., **679**, pp. 428–431 (2008).

ALBRECHT, A.J. ET AL.
«Report of the Dark Energy Task Force» (2006).

ALLEN, S.W., SCHMIDT, R.W. AND BRIDLE, S.L.
«A preference for a non-zero neutrino mass from cosmological data».
Mon. Not. Roy. Astron. Soc., **346**, p. 593 (2003).

ALPHER, R.A., BETHE, H. AND GAMOW, G.
«The Origin of Chemical Elements».
Physical Review, **73**, pp. 803–804 (1948).

ALPHER, R.A. AND HERMAN, R.
«Evolution of the Universe».
Nature , **162**, pp. 774–775 (1948).

ALPHER, R.A. AND HERMAN, R.C.
«Theory of the Origin and Relative Abundance Distribution of the Elements».
Reviews of Modern Physics, **22**, pp. 153–212 (1950).

AMENDOLA, L.
«Coupled quintessence».
Phys. Rev., **D62**, p. 043511 (2000).

AMENDOLA, L., BALDI, M. AND WETTERICH, C.
«Growing Matter».
Phys. Rev., **D78**, p. 023015 (2008).

AMENDOLA, L. AND TOCCHINI-VALENTINI, D.
«Stationary dark energy: the present universe as a global attractor».
Phys. Rev., **D64**, p. 043509 (2001).

ANDERSON, G.W. AND CARROLL, S.M.
«Dark matter with time-dependent mass» (1997).

ARBOLINO, M.V. AND RUFFINI, R.
«The ratio between the mass of the halo and visible matter in spiral galaxies and limits on the neutrino mass».
A&A , **192**, pp. 107–116 (1988).

ARKANI-HAMED, N., FINKBEINER, D.P., SLATYER, T.R. AND WEINER, N.
«A Theory of Dark Matter».
Phys. Rev., **D79**, p. 015014 (2009).

ARMANDROFF, T.E., OLSZEWSKI, E.W. AND PRYOR, C.
≪The Mass-To-Light Ratios of the Draco and Ursa Minor Dwarf Spheroidal Galaxies.I. Radial Velocities from Multifiber Spectroscopy≫.
AJ, **110**, pp. 2131–+ (1995).

ARNABOLDI, C., ARTUSA, D.R., AVIGNONE, F.T., BALATA, M., BANDAC, I., BARUCCI, M., BEEMAN, J.W., BROFFERIO, C., BUCCI, C., CAPELLI, S. ET AL.
≪New Limit on the Neutrinoless $\beta\beta$ Decay of ^{130}Te≫.
Phys. Rev. Lett. , **95(14)**, pp. 142501–+ (2005).

BAHCALL, N.A. AND BURGETT, W.S.
≪Are superclusters correlated on a very large scale?≫
ApJ , **300**, pp. L35–L39 (1986).

BAHCALL, N.A. AND SONEIRA, R.M.
≪The spatial correlation function of rich clusters of galaxies≫.
ApJ , **270**, pp. 20–38 (1983).

BALTZ, E.A. ET AL.
≪Pre-launch estimates for GLAST sensitivity to Dark Matter annihilation signals≫.
JCAP, **0807**, p. 013 (2008).

BARGER, V., KNELLER, J.P., LANGACKER, P., MARFATIA, D. AND STEIGMAN, G.
≪Hiding relativistic degrees of freedom in the early universe≫.
Phys. Lett., **B569**, pp. 123–128 (2003a).

BARGER, V., KNELLER, J.P., LEE, H.S., MARFATIA, D. AND STEIGMAN, G.
≪Effective number of neutrinos and baryon asymmetry from BBN and WMAP≫.
Phys. Lett., **B566**, pp. 8–18 (2003b).

BARGER, V., MARFATIA, D. AND TREGRE, A.
≪Neutrino mass limits from SDSS, 2dFGRS and WMAP≫.
Phys. Lett., **B595**, pp. 55–59 (2004).

BASHINSKY, S. AND SELJAK, U.
≪Signatures of relativistic neutrinos in CMB anisotropy and matter clustering≫.
Phys. Rev., **D69**, p. 083002 (2004).

BEAN, R. AND DORE, O.
≪Probing dark energy perturbations: the dark energy equation of state and speed of sound as measured by WMAP≫.
Phys. Rev., **D69**, p. 083503 (2004).

BEAN, R., FLANAGAN, E.E., LASZLO, I. AND TRODDEN, M.
«Constraining Interactions in Cosmology's Dark Sector».
Phys. Rev., **D78**, p. 123514 (2008a).

BEAN, R., FLANAGAN, E.E. AND TRODDEN, M.
«Adiabatic instability in coupled dark energy-dark matter models».
Phys. Rev., **D78**, p. 023009 (2008b).

BEAN, R., FLANAGAN, E.E. AND TRODDEN, M.
«The Adiabatic Instability on Cosmology's Dark Side».
New J. Phys., **10**, p. 033006 (2008c).

BEAUDET, G. AND GORET, P.
«Leptonic numbers and the neutron to proton ratio in the hot big bang model».
A&A , **49**, pp. 415–419 (1976).

BELYAEV, S. AND BUDKER, G.
«Relativistic Kinetic Equation».
DAN SSSR, **107**, pp. 807–810 (1956).

BENNETT, C.L. ET AL.
«First Year Wilkinson Microwave Anisotropy Probe (WMAP) Observations: Preliminary Maps and Basic Results».
Astrophys. J. Suppl., **148**, p. 1 (2003).

BERGSTROM, L., BERTONE, G., BRINGMANN, T., EDSJO, J. AND TAOSO, M.
«Gamma-ray and Radio Constraints of High Positron Rate Dark Matter Models Annihilating into New Light Particles».
Phys. Rev., **D79**, p. 081303 (2009).

BERGSTROM, L., BRINGMANN, T. AND EDSJO, J.
«New Positron Spectral Features from Supersymmetric Dark Matter - a Way to Explain the PAMELA Data?»
Phys. Rev., **D78**, p. 103520 (2008).

BERNARDINI, A.E. AND BERTOLAMI, O.
«Stationary condition in a perturbative approach for mass varying neutrinos».
Phys. Lett., **B662**, pp. 97–101 (2008).

BERTONE, G., HOOPER, D. AND SILK, J.
«Particle dark matter: evidence, candidates and constraints».
Phys. Rep. , **405**, pp. 279–390 (2005).

BERTONE, G., CIRELLI, M., STRUMIA, A. AND TAOSO, M.
«Gamma-ray and radio tests of the e+e- excess from DM annihilations».
JCAP, **0903**, p. 009 (2009).

BERTONE, G., HOOPER, D. AND SILK, J.
«Particle dark matter: Evidence, candidates and constraints».
Phys. Rept., **405**, pp. 279–390 (2005).

BIANCO, C.L., RUFFINI, R., VERESHCHAGIN, G. AND XUE, S.S.
«Equations of motion, initial and boundary conditions for GRB».
J.Korean Phys.Soc., **49**, pp. 722–731 (2006).

BIANCONI, A., LEE, H.W. AND RUFFINI, R.
«Limits from cosmological nucleosynthesis on the leptonic numbers of the universe».
A&A , **241**, pp. 343–357 (1991).

BISNOVATYI-KOGAN, G.S. AND NOVIKOV, I.D.
«Cosmology with a Nonzero Neutrino Rest Mass».
Soviet Astronomy, **24**, pp. 516–+ (1980).

BJAELDE, O.E. ET AL.
«Neutrino Dark Energy – Revisiting the Stability Issue».
JCAP, **0801**, p. 026 (2008).

BLANCHARD, A., DOUSPIS, M., ROWAN-ROBINSON, M. AND SARKAR, S.
«An alternative to the cosmological 'concordance model'».
Astron. Astrophys., **412**, pp. 35–44 (2003).

BOND, J.R., EFSTATHIOU, G. AND SILK, J.
«Massive neutrinos and the large-scale structure of the universe».
Phys. Rev. Lett. , **45**, pp. 1980–1984 (1980).

BONN, J. ET AL.
«Limits on neutrino masses from tritium beta decay».
Nucl. Phys. Proc. Suppl., **110**, pp. 395–397 (2002).

BOWERS, R.L. AND WILSON, J.R.
Numerical modeling in applied physics and astrophysics (1991).

BRAX, P., VAN DE BRUCK, C., DAVIS, A.C., KHOURY, J. AND WELTMAN, A.
«Detecting dark energy in orbit: The cosmological chameleon».
Phys. Rev., **D70**, p. 123518 (2004).

BRINGMANN, T.
«Particle Models and the Small-Scale Structure of Dark Matter».
New J. Phys., **11**, p. 105027 (2009).

BROOKFIELD, A.W., VAN DE BRUCK, C., MOTA, D.F. AND TOCCHINI-VALENTINI, D.
«Cosmology with massive neutrinos coupled to dark energy».
Phys. Rev. Lett., **96**, p. 061301 (2006a).

BROOKFIELD, A.W., VAN DE BRUCK, C., MOTA, D.F. AND TOCCHINI-VALENTINI, D.
«Cosmology of mass-varying neutrinos driven by quintessence: Theory and observations».
Phys. Rev., **D73**, p. 083515 (2006b).

BUCHMULLER, W., DI BARI, P. AND PLUMACHER, M.
«Some Aspects of Thermal Leptogenesis».
New J. Phys., **6**, p. 105 (2004).

BULLOCK, J.S. ET AL.
«Profiles of dark haloes: evolution, scatter, and environment».
Mon. Not. Roy. Astron. Soc., **321**, pp. 559–575 (2001).

BURKERT, A.
«The Structure of dark matter halos in dwarf galaxies».
IAU Symp., **171**, p. 175 (1996).

CALDWELL, R.R., DAVE, R. AND STEINHARDT, P.J.
«Cosmological Imprint of an Energy Component with General Equation-of-State».
Phys. Rev. Lett., **80**, pp. 1582–1585 (1998).

CALDWELL, R.R. AND KAMIONKOWSKI, M.
«The Physics of Cosmic Acceleration» (2009).

CALZETTI, D., GIAVALISCO, M. AND RUFFINI, R.
«The normalization of the correlation functions for extragalactic structures».
A&A , **198**, pp. 1–2 (1988).

CALZETTI, D., GIAVALISCO, M., RUFFINI, R., EINASTO, J. AND SAAR, E.
«The correlation function of galaxies in the direction of the Coma cluster».
Ap&SS, **137**, pp. 101–106 (1987).

CASAS, A., CHENG, W.Y. AND GELMINI, G.
«Generation of large lepton asymmetries».
Nucl. Phys., **B538**, pp. 297–308 (1999).

CAVALLO, G. AND REES, M.J.
«A qualitative study of cosmic fireballs and gamma-ray bursts».
MNRAS , **183**, pp. 359–365 (1978).

CHANG, J. ET AL.
«An excess of cosmic ray electrons at energies of 300.800 GeV».
Nature, **456**, pp. 362–365 (2008).

CHEN, H., WILKS, S.C., BONLIE, J.D., LIANG, E.P., MYATT, J., PRICE, D.F., MEYERHOFER, D.D. AND BEIERSDORFER, P.
«Relativistic Positron Creation Using Ultraintense Short Pulse Lasers».
Phys. Rev. Lett. , **102(10)**, pp. 105001–+ (2009).

CHEVALLIER, M. AND POLARSKI, D.
«Accelerating universes with scaling dark matter».
Int. J. Mod. Phys., **D10**, pp. 213–224 (2001).

CHIBA, T., TAKAHASHI, F. AND YAMAGUCHI, M.
«Baryogenesis in a flat direction with neither baryon nor lepton charge».
Phys. Rev. Lett., **92**, p. 011301 (2004).

CHOLIS, I., DOBLER, G., FINKBEINER, D.P., GOODENOUGH, L. AND WEINER, N.
«The Case for a 700+ GeV WIMP: Cosmic Ray Spectra from ATIC and PAMELA» (2008).

CHRISTENSEN, N., MEYER, R., KNOX, L. AND LUEY, B.
«II: Bayesian Methods for Cosmological Parameter Estimation from Cosmic Microwave Background Measurements».
Class. Quant. Grav., **18**, p. 2677 (2001).

CHURAZOV, E., SUNYAEV, R., SAZONOV, S., REVNIVTSEV, M. AND VARSHALOVICH, D.
«Positron annihilation spectrum from the Galactic Centre region observed by SPI/INTEGRAL».
MNRAS , **357**, pp. 1377–1386 (2005).

CIRELLI, M., FRANCESCHINI, R. AND STRUMIA, A.
«Minimal Dark Matter predictions for galactic positrons, anti-protons, photons».
Nucl. Phys., **B800**, pp. 204–220 (2008).

CIRELLI, M., KADASTIK, M., RAIDAL, M. AND STRUMIA, A.
«Model-independent implications of the e+, e-, anti-proton cosmic ray spectra on properties of Dark Matter».
Nucl. Phys., **B813**, pp. 1–21 (2009).

CIRELLI, M. AND PANCI, P.
«Inverse Compton constraints on the Dark Matter e+e- excesses».
Nucl. Phys., **B821**, pp. 399–416 (2009).

CIRELLI, M. AND STRUMIA, A.
«Minimal Dark Matter predictions and the PAMELA positron excess» (2008).

CIRELLI, M., STRUMIA, A. AND TAMBURINI, M.
«Cosmology and Astrophysics of Minimal Dark Matter».
Nucl. Phys., **B787**, pp. 152–175 (2007).

COLE, S. ET AL.
«The 2dF Galaxy Redshift Survey: Power-spectrum analysis of the final dataset and cosmological implications».
Mon. Not. Roy. Astron. Soc., **362**, pp. 505–534 (2005).

COLEMAN, P.H. AND PIETRONERO, L.
«The fractal structure of the universe.»
Phys. Rep. , **213**, pp. 311–389 (1992).

COPELAND, E.J., SAMI, M. AND TSUJIKAWA, S.
«Dynamics of dark energy».
Int. J. Mod. Phys., **D15**, pp. 1753–1936 (2006).

CORASANITI, P.S. AND COPELAND, E.J.
«A model independent approach to the dark energy equation of state».
Phys. Rev., **D67**, p. 063521 (2003).

CROTTY, P., LESGOURGUES, J. AND PASTOR, S.
«Measuring the cosmological background of relativistic particles with WMAP».
Phys. Rev., **D67**, p. 123005 (2003).

CROTTY, P., LESGOURGUES, J. AND PASTOR, S.
«Current cosmological bounds on neutrino masses and relativistic relics».
Phys. Rev., **D69**, p. 123007 (2004).

CUMBERBATCH, D.T., ZUNTZ, J., ERIKSEN, H.K.K. AND SILK, J.
«Can the WMAP Haze really be a signature of annihilating neutralino dark matter?» (2009).

CUOCO, A. ET AL.
«Present status of primordial nucleosynthesis after WMAP: results from a new BBN code».
Int. J. Mod. Phys., **A19**, pp. 4431–4454 (2004).

DAS, S., CORASANITI, P.S. AND KHOURY, J.
«Super-acceleration as signature of dark sector interaction».
Phys. Rev., **D73**, p. 083509 (2006).

DE BARROS, G., RUFFINI, R. AND VERESHCHAGIN, G.V.
«On hydrodynamic phase of grb sources».
Astronomy and Astrophysics, **submitted** (2009).

DE BERNARDIS, P., ADE, P.A.R., BOCK, J.J., BOND, J.R., BORRILL, J., BOSCALERI, A., COBLE, K., CONTALDI, C.R., CRILL, B.P., DE TROIA, G. ET AL.
≪Multiple Peaks in the Angular Power Spectrum of the Cosmic Microwave Background: Significance and Consequences for Cosmology≫.
ApJ , **564**, pp. 559–566 (2002).

DE BOER, W.
≪Indirect Dark Matter Signals from EGRET and PAMELA compared≫.
AIP Conf. Proc., **1166**, pp. 169–178 (2009).

DE GOUVEIA DAL PINO, E.M., HETEM, A., HORVATH, J.E., DE SOUZA, C.A.W., VILLELA, T. AND DE ARAUJO, J.C.N.
≪Evidence for a very large scale fractal structure in the universe from COBE measurements≫.
ApJ , **442**, pp. L45–L48 (1995).

DEHNEN, W. AND MCLAUGHLIN, D.
≪Dynamical insight into dark-matter haloes≫.
Mon. Not. Roy. Astron. Soc., **363**, pp. 1057–1068 (2005).

DI BARI, P.
≪Update on neutrino mixing in the early universe≫.
Phys. Rev., **D65**, p. 043509 (2002).

DI BARI, P. AND FOOT, R.
≪Active-sterile neutrino oscillations in the early universe: Asymmetry generation at low —delta(m**2)— and the Landau-Zener approximation≫.
Phys. Rev., **D65**, p. 045003 (2002).

DI BARI, P.
≪Addendum to: Update on neutrino mixing in the early universe≫.
Phys. Rev., **D67**, p. 127301 (2003).

DIEMAND, J. ET AL.
≪Clumps and streams in the local dark matter distribution≫.
Nature, **454**, pp. 735–738 (2008).

DIEMAND, J., KUHLEN, M. AND MADAU, P.
≪Formation and evolution of galaxy dark matter halos and their substructure≫.
Astrophys. J., **667**, p. 859 (2007).

DOLGOV, A.D.
≪NonGUT baryogenesis≫.
Phys. Rept., **222**, pp. 309–386 (1992).

DOLGOV, A.D.
«Neutrinos in cosmology».
Phys. Rep. , **370**, pp. 333–535 (2002).

DOLGOV, A.D., HANSEN, S.H., PASTOR, S., PETCOV, S.T., RAFFELT, G.G. AND SEMIKOZ, D.V.
«Cosmological bounds on neutrino degeneracy improved by flavor oscillations».
Nuclear Physics B, **632**, pp. 363–382 (2002).

DOLGOV, A.D., HANSEN, S.H., PASTOR, S. AND SEMIKOZ, D.V.
«Neutrino oscillations in the early universe: How large lepton asymmetry can be generated?»
Astropart. Phys., **14**, pp. 79–90 (2000).

DOLGOV, A.D., HANSEN, S.H. AND SEMIKOZ, D.V.
«Non-equilibrium corrections to the spectra of massless neutrinos in the early universe».
Nucl. Phys., **B503**, pp. 426–444 (1997).

DOLGOV, A.D. AND TAKAHASHI, F.
«Do neutrino flavor oscillations forbid large lepton asymmetry of the universe?»
Nucl. Phys., **B688**, pp. 189–213 (2004a).

DOLGOV, A.D. AND TAKAHASHI, F.
«Suppressed neutrino oscillations and large lepton asymmetries» (2004b).

DOLGOV, A.D. ET AL.
«Cosmological bounds on neutrino degeneracy improved by flavor oscillations».
Nucl. Phys., **B632**, pp. 363–382 (2002).

DONATO, F., MAURIN, D., BRUN, P., DELAHAYE, T. AND SALATI, P.
«Constraints on WIMP Dark Matter from the High Energy PAMELA $\bar{p}/p$ data».
Phys. Rev. Lett., **102**, p. 071301 (2009).

DOROSHKEVICH, A.G. AND KHLOPOV, M.Y.
«The formation of structure in the neutrino universe».
AZh, **58**, pp. 913–924 (1981).

DOROSHKEVICH, A.G., NOVIKOV, I.D., SUNYAEV, R.A. AND ZELDOVICH, Y.B.
«Helium Production in the Different Cosmological Models».
Highlights of Astronomy, **2**, pp. 318–+ (1971).

DOUSPIS, M., ZOLNIEROWSKI, Y., BLANCHARD, A. AND RIAZUELO, A.
«What can we learn about dark energy evolution?» (2006).

DUNKLEY, J. ET AL.
«Five-Year Wilkinson Microwave Anisotropy Probe (WMAP) Observations: Likelihoods and Parameters from the WMAP data».
Astrophys. J. Suppl., **180**, pp. 306–329 (2009).

DURRER, R. AND LABINI, F.S.
«A fractal galaxy distribution in a homogeneous universe?»
A&A , **339**, pp. L85–L88 (1998).

EGUCHI, K. ET AL.
«First results from KamLAND: Evidence for reactor anti- neutrino disappearance».
Phys. Rev. Lett., **90**, p. 021802 (2003).

EINSTEIN, A.
«Kosmologische Betrachtungen zur allgemeinen Relativitätstheorie».
Sitzungsberichte der Königlich Preußischen Akademie der Wissenschaften (Berlin), Seite 142-152., pp. 142–152 (1917).

ELGAROY, O. ET AL.
«A new limit on the total neutrino mass from the 2dF galaxy redshift survey».
Phys. Rev. Lett., **89**, p. 061301 (2002).

ELGAROY, O. AND LAHAV, O.
«Upper limits on neutrino masses from the 2dFGRS and WMAP: the role of priors».
JCAP, **0304**, p. 004 (2003).

EVANS, N.W., FERRER, F. AND SARKAR, S.
«A 'Baedecker' for the dark matter annihilation signal».
Phys. Rev., **D69**, p. 123501 (2004).

FALCONE, D. AND TRAMONTANO, F.
«Leptogenesis and neutrino parameters».
Phys. Rev., **D63**, p. 073007 (2001).

FARDON, R., NELSON, A.E. AND WEINER, N.
«Dark Energy from Mass Varying Neutrinos».
JCAP, **0410**, p. 005 (2004).

FARRAR, G.R. AND PEEBLES, P.J.E.
«Interacting Dark Matter and Dark Energy».
Astrophys. J., **604**, pp. 1–11 (2004).

FOOT, R., THOMSON, M.J. AND VOLKAS, R.R.
«Large neutrino asymmetries from neutrino oscillations».
Phys. Rev., **D53**, pp. 5349–5353 (1996).

FOOT, R. AND VOLKAS, R.R.
«How neutrino oscillations can induce an effective neutrino number of less than 3 during big bang nucleosynthesis».
Phys. Rev., **D56**, pp. 6653–6664 (1997).

FRANCA, U., LATTANZI, M., LESGOURGUES, J. AND PASTOR, S.
«Model independent constraints on mass-varying neutrino scenarios».
Phys. Rev., **D80**, p. 083506 (2009).

FRANCA, U. AND ROSENFELD, R.
«Age constraints and fine tuning in variable-mass particle models».
Phys. Rev., **D69**, p. 063517 (2004).

FREEDMAN, W.L. ET AL.
«Final Results from the Hubble Space Telescope Key Project to Measure the Hubble Constant».
Astrophys. J., **553**, pp. 47–72 (2001).

FREESE, K., KOLB, E.W. AND TURNER, M.S.
«MASSIVE, DEGENERATE NEUTRINOS AND COSMOLOGY».
Phys. Rev., **D27**, p. 1689 (1983).

FRIEDMAN, A.
«Über die Krümmung des Raumes».
Zeitschrift fur Physik, **10**, pp. 377–386 (1922).

FRIEMAN, J., TURNER, M. AND HUTERER, D.
«Dark Energy and the Accelerating Universe».
Ann. Rev. Astron. Astrophys., **46**, pp. 385–432 (2008).

GAITE, J., DOMÍNGUEZ, A. AND PÉREZ-MERCADER, J.
«The Fractal Distribution of Galaxies and the Transition to Homogeneity».
ApJ , **522**, pp. L5–L8 (1999).

GALLI, S., IOCCO, F., BERTONE, G. AND MELCHIORRI, A.
«CMB constraints on Dark Matter models with large annihilation cross-section».
Phys. Rev., **D80**, p. 023505 (2009).

GAMOW, G.
«Expanding Universe and the Origin of Elements».
Physical Review, **70**, pp. 572–573 (1946).

GAMOW, G.
≪The Origin of Elements and the Separation of Galaxies≫.
Physical Review, **74**, pp. 505–506 (1948).

GAO, J.G. AND RUFFINI, R.
≪Relativistic limits on the masses of self-gravitating systems of degenerate neutrinos.≫
Physics Letters B, **97**, pp. 388–390 (1980).

GAO, L.
Mon. Not. Roy. Astron. Soc., **387**, p. 536 (2008).

GAVELA, M.B., HERNANDEZ, D., HONOREZ, L.L., MENA, O. AND RIGOLIN, S.
≪Dark coupling≫.
JCAP, **0907**, p. 034 (2009).

GENTILE, G., SALUCCI, P., KLEIN, U., VERGANI, D. AND KALBERLA, P.
≪The cored distribution of dark matter in spiral galaxies≫.
Mon. Not. Roy. Astron. Soc., **351**, p. 903 (2004).

GIAVALISCO, M.
Ph.D. thesis, University of Rome "La Sapienza" (1992).

GIOCOLI, C., PIERI, L. AND TORMEN, G.
≪Analytical approach to subhalo population in dark matter haloes≫.
MNRAS , **387**, pp. 689–697 (2008).

GIOCOLI, C., PIERI, L., TORMEN, G. AND MORENO, J.
≪A merger tree with microsolar mass resolution: application to γ-ray emission from subhalo population≫.
MNRAS , **395**, pp. 1620–1630 (2009).

GIUDICE, G.F., KOLB, E.W. AND RIOTTO, A.
≪Largest temperature of the radiation era and its cosmological implications≫.
Phys. Rev., **D64**, p. 023508 (2001).

GIUSARMA, E., PANDOLFI, S., LATTANZI, M. AND MELCHIORRI, A.
≪In preparation≫ (????).

GOODMAN, J.
≪Are gamma-ray bursts optically thick?≫
ApJ , **308**, pp. L47–L50 (1986).

GOULD, R.J.
≪Kinetic theory of relativistic plasmas≫.
Physics of Fluids, **24**, pp. 102–107 (1981).

GRAJEK, P., KANE, G., PHALEN, D., PIERCE, A. AND WATSON, S.
«Is the PAMELA Positron Excess Winos?»
Phys. Rev., **D79**, p. 043506 (2009).

GREEN, A.M., HOFMANN, S. AND SCHWARZ, D.J.
«The power spectrum of SUSY-CDM on sub-galactic scales».
Mon. Not. Roy. Astron. Soc., **353**, p. L23 (2004).

GREEN, A.M., HOFMANN, S. AND SCHWARZ, D.J.
«The first WIMPy halos».
JCAP, **0508**, p. 003 (2005).

GRIMSRUD, O.M. AND WASSERMAN, I.
«Non-equilibrium effects in steady relativistic $e^+ + e^-$-gamma winds».
MNRAS , **300**, pp. 1158–1180 (1998).

GU, P., WANG, X. AND ZHANG, X.
«Dark Energy and Neutrino Mass Limits from Baryogenesis».
Phys. Rev., **D68**, p. 087301 (2003).

HANNESTAD, S.
«Cosmological limit on the neutrino mass».
Phys. Rev., **D66**, p. 125011 (2002).

HANNESTAD, S.
«Can cosmology detect hierarchical neutrino masses?»
Phys. Rev., **D67**, p. 085017 (2003a).

HANNESTAD, S.
«Neutrino masses and the number of neutrino species from WMAP and 2dFGRS».
JCAP, **0305**, p. 004 (2003b).

HANNESTAD, S.
«Constraints on the sound speed of dark energy».
Phys. Rev., **D71**, p. 103519 (2005).

HANNESTAD, S.
«Primordial Neutrinos».
Ann. Rev. Nucl. Part. Sci., **56**, pp. 137–161 (2006).

HANNESTAD, S. AND RAFFELT, G.
«Cosmological mass limits on neutrinos, axions, and other light particles».
JCAP, **0404**, p. 008 (2004).

HANNESTAD, S., TU, H. AND WONG, Y.Y.Y.

≪Measuring neutrino masses and dark energy with weak lensing tomography≫.
JCAP, **0606**, p. 025 (2006).

HANSEN, S.H., MANGANO, G., MELCHIORRI, A., MIELE, G. AND PISANTI, O.
≪Constraining neutrino physics with BBN and CMBR≫.
Phys. Rev., **D65**, p. 023511 (2002).

HANSEN, S.H., MANGANO, G., MELCHIORRI, A., MIELE, G. AND PISANTI, O.
≪Constraining neutrino physics with big bang nucleosynthesis and cosmic microwave background radiation≫.
Phys. Rev. D, **65(2)**, pp. 023511–+ (2002).

HARVEY, J.A. AND KOLB, E.W.
≪GRAND UNIFIED THEORIES AND THE LEPTON NUMBER OF THE UNIVERSE≫.
Phys. Rev., **D24**, p. 2090 (1981).

HAWKINS, E., MADDOX, S., COLE, S., LAHAV, O., MADGWICK, D.S., NORBERG, P., PEACOCK, J.A., BALDRY, I.K., BAUGH, C.M., BLAND-HAWTHORN, J. ET AL.
≪The 2dF Galaxy Redshift Survey: correlation functions, peculiar velocities and the matter density of the Universe≫.
MNRAS , **346**, pp. 78–96 (2003).

HAYASHI, E., NAVARRO, J.F., TAYLOR, J.E., STADEL, J. AND QUINN, T.R.
≪The Structural Evolution of Substructure≫.
Astrophys. J., **584**, pp. 541–558 (2003).

HINSHAW, G. ET AL.
≪First Year Wilkinson Microwave Anisotropy Probe (WMAP) Observations: Angular Power Spectrum≫.
Astrophys. J. Suppl., **148**, p. 135 (2003).

HISANO, J., MATSUMOTO, S. AND NOJIRI, M.M.
≪Explosive dark matter annihilation≫.
Phys. Rev. Lett., **92**, p. 031303 (2004).

HISANO, J., MATSUMOTO, S., NOJIRI, M.M. AND SAITO, O.
≪Non-perturbative effect on dark matter annihilation and gamma ray signature from galactic center≫.
Phys. Rev., **D71**, p. 063528 (2005).

HOFMANN, S., SCHWARZ, D.J. AND STOECKER, H.
≪Damping scales of neutralino cold dark matter≫.

Phys. Rev., **D64**, p. 083507 (2001).

HOOPER, D., BLASI, P. AND SERPICO, P.D.
«Pulsars as the Sources of High Energy Cosmic Ray Positrons».
JCAP, **0901**, p. 025 (2009a).

HOOPER, D., FINKBEINER, D.P. AND DOBLER, G.
«Evidence Of Dark Matter Annihilations In The WMAP Haze».
Phys. Rev., **D76**, p. 083012 (2007).

HOOPER, D., STEBBINS, A. AND ZUREK, K.M.
«Excesses in cosmic ray positron and electron spectra from a nearby clump of neutralino dark matter».
Phys. Rev., **D79**, p. 103513 (2009b).

HOOPER, D. AND ZUREK, K.M.
«The PAMELA and ATIC Signals From Kaluza-Klein Dark Matter».
Phys. Rev., **D79**, p. 103529 (2009).

HU, W.
«Structure Formation with Generalized Dark Matter».
Astrophys. J., **506**, pp. 485–494 (1998).

HU, W., EISENSTEIN, D.J. AND TEGMARK, M.
«Weighing neutrinos with galaxy surveys».
Phys. Rev. Lett., **80**, pp. 5255–5258 (1998).

HUBBLE, E.
«A Relation between Distance and Radial Velocity among Extra-Galactic Nebulae».
Proceedings of the National Academy of Science, **15**, pp. 168–173 (1929).

HUEY, G. AND WANDELT, B.D.
«Interacting quintessence, the coincidence problem and cosmic acceleration».
Phys. Rev., **D74**, p. 023519 (2006).

IBATA, R.A., WYSE, R.F.G., GILMORE, G., IRWIN, M.U. AND SUNTZEFF, N.B.
«The Kinematics, Orbit, and Survival of the Sagittarius Dwarf Spheroidal Galaxy».
Astron. J., **113**, pp. 634–655 (1997).

ICHIKI, K. AND KEUM, Y.Y.
«Primordial Neutrinos, Cosmological Perturbations in Interacting Dark-Energy Model: CMB and LSS».
JCAP, **0806**, p. 005 (2008).

JOYCE, M., SYLOS LABINI, F., GABRIELLI, A., MONTUORI, M. AND PIETRONERO, L.
«Basic properties of galaxy clustering in the light of recent results from the Sloan Digital Sky Survey».
A&A , **443**, pp. 11–16 (2005).

KAMIONKOWSKI, M. AND PROFUMO, S.
«Early Annihilation and Diffuse Backgrounds in Models of Weakly Interacting Massive Particles in Which the Cross Section for Pair Annihilation Is Enhanced by 1/v».
Phys. Rev. Lett., **101**, p. 261301 (2008).

KATRIN COLLABORATION.
«KATRIN: A next generation tritium beta decay experiment with sub-eV sensitivity for the electron neutrino mass».
ArXiv High Energy Physics - Experiment e-prints (2001).

KATZ, J.I.
«A Cubic Micron of Equilibrium Pair Plasma?»
ApJS , **127**, pp. 371–373 (2000).

KAWASAKI, M., TAKAHASHI, F. AND YAMAGUCHI, M.
«Large lepton asymmetry from Q-balls».
Phys. Rev., **D66**, p. 043516 (2002).

KITCHING, T.D., HEAVENS, A.F., VERDE, L., SERRA, P. AND MELCHIORRI, A.
«Finding Evidence for Massive Neutrinos using 3D Weak Lensing».
Phys. Rev., **D77**, p. 103008 (2008).

KLAPDOR-KLEINGROTHAUS, H.V., DIETZ, A., BAUDIS, L., HEUSSER, G., KRIVOSHEINA, I.V., MAJOROVITS, B., PAES, H., STRECKER, H., ALEXEEV, V., BALYSH, A. ET AL.
«Latest results from the HEIDELBERG-MOSCOW double beta decay experiment».
European Physical Journal A, **12**, pp. 147–154 (2001).

KLAPDOR-KLEINGROTHAUS, H.V., DIETZ, A., HARNEY, H.L. AND KRIVOSHEINA, I.V.
«Evidence for Neutrinoless Double Beta Decay».
Mod. Phys. Lett., **A16**, pp. 2409–2420 (2001).

KLAPDOR-KLEINGROTHAUS, H.V., DIETZ, A., KRIVOSHEINA, I.V., DORR, C. AND TOMEI, C.
«Support of evidence for neutrinoless double beta decay».
Phys. Lett., **B578**, pp. 54–62 (2004).

KLYPIN, A.A. AND KOPYLOV, A.I.
«The Spatial Covariance Function for Rich Clusters of Galaxies».
Soviet Astronomy Letters, **9**, pp. 41–+ (1983).

KNELLER, J.P., SCHERRER, R.J., STEIGMAN, G. AND WALKER, T.P.
«How does the cosmic microwave background plus big bang nucleosynthesis constrain new physics?»
Phys. Rev. D, **64(12)**, pp. 123506–+ (2001).

KNELLER, J.P., SCHERRER, R.J., STEIGMAN, G. AND WALKER, T.P.
«How Does CMB + BBN Constrain New Physics?»
Phys. Rev., **D64**, p. 123506 (2001).

KOGUT, A. ET AL.
«Wilkinson Microwave Anisotropy Probe (WMAP) First Year Observations: TE Polarization».
Astrophys. J. Suppl., **148**, p. 161 (2003).

KOIVISTO, T. AND MOTA, D.F.
«Dark Energy Anisotropic Stress and Large Scale Structure Formation».
Phys. Rev., **D73**, p. 083502 (2006).

KOLB, E.W. AND TURNER, M.S.
The Early Universe (Frontiers in Physics, Reading, MA: Addison-Wesley, 1990).

KOMATSU, E. ET AL.
«Five-Year Wilkinson Microwave Anisotropy Probe (WMAP) Observations:Cosmological Interpretation».
Astrophys. J. Suppl., **180**, pp. 330–376 (2009).

KOWALSKI, M. ET AL.
«Improved Cosmological Constraints from New, Old and Combined Supernova Datasets».
Astrophys. J., **686**, pp. 749–778 (2008).

KRAUS, C., BORNSCHEIN, B., BORNSCHEIN, L., BONN, J., FLATT, B., KOVALIK, A., OSTRICK, B., OTTEN, E.W., SCHALL, J.P., THÜMMLER, T. ET AL.
«Final results from phase II of the Mainz neutrino mass searchin tritium β decay».
European Physical Journal C, **40**, pp. 447–468 (2005).

KUO, C.L. ET AL.
«High Resolution Observations of the CMB Power Spectrum with ACBAR».
Astrophys. J., **600**, pp. 32–51 (2004).

KUZMIN, V.A., RUBAKOV, V.A. AND SHAPOSHNIKOV, M.E.
≪On the Anomalous Electroweak Baryon Number Nonconservation in the Early Universe≫.
Phys. Lett., **B155**, p. 36 (1985).

LA VACCA, G., KRISTIANSEN, J.R., COLOMBO, L.P.L., MAININI, R. AND BONOMETTO, S.A.
≪Do WMAP data favor neutrino mass and a coupling between Cold Dark Matter and Dark Energy?≫
JCAP, **0904**, p. 007 (2009).

LATTANZI, M., RUFFINI, R. AND VERESHCHAGIN, G.
≪On the possible role of massive neutrinos in cosmological structure formation≫.
In M. Novello and S.E. Perez Bergliaffa (eds.), *Cosmology and Gravitation*, volume 668 of *American Institute of Physics Conference Series*, pp. 263–287 (2003).

LATTANZI, M., RUFFINI, R. AND VERESHCHAGIN, G.V.
≪Joint constraints on the lepton asymmetry of the Universe and neutrino mass from the Wilkinson Microwave Anisotropy Probe≫.
Phys. Rev. D, **72(6)**, pp. 063003–+ (2005).

LATTANZI, M., RUFFINI, R. AND VERESHCHAGIN, G.V.
≪Do WMAP data constraint the lepton asymmetry of the Universe to be zero?≫
In *Albert Einstein Century International Conference*, volume 861 of *American Institute of Physics Conference Series*, pp. 912–919 (2006).

LATTANZI, M. AND SILK, J.
≪Can the WIMP annihilation boost factor be boosted by the Sommerfeld enhancement?≫
Phys. Rev., **D79**, p. 083523 (2009).

LAVALLE, J., YUAN, Q., MAURIN, D. AND BI, X.
≪Full calculation of clumpiness boost factors for antimatter cosmic rays in the light of ΛCDM N-body simulation results. Abandoning hope in clumpiness enhancement?≫
A&A , **479**, pp. 427–452 (2008).

LEE, B.W. AND WEINBERG, S.
≪Cosmological lower bound on heavy-neutrino masses≫.
Phys. Rev. Lett. , **39**, pp. 165–168 (1977).

LEMAÎTRE, A.G.
≪Contributions to a British Association Discussion on the Evolution of the Universe.≫

Nature , **128**, pp. 704–706 (1931a).

LEMAÎTRE, G.
«Un Univers homogène de masse constante et de rayon croissant rendant compte de la vitesse radiale des nébuleuses extra-galactiques».
Annales de la Societe Scietifique de Bruxelles, **47**, pp. 49–59 (1927).

LEMAÎTRE, G.
«The Beginning of the World from the Point of View of Quantum Theory.»
Nature , **127**, pp. 706–+ (1931b).

LESGOURGUES, J. AND PASTOR, S.
«Massive neutrinos and cosmology».
Phys. Rep. , **429**, pp. 307–379 (2006).

LESGOURGUES, J. AND LIDDLE, A.R.
«The lepton asymmetry: The last chance for a critical- density cosmology?»
Mon. Not. Roy. Astron. Soc., **327**, p. 1307 (2001).

LESGOURGUES, J. AND PASTOR, S.
«Cosmological implications of a relic neutrino asymmetry».
Phys. Rev., **D60**, p. 103521 (1999).

LESGOURGUES, J. AND PASTOR, S.
«Massive neutrinos and cosmology».
Phys. Rept., **429**, pp. 307–379 (2006).

LESGOURGUES, J., PEROTTO, L., PASTOR, S. AND PIAT, M.
«Probing neutrino masses with CMB lensing extraction».
Phys. Rev., **D73**, p. 045021 (2006).

LESGOURGUES, J., VALKENBURG, W. AND GAZTANAGA, E.
«Constraining neutrino masses with the ISW-galaxy correlation function».
Phys. Rev., **D77**, p. 063505 (2008).

LEWIS, A. AND BRIDLE, S.
«Cosmological parameters from CMB and other data: a Monte- Carlo approach».
Phys. Rev., **D66**, p. 103511 (2002).

LEWIS, A., CHALLINOR, A. AND LASENBY, A.
«Efficient Computation of CMB anisotropies in closed FRW models».
Astrophys. J., **538**, pp. 473–476 (2000).

LINDEN, S. AND VIREY, J.M.

«A test of the CPL parameterization for rapid dark energy equation of state transitions».
Phys. Rev., **D78**, p. 023526 (2008).

LINDER, E.V.
«Exploring the expansion history of the universe».
Phys. Rev. Lett., **90**, p. 091301 (2003).

LINDER, E.V.
«Mapping the Cosmological Expansion».
Rept. Prog. Phys., **71**, p. 056901 (2008).

LIU, J., YIN, P.F. AND ZHU, S.H.
«Prospects for Detecting Neutrino Signals from Annihilating/Decaying Dark Matter to Account for the PAMELA and ATIC results».
Phys. Rev., **D79**, p. 063522 (2009).

LOBASHEV, V.M.
«The search for the neutrino mass by direct method in the tritium beta-decay and perspectives of study it in the project KATRIN».
Nuclear Physics A, **719**, pp. 153–+ (2003).

LOEB, A. AND WYITHE, S.
«Precise Measurement of the Cosmological Power Spectrum With a Dedicated 21cm Survey After Reionization».
Phys. Rev. Lett., **100**, p. 161301 (2008).

LOEB, A. AND ZALDARRIAGA, M.
«Measuring the small-scale power spectrum of cosmic density fluctuations through 21-cm tomography prior to the epoch of structure formation».
Phys. Rev. Lett., **92**, p. 211301 (2004).

LOEB, A. AND ZALDARRIAGA, M.
«The small-scale power spectrum of cold dark matter».
Phys. Rev., **D71**, p. 103520 (2005).

LUO, X. AND SCHRAMM, D.N.
«Fractals and cosmological large-scale structure».
Science, **256**, pp. 513–515 (1992).

MA, C.P. AND BERTSCHINGER, E.
«Cosmological perturbation theory in the synchronous and conformal Newtonian gauges».
Astrophys. J., **455**, pp. 7–25 (1995).

MACK, G.D., JACQUES, T.D., BEACOM, J.F., BELL, N.F. AND YUKSEL, H.

«Conservative Constraints on Dark Matter Annihilation into Gamma Rays».
Phys. Rev., **D78**, p. 063542 (2008).

MAJEROTTO, E., VALIVIITA, J. AND MAARTENS, R.
«Adiabatic initial conditions for perturbations in interacting dark energy models» (2009).

MALTONI, M., SCHWETZ, T., TÓRTOLA, M. AND VALLE, J.W.F.
«Status of global fits to neutrino oscillations».
New Journal of Physics, **6**, pp. 122–+ (2004).

MANDELBROT, B.B.
The fractal geometry of nature /Revised and enlarged edition/ (New York, W.H. Freeman and Co., 1983, 495 p., 1983).

MANGANO, G., MIELE, G., PASTOR, S. AND PELOSO, M.
«A precision calculation of the effective number of cosmological neutrinos».
Phys. Lett., **B534**, pp. 8–16 (2002).

MANGANO, G. ET AL.
«Relic neutrino decoupling including flavour oscillations».
Nucl. Phys., **B729**, pp. 221–234 (2005).

MAO, Y., TEGMARK, M., MCQUINN, M., ZALDARRIAGA, M. AND ZAHN, O.
«How accurately can 21 cm tomography constrain cosmology?»
Phys. Rev., **D78**, p. 023529 (2008).

MARCH-RUSSELL, J., MURAYAMA, H. AND RIOTTO, A.
«The small observed baryon asymmetry from a large lepton asymmetry».
JHEP, **11**, p. 015 (1999).

MARCH-RUSSELL, J., WEST, S.M., CUMBERBATCH, D. AND HOOPER, D.
«Heavy Dark Matter Through the Higgs Portal».
JHEP, **07**, p. 058 (2008).

MARCH-RUSSELL, J.D. AND WEST, S.M.
«WIMPonium and Boost Factors for Indirect Dark Matter Detection».
Phys. Lett., **B676**, pp. 133–139 (2009).

MCDONALD, J.
«Naturally large cosmological neutrino asymmetries in the MSSM».
Phys. Rev. Lett., **84**, pp. 4798–4801 (2000).

MÉSZÁROS, P., LAGUNA, P. AND REES, M.J.
«Gasdynamics of relativistically expanding gamma-ray burst sources - Kinematics, energetics, magnetic fields, and efficiency».
ApJ , **415**, pp. 181–190 (1993).

MIHALAS, D. AND MIHALAS, B.W.
Foundations of Radiation Hydrodynamics (New York, Oxford University Press, 1984).

MIRALDA-ESCUDÉ, J.
«A Test of the Collisional Dark Matter Hypothesis from Cluster Lensing».
ApJ , **564**, pp. 60–64 (2002).

MOTA, D.F., KRISTIANSEN, J.R., KOIVISTO, T. AND GROENEBOOM, N.E.
«Constraining Dark Energy Anisotropic Stress».
Mon. Not. Roy. Astron. Soc., **382**, pp. 793–800 (2007).

MUSTAFA, M.G. AND KÄMPFER, B.
«Gamma flashes from relativistic electron-positron plasma droplets».
Phys. Rev. A, **79(2)**, pp. 020103–+ (2009).

MYATT, J., DELETTREZ, J.A., MAXIMOV, A.V., MEYERHOFER, D.D., SHORT, R.W., STOECKL, C. AND STORM, M.
«Optimizing electron-positron pair production on kilojoule-class high-intensity lasers for the purpose of pair-plasma creation».
Phys. Rev. E, **79(6)**, pp. 066409–+ (2009).

NAVARRO, J.F. ET AL.
«The Diversity and Similarity of Cold Dark Matter Halos» (2008).

ORITO, M., KAJINO, T., MATHEWS, G.J. AND BOYD, R.N.
«Primordial nucleosynthesis and neutrinos with mass and degeneracy».
Nuclear Physics A, **688**, pp. 17–20 (2001).

ORITO, M., KAJINO, T., MATHEWS, G.J. AND WANG, Y.
«Constraints on neutrino degeneracy from the cosmic microwave background and primordial nucleosynthesis».
Phys. Rev. D, **65(12)**, pp. 123504–+ (2002).

PAGE, L. ET AL.
«First Year Wilkinson Microwave Anisotropy Probe (WMAP) Observations: Interpretation of the TT and TE Angular Power Spectrum Peaks».
Astrophys. J. Suppl., **148**, p. 233 (2003).

PATO, M., PIERI, L. AND BERTONE, G.
«Multi-messenger constraints on the annihilating dark matter interpretation of the positron excess» (2009).

PEACOCK, J.A.
≪Studying Large-scale Structure with the 2dF Galaxy Redshift Survey≫.
In N. Metcalfe and T. Shanks (eds.), *A New Era in Cosmology*, volume 283 of *Astronomical Society of the Pacific Conference Series*, pp. 19–+ (2002).

PEACOCK, J.A., COLE, S., NORBERG, P., BAUGH, C.M., BLAND-HAWTHORN, J., BRIDGES, T., CANNON, R.D., COLLESS, M., COLLINS, C., COUCH, W. ET AL.
≪A measurement of the cosmological mass density from clustering in the 2dF Galaxy Redshift Survey≫.
Nature , **410**, pp. 169–173 (2001).

PEARSON, T.J. ET AL.
≪The Anisotropy of the Microwave Background to l = 3500: Mosaic Observations with the Cosmic Background Imager≫.
Astrophys. J., **591**, pp. 556–574 (2003).

PECCEI, R.D.
≪Neutrino models of dark energy≫.
Phys. Rev., **D71**, p. 023527 (2005).

PEEBLES, P.J.E.
≪Primeval adiabatic perturbations - Effect of massive neutrinos≫.
ApJ , **258**, pp. 415–424 (1982).

PEEBLES, P.J.E.
Principles of physical cosmology (Princeton Series in Physics, Princeton, NJ: Princeton University Press, —c1993, 1993).

PEEBLES, P.J.E. AND RATRA, B.
≪The cosmological constant and dark energy≫.
Rev. Mod. Phys., **75**, pp. 559–606 (2003).

PEIRIS, H.V. ET AL.
≪First year Wilkinson Microwave Anisotropy Probe (WMAP) observations: Implications for inflation≫.
Astrophys. J. Suppl., **148**, p. 213 (2003).

PENZIAS, A.A. AND WILSON, R.W.
≪A Measurement of Excess Antenna Temperature at 4080 Mc/s.≫
ApJ , **142**, pp. 419–421 (1965).

PERLMUTTER, S. ET AL.
≪Measurements of Omega and Lambda from 42 High-Redshift Supernovae≫.
Astrophys. J., **517**, pp. 565–586 (1999).

PIERI, L., BERTONE, G. AND BRANCHINI, E.
«Dark Matter Annihilation in Substructures Revised».
Mon. Not. Roy. Astron. Soc., **384**, p. 1627 (2008).

PIERI, L., PIZZELLA, A., CORSINI, E.M., BONTA', E.D. AND BERTOLA, F.
«Could the Fermi-LAT detect gamma-rays from dark matter annihilation in the dwarf galaxies of the Local Group?»
Astron. Astrophys., **496**, p. 351 (2009a).

PIERI, L., LATTANZI, M. AND SILK, J.
«Constraining the Sommerfeld enhancement with Cherenkov telescope observations of dwarf galaxies» (2009b).

PIERPAOLI, E.
«Constraints on the cosmic neutrino background».
Mon. Not. Roy. Astron. Soc., **342**, p. L63 (2003).

PIRAN, T.
«Gamma-ray bursts and the fireball model».
Phys. Rep. , **314**, pp. 575–667 (1999).

PIRAN, T., SHEMI, A. AND NARAYAN, R.
«Hydrodynamics of Relativistic Fireballs».
MNRAS , **263**, pp. 861–867 (1993).

POSPELOV, M. AND RITZ, A.
«Astrophysical Signatures of Secluded Dark Matter».
Phys. Lett., **B671**, pp. 391–397 (2009).

PRITCHARD, J.R. AND PIERPAOLI, E.
«Constraining massive neutrinos using cosmological 21 cm observations».
Phys. Rev., **D78**, p. 065009 (2008).

PROFUMO, S.
«TeV gamma-rays and the largest masses and annihilation cross sections of neutralino dark matter».
Phys. Rev., **D72**, p. 103521 (2005).

PROFUMO, S., SIGURDSON, K. AND KAMIONKOWSKI, M.
«What mass are the smallest protohalos?»
Phys. Rev. Lett., **97**, p. 031301 (2006).

QUARTIN, M., CALVAO, M.O., JORAS, S.E., REIS, R.R.R. AND WAGA, I.
«Dark Interactions and Cosmological Fine-Tuning».
JCAP, **0805**, p. 007 (2008).

RIESS, A.G. ET AL.
«Observational Evidence from Supernovae for an Accelerating Universe and a Cosmological Constant».
Astron. J., **116**, pp. 1009–1038 (1998).

RIESS, A.G. ET AL.
«A Redetermination of the Hubble Constant with the Hubble Space Telescope from a Differential Distance Ladder».
Astrophys. J., **699**, pp. 539–563 (2009).

ROBERTSON, B. AND ZENTNER, A.
«Dark Matter Annihilation Rates with Velocity-Dependent Annihilation Cross Sections».
Phys. Rev., **D79**, p. 083525 (2009).

ROSENFELD, R.
«Reconstruction of interacting dark energy models from parameterizations».
Phys. Rev., **D75**, p. 083509 (2007).

RUFFINI, R.
«On the de Vaucouleurs density-radius relation and the cellular intermediate large-scale structure of the universe».
In H.G. Corwin Jr. and L. Bottinelli (eds.), *World of Galaxies (Le Monde des Galaxies)*, pp. 461–472 (1989).

RUFFINI, R., AKSENOV, A.G., BERNARDINI, M.G., BIANCO, C.L., CAITO, L., CHARDONNET, P., DAINOTTI, M.G., DE BARROS, G., GUIDA, R., IZZO, L. ET AL.
«The Blackholic energy and the canonical Gamma-Ray Burst IV: the "long," "genuine short" and "fake-disguised short" GRBs».
In M. Novello and S. Perez (eds.), *American Institute of Physics Conference Series*, volume 1132 of *American Institute of Physics Conference Series*, pp. 199–266 (2009a).

RUFFINI, R., SALMONSON, J.D., WILSON, J.R. AND XUE, S.S.
«On the pair electromagnetic pulse of a black hole with electromagnetic structure».
A&A , **350**, pp. 334–343 (1999).

RUFFINI, R., SALMONSON, J.D., WILSON, J.R. AND XUE, S.S.
«On the pair-electromagnetic pulse from an electromagnetic black hole surrounded by a baryonic remnant».
A&A , **359**, pp. 855–864 (2000).

RUFFINI, R. AND SONG, D.J.

≪On the Jeans mass of weakly interacting, neutral, massive leptons.≫
In F. Melchiorri and R. Ruffini (eds.), *Gamow cosmology, p. 370 - 385*, pp. 370–385 (1986).

RUFFINI, R., SONG, D.J. AND STELLA, L.
≪On the statistical distribution off massive fermions and bosons in a Friedmann universe≫.
A&A , **125**, pp. 265–270 (1983).

RUFFINI, R., SONG, D.J. AND TARAGLIO, S.
≪The 'ino' mass and the cellular large-scale structure of the universe≫.
A&A , **190**, pp. 1–2 (1988).

RUFFINI, R., VERESHCHAGIN, G. AND XUE, S.S.
≪Electron-positron pairs in physics and astrophysics≫.
Physics Reports, p. accepted (2009b).

SALUCCI, P. ET AL.
≪The universal rotation curve of spiral galaxies. II: The dark matter distribution out to the virial radius≫.
Mon. Not. Roy. Astron. Soc., **378**, pp. 41–47 (2007).

SAVAGE, M.J., MALANEY, R.A. AND FULLER, G.M.
≪Neutrino oscillations and the leptonic charge of the universe≫.
ApJ , **368**, pp. 1–11 (1991).

SCOTT, P.F. ET AL.
≪First results from the Very Small Array – III. The CMB power spectrum≫.
Mon. Not. Roy. Astron. Soc., **341**, p. 1076 (2003).

SELJAK, U. AND ZALDARRIAGA, M.
≪A Line of Sight Approach to Cosmic Microwave Background Anisotropies≫.
Astrophys. J., **469**, pp. 437–444 (1996).

SHECTMAN, S.A., LANDY, S.D., OEMLER, A., TUCKER, D.L., LIN, H., KIRSHNER, R.P. AND SCHECHTER, P.L.
≪The Las Campanas Redshift Survey≫.
ApJ , **470**, pp. 172–+ (1996).

SHEMI, A. AND PIRAN, T.
≪The appearance of cosmic fireballs≫.
ApJ , **365**, pp. L55–L58 (1990).

SILK, J. AND SREDNICKI, M.
≪Cosmic-ray antiprotons as a probe of a photino-dominated universe≫.
Phys. Rev. Lett., **53**, p. 624 (1984).

SJOSTRAND, T. ET AL.
«High-energy physics event generation with PYTHIA 6.1».
Comput. Phys. Commun., **135**, pp. 238–259 (2001).

SOMMERFELD, A.
«».
Annalen der Physik, **403**, p. 257 (1931).

SPERGEL, D.N. ET AL.
«First Year Wilkinson Microwave Anisotropy Probe (WMAP) Observations: Determination of Cosmological Parameters».
Astrophys. J. Suppl., **148**, pp. 175–194 (2003).

SPRINGEL, V. ET AL.
«Prospects for detecting supersymmetric dark matter in the Galactic halo».
Nature, **456N7218**, pp. 73–80 (2008a).

SPRINGEL, V. ET AL.
«A blueprint for detecting supersymmetric dark matter in the Galactic halo» (2008b).

SPRINGEL, V. ET AL.
«The Aquarius Project: the subhalos of galactic halos».
Mon. Not. Roy. Astron. Soc., **391**, pp. 1685–1711 (2008c).

STEPNEY, S.
«Two-body relaxation in relativistic thermal plasmas».
MNRAS , **202**, pp. 467–481 (1983).

STRONG, A.W., MOSKALENKO, I.V. AND REIMER, O.
«A new determination of the extragalactic diffuse gamma-ray background from EGRET data».
Astrophys. J., **613**, pp. 956–961 (2004).

STRUMIA, A. AND VISSANI, F.
«Implications of neutrino data circa 2005».
Nuclear Physics B, **726**, pp. 294–316 (2005).

TAKAHASHI, F. AND YAMAGUCHI, M.
«Spontaneous baryogenesis in flat directions».
Phys. Rev., **D69**, p. 083506 (2004).

TEGMARK, M. ET AL.
«Cosmological parameters from SDSS and WMAP».
Phys. Rev., **D69**, p. 103501 (2004).

TEGMARK, M. ET AL.
«Cosmological Constraints from the SDSS Luminous Red Galaxies».
Phys. Rev., **D74**, p. 123507 (2006).

THOMA, M.H.
«Colloquium: Field theoretic description of ultrarelativistic electron-positron plasmas».
Reviews of Modern Physics, **81**, pp. 959–968 (2009).

TORMEN, G., MOSCARDINI, L. AND YOSHIDA, N.
«Properties of cluster satellites in hydrodynamical simulations».
MNRAS , **350**, pp. 1397–1408 (2004).

TREMAINE, S. AND GUNN, J.E.
«Dynamical role of light neutral leptons in cosmology».
Phys. Rev. Lett. , **42**, pp. 407–410 (1979).

VALIVIITA, J., MAARTENS, R. AND MAJEROTTO, E.
«Observational constraints on an interacting dark energy model» (2009).

VALIVIITA, J., MAJEROTTO, E. AND MAARTENS, R.
«Instability in interacting dark energy and dark matter fluids».
JCAP, **0807**, p. 020 (2008).

VASS, I., VALLURI, M., KRAVTSOV, A. AND KAZANTZIDIS, S.
«Evolution of the Dark Matter Phase-Space Density Distributions of LCDM Halos».
Mon. Not. Roy. Astron. Soc., **395**, pp. 1225–1236 (2009).

VERDE, L. ET AL.
«First Year Wilkinson Microwave Anisotropy Probe (WMAP) Observations: Parameter Estimation Methodology».
Astrophys. J. Suppl., **148**, p. 195 (2003).

WALKER, M.G., MATEO, M., OLSZEWSKI, E.W., GNEDIN, O.Y., WANG, X., SEN, B. AND WOODROOFE, M.
«Velocity Dispersion Profiles of Seven Dwarf Spheroidal Galaxies».
ApJ , **667**, pp. L53–L56 (2007).

WALKER, M.G. ET AL.
«A Universal Mass Profile for Dwarf Spheroidal Galaxies».
Astrophys. J., **704**, pp. 1274–1287 (2009).

WEINBERG, S.
Gravitation and Cosmology: Principles and Applications of the General Theory of Relativity (Gravitation and Cosmology: Principles and Applications of the General Theory of Relativity, by Steven Weinberg, pp. 688. ISBN 0-471-92567-5. Wiley-VCH , July 1972., 1972).

WEINBERG, S.
«Damping of tensor modes in cosmology».
Phys. Rev., **D69**, p. 023503 (2004).

WEINHEIMER, C. ET AL.
«High precision measurement of the tritium beta spectrum near its endpoint and upper limit on the neutrino mass».
Phys. Lett., **B460**, pp. 219–226 (1999).

WELLER, J. AND LEWIS, A.M.
«Large Scale Cosmic Microwave Background Anisotropies and Dark Energy».
Mon. Not. Roy. Astron. Soc., **346**, pp. 987–993 (2003).

WETTERICH, C.
«Growing neutrinos and cosmological selection».
Phys. Lett., **B655**, pp. 201–208 (2007).

WEYL, H.
Space Time Matter (Dover Publications, New York, 1952).

WILKS, S.C., KRUER, W.L., TABAK, M. AND LANGDON, A.B.
«Absorption of ultra-intense laser pulses».
Physical Review Letters, **69**, pp. 1383–1386 (1992).

WILSON, J.R. AND MATHEWS, G.J.
Relativistic Numerical Hydrodynamics (2003).

WONG, Y.Y.Y.
«Analytical treatment of neutrino asymmetry equilibration from flavour oscillations in the early universe».
Phys. Rev., **D66**, p. 025015 (2002).

YAMAGUCHI, M.
«Generation of cosmological large lepton asymmetry from a rolling scalar field».
Phys. Rev., **D68**, p. 063507 (2003).

YUKSEL, H., KISTLER, M.D. AND STANEV, T.
«TeV Gamma Rays from Geminga and the Origin of the GeV Positron Excess».
Phys. Rev. Lett., **103**, p. 051101 (2009).

ZEHAVI, I., ZHENG, Z., WEINBERG, D.H., FRIEMAN, J.A., BERLIND, A.A., BLANTON, M.R., SCOCCIMARRO, R., SHETH, R.K., STRAUSS, M.A., KAYO, I. ET AL.

≪The Luminosity and Color Dependence of the Galaxy Correlation Function≫.
ApJ , **630**, pp. 1–27 (2005).

ZELDOVICH, Y.B. AND SYUNYAEV, R.A.
≪Astrophysical implications of the neutrino rest mass. I - The universe≫.
Pis ma Astronomicheskii Zhurnal, **6**, pp. 451–456 (1980).

ZHAO, G.B., XIA, J.Q. AND ZHANG, X.M.
≪Probing for variation of neutrino mass with current observations≫.
JCAP, **0707**, p. 010 (2007).